DESIGN AND ANALYSIS OF DEPLOYABLE RECIPROCAL FRAMES

A Thesis Submitted to the
Graduate School of Engineering and Science
İzmir Institute of Technology
in Partial Fulfillment of the Requirements for the Degree of

DOCTOR OF PHILOSOPHY

in Architecture

by
Gülçin ÖZEN

July 2022
İZMİR

ACKNOWLEDGEMENTS

Firstly, I would like to thank and pay my respects to my thesis advisor Prof. Dr. Koray Korkmaz, who guided me with his experiences and feedback, and always motivated and supported me during my Ph.D. study.

Besides, I would like to express my sincere thanks to Assoc. Prof. Dr. Gökhan Kiper for his scientific guidance, feedback, and continuous support.

I would like to thank my thesis committee, Asst. Prof. Dr. Uğur Demir, Asst. Prof. Dr. Halit Coza and Assoc. Prof. Dr. Ahmet Vefa Orhon contributed to the thesis with their constructive feedback, valuable suggestions, and comments.

I would like to thank my friends Mümine Gerçek Şen, Mina Yavuz Aslan, İlker Güçü, Keziban Çelik, Fulya Atarer and Şüheda Köse for their great support and warm friendship.

I would like to thank my family, who are always there for me.

ABSTRACT

DESIGN AND ANALYSIS OF DEPLOYABLE RECIPROCAL FRAMES

A reciprocal frame (RF) is a type of structure used since early times. It consists of mutually supporting bars that can span large distances greater than the length of the bar. Although there are deficiencies in previous studies, there are movable RFs, but we cannot talk about the existence of a 3-dimensional deployable RF network. This study aims to contribute to the missing knowledge for movable RF fans and develop a deployable RF network.

The study has conducted a comprehensive literature review to gain knowledge and identify the deficiencies of RFs. There are many studies about RFs, but it has been observed that very limited research has been done on movable RFs, and some geometric properties have not been made yet. Firstly, missing geometric knowledge has been found, which are the positions and orientations of the joints by using Denavit-Hartenberg parameters. Also, the effect of engagement length on the fan height and base edge is analyzed. A reconfigurable demountable RF fan is created with the obtained geometric knowledge.

Then, mobility calculations are made, and kinematic diagrams are drawn for zero, single, and multi degrees of freedom (DoF) triangular, quadrilateral, and pentagonal fans. Their motions are investigated, and 3-dimensional (3d) simulations are generated.

A two DoF quadrilateral fan with prismatic and revolute joints is produced. Then the possibilities of assembling the two DoF fans are searched to create a deployable RF network. While the network has a single DoF in the direction of vault curvature, it has multi DoF in the thickness direction. The network takes the form of a roll in its most closed state, and it takes the form of a vault in its most open state. The section of the curvature of the deployable network is the same as the Da Vinci bridge. However, while simple joints were used in the Da Vinci Bridge, revolute and prismatic joints are used in the proposed deployable RF network.

ÖZET

HAREKETLİ KARŞILIKLI/KİLİTLİ ÇERÇEVELERİN TASARIMI VE ANALİZİ

Karşılıklı/Kilitli Çerçeveler (RF) (Kılıç and Orhon, 2019) eski zamanlardan beri kullanılan bir yapı türüdür. Bu yapılar birbirini destekleyen çubuk elemanlardan oluşmakta ve kendi uzunluğundan büyük açıklıkları geçebilmektedir. Daha önceki çalışmalarda eksiklikler olsa da hareketli RF'lerle ilgili çalışmalar vardır ancak katlanabilir bir RF kafes sisteminin varlığından söz etmek mümkün değildir. Bu çalışma, hareketli RF'ler için eksik bilgilerin geliştirilmesini ve katlanabilir bir RF kafes yapısı geliştirmeyi amaçlamaktadır.

Çalışmada, karşılıklı/kilitli çerçevelerle ilgili bilgi edinmek ve konuyla ilgili eksiklikleri bulmak için kapsamlı bir literatür taraması yapılmıştır. RF'lerle ilgili olarak yapılmış pek çok çalışma olmasına rağmen, hareketli RF'ler üzerine yapılmış çalışmaların çok sınırlı olduğu ve bazı geometrik özelliklerin henüz bulunmadığı tespit edilmiştir. İlk olarak mafsalların nereye yerleştirildiğini, nasıl yönlendirildiğini ve birbirlerine göre nasıl konumlandırıldıklarının bilgisi Denavit-Hartenberg parametreleri kullanılarak bulunmuştur. Ayrıca, mafsallar arasındaki mesafenin, modül yüksekliği ve modülün zemine değen noktalarının birbirine olan mesafesi üzerindeki etkisi analiz edilmiştir. Elde edilen geometrik bilgilerle, farklı şekillerde tekrar bir araya getirilebilir, sökülüp takılabilen dört çubuklu RF modülü tasarlanmıştır.

Daha sonra sıfır, tek ve çok serbestlik dereceli üç çubuklu, dört çubuklu ve beş çubuklu modüller için mobilite hesapları yapılmış ve kinematik diyagramları çizilmiştir. Hareketlerini incelemek amacıyla üç boyutlu simülasyonları oluşturulmuştur.

Çalışmanın devamında kayar ve döner mafsallara sahip iki serbestlik dereceli dört çubuklu bir modül üretilmiş ve katlanabilir kafes yapı elde edebilmek için bu iki serbestlik dereceli modüllerin bir araya getirilme olanakları araştırılmıştır. Bu modüller çoğaltılarak bir sarmal kafes sistem elde edilmiştir. Gerekli serbestlik derecesi çalışmaları yapılarak tonoz eğriliği yönünde tek, tonoz kalınlığı yönünde çok serbestlik derecesi elde edilmiştir. Kafes, en kapalı halinde sarmal şeklini alırken, en açık halinde tonoz biçimini almaktadır. Kafes sistemin tonoz eğriliği yönündeki kesiti Da Vinci köprüsüyle aynıdır. Ancak Da Vinci köprüsünde basit mafsallar kullanılırken, önerilen kafes yapıda döner ve kayar mafsallar kullanılmıştır.

TABLE OF CONTENTS

LIST OF FIGURES

Figure **Page**

Figure **Page**

Figure **Page**

Figure **Page**

Figure **Page**

Figure **Page**

Figure **Page**

Figure **Page**

LIST OF TABLES

CHAPTER 1

INTRODUCTION

1.1. Definition of the Study

People's needs constantly change, and every area of life needs to keep up with this change. Anything that cannot adapt to the change is eliminated. Therefore, the necessity of constructing structures that can respond to rapidly changing spatial needs arises. Advances in construction technology, materials science, and architectural computing technologies have made it possible to build deployable structures that can meet changing human needs.

Deployable structures are described as prefabricated structures that can be transformed from a closed compact to a predefined expanded form that can carry loads. Scissor-like elements (SLE) are the most commonly used units of deployable structures (Gantes, 1991). There are many studies on deployable structures made so far with SLEs. Spanish architect Emilio Perez Pinero pioneered SLEs and presented the notion of scissor structure in 1961. Pinero designed a deployable roof structure for the Itinerant Theater in London in 1961 from SLEs and motivated many architects and engineers to work on these mechanisms. The deployable structure composed of rigid bars and cables required the use of some additional cables to lock the system and provide the necessary stabilization after folding (Gantes, 1991). Then, Escrig studied how three-dimensional structures can be obtained by intersecting SLEs in multiple directions on a grid. Escrig investigated how three-dimensional structures can be created by intersecting SLEs in numerous directions on a grid and how curvature can be achieved in such a grid by changing the position of the intermediate hinge of SLEs. New spherical grid structures consisting of two-way and three-way scissors are proposed by Escrig, in collaboration with Jose Sanchéz and Juan Pérez Valcárcel, and they suggested various connection details for the designs (Gantes, 1991). The units are planar in SLEs composed of translational angulated or polar scissor units, and the researchers try to create 3-dimensional (3d) deployable structures by adding scissor units in different ways. This thesis study questions whether a deployable structure can be made with 3d units: Reciprocal Frames (RF). RFs consist of bars that mutually

support each other. The bars of the RFs support each other at the intermediate points and are supported by another bar at the one end of the bar. RFs are three-dimensional because of the bar eccentricity and the system of mutual benefit of the bars. Graham Brown coined the name 'reciprocal frame.' The etymology of 'reciprocal' comes from the Latin word 'reciprocus' while recus means backward, procous means forwards. Therefore, reciprocity means back and forth, providing an exchange for mutual benefit (Parigi and Pugnale, 2014). Baverel used the term 'nexorade' to explain RFs. The etymology of nexorade comes from the Latin word 'nexor' meaning link. Nexorade implies the assembly of nexors. The notion creates complications with Graham Brown's RF, but they mean the same thing (Baverel, 2000).

Although there are studies on movable RF units in the literature, there are some deficiencies. Moreover, there is no study on 3d deployable RF networks. The fact that RFs have the characteristics to meet the needs in changing situations is a source of motivation for developing movable RF fans and deployable RF networks for this study.

1.2. Aim of the Thesis

In the research that has been done until today, the geometry of RF, form-finding issues, connections, structural behavior, fabrication methods, and movable RFs were studied. But there is a very limited number of studies about movable RF fans and no studies for 3-dimensional deployable RF networks. The first aim of this dissertation is to explore the missing geometric knowledge for movable RF fans and make the necessary motion studies. The second aim of this dissertation is to search for possible ways to assemble the movable RF fans and construct a deployable RF network.

1.3. Methodology

Simulation and modeling are used as the primary research methodology. Simulation and modeling include mathematical models and computer simulations.

The study starts by examining the literature. The literature review has been done regarding the components that form an RF, architectural applications, and previous work review.

After having groundwork about the topic, the study focused on the geometry, motion capabilities, kinematic properties, and multiplication processes of RF fans. Microsoft Excel is used to develop mathematical models. In addition to these mathematical models, kinematic diagrams are drawn in Autodesk Autocad. 3d computer models are constructed by using Solidworks to understand the motion capabilities of the fans and networks. By preserving the parameters in Solidworks, physical models are produced with a 3d printer, and wood and metal workshops are used for cutting.

1.4. Outline of the Thesis

This thesis consists of nine chapters.

Chapter 1 presents the definition, aim, and methodology of the study.

In Chapter 2, a literature review has been done. The definition of the RF and its elements are presented. Then architectural applications of reciprocity and a review of the previous work are introduced.

After getting the necessary information, the geometric properties of RF fans are investigated in Chapter 3. The joints' positions and orientations are found using Denavit-Hartenberg parameters. This information gives where the joints are placed, how they are oriented, and take positions according to one another. Besides, the influence of engagement length on the fan height and the base edge is analyzed. Based on the geometric properties that are proposed, case studies are done. Moreover, a physical model of a reconfigurable demountable RF fan is produced.

Chapter 4 focuses on calculating the mobility of the three-, four- and five-nexor fans. Fans are divided into three sub-groups within themselves: zero DoF, single DoF, and multi DoF triangular, quadrilateral, or pentagonal fans.

Chapter 5 studies the motion of the single DoF triangular and quadrilateral fans. Firstly, fans are connected without using any sliding joints. Then the fans with sliding joints are produced. Necessary joints – revolute or prismatic- are assembled to reach a single DoF in these fans. By creating computer models, their motions are simulated.

Networks are formed from quadrilateral fans by using only revolute joints in Chapter 6. The aim is to have a single DoF network. The networks are divided into two categories as type one and type two. Type one is composed of only leftward fans, and type two is composed of both leftward and rightward fans. Types of networks are

categorized in themselves into three according to the joint series that are used. The networks are modeled in Solidworks, and their motions are simulated.

Chapter 7 focuses on the motion analysis of single DoF triangular and quadrilateral RFs with the minimum number of orthogonal revolute joints. Motion analyses are performed by reducing the orthogonally connected revolute joints in the fans.

In Chapter 8, motion analysis of two DoF quadrilateral fan is searched. Two motion modes are found for the fan. Then two networks are developed. Their mobilities are calculated, and by creating computer models, the motions of the networks are simulated. Moreover, physical models are created to see the performance.

In Chapter 9, the study is concluded with the main achievements obtained and the study's contributions to the field.

CHAPTER 2

REVIEW OF THE PREVIOUS WORK

This chapter presents a review of RFs studied in the literature. The components that form an RF fan and their relations are studied in detail to understand the essential design principles of the RFs. Then, former structures and studies are presented in the subsections of architectural applications of reciprocity and the previous work.

2.1. Reciprocal Frames

The closed-circuit system consisting of short bars that can span large openings greater than the length of the individual bar and support one another is called Reciprocal Frames (RF) (Figure 2.1). In RFs, whatever the composition is, the geometry should always have two connected members at a time. Moreover, at least three members should be connected to create a frame, but there is no limit to the maximum (Baverel and Saidani, 1999).

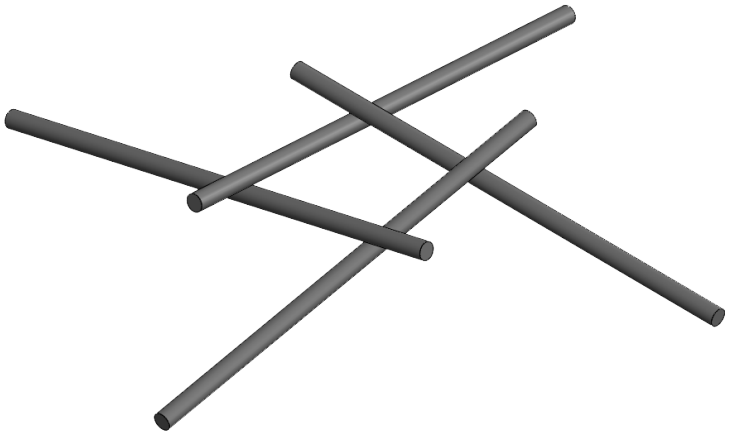

Figure 2.1. A reciprocal frame.

Each member of the nexorade is described as 'nexor' (Figure 2.2a). The simplest form of a nexorade is called 'fan'. In other words, it is the most elementary arrangement

of a nexorade. Three or more nexors are coming together and generating a fan. In Figure 2.2b, a four-nexor fan and three-nexor fan arrangements can be seen (Baverel, 2000).

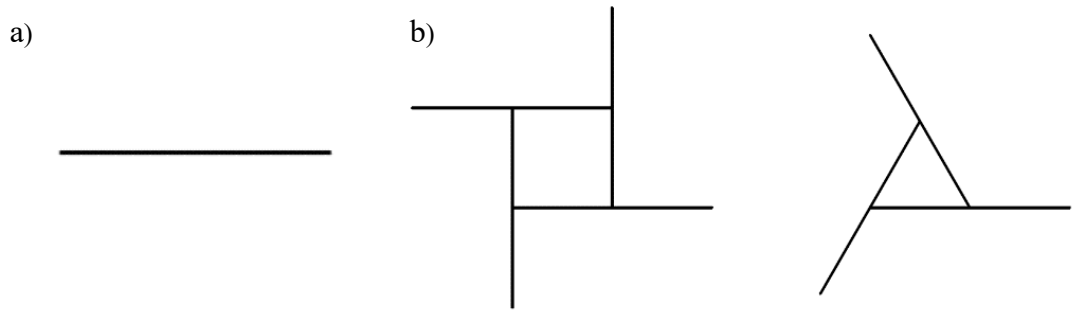

Figure 2.2. a) Nexor, b) A fan.

L_n is referred to indicate the length of each nexor. The distance between one end of a nexor and an intersection point is 'engagement length' (Figure 2.3) and is denoted by λ. A polygon created at the center of the fan is called an 'engagement window' (Baverel, 2000).

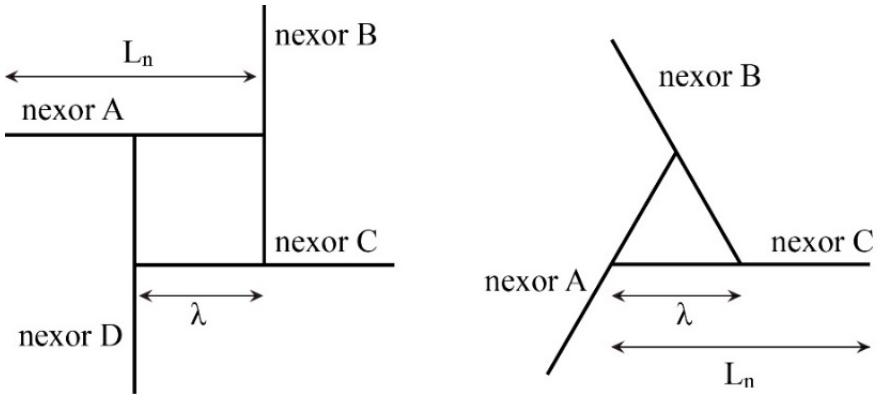

Figure 2.3. Plan view of a fan.

A nexor can be an upward or downward position with its supporting nexor. Nexor's two endpoints can be both above or below, or one can be above and the other in the below position (Figure 2.4) (Baverel, 2000).

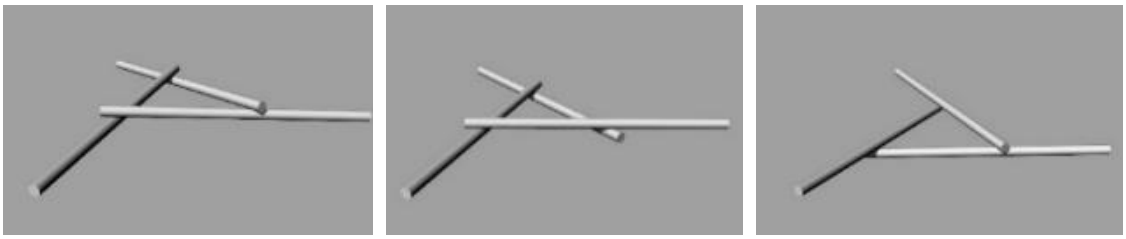

Figure 2.4. Different end dispositions of a nexor.

If the ends of nexors shown in Figure 2.5 create an anticlockwise moment, it is called a 'leftward fan.' Otherwise, if it makes a clockwise moment, it is called a 'rightward fan' (Baverel, 2000). The term “chiral” is used to denote an object whose mirror image cannot be superimposed on it (Conway, Burgiel, and Goodman-Strauss, 2008). An RF fan is chiral since the mirror image is not the same with itself (Figure 2.5). There is chirality in the networks formed from the fans, but there are also networks without chirality. Examples are given in the following sections.

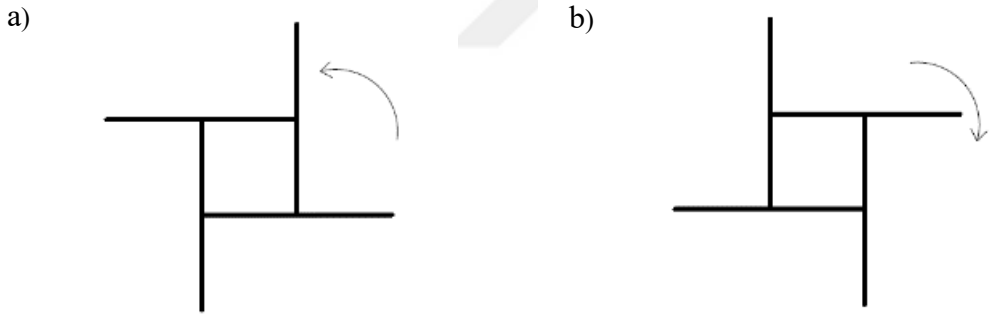

Figure 2.5. a) Leftward fan, b) Rightward fan.

At the connection of two nexors, the minimum perpendicular distance between the centroids of these cross-sections is referred to as 'eccentricity' and denoted by e (Figure 2.6). Even though the angle between two nexors changes, the eccentricity does not (Baverel, 2000).

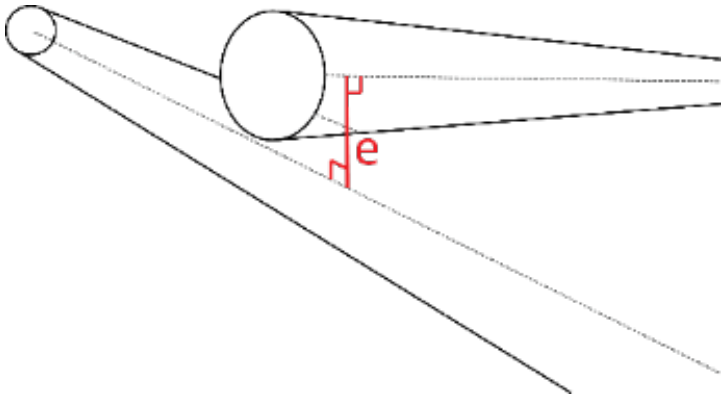

Figure 2.6. Eccentricity.

If nexors have circular cross-sections, their eccentricity is the sum of radiuses of two nexors. In flat fans, all the nexors are on the same level, which means e = 0. In the situation of e > 0, the supported nexors are in a higher position than the support nexors (Thönnissen, 2014).

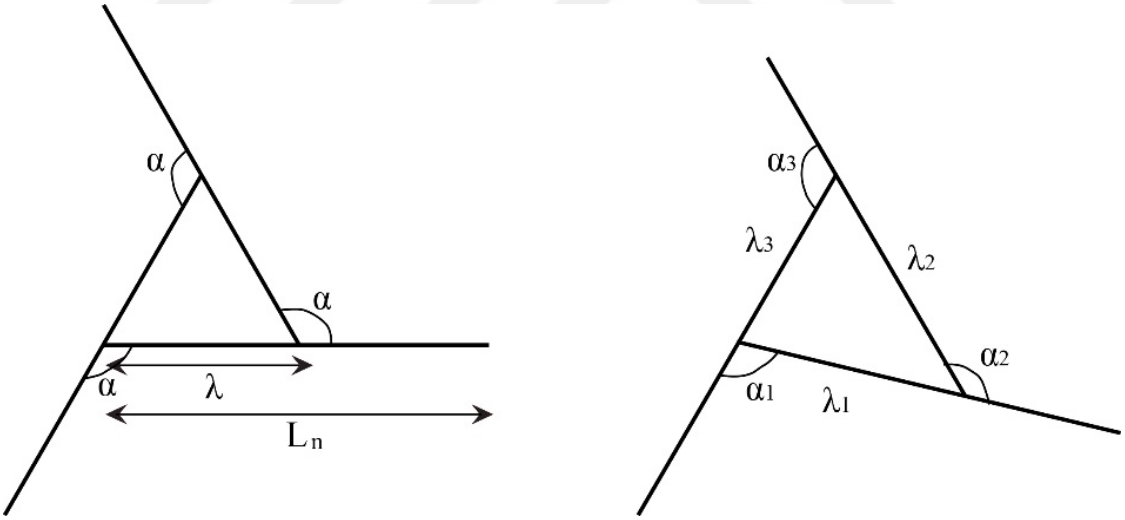

Figure 2.7. Fans with identical and varied engagement lengths.

A nexorade can be composed of both identical engagement lengths and varied engagement lengths, and this length can vary between 0 to L_n (Figure 2.7) (Baverel, 2000).

2.2. Architectural Applications of Reciprocity

Since antiquity, the principle of spanning long distances with mutually supported short bars has been known. The first examples of structures similar to RF are Indian Tepee and Hogan dwelling. They both depend on mutually supported elements. Indian tepees are built quickly, and they are portable and reusable. The wooden bars of the tepees serve as the main load-bearing system. They meet at one point and are connected with a lash to stabilize the structure (Figure 2.8). The structure is covered with animal skin for weather protection (Popovic Larsen, 2007).

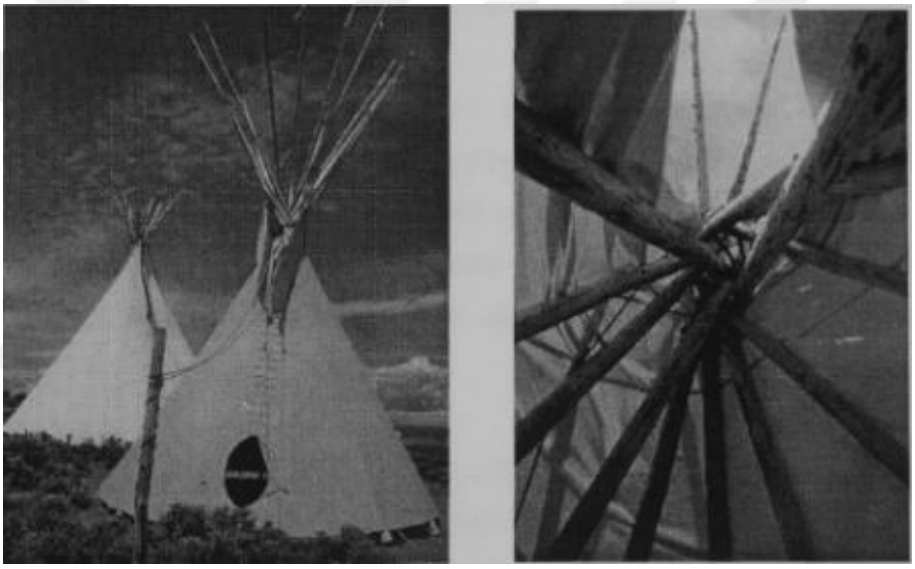

Figure 2.8. Indian tepee.
(Source: Popovic, 1996)

On the other hand, Hogan dwellings resemble a complex reciprocal system consisting of several reciprocal grillages. Each RF has a larger diameter and consists of laying beams on top of each other. This process continues until the opening gets smaller. Because of this installation process, the Hogan is shaped like a domed roof (Figure 2.9). The structure of the wooden frame is usually plastered with mud. The mud stabilizes the connection between the wooden beams and provides climate protection (Popovic Larsen, 2007).

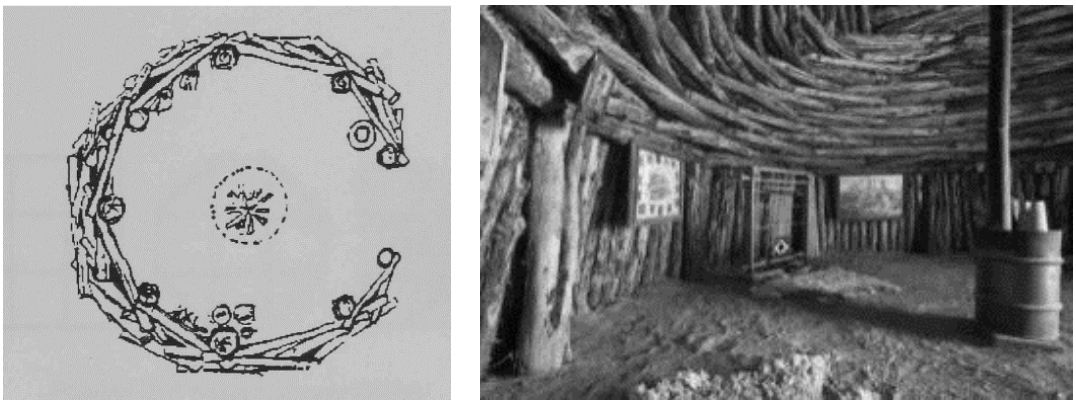

Figure 2.9. Hogan dwelling.
(Source: Popovic, 1996)

A bridge over the Rhine (Figure 2.10) built during the Roman Empire by Julius Caesar is another example of the early use of RF. It consists of interlocked timber beams, and the reason for using RF is to have simple connections for fast constructability (Gustafsson, 2016).

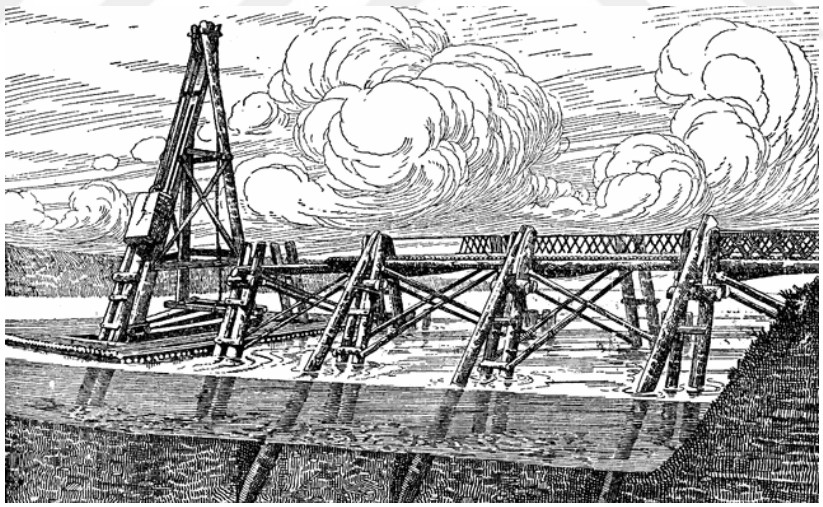

Figure 2.10 Bridge over the Rhine.
(Source: Clip Art ETC, n.d.)

There are two inspirational concepts in Asia for using RFs: structural concept inspired by bamboo baskets with interwoven strips and religious concept inspired by mandala. Wood construction procedures developed in China between the 9th and 12th

centuries include construction methods inspired by bamboo baskets with interwoven strips. At Rainbow Bridge in Shandong (Figure 2.11), it is seen that the beam series are constructed according to the reciprocal support scheme (di Carlo, 2008).

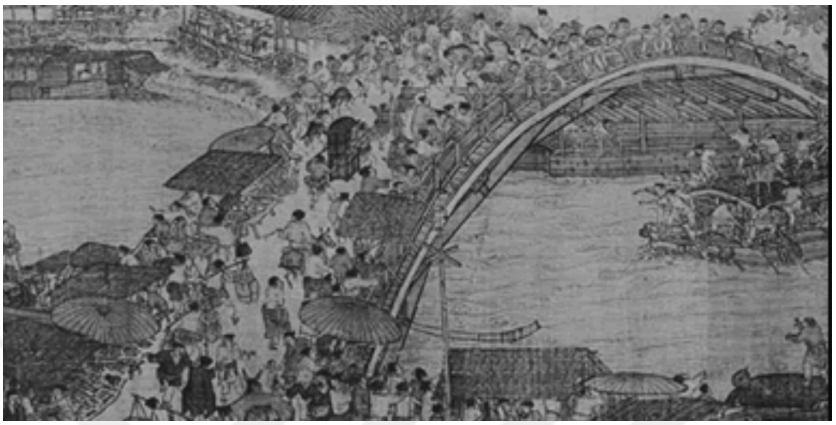

Figure 2.11 Rainbow bridge in Shandong.
(Source: Karakoç, 2017)

In the second half of the 12th century, shrines and temples were built according to the technique that a Buddhist monk Chogen established: a spiral layering of wooden beams. Even though no built examples remain, the technique used by Chogen is the same with the RFs. The geometric form used in these temples resembles the religious concept of the mandala, which is used as a symbol of divinities in Buddhist mediations. Since the forms of the temple plans are analogous to the mandala, 'mandala dach' (mandala roof) is used instead of RF as a term in Germany. The mandala is a pattern composed of circles and squares and is one of the oldest religious symbols (Figure 2.12). They can be seen on the ceilings as paintings in religious buildings (Popovic Larsen, 2007).

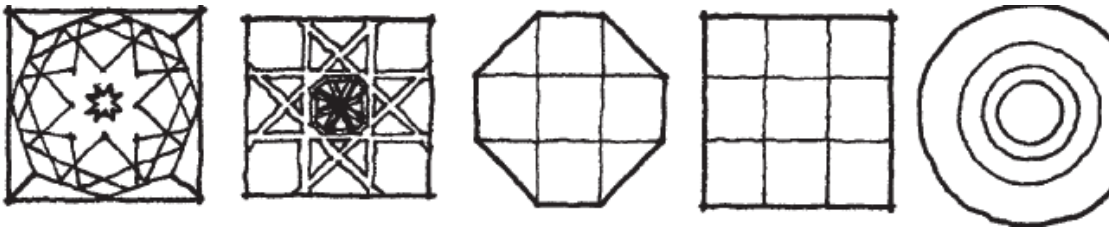

Figure 2.12 Mandala geometry.
(Source: Popovic Larsen, 2007)

In medieval times, the floors of most buildings are constructed from timber in Europe. While small size buildings like houses or farm buildings are built with timber, larger buildings like churches or palaces are built with stone. In both situations, timber is used as a flooring material to span between walls or create levels. As larger buildings are constructed, the need for timber increases in longer lengths to span greater distances. At this point, the beam grillage system becomes a solution for spanning longer distances with available beams. This beam grillage system is similar to the RF's working procedure (Popovic Larsen, 2007). Figure 2.13a shows a four-beam-supported medieval floor, mostly used to frame stairwells (Chilton, Choo, and Yu, 1994). In the first half of the 13th century in Europe, Villard de Honnecourt, the medieval architect, describes a joisting installation method in his book for flooring construction (Figure 2.13b). Villard de Honnecourt explains his method as "the construction of a house or a tower if the wooden beams are too short" (Popovic Larsen, 2007).

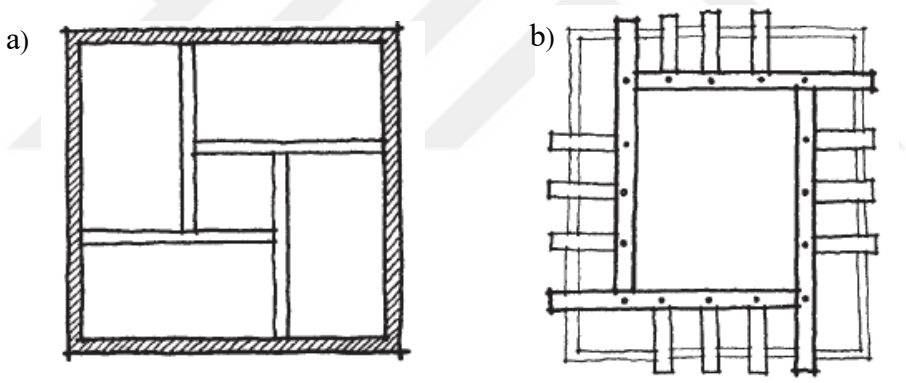

Figure 2.13. a) Medieval floor grillage assembly, b) Planar grillage assembly by Honnecourt (Source: Popovic Larsen, 2007).

Another building with an RF system was the roof of the chapter house of Lincoln Cathedral, which was designed and built between 1220 and 1235 by Alexander (Figure 2.14). The principle of reciprocity is used in the regular decagon-based pyramidal roof of the building. The ten-sided polygonal planned roof is composed of two parts. The lower part forms the planar reciprocal system, and the upper part forms the pyramid (Hewett, 1974).

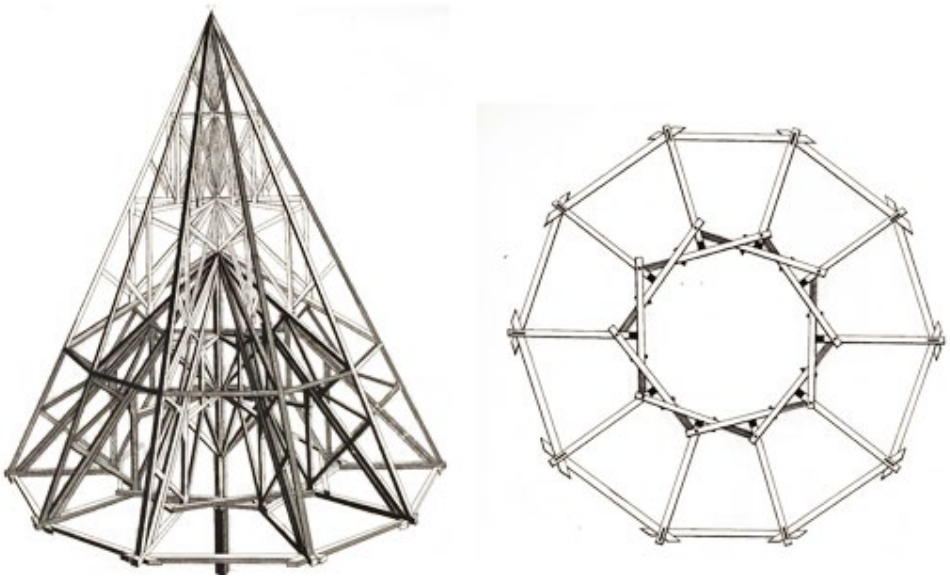

Figure 2.14. Roof of the association building of Lincoln Cathedral.
(Source: Hewett, 1974)

According to Pizzigoni, Brunelleschi uses a construction method similar to RF in the dome of Florence's Cathedral, La Basilica di Santa Maria del Fiore. The row of bricks that make up the vault is designed to carry each other. The procedure that is used belongs to Brunelleschi and involves the formation of a layered spiral pattern with bricks called herringbone (Figure 2.15) (Pizzigoni, 2015). The Herringbone is an example of chirality.

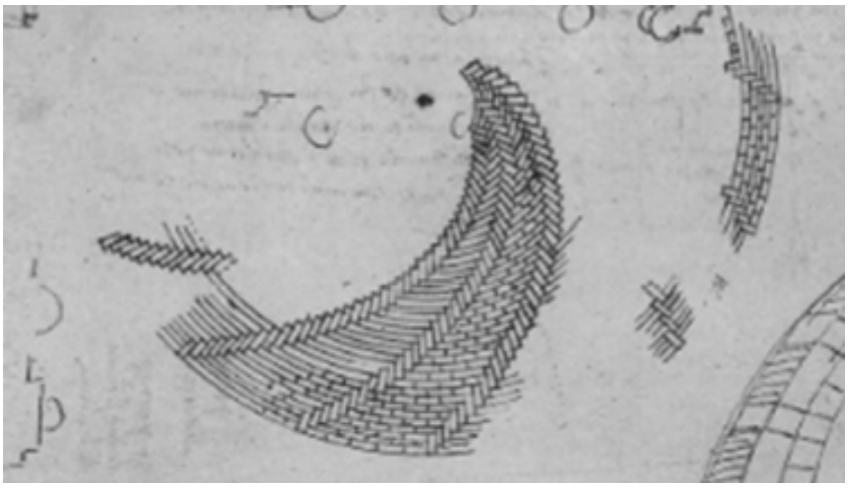

Figure 2.15. Herringbone.
(Source: Pizzigoni, 2015)

Later in the 16th century Leonardo da Vinci, who set the foundation for a scientific study of RFs, discovered various two- and three-dimensional RF structures. The planar grillage of four beams sketched in Codex Madrid is similar to the main grillage system that Honnecourt suggested (Figure 2.16) (Popovic, 1996).

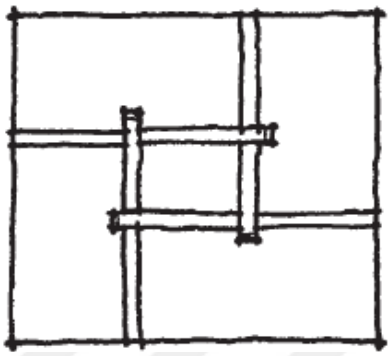

Figure 2.16. Flat beam grillage by Leonarda da Vinci.
(Source: Popovic Larsen, 2007)

He also has sketches for beam grillage assemblies in Codex Atlantico for passing spans with regular and irregular geometric constructs (Figure 2.17) (Popovic, 1996).

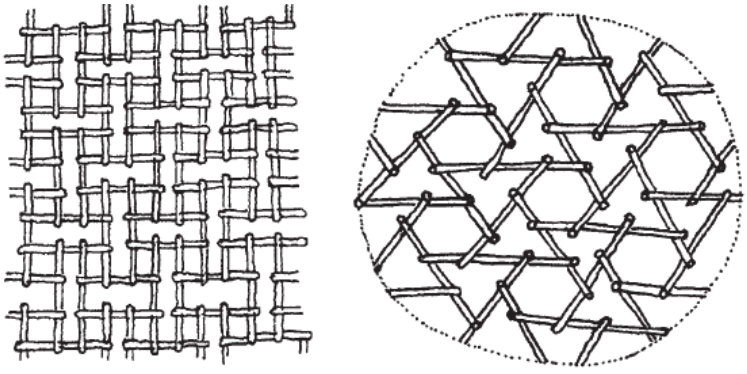

Figure 2.17. Sketches of grillage assemblies by Leonardo da Vinci.
(Source: Popovic Larsen, 2007)

He illustrates the three-dimensional arch structures for domes and bridges (Figure 2.18) (Rizzuto, Saidani, and Chilton, 2002). Each of these beams is supported by one another. The bridge designs of Da Vinci are not chiral since symmetric RF fans are used.

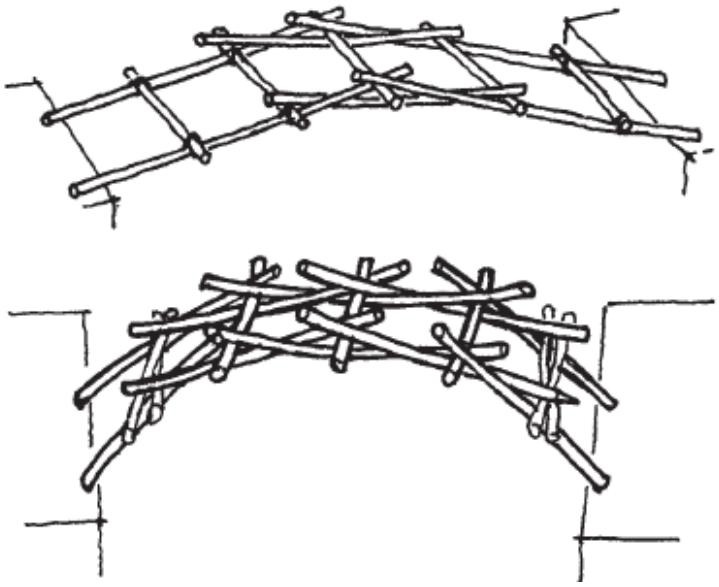

Figure 2.18 Bridge designs by Leonardo da Vinci.
(Source: Popovic Larsen, 2007)

The German engineer Feirdrich Zollinger (1880-1945) developed the lamella dome system using short wooden elements due to its ease and fast construction (Figure 2.19). Short wooden elements do not join at a single point; instead, they form an RF. The system was developed after the first world war because it was fast and cheap to meet the housing need. Later, Pier Luigi Nervi designed the Orvieto hangar structure with a lamella dome, but it was demolished in World War II (Figure 2.20). Moreover, the Copenhagen School of Architecture's canteen was constructed from a steel lamella dome (Figure 2.21) (Popovic Larsen, 2014).

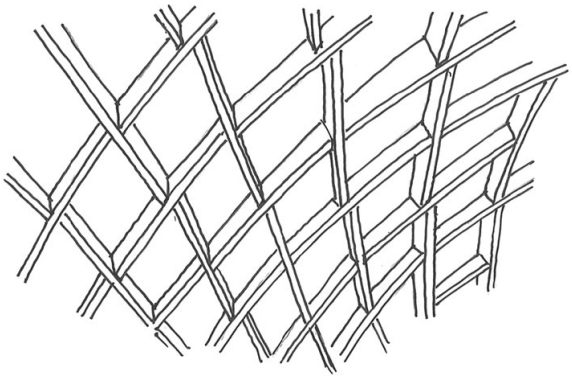

Figure 2.19. Zollinger lamella structure.
(Source: Popovic Larsen, 2014)

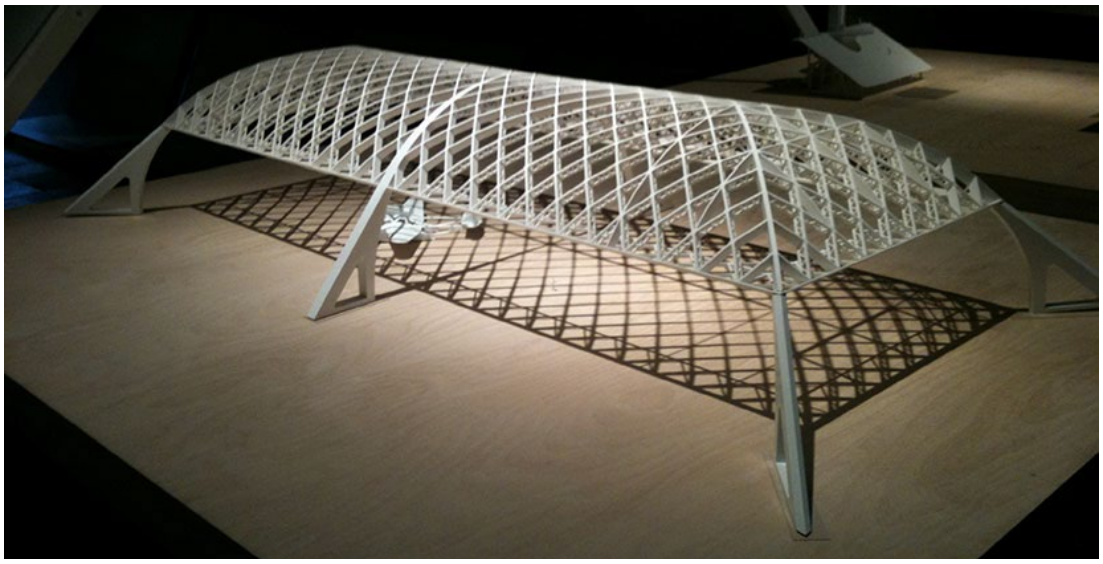

Figure 2.20. The Orvietro hangar's physical model by Pier Luigi Nervi.
(Source: Popovic Larsen, 2014)

Figure 2.21. Copenhagen School of Architecture canteen from steel lamella structure.
(Source: Popovic Larsen, 2014)

A pedestrian bridge in Rio de Janerio from bamboos is similar to the Leonardo da Vinci bridge (Figure 2.22) (Popovic Larsen, 2007).

Figure 2.22. Pedestrian RF bridge.
(Source: Popovic Larsen, 2007)

Similarly, a solution to the question of building planar ceilings and roofs larger than the beams available appeared in Sebastiano Serlio's book dated 1556. The grillage is similar to Honnecourt's flooring construction (Figure 2.23) (Baverel, 2000).

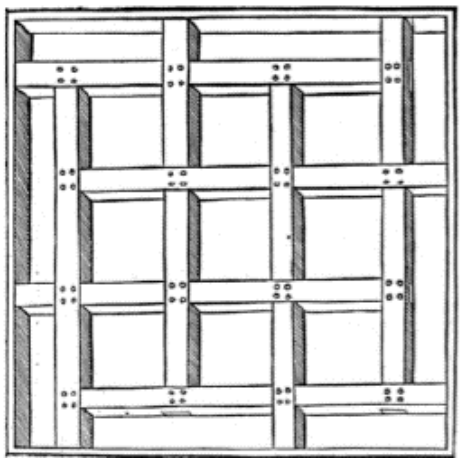

Figure 2.23. Serlio's solution for building planar ceilings and roofs.
(Source: Baverel, 2000)

John Wallis, another European mathematician who studied the RFs, described planar assemblies' geometry and studied their structural behavior in his Opera Mathematica (Figure 2.24) (Houlsby, 2014).

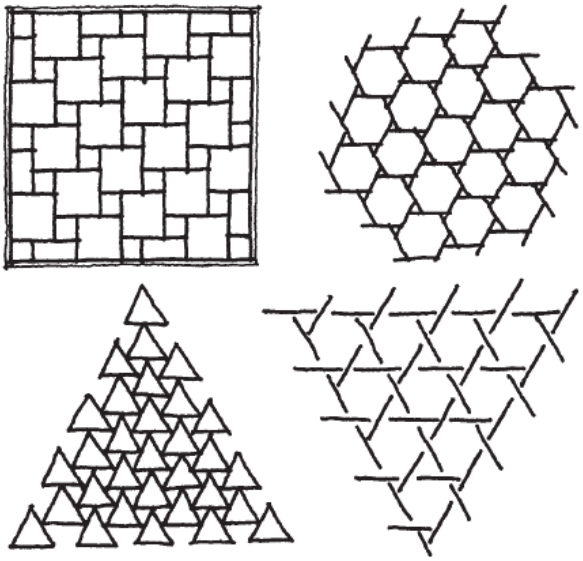

Figure 2.24. Planar morphology of grillage structures.
(Source: Popovic Larsen, 2007)

A. R. Emy, a professor of Fortification at the Royal Military School Saint-Cyr, explained a grid floor in his treatise about Carpentry very similar to RFs (Figure 2.25) (Pugnale et al., 2011).

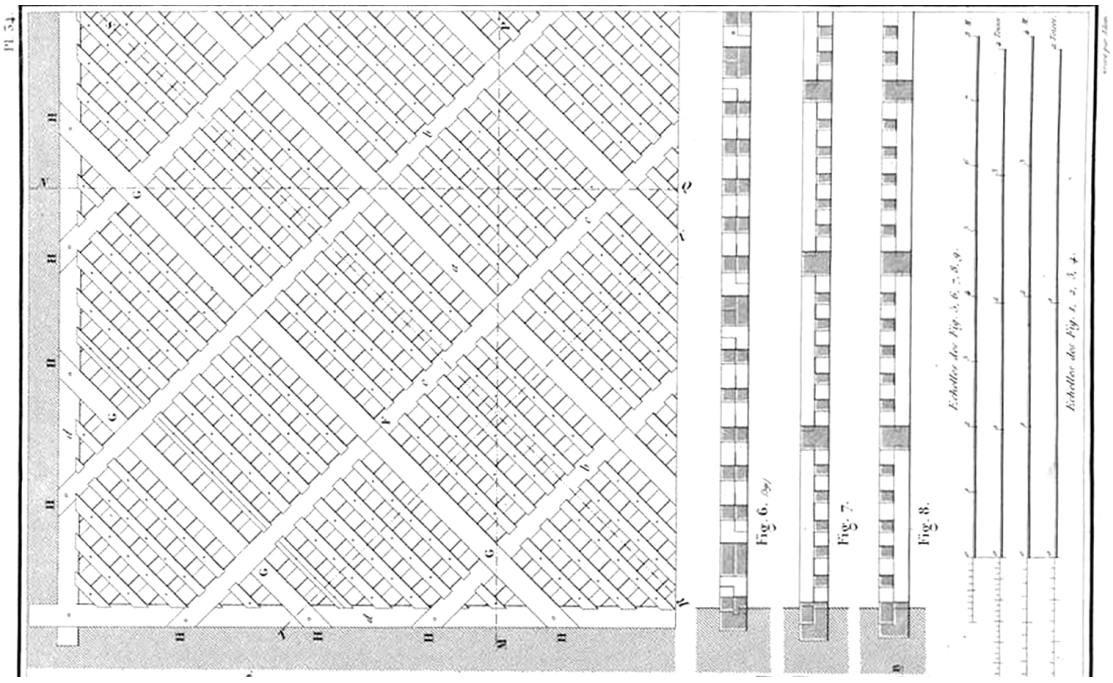

Figure 2.25. Flooring Emy suggested in his treatise.
(Source: Roberti et al., 2021)

In the 19th and 20th centuries, some designers also used RFs in their designs. Architect Jose Maria Jujol designed the Casa Negre (1915) (Figure 2.26a) and Casa Bofarul (1913-1918) (Figure 2.26b). The roofs of these projects are 3d grillage structures that support each other and rise spirally (Popovic, 1996).

Figure 2.26. a) Casa Negre roof. (Source: Pugnale and Sassone, 2014), b) Case Bofarul roof (Source: Bautista, n.d.).

In 1952-1953, architect Louis Kahn used a four-beam planar grillage in a multi-story building to design the Mill Creek social housing project in Philadelphia (Figure 2.27a). The main advantage of using planar beams in this housing project is to prevent the columns in the plan and thus facilitate spatial organization. In the project, the 15-meter span is crossed with medieval quadratic planar beams (Popovic Larsen, 2007).

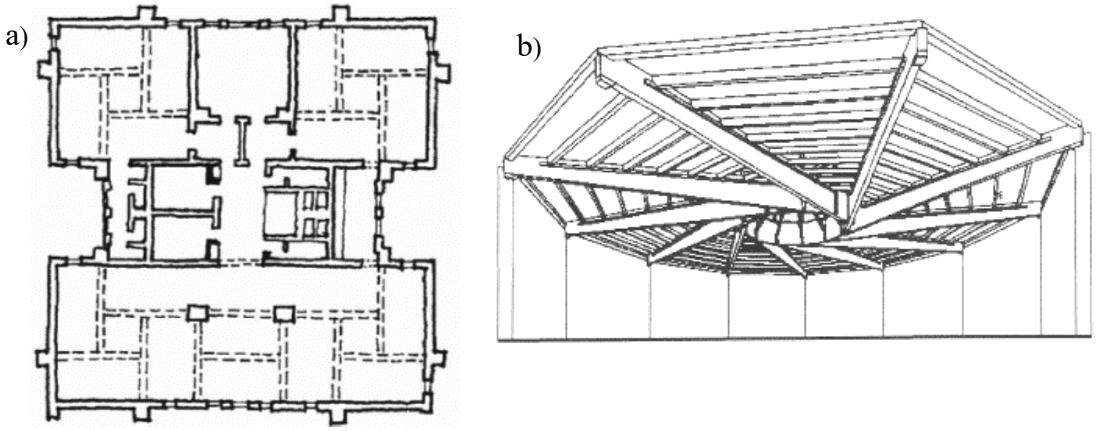

Figure 2.27. a) The Mill Creek social housing project, b) Salt storage building in Lausanne in Switzerland (Source: Popovic Larsen, 2007).

Another RF example is the roof of a salt storage building in Lausanne designed by Atelier Gamme Architecture in 1989 (Figure 2.27b). The regular polygonal plan of this building is covered with eleven glulam beams that span 26 meters (Rizzuto, Saidani, and Chilton, 2000).

Palazzo Piccolomini in Pienza has a ceiling with RF timber beams in the music room. The room is one of the smallest rooms, with short beams spanning the distance (Figure 2.28) (Pugnale and Sassone, 2014).

Figure 2.28. Ceiling of the music room in Palazzo Piccolomini.
(Source: Pugnale and Sassone, 2014)

Chilton (2009) reports that Graham Brown designed the Whisky Barrel and Ferryhill homes' roof structures as RFs (Figure 2.29). Whisky Barrel house has seven beams RF, which form a heptagonal roof window at the center of the roof. House at Ferryhill has ten beams RF, which creates a decahedral form at the center of the roof (Chilton, 2009).

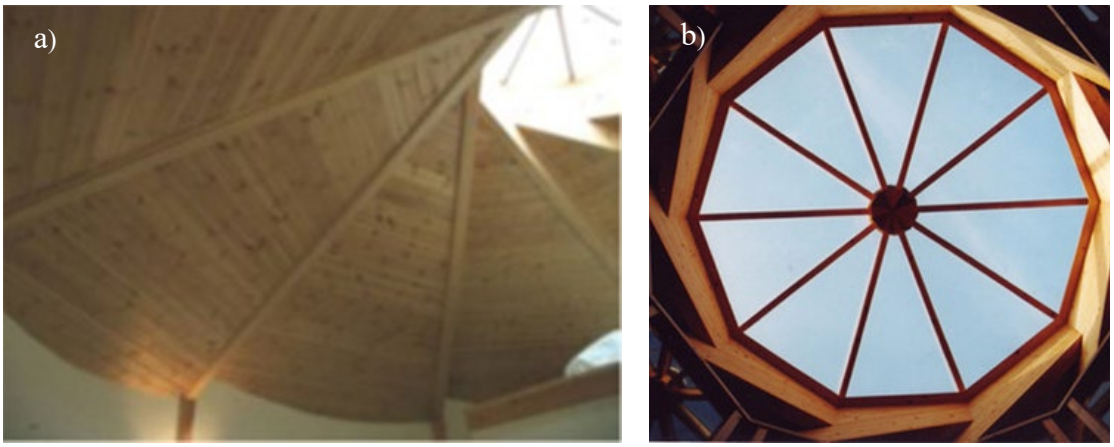

Figure 2.29. a) Whisky Barrel House, b) House at Ferryhill.
(Source: Chilton, 2009)

RFs are used as a roof in the buildings of Seiwa Bunraku Puppet Theater and Sukiya Yu House, designed by Kazuhiro Ishii (Figure 2.30). The Seiwa Bunraku Puppet Theater exhibition hall, which was completed in 1992, is 13 meters high and 7 meters wide. In the theater's auditorium, a planar beam was designed to form a suspended ceiling, and the used grillage system is quite heavy to give the feeling of sadness in the performed plays. The beams are one meter in height; and one end is supported by another beam, and one end supports the other with the use of a steel anchor (Popovic Larsen, 2009).

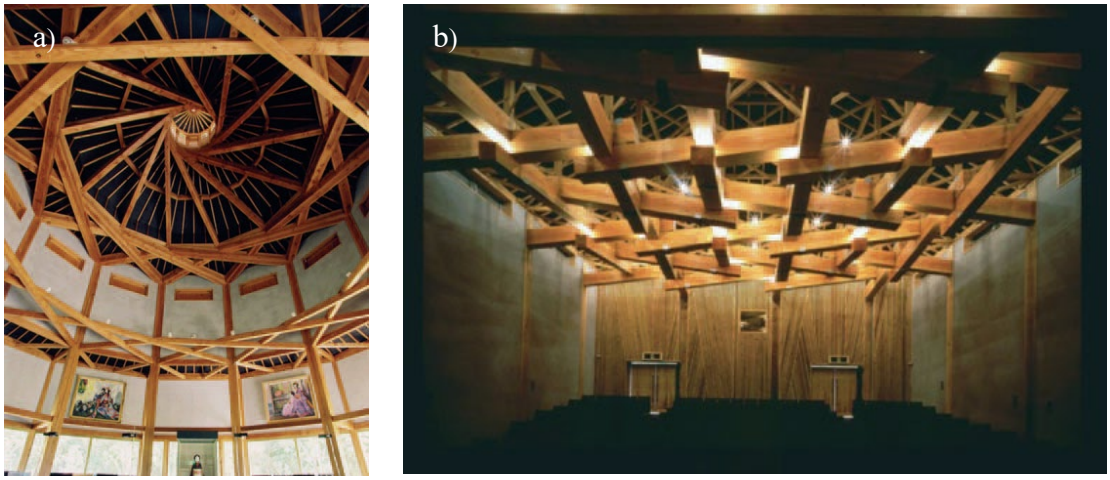

Figure 2.30. a) The exhibition hall of the Seiwa Bunraku Puppet Theater, b) The auditorium at Puppet Theatre (Source: Popovic Larsen, 2007 and Popovic Larsen, 2009).

The 7-meter-diameter wooden geodesic dome covering the Yu-an guest house of the Sukiya House, built in 1990, was supported by a reciprocal beam system (Figure 2.31) (Popovic Larsen, 2007).

Figure 2.31. Wooden geodesic dome of Sukiya Yu.
(Source: Popovic Larsen, 2007)

Yasufumi Kijima designed Toyoson Stonemason Museum in 1993 using multiple RFs (Figure 2.32a). The building has three cylindrical volumes: an exhibition building, a multipurpose hall with conical roofs, and an administration building with a flat roof. The combination of triangular and hexagonal units constituted the roof of the apex, a hexagonal RF unit. Multiple RFs cause the in-between units to become four-sided regular polygons. (Popovic Larsen, 2007).

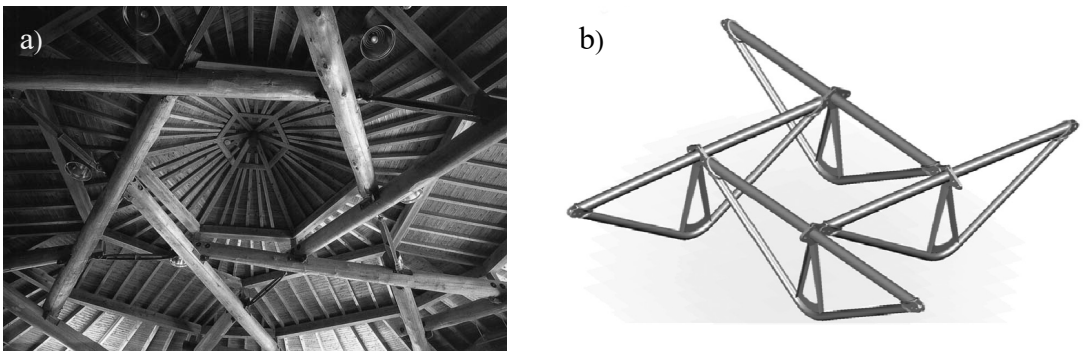

Figure 2.32. a) Toyoson Stonemason Museum (Source: Popovic Larsen, 2007), b) Principle of a nexorade that is used in the archeological site (Source: Gelez, Aubry, and Vaudeville, 2011)

In 2008, a shelter that covers an archeological excavation site was designed by architect Paul Andreu and engineers Bernard Vaudeville and Simon Aubry from aluminum in Bibracte, France (Figure 2.32b and Figure 2.33). The reason for the choice of aluminum is to have a light structure. The RF is covered with PVC fabric for weather protection (Gelez, Aubry, and Vaudeville, 2011).

Figure 2.33. View of the shelter from the south.
(Source: Gelez, Aubry, and Vaudeville, 2011)

In 2010, Hiroshi Ambuichi and Arup designed an RF for the Mount Rokko-Shidare Observatory (Figure 2.34). In the structure, 50 mm welded steel tubes are formed by hexagons and triangles, and the engagement windows are covered with other 15-20 mm thick wooden beams (Popovic Larsen, 2014).

Figure 2.34. Mount Rokko-Shidare Observatory.
(Source: Popovic Larsen, 2014)

Furthermore, a set of experimental works related to structural, geometrical, and constructive issues of RFs are appearing. Forest Park structure, Kreod pavilion, a pavilion in Palestine, and Coca Cola pavilion are some of the examples of experimental works. In those pavilions, the reciprocal principle has been explored by using different materials, element sections, joints, and planar or spatial configurations.

In 2002, Shigeru Ban and Cecil Balmond designed a fluctuating eave of intertwined bamboo boards spanning an area of about 11x11 meters for the Rice University campus. The Shigeru-Ban Architects states that the bamboo eaves of Rice University are working as a prototype for the larger-scale and permanent project of the Forest Park, St Louis Pavilion (Figure 2.35) (Shigeru Ban Architects, 2002).

Figure 2.35 Forest Park pavilion.
(Source: Shigeru Ban Architects, 2002)

Pavilion Architecture designed Kreod Pavilion for the London Olympic Games in 2014. In the structure, an RF design consisting of hexagons and triangles forms an inclined surface (Figure 2.36) (Popovic Larsen, 2014).

Figure 2.36. Kreod Pavilion.
(Source: Furuto, 2012)

In Palestine Jericho, the pavilion was designed by AAU Anastas from stone. Beams were cut to form curved surfaces and created a self-standing structure that came together according to a four-way RF (Figure 2.37) (Karakoç, 2017).

Figure 2.37. Pavilion in Palestine Jericho.
(Source: Griffiths, 2017)

AKT II designed the Coca-Cola Beatbox pavilion for London's 2012 Summer Olympic and Paralympic Games (Figure 2.38). 230 red and white translucent synthetic cushions are developed. 40 cushions out of 230 are sound-emitting and touch-sensitive to have an interactive façade. For a self-supporting 3d structure, the cushions are weaved together reciprocally (AKT II, 2012).

Figure 2.38. Coca Cola pavilion.
(Source: Anastas, Rhode-Barbarigos, and Adriaenssens, 2016)

Pizzigoni has designed an RF using precast concrete elements as a proposal for the Italian Pavilion at the Shanghai 2010 World's Fair (Figure 2.39). The real-scale model is made of high-resistance reinforced fiber concrete in suitable dimensions and weights to allow construction and dismantling. Mirrored S-shaped elements were designed due to the need to reduce notches in overlapping beams which weaken the elements (Pizzigoni, 2009).

Figure 2.39. RF design by Pizzigoni.
(Source: Pizzigoni, 2009)

Pantazis and Gerber designed a pergola in 2014. A module consists of two elements and questions the possibilities of materials and modules beyond traditional examples. In the developed module, curved panels carry each other instead of linear elements (Figure 2.40). The aim is to improve the structural performance and create a

three-dimensional hollow shell for a shaded environment. There is a notched connection system between these elements, which comes together with special angles. Twisted plywood was preferred as the material (Pantazis and Gerber, 2014).

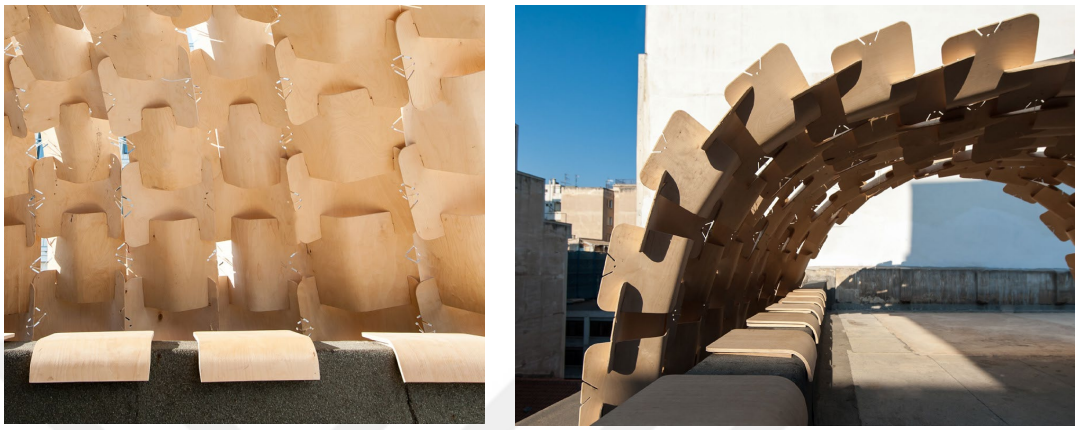

Figure 2.40. The pergola Pantazis and Gerber developed.
(Source: Pantazis and Gerber, 2014)

DigDesFab15 Research Pavilion is designed for practicing the applicability of timber and polymer concrete (Figure 2.41). Three-layer timber panels are temporarily fixed in the pavilion and then stiffened with polymer concrete. The pavilion was designed by the students and the instructors at the Digital Design and Full-Scale Fabrication seminar held at the University of Applied Arts Vienna (Gheorghe and Vierlinger, 2017).

Figure 2.41. DigDesFab15 Research Pavilion.
(Gheorghe and Vierlinger, 2017)

2.3. Review of the Previous Work

The principle of reciprocity draws the interest of designers and researchers, and it has become a topic for scientific research. The first patent was taken for lamella dome by Zollinger mentioned before. Then, Emilio Perez Pinero (1965) developed a foldable structure based on the mutually supporting beams (Figure 2.42a) (Pugnale and Sassone, 2014).

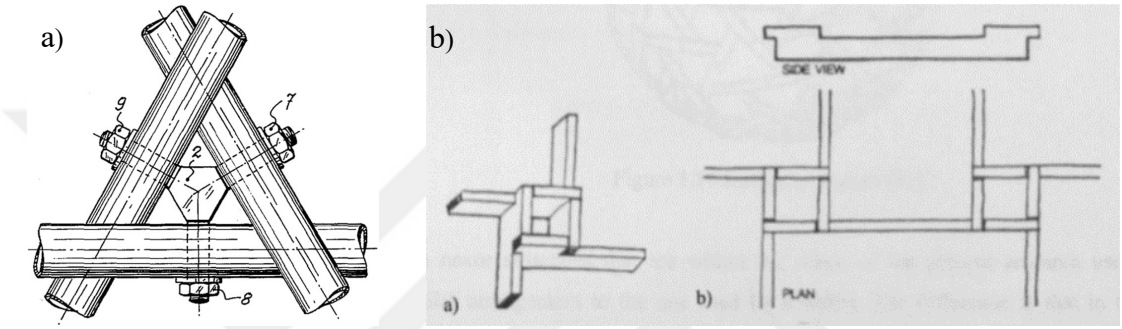

Figure 2.42. a) Emilio Perez Pinero's patent (Source: Pugnale and Sassone, 2014), b) Gat's system (Source: Baverel, 2000).

Daniel Gat patented a self-supporting system in 1978 (Figure 2.42b). The system that he called SIGMA (Self-supporting Interlocking Grids for Multiple Applications) was described as pre-uniform prefabricated structural elements that did not require qualified workmanship and could be standardized for use in roof and floor beams. It was very similar to the John Wallis system, but the difference was that Gat used a unique wedge spacer to create a slope between elements to have a 3d form (Baverel, 2000).

The RF was patented by Graham Brown in the UK in 1989 under 'Three Dimensional Structures' to explain the grillage structure in which the bars mutually support each other (Figure 2.43a) (Chilton and Choo, 1992).

Another system created in 1992 by Simple Science Toys based in Eugene was The Rotegrity system which was a continuation of John Wallis's arrangements. But in this system, interwoven bent elements were used (Figure 2.43b) (Baverel, 2000).

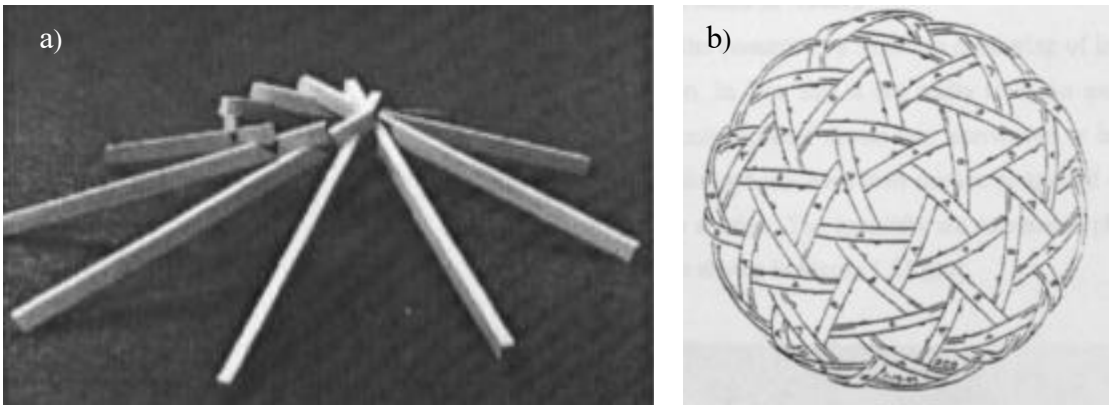

Figure 2.43. a) Graham Brown's system, b) Rotegrity system.
(Source: Baverel, 2000)

In terms of geometric properties, Chilton and Choo (1992) were the first using, defining, and describing RF in a scientific paper and specify the principles of RF. Chilton and Choo (1992) explained the main parameters of the static RFs as follows (Figure 2.44) (Chilton and Choo, 1992):

n – the number of nexors

r_0 – outer radius

r_i- inner radius

H- vertical rise between the outer supports and nexor intersection points

h_2- vertical spacing between nexor centerlines

L_n- nexor length

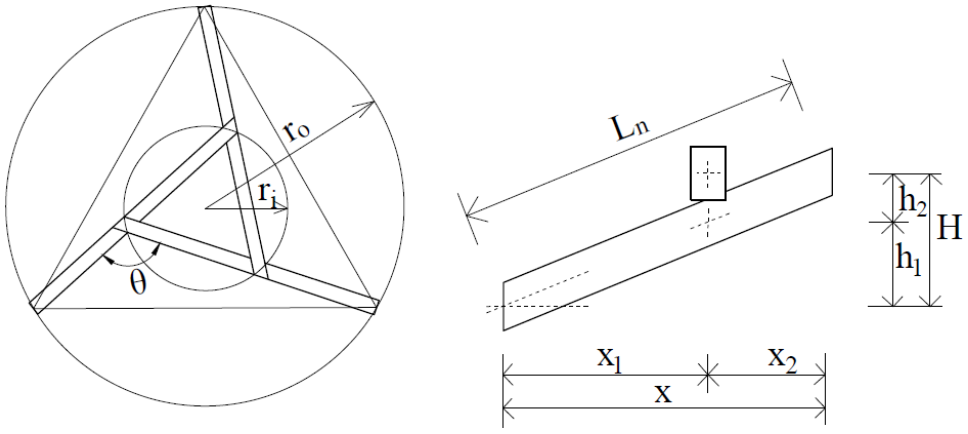

Figure 2.44. Geometrical parameters that define a fan.
(Source: Larsen, 1996)

Chilton and Choo (1992) have presented the parameters that define the geometry of a static RF and their relation to each other by having rectangular cross-sectioned nexors by using basic trigonometry (Chilton and Choo, 1992).

Olga Popovic Larsen was the first who study architectural and practical aspects of RFs in a Ph.D. thesis in 1996 in consultation with John Chilton. She focused on the history of RF, architectural and structural applications, and geometrical considerations. Popovic (1996) reports that Chilton and Choo (1992) have presented the parameters that define the geometry of a static RF and their relation to each other by having rectangular cross-sectioned nexors, and they can be determined by the following equations using basic trigonometry (Figure 2.45) (Popovic, 1996):

$$\theta = \frac{360}{n}$$

$$x_2 = 2r_i \sin\frac{\theta}{2}$$

$$x_1 = \left[r_0^2 - \left(r_i \cos\frac{\theta}{2}\right)^2\right]^{\frac{1}{2}} - \frac{x_2}{2}$$

$$x = x_1 + x_2$$

$$h_1 = H\frac{x_1}{x}$$

$$h_2 = H - h_1$$

$$L_n = (x^2 + H^2)^{\frac{1}{2}}$$

Figure 2.45. Trigonometric equations.
(Source: Popovic, 1996)

Popovic (1996) used the same parameters with the static RFs to find the retractable RF geometry. She analyzed the relationship between ratio h_2/H and number of beams; ratio L_n/r_o and the number of beams; and horizontal angle (angle between nexors) and vertical angle (slope) (Figure 2.46) (Popovic, 1996).

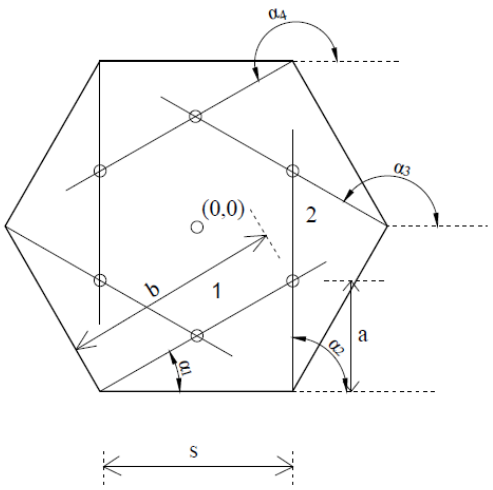

$$\alpha_2 = \alpha_1 + \frac{360}{n}$$

$$a = \frac{s}{\left[\left(\frac{\cos\alpha_1 \sin\alpha_2}{\sin\alpha_1}\right) - \cos\alpha_2\right]}$$

$$b = a\frac{\sin\alpha_2}{\sin\alpha_1}$$

$$\beta = \sin^{-1}\left(\frac{d}{b-a}\right)$$ (β is beam slope angle)

Figure 2.46. Plan geometry of a retractable RF and trigonometric equations.
(Source: Larsen, 1996)

Chilton, Choo, and Wilkinson (1998) analyzed the relationship between nexor length (L_n) and angle between nexors (θ); engagement length (λ) and angle θ; ratio λ / L_n and angle θ; inner radius and angle θ for planar RFs and ratio λ / L_n and height for three-dimensional RFs with the different number of beams (Figure 2.47) (Chilton, Choo, and Wilkinson, 1998)

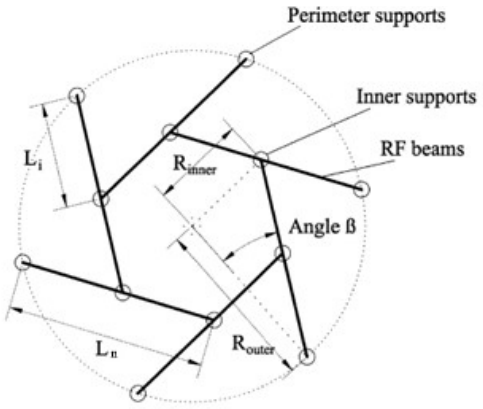

Figure 2.47. Plan of an RF.
(Source: Chilton, Choo, and Wilkinson, 1998)

Oliver Baverel's Ph.D. thesis was a major step in providing an identification of RFs in the modern age. He founded Multi Reciprocal Grid (MRG) which several RFs came together at the outer end of each member to create Multi-Reciprocal Grid (MRG)

structures. The concept in MRG was to generate a structure using grids instead of adding a few members. Baverel (2000) defined the main parameters that create an elementary configuration different than Chilton and Choo (1992) as follows (Baverel, 2000):

λ, engagement length

L_n, nexor length

D, the diameter of a nexor

α, the angle between nexors

Three-dimensional static MRGs are studied using analytic geometry and later genetic algorithm in Baverel's thesis. In the study, analytic geometry is used for the RFs based on regular and semi-regular polyhedra, and genetic algorithm is used to create a wide range of configurations of RF. There are three ways to transform an initial elementary configuration into a nexorade: translation, rotation, and extended translation. The genetic algorithm method is used to transform an elementary configuration without eccentricity and engagement length into a nexorade (Baverel, 2000).

Baverel and Douthe (2009) suggested the Dynamic Relaxation Method, which converts corners of the polyhedrons into regular polygons to have nexorades. After generating the fans from regular polygons, beams are bent to be linked with the adjacent beam with the appropriate engagement length, style, and end disposition (Douthe and Baverel, 2009).

Figure 2.48. Transformation of a frame made of three beams using the dynamic relaxation method (Source: Douthe and Baverel, 2009)

The RFs can, in theory, be produced from all basic building materials such as wood, steel, and reinforced concrete. Bertin created a model that is a 10-meter dome from bamboo. 1,5 m long and 4 cm diameter bamboo sticks were used. The dome shown in Figure 2.49 consists of triangles and hexagons and is connected by plastic clamps to increase friction between the elements (Popovic Larsen, 2007).

Figure 2.49. Bertin's dome model.
(Source: Popovic Larsen, 2007)

In the 20th century, it was possible to see that steel and precast concrete elements were also used in RFs. Garavaglia examined the collapse behavior of Pizzigoni's S-shaped 3-nexor RF fan made of fiber-reinforced concrete (Figure 2.50) (Garavaglia et al., 2013).

Figure 2.50. S-shaped 3-nexor RF fan.
(Source: Garavaglia et al., 2013)

Godthelp developed a computational design to production tool to obtain vaulted timber RFs by optimizing connection typology in his master thesis. The parametric models are made in 'The Timber Reciprocal Frame Designer' (RFD) (the tool he proposed) in Figure 2.51 (Godthelp, 2019).

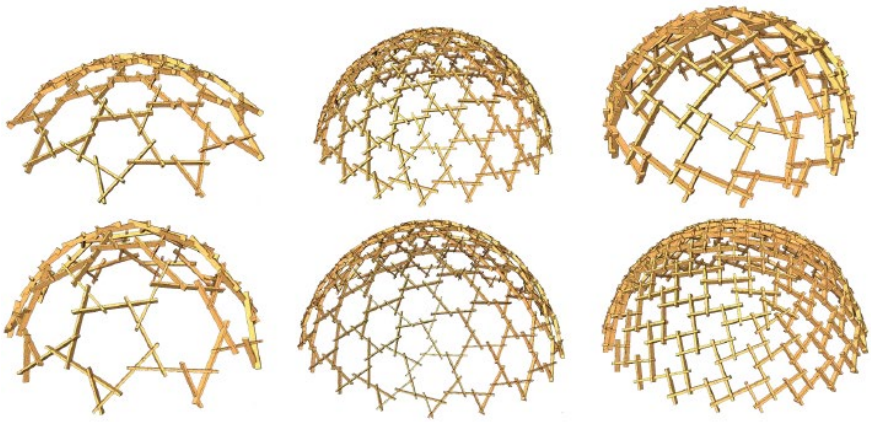

Figure 2.51 RF design developed in RFD.
(Source: Godthelp, 2019)

In terms of joints, Joel Gustafsson studied connections in timber RFs in his thesis. He investigated the effects of connection types in RFs regarding production, assembly, disassembly, appearance, and structural behavior. He especially emphasizes the notched and superposition connection types (Gustafsson, 2016).

Rizzuto considered various connection types in RFs. Bolted 3-nexor fans were analyzed to get information about the risk of yielding. According to the study, it has been found that the use of notches weakens the structure due to the subtraction of the cross-section of bars (Rizzuto and Popovic Larsen, 2010).

Puyol studied the notched linear plywood plate elements manufactured by six-axis robots. He explores how free-form structures are fabricated and assembled following an RF pattern by algorithmically designing their segmentation into mass-customized planar members (Figure 2.52) (Puyol, 2015).

Figure 2.52 Framework built with rectangular boards.
(Source: Puyol, 2015)

Perez-Valcarcel et al. (2021) investigated deployable structures' geometrical and kinematic viability with reciprocal linkages. 4-nexor RF was analyzed, and four nexors were attached to a hollow square prism called a linkage in the study to increase the rigidity. They propose equations to investigate the relationship between the diameter of the nexor and the width of the linkage. Their analysis continues by finding the horizontal plane's angle by knowing the fan's height and span. Then the study focuses on mesh geometry (Figure 2.53a) (Pérez-Valcárcel et al., 2021a). Afterward, they propose a vault composed of reciprocal linkages at the end of the bars (Figure 2.53b) (Pérez-Valcárcel et al., 2021b).

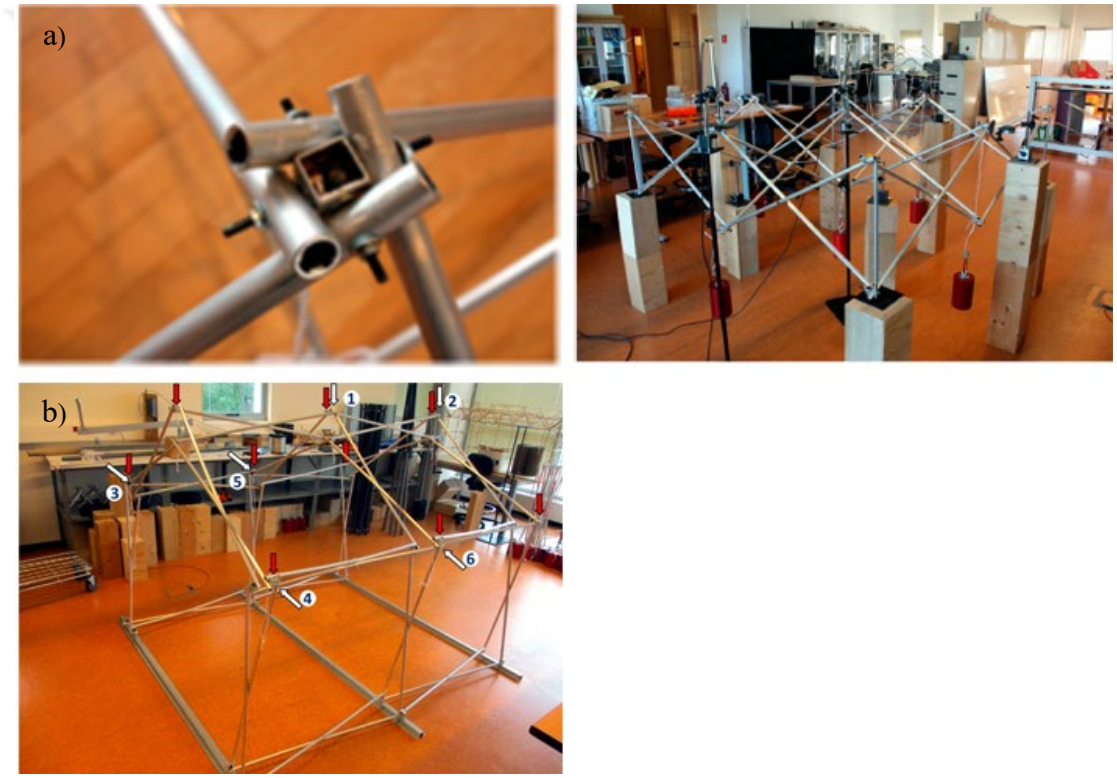

Figure 2.53. a) Reciprocal linkages and deployable structure, b) Vault (Pérez-Valcárcel et al., 2021b).

Joints, the links of which are kept in contact by external forces, are called force-closed. If joints, the links of which are constrained to come into contact with each other through certain geometric are form-closed joints (“IFTooM Dictionaries Online”, n.d.). RFs are force-closed mechanisms in theory (Figure 2.1). However, as seen from the studies in the literature, they become form-closed for practical reasons.

From the parametric studies perspective, Parigi held a workshop with architecture students at Aalborg University about un-notched three-dimensional configurations of RFs in 2014 (Parigi and Pugnale, 2014). Finally, he developed a reciprocalizer, a Grasshopper plugin to design RFs. The plugin has the geometric information that is necessary to create an RF. This tool was developed to predict and control the geometry of large grids (Parigi and Kirkegaard, 2014).

Song et al. developed a computational tool using C++ and OpenGL to design RF over a 3d guiding surface (Figure 2.54). The tool works in three stages. First, the reciprocal grid is defined as two-dimensional with regular polygons. Second, the defined grid is lifted to the 3d guiding surface. And finally, the optimization process guarantees the collinearity of contact joints (Song et al., 2013).

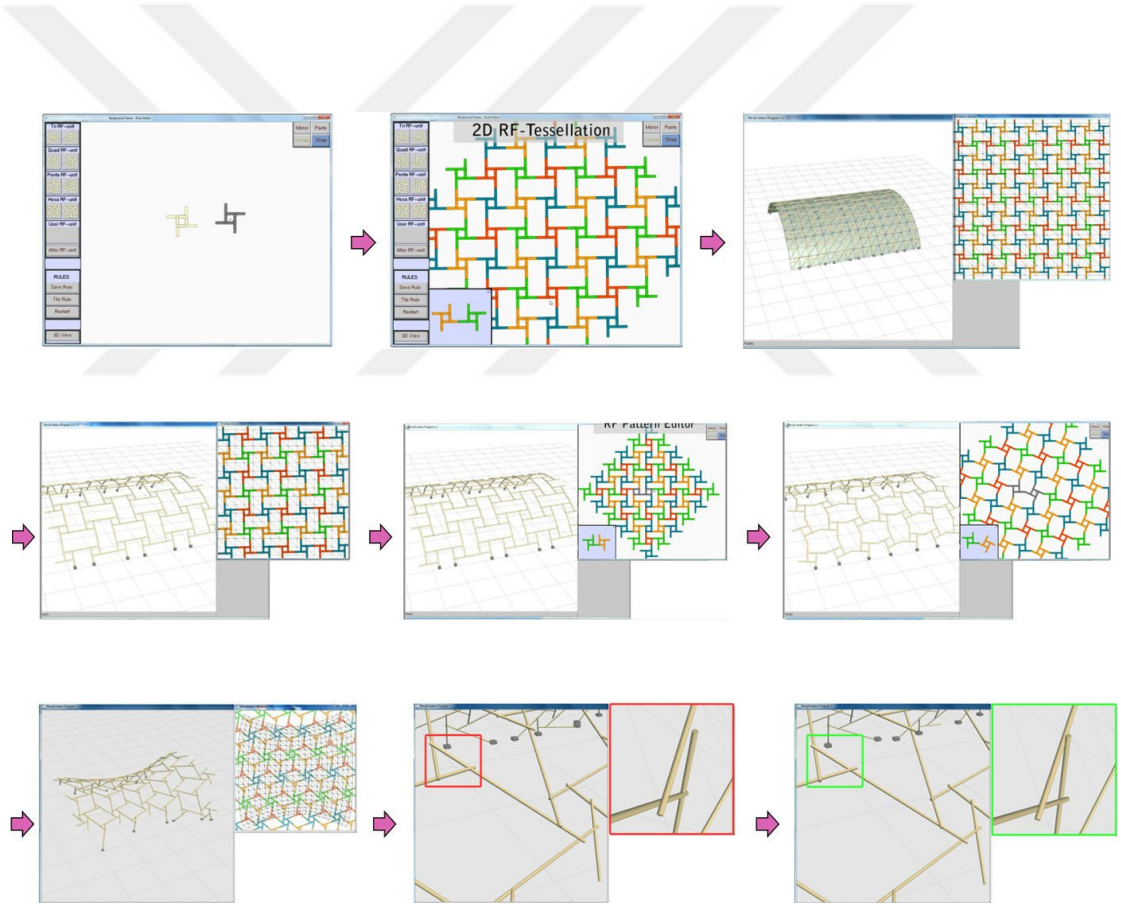

Figure 2.54. Process of using the tool to design a 3d RF.
(Source: Song et al., 2014)

Anastas et al. presented a parametric model for design to construction workflow through the cell-based pattern for RFs (Figure 2.55). A 3d surface is divided into

triangular or rectangular surfaces, and then bars are defined into these cells. After they are all connected, a network is acquired. The researchers also make structural analysis and fabrication processes (Anastas, Rhode-Barbarigos, and Adriaenssens, 2016).

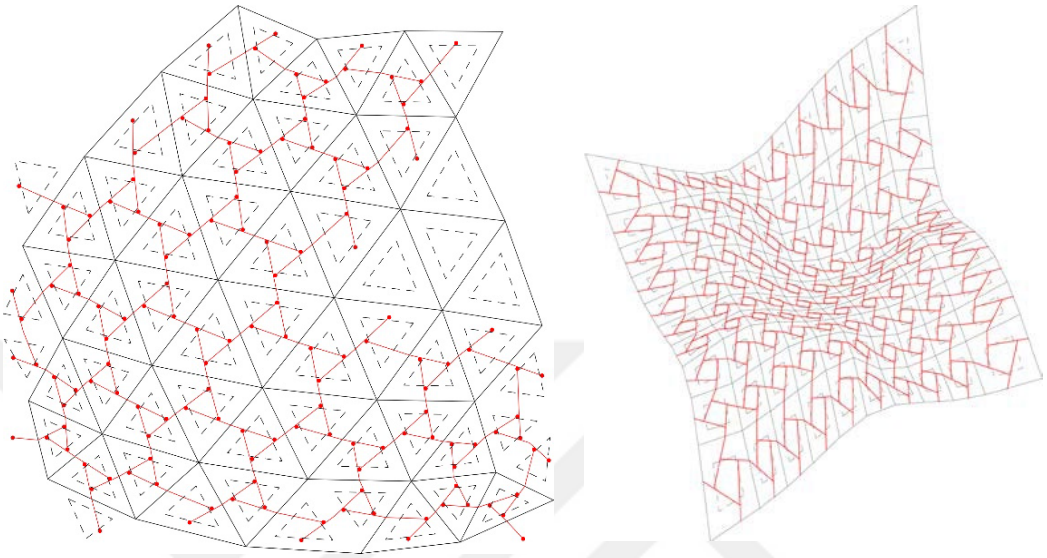

Figure 2.55. Network of RFs on triangular and rectangular surfaces.
(Source: Anastas, Rhode-Barbarigos, and Adriaenssens, 2016)

Furthermore, Arias and Diaz (2019) developed software where users can easily change the variables and get a graphical answer about the designs, transformations, and studies made up of RFs (Arias and Díaz, 2019).

Regarding movable studies, according to Choo et al., sports stadia and long-span multipurpose spaces can be covered with retractable RF roofs. Choo et al. (1994) claimed that a retractable RF roof does not need extensive running rails compared with other structures. During the retraction process, each nexor rotates around its outer support and slides on the supporting nexor. There are two options for the driving mechanism. The first one is the individually synchronized motors which rotate nexors of the roof. The second one is to create an outer ring connecting nexors that is mechanically rotated (Choo, Couliette, and Chilton, 1994).

Larsen (1996) proposed some new equations to understand the geometry of retractable RFs in addition to static RF equations. Moreover, she explained two mechanisms for the retraction research: one of them allows rotation at the hinges but

constrains sliding at the outer support. The other one allows rotation and translation at the outer support (Popovic, 1996).

Saidani and Baverel (1998) described a deployable system from RFs, which consists of a rotation of nodes of the structure. The study is based on 3- and 4-nexor fan networks. While 3-nexor fans are rigid, 4-nexor fans can deploy (Figure 2.56) (Saidani and Baverel, 1998).

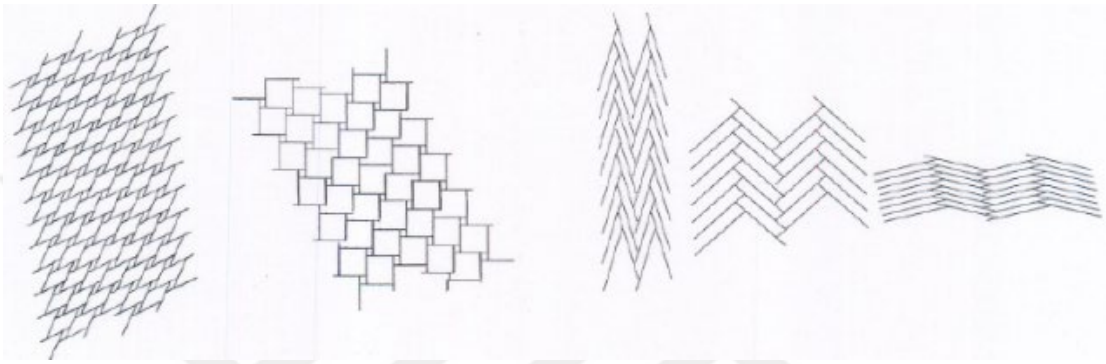

Figure 2.56. Retraction processes.
(Source: Saidani and Baverel, 1998)

Chilton et al. (1998) explored the static and retractable RF geometries and their structural behaviors through parametric analysis. Parametric studies are made in three stages. The first stage was to analyze planar RF. Secondly, the analysis was made with a 3d RF grillage structure to investigate how the structure's height alters with a variable aperture. At the final stage, the load distribution of the planar RF to the supports was examined and forces and moments were calculated involved in the load transfer (Chilton, Choo, and Wilkinson, 1998).

Parigi and Sassone (2010) investigated 4-nexor planar movable RFs having a single degree of freedom with rotational and translational hinges (Figure 2.57) (Parigi and Sassone, 2010). Parigi et al. (2014) proposed a formulation for pinned joint RFs for assessing the static and kinematic behavior of RFs (Parigi et al., 2014).

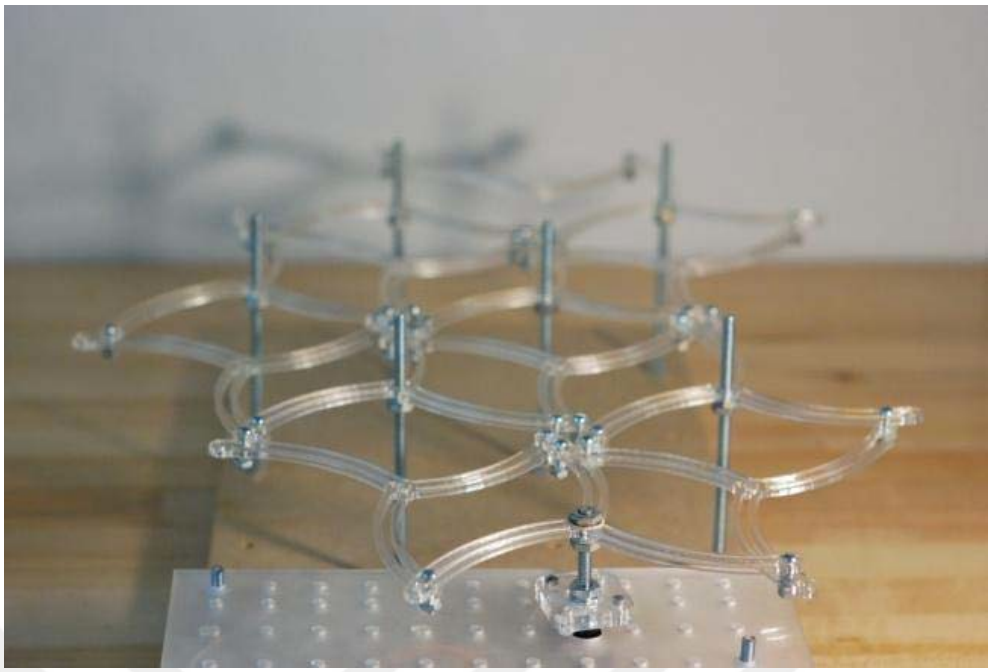

Figure 2.57 Pinned bar assembly made by Parigi and Sassone.
(Source: Parigi and Sassone, 2010)

Popovic Larsen and Sang-Hoon Lee carried out a workshop with students, and they developed some designs for deployable emergency shelters, which are easily and quickly constructed. "arch-type" for Da Vinci's bridge, "plane-type" for Serlio's designs, and "hanging-type" RFs were a starting point. In Figure 2.58, three designs that are offered as a result of the workshop can be seen (Popovic Larsen and Sang-Hoon Lee, 2013).

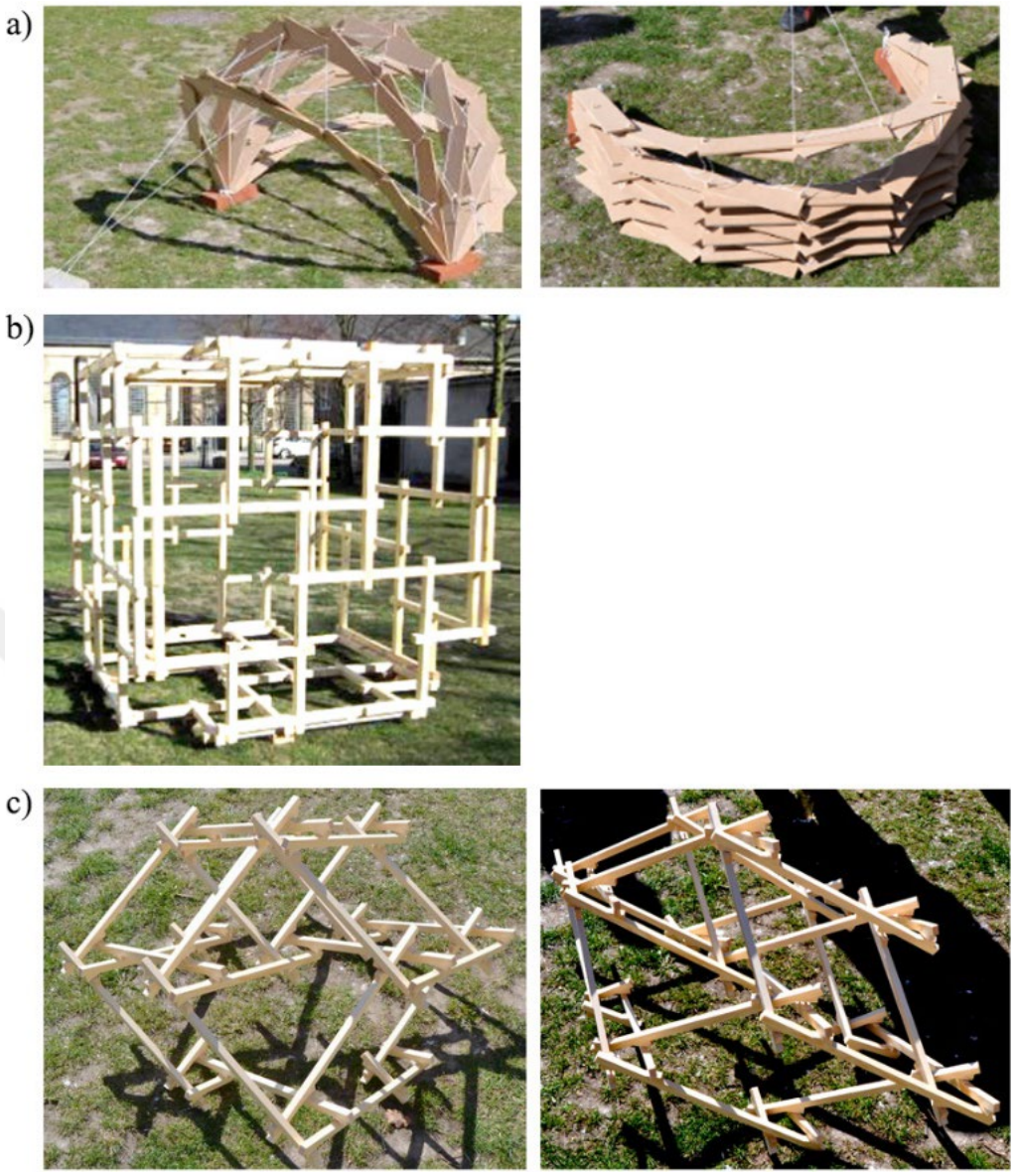

Figure 2.58 a) Arch-type RF b) Plane type RF c) Hanging-type RF.
(Source: Popovic Larsen and Sang-Hoon Lee, 2013)

Muñoz-Vidal et al. (2019) proposed a transportable foldable RF (Figure 2.59). The form of the design is inspired by reminiscent of the classic yurt. They use arc-type bars instead of straight ones to provide enclosure. Their aim is to design transportable, quickly assembled, robust, and expandable RF prototypes. If the appropriate screws are removed, the structure can be folded (Muñoz-Vidal et al., 2019).

Figure 2.59. Foldable crossed arches designed by Muñoz-Vidal et al.
(Source: Muñoz-Vidal et al., 2019)

Looking at the studies, in conclusion, it can be claimed that none of the existing studies is considered highly useful for creating movable RFs and deployable RF networks due to the deficiencies in geometric and kinematic analysis, mobility calculation, motion analysis, and RFs with different joint variations.

CHAPTER 3

GEOMETRIC PROPERTIES OF RFS

In RFs, every nexor supports and is supported by the adjacent nexor. The position and the orientation of every nexor determines and is determined by the adjacent one, which means all parameters are dependent on each other. Any change in one of these parameters also means a change in the form of the RF. For this reason, geometric properties should be known in detail to design RFs.

There are some deficiencies in geometric properties in the previous studies about RFs. In this chapter, the joints' positions and orientations are found using the Denavit-Hartenberg parameters. This information gives where the joints are placed and how they are oriented and take position according to one another. Moreover, the engagement length, eccentricity, and height relationship have been examined previously, but the influence of engagement length on the height and the base edge has not been reported. These omitted parameters and relationships are discussed in this chapter.

3.1. Denavit Hartenberg Convention

The Denavit Hartenberg (DH) convention can be used to understand the geometric properties of an RF fan. DH convention is used for describing the geometry of the links and the relative positions of links with respect to each other. It can be used for linkages, which are mechanisms with joints that have surface contact, such as revolute (R), prismatic (P), helical (H), cylindrical (C), universal (U), and spherical (S) joints. Joints with multi-degree-of-freedom (DoF) can be considered as combinations of single DoF joints. A C joint is a combination of an R and a P joint where the R joint axes are in the P joint direction. A U joint is composed of two perpendicularly intersecting R joints, and an S joint can be modeled as a series of three intersecting R joint axes.

If the axis of the nexor is parallel to the axis of the joint, the joint is represented with a subscript $\parallel$, and if the axis of the nexor is perpendicular to the axis of the joint, the joint is represented with a subscript $\perp$ in this study. This representation is valid only for R joints.

Every link connects two or more joints, and every joint connects two and only two links. In DH convention, a Cartesian coordinate system is attached to each link. First, the axes of single DoF joints are numbered (an exception is a C joint where it is not necessary to dissect into R and P joints). The coordinate system attached to each joint axis i is defined according to the following rules:

• z_i-axis is on a joint axis i.

• x_i axis is on the common perpendicular of z_{i-1} and z_i axes.

Four parameters are needed to be known to describe how a frame (i) relates to the previous frame (i - 1). The four parameters are a, α, d, and θ. While a and α are called link parameters, d and θ are joint parameters. They have named link length (a), twist angle (α), link offset (d), and joint angle (θ), respectively. The reason for giving these names is the geometric relationships between two coordinate frames. Link parameters are measured about and along x-axes, and joint parameters are measured about and along z-axes. The right-hand rule is used for finding the direction of α and θ: while the clockwise direction is negative, the counterclockwise direction is positive (Lynch and Park, 2017).

In DH convention, some rules are needed to be followed for finding parameters (McCarthy and Soh, 2010):

• a_{ij} is the distance between the two joint axes, from z_i to z_j along x_j axis, where $j = i + 1$.

• α_{ij} is the twist angle between z_i and z_j measured about x_i.

• d_i is the link offset from x_{i-1} to x_i along z_{i-1} axis.

• θ_i is the joint angle between x_{i-1} to x_i measured about z_{i-1}.

A_i^j indicates a homogeneous transformation matrix from frame i to frame $j = i + 1$ (1). The homogeneous transformation matrix is a 4 x 4 matrix to find the position and orientation from one coordinate frame to another. The homogeneous transformation matrix from frame i to j is as follows:

$$A_i^j = \begin{bmatrix} \cos\theta_i & -\cos\alpha_{ij}\sin\theta_i & \sin\alpha_{ij}\sin\theta_i & a_{ij}\cos\theta_i \\ \sin\theta_i & \cos\alpha_{ij}\cos\theta_i & -\sin\alpha_{ij}\cos\theta_i & a_{ij}\cos\theta_i \\ 0 & \sin\alpha_{ij} & \cos\alpha_{ij} & d_i \\ 0 & 0 & 0 & 1 \end{bmatrix} \quad (1)$$

A Cartesian coordinate system is defined on the links in compliance with DH convention (Figure 3.1). Figure 3.1 is a closed-loop kinematic chain like an RF, and the n^{th} coordinate system is identical with the initial (0^{th}) coordinate system (Tsai, 1999).

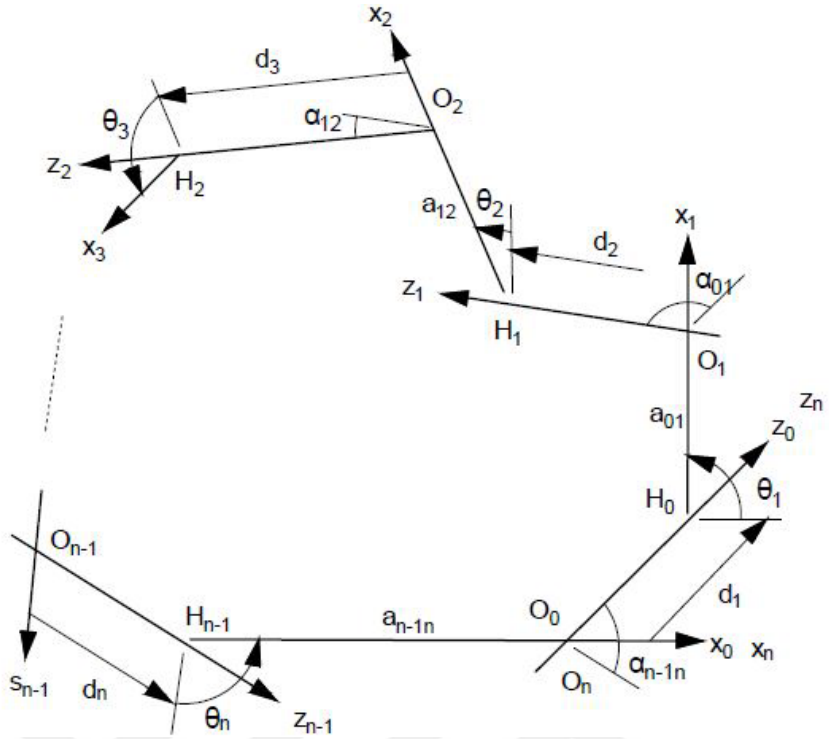

Figure 3.1 DH parameters on a closed-loop kinematic chain (Source: Tsai, 1999)

After the coordinates are taken properly, the matrices are created. The changes of the coordinates start with (x_0, y_0, z_0), turn around the loop, and return to (x_0, y_0, z_0). After multiplying the matrices (2) for each coordinate frame, the result is an identity matrix (3) since it is a closed loop and the kinematic chain turns back to the starting point at the end (Tsai, 1999).

$$I = A_1^n = A_1^2\, A_2^3\, A_3^4 \dots\dots\dots A_{n-2}^{n-1}\, A_{n-1}^n \tag{2}$$

$$I = A_1^n = \begin{bmatrix} 1 & 0 & 0 & 0 \\ 0 & 1 & 0 & 0 \\ 0 & 0 & 1 & 0 \\ 0 & 0 & 0 & 1 \end{bmatrix} \tag{3}$$

3.2. Denavit Hartenberg Convention in RFs

Two nexors can be connected with a series of $CR_{\perp}C$ (cylindrical, revolute, cylindrical) joints in RFs. While C joints are set along the link axes, R joints are set along the contact normals. C joint provides rotation around and translation along the defined

axis and is a 2-DoF joint. R joint provides rotation between two paired elements and is a 1-DoF joint (Tsai, 1999). A 4-nexor RF having $CR_{\perp}C$ joint series has mobility of 9 (including self-motions of links about their axes).

For a 4-nexor RF with a $CR_{\perp}C$ joint series, the coordinate frames are placed on the mechanism, and parameters are defined. "a_{ij}" is the distance between z_i to z_j axes. For RF, all a_{ij} are 0, because all consecutive joint axes intersect. "α_{ij}" is the angle measured from z_i axis to z_j axis about x_j axis. For example, α_{121} in Figure 3.2 is the angle measured from z_{12} axis to z_1 axis about x_1 axis, which is 270 º. "d_i" is the distance between x_{i-1} axis to x_i axis. d_1 can be measured from x_{12} to x_1 axis in Figure 3.2. The distance between x_{12} to x_1 gives the eccentricity or diameter of the nexor, which is denoted as e in Table 3.1. Finally, "θ_i" is measured about z_{i-1} axis from x_{i-1} axis to x_i axis. The angle measured from x_{12} to x_1 axis about z_{12} axis gives θ_1 angle (Figure 3.2). The parameters are listed in Table 3.1.

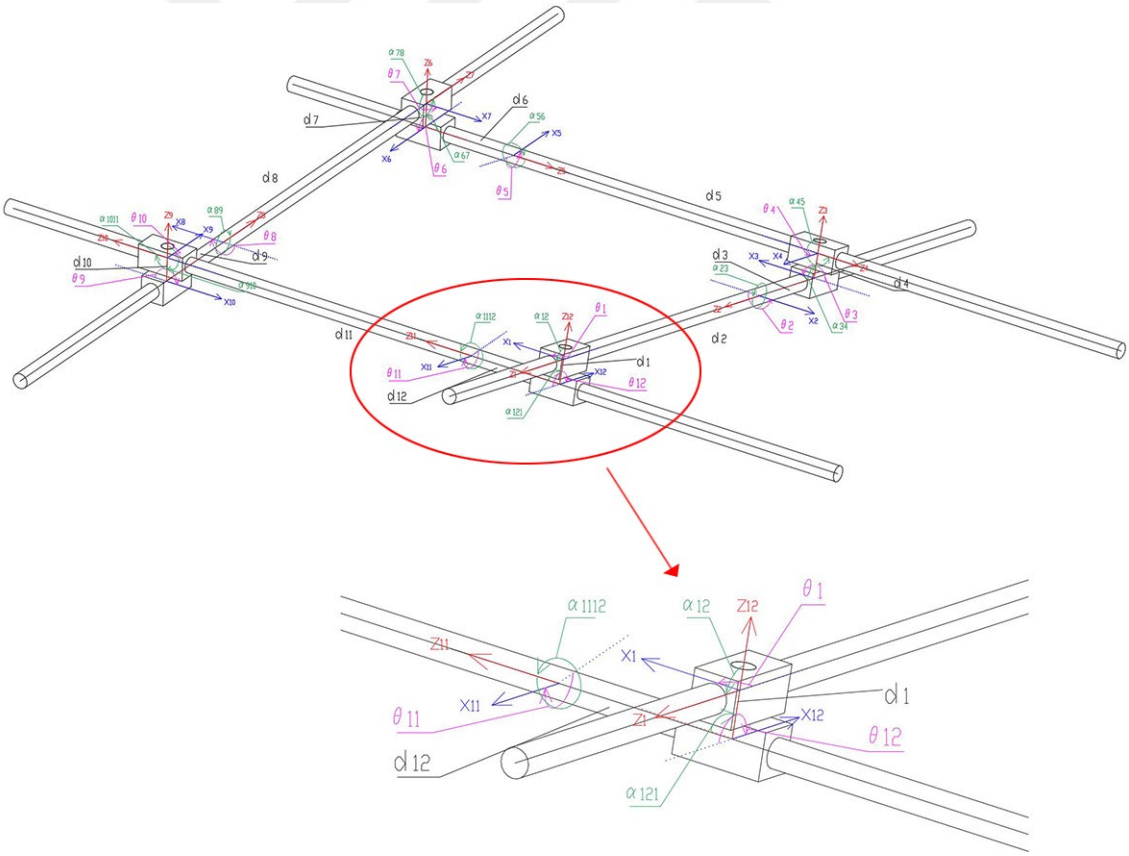

Figure 3.2. Local coordinate frames for a 4-nexor fan.

Table 3.1. DH parameters for a 4-nexor RF for CR⊥C joint series.

i	a_{ij}	d_i	α_{ij}	θ_i
1	0	e	270º	θ_1
2	0	d_2	0º	θ_2
3	0	d_3	90º	180º
4	0	e	270º	θ_4
5	0	d_5	0º	θ_5
6	0	d_6	90º	180º
7	0	e	270 º	θ_7
8	0	d_8	0 º	θ_8
9	0	d_9	90º	180º
10	0	e	270º	θ_{10}
11	0	d_{11}	0º	θ_{11}
12	0	d_{12}	90º	180º

RFs comprise closed-loop kinematic chains. Therefore, the loop closure equations give the identity matrix as a result (4).

$$I = A_1^{12} = A_1^2\, A_2^3\, A_3^4\, A_4^5\, A_5^6\, A_6^7\, A_7^8\, A_8^9\, A_9^{10}\, A_{10}^{11}\, A_{11}^{12}\, A_{12}^1 \tag{4}$$

Equation (5) shows the homogeneous transformation matrix from frame i to j. While the left 3 x 3 matrix (red) represents rotation, the right 3 x 1 matrix (blue) represents translation. For example, suppose one wants to find the angle between one coordinate frame to another. In that case, the values in the red rectangle should be analyzed. Or, if one wants to know the position or distance from one point to another, the values in the blue rectangle should be analyzed (5).

$$A_i^j = \begin{bmatrix} x_x & y_x & z_x & d_x \\ x_y & y_y & z_y & d_y \\ x_z & y_z & z_z & d_z \\ 0 & 0 & 0 & 1 \end{bmatrix} \tag{5}$$

Equation 1 Homogeneous transformation matrix (Almaged, 2017)

The distance between opposite frames (Figure 3.3) whose coordinates are known can be found with Equation (6).

$$k = \sqrt{(x_2 - x_1)^2 + (y_2 - y_1)^2 + (z_2 - z_1)^2} \quad (6)$$

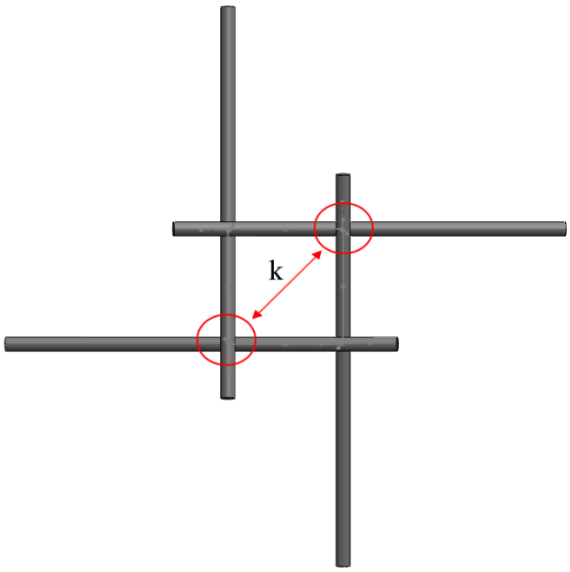

Figure 3.3. Distance between opposite coordinate frames (k).

The homogeneous transformation matrices give critical geometric knowledge, rotation, and translation data. Constructive details should be considered to create movable RFs, and DH parameters will provide this information. The orientation of the coordinate frames or the position of the joints will be decided according to these parameters. This is illustrated with a case study with changing engagement lengths.

3.2.1. Case Study for a $CR_{\perp}C$ Joint Series RF Fan

DH parameters are found for $\lambda = 40$ cm and $\lambda = 50$ cm where $L_n = 140$ cm and $e = 4$ cm for $CR_{\perp}C$ joint series RF (Table 3.2 and Table 3.3). To find the translation or rotation of the sixth coordinate frame according to first, matrices from first to sixth should be multiplied. These x, y, and z coordinates can be used to find the distance between opposite corners. The distance is denoted as k_1 for $\lambda = 40$ cm and k_2 for $\lambda = 50$ cm.

Table 3.2. DH parameters for λ = 40 cm $CR_{\perp}C$ joint series RF fan.

i	a_{ij}	d_i	α_{ij}	θ_i
1	0	4	270°	90°
2	0	-30	0°	190,6°
3	0	-10	90°	180°
4	0	4	270°	88,9°
5	0	-30	0°	192,0°
6	0	-10	90°	180°
7	0	4	270°	90°
8	0	-30	0°	190,6°
9	0	-10	90°	180°
10	0	4	270°	88,9°
11	0	-30	0°	192,0°
12	0	-10	90°	180°

$$A_1^6 = \begin{bmatrix} -0{,}9779 & -0{,}019546443 & -0{,}208384 & 40{,}78186 \\ -0{,}0195 & -0{,}982779644 & 0{,}183748287 & 40{,}0463 \\ -0{,}2084 & 0{,}183744682 & 0{,}960631394 & 0{,}582082 \\ 0 & 0 & 0 & 1 \end{bmatrix}$$

The left 3 x 3 rotation matrix elements give the cosine of the angles between the axes of coordinate frames. The angles between the 1st and 6th joint axes in λ= 40 cm are:

x_x= 168° y_x=91° z_x=102°

x_y=91° y_y=169° z_y=79°

x_z=102° y_z=79° z_z=16°

The right 3 x 1 matrix gives the coordinates of the origin of the sixth frame. Since the first frame's coordinates are (0,0,0), the distance of the origin of the 6th frame can be found as:

$$\mathbf{k_1} = \sqrt{(\mathbf{40,8})^2 + (\mathbf{40,04})^2 + (\mathbf{0,58})^2} = \mathbf{57,16\ cm}$$

Table 3.3. DH parameters for λ = 50 cm CR⊥C joint series RF fan.

i	a_{ij}	d_i	α_{ij}	θ_i
1	0	4	270°	90°
2	0	-40	0°	188,5°
3	0	-10	90°	180°
4	0	4	270°	89,3°
5	0	-40	0°	189,7°
6	0	-10	90°	180°
7	0	4	270°	90°
8	0	-40	0°	188,5°
9	0	-10	90°	180°
10	0	4	270°	89,3°
11	0	-40	0°	189,7°
12	0	-10	90°	180°

$$\mathbf{A_1^6} = \begin{bmatrix} \mathbf{-0,98554} & \mathbf{-0,01256604} & \mathbf{-0,168992126} & \mathbf{50,628302} \\ \mathbf{-0,01261} & \mathbf{-0,98904071} & \mathbf{0,147103244} & \mathbf{50,040511} \\ \mathbf{-0,16899} & \mathbf{0,147107296} & \mathbf{0,97457801} & \mathbf{0,6011105} \\ \mathbf{0} & \mathbf{0} & \mathbf{0} & \mathbf{1} \end{bmatrix}$$

The angle between 1st and 6th joint' axes for the λ = 50 cm case are:

x_x= 170° y_x=91° z_x=100°

x_y=91° y_y=172° z_y=82°

x_z=100° y_z=82° z_z=13°

Also, the distance between the first and sixth frames can be found as:

$$k_2 = \sqrt{(50{,}6)^2 + (50{,}04)^2 + (0{,}6)^2} = 71{,}18 \text{ cm}$$

As can be seen from the results, the orientation and position of the frames change with different engagement lengths. It is essential knowledge while designing movable RFs. One can decide where the joints should be located with the found position and orientation information.

3.3. The Impact of Engagement Length on Base Edge and Height

To create a 4-nexor fan, engagement length ($\lambda = 2\,l$) and eccentricity (e) are given as input and twist angle (β), the angle between the nexor and the horizontal plane (Ψ), the height of the structure (h), the distance between nexor midpoint and structure's center (b), and base edge (c) are found as an output (Figure 3.4). The necessary formulations are derived to find these parameters.

In Figure 3.4, there are n = 4 identical nexors and, $\gamma = 2\pi / n$. In the initial state, the symmetry axes of all nexors (such as OP and OT) are on the same plane. Then all nexors are rotated around their midpoints by an angle Ψ until they are tangent to the adjacent nexors. Since all nexors are rotated with the same angle, the contact points, such as R, are coplanar on the xy- plane.

Let nexor length $L_n = L_1 + L_2$, $|PQ| = |TS| = l$ and the radius of the nexors be $r = |QR| = |RS|$. Then $|QR| + |RS| = 2r = e$ which is eccentricity. Let $|OP| = |OT| = b$ and $|AB| = c$. Ψ, b, h, β, and c are unknown for the configuration. Ψ and b can be found with Equation (7) and Equation (8).

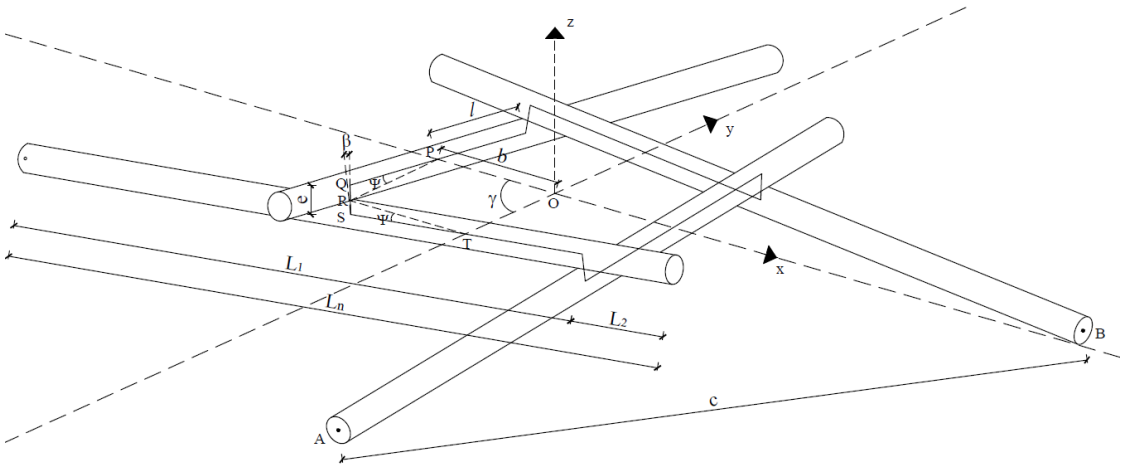

Figure 3.4. 4-nexor fan parameters.

$$\Psi = \cos^{-1}\left(\sqrt{\frac{(l)^2(1-\cos\gamma)(3-\cos\gamma)+r^2\sin^2\gamma \pm \sqrt{[(l)^2(1-\cos\gamma)(3-\cos\gamma)+r^2\sin^2\gamma]^2-8(l)^4(1-\cos\gamma)^3}}{2(l)^2(1-\cos\gamma)^2}}\right) \quad (7)$$

$$b = \frac{(2 - (1 - \cos\gamma)\cos^2\Psi)}{\sin\gamma\cos\Psi} l \tag{8}$$

If this structure is considered as a roof, Ψ gives the slope, and h is the height of the roof (Figure 3.5). Taking the total length of one nexor as L_n, which is a known parameter, h can be found by the following equation (9):

$$h = \sin\Psi * L_n \tag{9}$$

After Ψ is found, the twist angle (β) of the nexors can be calculated as two times the angle between SQ and a line perpendicular to TS and parallel to yz- plane (10). β is α_{ij} in DH parameters.

$$\beta = 2\cos^{-1}\left(\frac{l\ \tan\Psi}{r}\right) \tag{10}$$

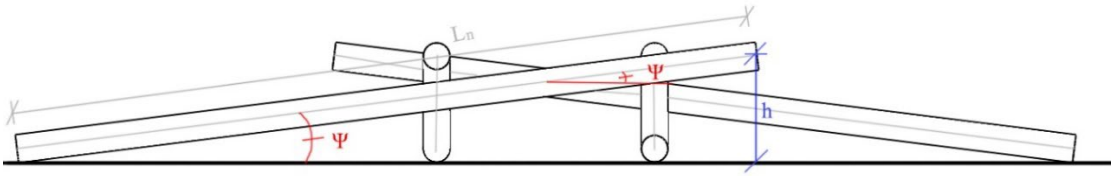

Figure 3.5. Side view of a 4-nexor fan.

The area that the RF covers is an important issue from the design point of view. The endpoints of the nexor create a square on the ground for this study. One edge of a square which is named the base edge (c), can be calculated with the formula as follows (11):

$$|AB| = c = \sqrt{2 * [b^2 + [(L_1 - l) * \cos\Psi]^2]} \tag{11}$$

For the inverse solution, to find l and e for given b and Ψ, one needs to use Equation (12) and Equation (13).

$$l = \frac{2b \sin\gamma \cos\Psi}{2 - (1 - \cos\gamma)\cos^2\Psi} \tag{12}$$

$$e = 2r = 2b\sqrt{\frac{(1 - \cos\gamma)\sin^2\Psi}{2 - (1 - \cos\gamma)\cos^2\Psi}} \tag{13}$$

3.3.1 Case Study to Analyze the Impact of Engagement Length on Base Edge and Height

n = 4, L_1 = 135 cm, L_2=5 cm, L_n=140 cm, l = 25 cm, e = 4 cm (r = 2 cm)

In the RF, *l* is 25 cm, and e is 4 cm. For the given *l* and e, Ψ, b, h, β, and c are calculated.

$\Psi = \cos^{-1}\left(\sqrt{\frac{(25)^2(1-\cos 90)(3-\cos 90)+(2)^2\sin^2 90 \pm \sqrt{[(25)^2(1-\cos 90)(3-\cos 90)+(2)^2\sin^2 90]^2 - 8(25)^4(1-\cos 90)^3}}{50(1-\cos 90)^2}}\right) =$ 4,6°

$$b = \frac{(2 - (1 - \cos 90)\cos^2(4{,}55))}{\sin 90 \cos(4{,}55)} 25 = 25{,}2 \text{ cm}$$

$$h = \sin(4{,}55) * 140 = 11{,}1 \text{ cm}$$

$$\beta = 2\cos^{-1}\left(\frac{25 * \tan(4{,}55)}{2}\right) = 9{,}1^o$$

$$c = \sqrt{2 * [(25{,}2)^2 + [(135 - 25) * \cos(4{,}6)]^2]} = 159{,}1 \text{ cm}$$

Inverse solution for the desired b = 25,2 cm and Ψ = 4,6° :

$$l = \frac{25{,}2 * \sin 90 * \cos(4{,}6)}{2 - (1 - \cos 90) * \cos^2(4{,}6)} = 25 \text{ cm}$$

$$e = 2 * 25{,}2\sqrt{\frac{(1 - \cos 90)\sin^2(4{,}6)}{2 - (1 - \cos 90)\cos^2(4{,}6)}} = 4 \text{ cm}$$

Formulas are applied to different engagement lengths from 1 cm to 135 cm to see the change in Ψ, b, h, β, and c. θ value is taken from the DH parameters to see the relation with the other parameters.

Table 3.4. Changing parameters with the variable engagement lengths.

L_1	L_2	L_n	n	λ	$l = \lambda/2$	Ψ (degrees)	b	h	β (degrees)	c	θ (degrees)
135	5	140	4	1	0.5	71.0	2.9	132.4	86.8	62.0	26.6
135	5	140	4	2	1	56.9	3.1	117.3	79.9	103.5	45.5
135	5	140	4	3	1.5	47.1	3.4	102.5	72.4	128.6	57.6
135	5	140	4	6	3	30.7	4.4	71.5	54.1	160.6	74.9
135	5	140	4	7	3.5	27.4	4.8	64.5	49.5	165.1	77.7
135	5	140	4	9	4.5	22.5	5.6	53.7	41.9	170.6	81.6
135	5	140	4	10	5	20.7	6.0	49.4	38.9	172.1	82.8
135	5	140	4	11	5.5	19.1	6.4	45.7	36.2	173.2	83.9
135	5	140	4	12	6	17.7	6.9	42.5	33.8	174.0	84.7
135	5	140	4	15	7.5	14.5	8.2	35.1	28.1	174.9	86.4
135	5	140	4	20	10	11.1	10.6	27.0	21.8	174.0	87.9
135	5	140	4	25	12.5	9.0	13.0	21.9	17.7	172.0	88.6
135	5	140	4	30	15	7.5	15.4	18.3	14.9	169.6	89.0
135	5	140	4	40	20	5.7	20.3	13.9	11.3	164.3	89.4
135	5	140	4	50	25	4.6	25.2	11.1	9.1	159.0	89.6
135	5	140	4	70	35	3.3	35.2	8.0	6.5	149.6	89.8
135	5	140	4	90	45	2.5	45.1	6.2	5.1	142.2	89.9
135	5	140	4	110	55	2.1	55.1	5.1	4.2	137.2	89.9
135	5	140	4	135	67.5	1.7	67.6	4.1	3.4	134.9	89.9

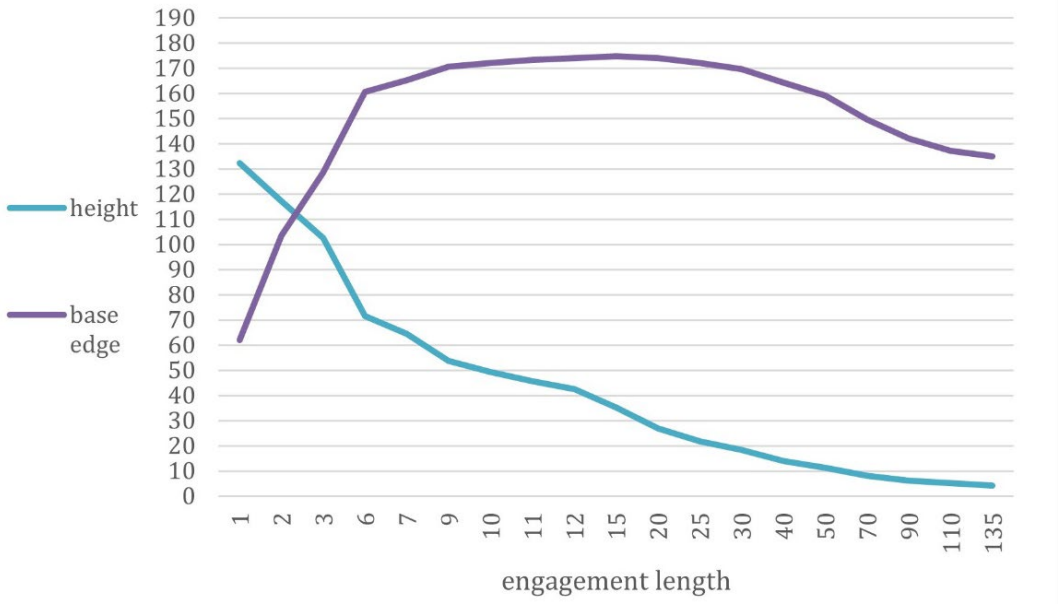

Figure 3.6. The influence of engagement lengths on fan heights and base edges.

Nexor length, eccentricity, and the number of nexors are kept constant while engagement length is increased. It is known from the previous studies that RF gets lower as the engagement length increases. As a result, it can be guessed that Ψ gets smaller as

the RF gets closer to the ground. As engagement length increases, the engagement window gets bigger, which means b increases. The twist angle β takes smaller values as the frame gets closer to the ground. θ takes bigger values, and its value reaches almost 90º. All the parameters monotonically increase or decrease except one. While the base edge is expected to have a maximum value with minimum height and maximum engagement length, it has the maximum amount when λ = 15 cm, and then it starts to decrease (Table 3.4). The graph in Figure 3.6 shows how the heights and base edges change with the increasing engagement lengths.

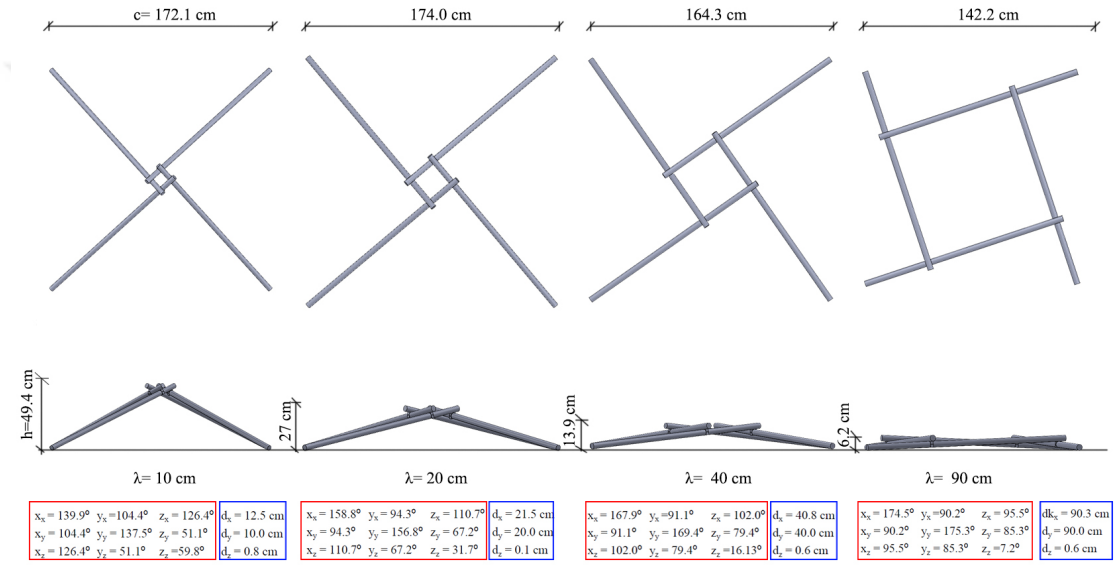

Figure 3.7. RF fan showing the influence of engagement lengths on fan heights and base edges.

With this part of the study, it is seen that it is possible to obtain different assemblies that can be demountable. When the required nexor lengths for the desired heights or base edges are found, the position and orientation of the joints connecting the nexors are determined (Figure 3.7). Thus, by drilling holes on the nexor for the joints (Figure 3.8), RFs with different heights, base edges, and engagement lengths can be disassembled and reassembled as needed.

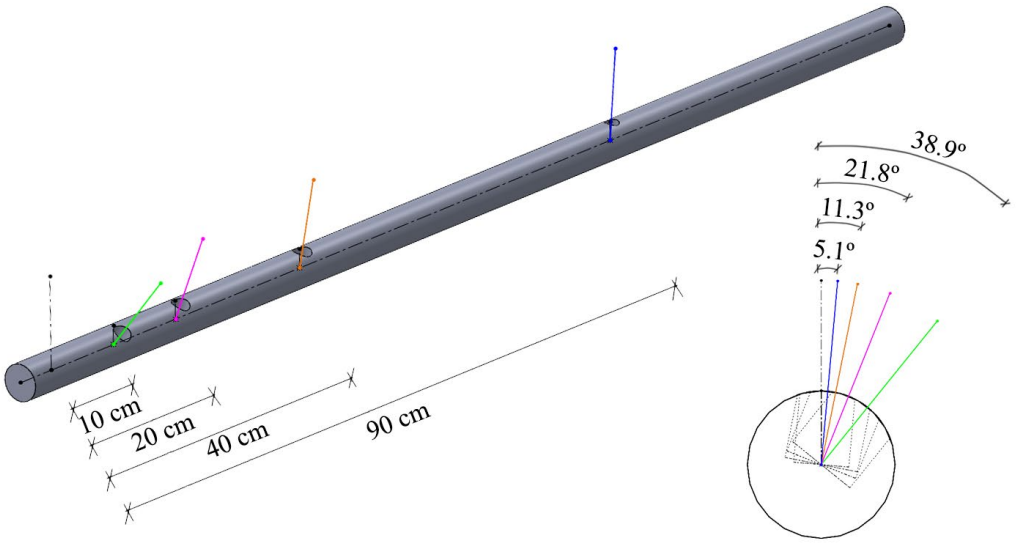

Figure 3.8. Nexor with several holes for different engagement lengths.

A reconfigurable demountable fan is produced with the information obtained. The nexors are printed in a 3d printer. The nexor lengths are defined as 25 cm, and the engagement lengths are specified as 1, 3, 9, 15, and 20 cm (Figure 3.9a). The axes of holes are obtained from data based on the engagement lengths and eccentricities. The radiuses of the holes are determined according to the screws to be used. 3 mm screws and union nuts are used to connect nexors (Figure 3.9b).

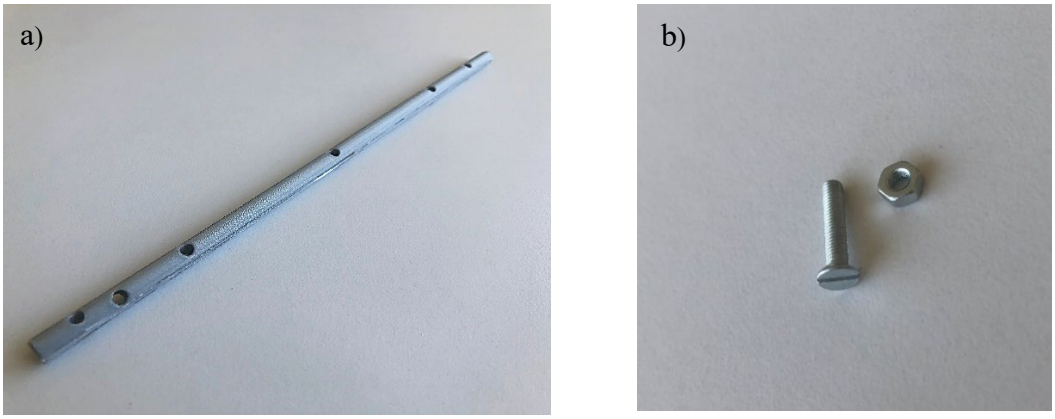

Figure 3.9. a) Nexor b) Screw and union nut.

Different assemblies can be achieved by changing the hole (Figure 3.10). Thus, the fan's desired height and base edge can be created according to the changing needs.

Figure 3.10. Demountable fan.

3.4. Conclusion

The RF fan is modeled as a kinematic chain with DH parameters for the given eccentricity and engagement length in this chapter. Homogenous transformation matrices are obtained by using the model and parameters. Thus, it is possible to find the position and orientation of a coordinate frame from these transformation matrices. These position and orientation data are necessary to solve the constructive details when designing movable or demountable RFs. Then, relationships among design parameters are presented to find unknown parameters such as twist angle, the angle between the nexors and the horizontal plane, the height of the mechanism, the distance between the nexor midpoint and the structure's center, and the base edge. Their relations with the increasing engagement lengths are shown in a table. It is not possible to specify the maximum height and maximum base edge independently at the same time with the same engagement lengths. In order to reach the optimum result, the designer can follow the method suggested in this study or make use of the graph in Figure 3.6, where the same nexor dimensions are used in the fan.

A reconfigurable demountable physical model is produced with a 3d printer. The positions and the orientation of the holes on a nexor are determined according to the data obtained from the calculations.

To conclude, one can find the values of the necessary parameters to obtain different assemblies by demounting the RF and remounting it again using alternative holes on the nexors. Moreover, the geometric information found can be used to design movable RFs.

CHAPTER 4

MOBILITY ANALYSIS OF RFS

Mobility (M) can also be referred to as degrees of freedom (DoF). Some independent parameters are needed to define the position of links in the mechanism. Mobility is the number of these independent parameters. In other words, it is the total DoF to be controlled in a mechanism for the links in a specific position. It is about the motion capability of the mechanism (Mufazzal, 2017). The mechanism's mobility depends on the link arrangement and the type of the joints.

In RFs, revolute (R), prismatic (P), cylindrical (C), slotted cylinder (C_s), and universal (U) joints can be used to connect two nexors. A C joint is a combination of an R and a P joint where the R joint axes are in the P joint direction, a C_s joint has perpendicularly intersecting R and P joints, and the U joint is composed of two perpendicularly intersecting R joints (Figure 4.1) (Table 4.1).

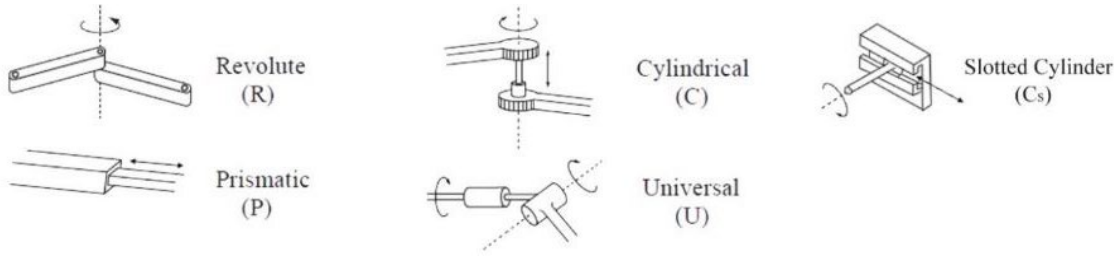

Figure 4.1. Joint types used in RFs.
(Source: Lynch and Park, 2017 and Söylemez, 2011)

Table 4.1. Joint types, their DoFs, and kinematic diagrams.

Name	Symbol	DoF	Rotational	Translational	Diagram
Revolute	R	1	1	0	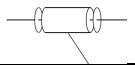
Prismatic	P	1	0	1	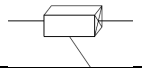
Cylindrical	C (RP)	2	1	1	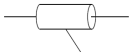
Slotted Cylinder	C_s (RP)	2	1	1	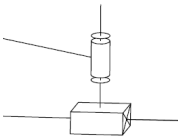
Universal	U (2R)	2	2	0	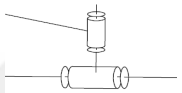

R and P joints are 1-DoF joints where the R joint allows rotation and the P joint allows translation. C and C_s joints have 2-DoF, which provides both translation and rotation. U joint is also a 2-DoF joint, but it provides rotations only.

The mobility of a mechanism that is composed of links and connected with joints can be calculated with Freudenstein and Alizade's mobility formula (14) (Freudenstein and Alizade, 1975):

$$M = \sum_{i=1}^{j} f_i - \sum_{k=1}^{L} \lambda_k \qquad (14)$$

M = mobility

j = number of joints

f_i = DoF of joint i

Σf_i = connectivity sum

L = number of independent loops

λ_k = DoF of space in which the loop k of the mechanism operates (λ_k = 2, 3, 4, 5, 6) (λ_k = 3 for planar mechanisms, λ_k = 6 for spatial mechanisms, RFs are λ_k = 6 mechanisms since they are spatial)

L is calculated by using Euler's formula:

$$L = j - l_l + 1 \tag{15}$$

$l_l =$ number of links

Assemblies with zero or negative DoF (M < 0 or M = 0) are called structures, and these mechanisms cannot move. Mechanisms having single or multi DoF can move and need more than one or more actuators to operate.

In this chapter, single-loop 3-, 4-, and 5-nexor fans are created, different joint series are applied, kinematic diagrams are drawn, and their mobilities are calculated. The fans are divided into three categories according to their motion capabilities: zero DoF, single DoF, and multi DoF fans.

4.1. Triangular Fans with Different Joint Connections

4.1.1. Zero DoF Triangular Fans

The mechanism's mobility is negative when three nexors are connected with three $R_\perp$ joints (Figure 4.2a). It means that this mechanism cannot move and is a structure. When three more $R_\parallel$ joints or P joints are added, the connectivity sum equals six, and M becomes zero (Figure 4.2b and Figure 4.2c). The fans are still unable to move.

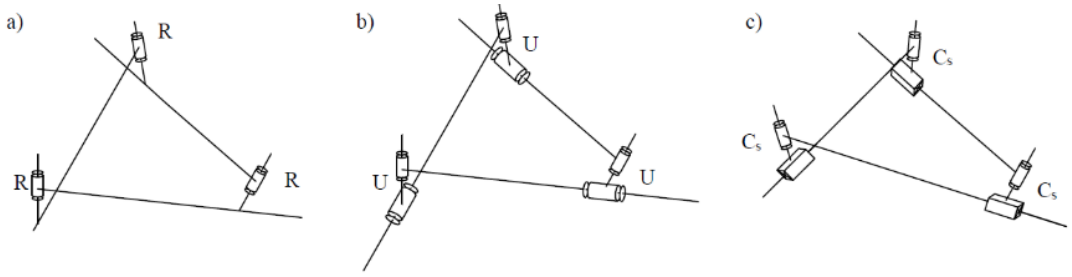

$\Sigma f_i = 3, \lambda_k = 6$
$M = 3 - 6 = -3$

$\Sigma f_i = 6, \lambda_k = 6$
$M = 6 - 6 = 0$

$\Sigma f_i = 6, \lambda_k = 6$
$M = 6 - 6 = 0$

Figure 4.2. Zero DoF 3- nexor fans a) $R_\perp$-$R_\perp$-$R_\perp$ fan, b) U-U-U fan, c) Cs-Cs-Cs fan.

According to the mobility formula, even though $UR_\parallel$-U-U joint series triangular fan's mobility equals one, it is a structure (Figure 4.3a). Because two $R_\parallel$ joints in one

nexor let the nexor turns around itself. But it does not change or affect the form of the fan, and one rotation for one nexor can be ignored from the mobility result. So excessive mobility can be deducted from the formula to get the correct mobility value as proposed by Alizade (2019) (16).

$$M = \sum_{i=1}^{j} f_i - \sum_{k=1}^{N} \lambda_k - E \tag{16}$$

E= Excessive mobility

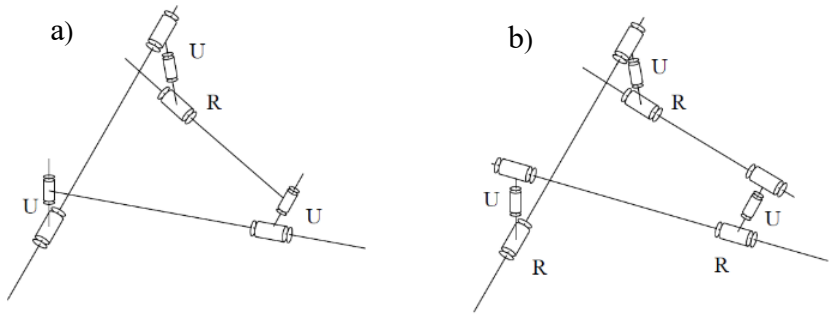

$\Sigma f_i = 7, \lambda_k = 6, E = 1,$
$M = 7 - 6 = 1 - 1 = 0$

$\Sigma f_i = 9, \lambda_k = 6, E = 3,$
$M = 9 - 6 - 3 = 0$

Figure 4.3. Zero DoF 3-nexor fans having excessive mobilities a) $UR_{\parallel}$-U-U fan, b) $UR_{\parallel}$-$UR_{\parallel}$-$UR_{\parallel}$ fan

The same situation for $UR_{\parallel}$-$UR_{\parallel}$-$UR_{\parallel}$ fan is valid (Figure 4.3b), and three rotations should be extracted from the equation since three nexors have two $R_{\parallel}$ joints simultaneously.

4.1.2. Single DoF Triangular Fans

For an n nexor closed-loop mechanism with 1-DoF joints, for the mobility to be one, Σf_i needs to be greater than λ_k. Since λ_k equals six for RFs, Σf_i should be seven. A single DoF triangular fan with 1-DoF joints can be created with PU-U-U joint series. The kinematic diagram and the motion of the fan can be seen in Figure 4.4.

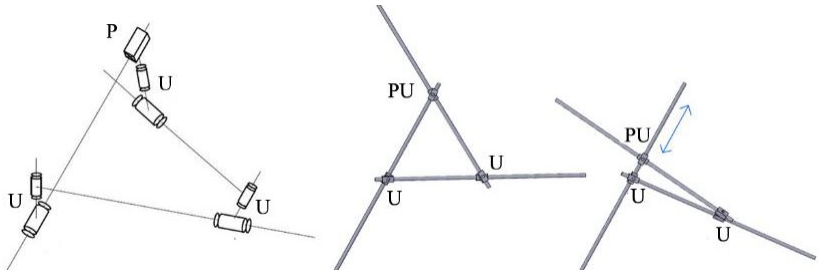

$\Sigma f_i = 7, \lambda_k = 6, M = 7 - 6 = 1$

Figure 4.4. PU-U-U fan and its motion in plan.

Fans with the 2-DoF joints can also be created for mobility to be one. 2-DoF joints are taken as two for f_i since they allow rotation and translation. $R_\perp$C-$R_\perp$C-$R_\perp$ (Fig. 74) and C_s-$R_\perp$C-U (Fig. 75) are two of the M = 1 fans with both 1-DoF and 2-DoF joints.

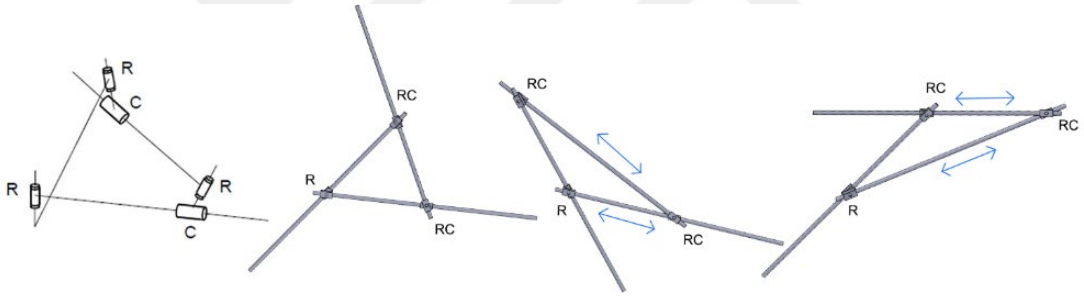

1 DoF joint= 3, 2 DoF joint=2, $\Sigma f_i = 7, \lambda_k = 6, M = 7 - 6 = 1$

Figure 4.5. $R_\perp$C-$R_\perp$C-$R_\perp$ fan and its motion in plan.

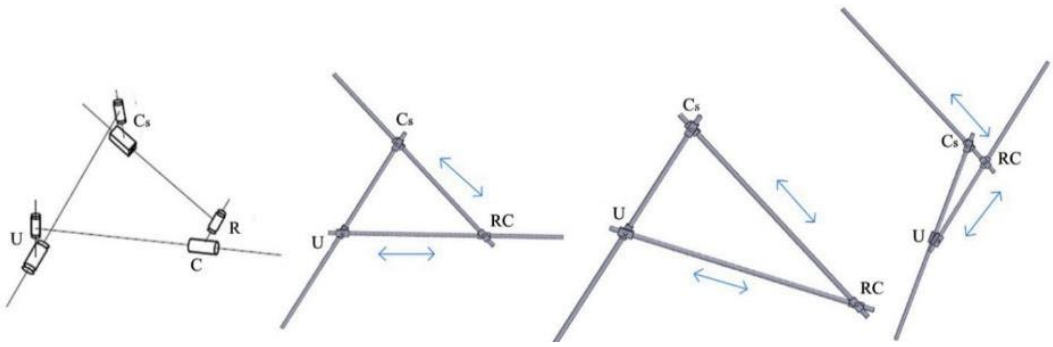

1 DoF joint= 5 , 2 DoF joint=1, $\Sigma f_i = 7, \lambda_k = 6, M = 7 - 6 = 1$

Figure 4.6. C_s-$R_\perp$C-U fan and its motion in plan.

4.1.3. Multi DoF Triangular Fans

PU-U-PU fan (Figure 4.7a) has eight 1-DoF joints, and its mobility equals two. Particular attention should be made not to have the same joints like two R joints or two P joints in one nexor to avoid excessive mobility. For the PU joint series fan (Figure 4.7b), M equals three, and the nexors which rotate about their axes do not exist since one nexor has one P and one R joint.

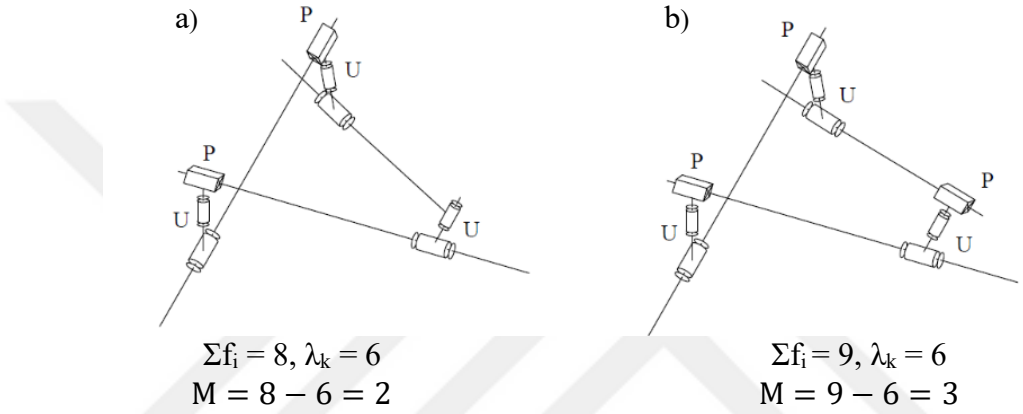

Figure 4.7. Multi DoF 3-nexor fans a) PU-U-PU fan, b) PU-PU-PU fan.

For $R_{\perp}C$ joint series, it can be assumed that there are two R and a P in one intersection point. Since there are three bars, Σf_i becomes nine (Figure 4.8a).

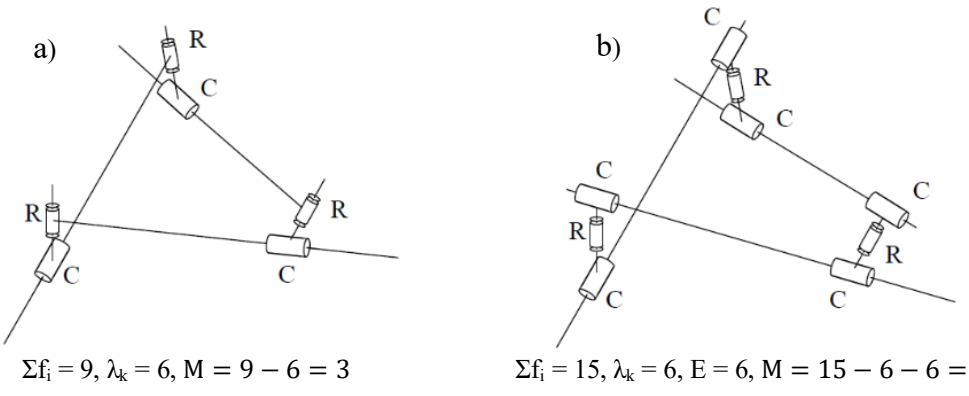

Figure 4.8. Multi DoF 3-nexor fans a) $R_{\perp}C$-$R_{\perp}C$-$R_{\perp}C$ fan, b) $CR_{\perp}C$-$CR_{\perp}C$-$CR_{\perp}C$ fan.

The maximum mobility value is assumed to be obtained by having three $R_{\perp}$ and six C joints in a configuration (Figure 4.8b). But the rotation of the nexors around their axes and sliding of the nexors back and forth exist at this fan. One nexor has one rotation and one sliding excessive mobility because of C. So, six excessive DoF should be taken away from the result for three nexors. As a result, the mobility of the $CR_{\perp}C$ joint series fan equals the mobility of the $R_{\perp}C$ joint series fan. But PU joint series fan's (Figure 4.7b) mobility is also three. This result shows that it is not necessary to use as many joints as possible or joints with as many DoFs as possible in the fan to have maximum mobility.

4.2. Quadrilateral Fans with Different Joint Connections

4.2.1. Zero DoF Quadrilateral Fans

The mechanism's mobility is negative when four nexors are connected with four $R_{\perp}$ joints (Figure 4.9a). It means that this mechanism cannot move and is a structure. The mechanism's mobility is zero until the connectivity sum reaches seven.

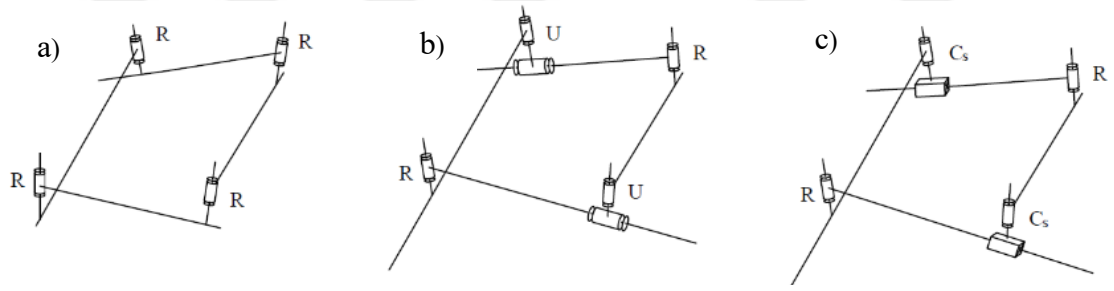

$\Sigma f_i = 4, \lambda_k = 6$
$M = 4 - 6 = -2$

$\Sigma f_i = 6, \lambda_k = 6$
$M = 6 - 6 = 0$

$\Sigma f_i = 6, \lambda_k = 6$
$M = 6 - 6 = 0$

Figure 4.9. Zero DoF 4-nexor fans a) $R_{\perp}$-$R_{\perp}$-$R_{\perp}$-$R_{\perp}$ fan, b) U-$R_{\perp}$-U-$R_{\perp}$ fan, c) C_s-$R_{\perp}$-C_s-$R_{\perp}$ fan.

4.2.2. Single DoF Quadrilateral Fans

For M = 1, the fan needs to have seven 1-DoF joints. It is possible to create U-U-$R_{\perp}$-U joint series (Figure 4.10) to reach mobility one with 1-DoF joints. To obtain M = 1 with both 1-DoF and 2-DoF joints, U-$R_{\perp}$- $R_{\perp}C$-$R_{\perp}$ (Figure 4.11) joint series fans can be created.

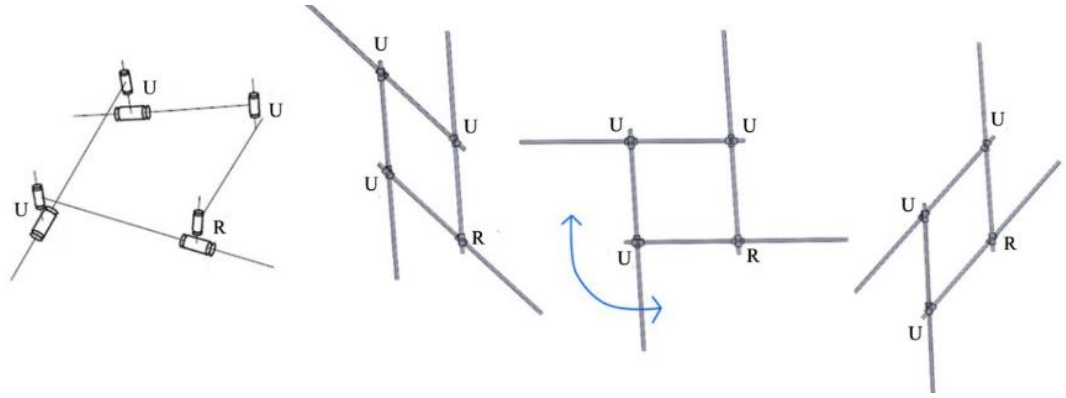

$\Sigma f_i = 7, \lambda_k = 6, M = 7 - 6 = 1$

Figure 4.10. U-U-R$_\perp$-U fan and its motion.

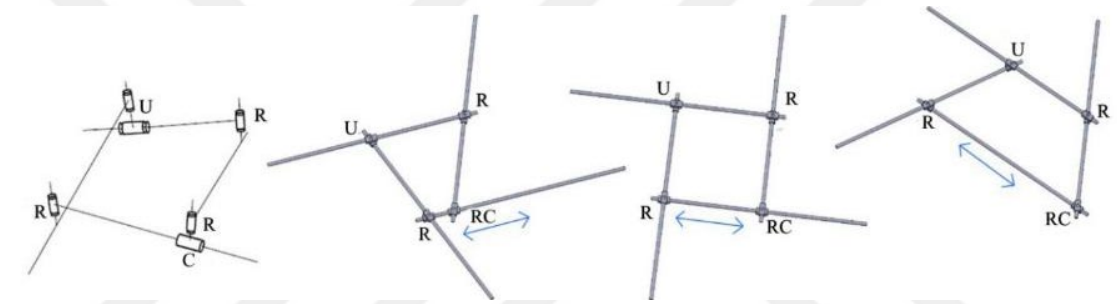

$\Sigma f_i = 7, \lambda_k = 6, M = 7 - 6 = 1$

Figure 4.11. U-R$_\perp$-R$_\perp$C-R$_\perp$ fan and its motion in plan.

4.2.3. Multi DoF Quadrilateral Fans

The fans that have multi DoF are shown in Figure 4.12 with having only 1-DoF joints or having both 1-DoF and 2-DoF joints. The fans having UR$_\parallel$ (Figure 4.12c) or C$_s$P (Figure 4.13a) joints at the intersection points have rotating or sliding nexors, so excessive mobility value should be extracted from the calculation.

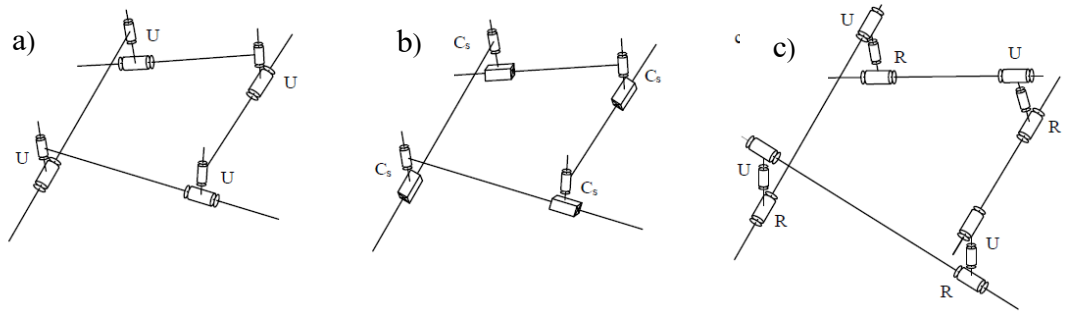

$\Sigma f_i = 8, \lambda_k = 6$ $\quad$ $\Sigma f_i = 8, \lambda_k = 6$ $\quad$ $\Sigma f_i = 12, \lambda_k = 6, E = 4$

$M = 8 - 6 = 2$ $\quad$ $M = 8 - 6 = 2$ $\quad$ $M = 12 - 6 - 4 = 2$

Figure 4.12. Multi DoF 4-nexor fans a) U-U-U-U fan, b) C_s- C_s- C_s- C_s fan, c) $UR_\perp$-$UR_\perp$-$UR_\perp$-$UR_\perp$ fan

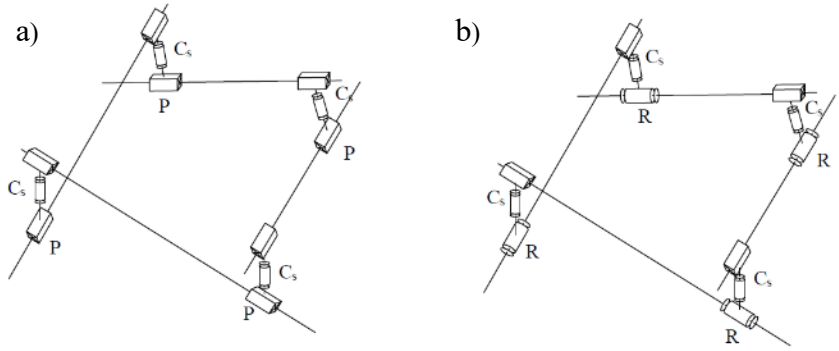

$\Sigma f_i = 12, \lambda_k = 6, E = 4$ $\quad$ $\Sigma f_i = 12, \lambda_k = 6$

$M = 12 - 6 - 4 = 2$ $\quad$ $M = 12 - 6 = 6$

Figure 4.13. Multi DoF 4-nexor fans a) C_sP-C_sP-C_sP-C_sP fan, b) $C_sR_\parallel$-$C_sR_\parallel$-$C_sR_\parallel$-$C_sR_\parallel$ fan.

Maximum mobility is assumed to be in the fan that has $CR_\perp C$ joint series at one intersection point. But the rotation of the nexors around their axes and sliding nexors back and forth exist at this fan. So, eight should be taken away from the result since there are four nexors. As a result, the mobility of the $CR_\perp C$ joint series (Figure 4.14b) fan equals the mobilities of $R_\perp C$ (Figure 4.14a) and $C_sR_\perp$ (Figure 4.13b) joint series fans.

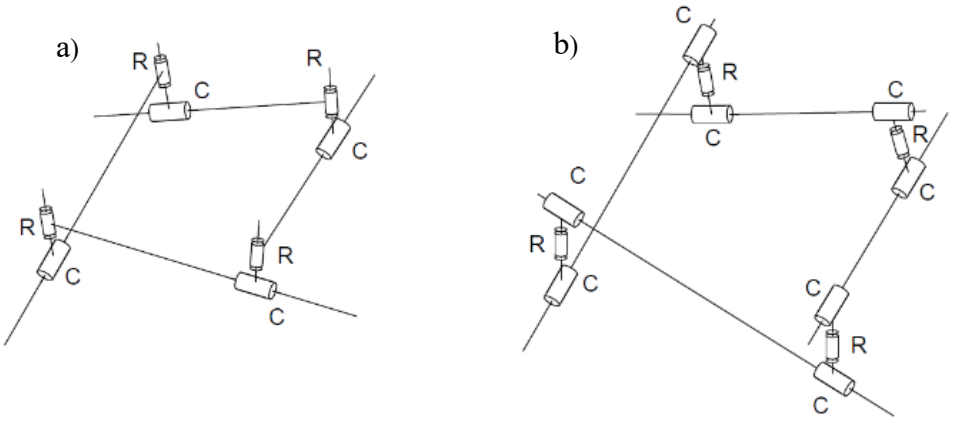

$\Sigma f_i = 12, \lambda_k = 6$
$M = 12 - 6 = 6$

$\Sigma f_i = 20, \lambda_k = 6, E = 8$
$M = 20 - 6 - 8 = 6$

Figure 4.14. Multi DoF 4-nexor fans a) $R_\perp$C-$R_\perp$C-$R_\perp$C-$R_\perp$C fan, b) $CR_\perp$C-$CR_\perp$C-$CR_\perp$C-$CR_\perp$C fan.

4.3. Pentagonal Fans with Different Joint Connections

4.3.1. Zero DoF Pentagonal Fans

The fan's mobility is negative when five nexors are connected with five $R_\perp$ joints (Figure 84a). It means that this fan cannot move and is a structure. The fan is still a structure even if added one more R joint. The fan's mobility is zero until Σf_i reaches seven.

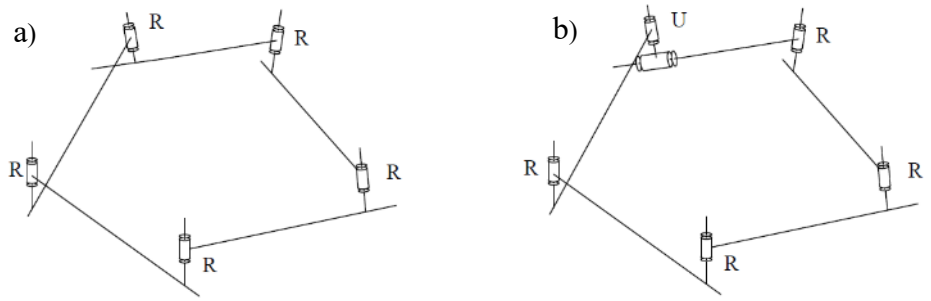

$\Sigma f_i = 5, \lambda_k = 6$
$M = 5 - 6 = -1$

$\Sigma f_i = 6, \lambda_k = 6$
$M = 6 - 6 = 0$

Figure 4.15. Zero DoF 5-nexor fans a) $R_\perp$-$R_\perp$-$R_\perp$-$R_\perp$-$R_\perp$ fan, b) U-$R_\perp$-$R_\perp$-$R_\perp$-$R_\perp$ fan.

4.3.2. Single DoF Pentagonal Fans

To have M = 1, the minimum number of joints is seven. Fans with a single DoF can be created using only 1-DoF (Figure 4.16) or both 1-DoF and 2-DoF (Figure 4.17) joints at the intersection points. In Figure 4.16, there is only rotation movement between nexors because of R joints. In Figure 4.17, there is still rotation between nexors, but one engagement length is variable because of the C joint.

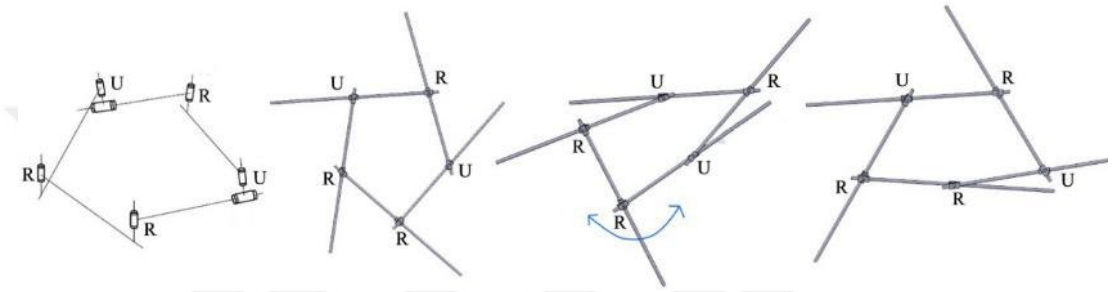

$\Sigma f_i = 7, \lambda_k = 6, M = 7 - 6 = 1$

Figure 4.16. U-R⊥-U-R⊥-R⊥ fan and its motion.

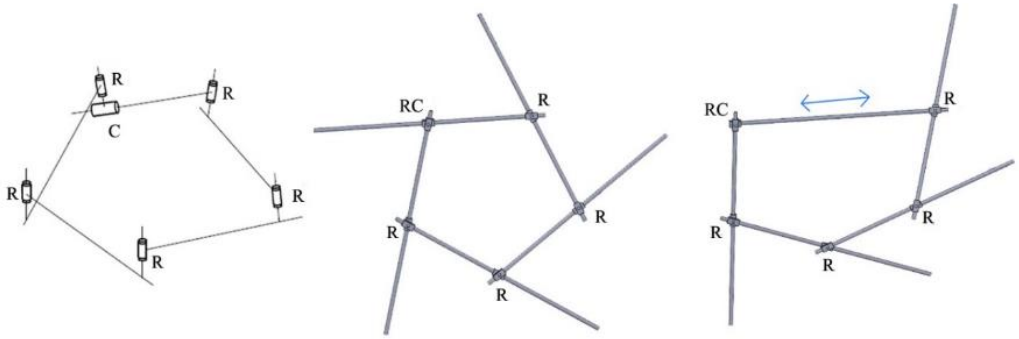

$\Sigma f_i = 7, \lambda_k = 6, M = 7 - 6 = 1$

Figure 4.17. R⊥C-R⊥-R⊥-R⊥-R⊥ fan and its motion.

4.3.3. Multi DoF Pentagonal Fans

Multi DoF fans can be seen in Figure 4.18 and Figure 4.19. U and UR⊥ joint series fans' (Figure 4.18b and Figure 4.18c) results are the same since the UR⊥ joint series fan

has rotating nexors around itself. Consequently, fans having U and $UR_{\perp}$ at the intersection points have the same motion capabilities.

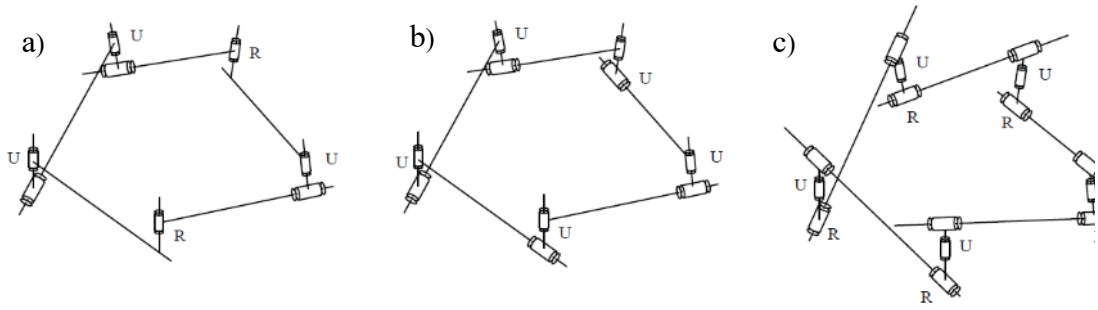

$\Sigma f_i = 8, \lambda_k = 6$ $\quad M = 8 - 6 = 2$

$\Sigma f_i = 10, \lambda_k = 6$ $\quad M = 10 - 6 = 4$

$\Sigma f_i = 15, \lambda_k = 6, E = 5$ $\quad M = 15 - 6 - 5 = 4$

Figure 4.18. Multi DoF 5-nexor fans a) U-$R_{\perp}$-U-$R_{\perp}$-U fan b) U-U-U-U-U fan, c) $UR_{\parallel}$-$UR_{\parallel}$-$UR_{\parallel}$-$UR_{\parallel}$-$UR_{\parallel}$ fan.

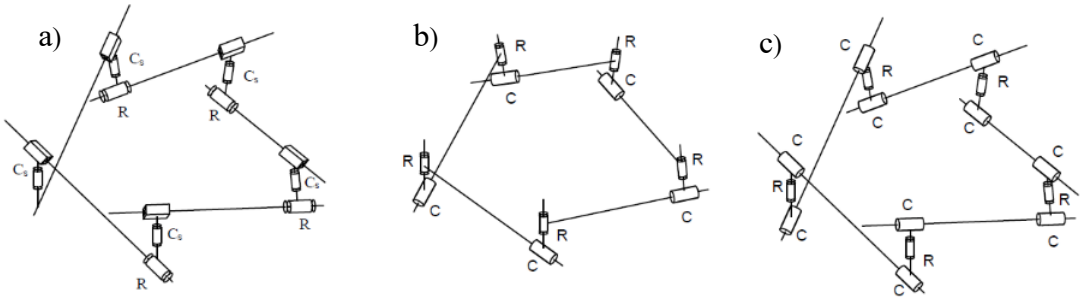

$\Sigma f_i = 15, \lambda_k = 6$ $\quad M = 15 - 6 = 9$

$\Sigma f_i = 15, \lambda_k = 6$ $\quad M = 15 - 6 = 9$

$\Sigma f_i = 25, \lambda_k = 6, E = 10$ $\quad M = 25 - 6 - 10 = 9$

Figure 4.19. Multi DoF 5-nexor fans a) $C_sR_{\parallel}$-$C_sR_{\parallel}$-$C_sR_{\parallel}$-$C_sR_{\parallel}$-C_s fan, b) $R_{\perp}$C-$R_{\perp}$C-$R_{\perp}$C-$R_{\perp}$C-$R_{\perp}$C fan, c) $CR_{\perp}$C-$CR_{\perp}$C-$CR_{\perp}$C-$CR_{\perp}$C-$CR_{\perp}$C fan

In Figure 4.19, the fans having maximum mobilities can be seen. Even though $CR_{\perp}$C joint series fan has the maximum number of Σf_i, its mobility equals $C_sR_{\parallel}$ and $R_{\perp}$C joint series fans' mobility. Because $CR_{\perp}$C joint series fan has two excessive mobility for each nexor. Since there are five nexors, ten should be extracted from the formula as excessive mobility. So, the mobility result equals nine, which is the maximum value for 5- nexor fans.

CHAPTER 5

MOTION ANALYSIS OF SINGLE DOF RFS WITH ORTHOGONAL R JOINTS VIA SIMULATIONS

In this chapter, the focus is on the motions of the fans. Since there are too many alternatives in multi-DoF fans and motion control is difficult, it is initially aimed to examine single DoF fans. This chapter of the thesis seeks to analyze how single DoF 3- and 4- nexor RFs with orthogonal R move. An orthogonal R joint means that two nexors are connected with an R joint, and the nexor's and R joint's axes are perpendicular to each other at every intersection point. The fans in this chapter have three orthogonal R joints for triangular fans and four orthogonal R joints for quadrilateral fans. Then, necessary joints are added to reach a single DoF fan regardless of type. There are two types of fans: fans created without any sliding joints and fans created with sliding joints. The motion analyses are evaluated by making an analogy as if the fan is two-dimensional, as seen from the top view.

4.4. Triangular Fans

In triangular fans, firstly, the fans created without any sliding joints are explained. In Figure 5.1a, every corner is connected with an orthogonal R joint, and then three more R joints are added. Thereby, every intersection point has a U joint, and the fan is a structure. There need to be seven DoF joints to have a single DoF fan. But adding an R joint to U joint series fan leads to excessive mobility (Figure 5.1b). That is to say; it is not possible to create a single DoF 3-nexor fan with only R joints.

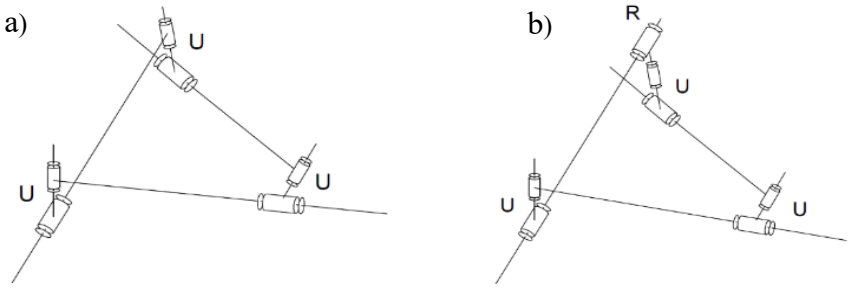

$\Sigma f_i = 6, \lambda_k = 6$

$M = 6 - 6 = 0$

$\Sigma f_i = 7, \lambda_k = 6, E=1$

$M = 7 - 6 - 1 = 0$

Figure 5.1. a)U-U-U fan, b) $R_{\parallel}$U-U-U fan.

Since a single DoF fan cannot be reached with only R joints, sliding joints are tried in the following fans. In Figure 5.2, one P joint is added to the support nexor. There are six R and a P joints, meaning one engagement length is variable. The engagement window area varies depending on the change in the engagement length with the help of R joints at the corners (Figure 5.3).

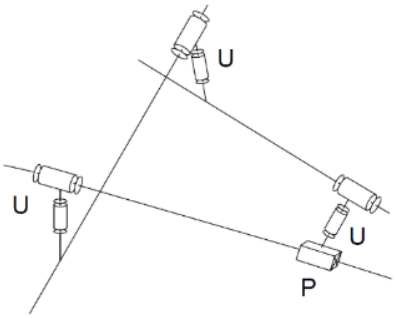

$\Sigma f_i = 7, \lambda_k = 6$

$M = 7 - 6 = 1$

Figure 5.2. U-UP-U fan.

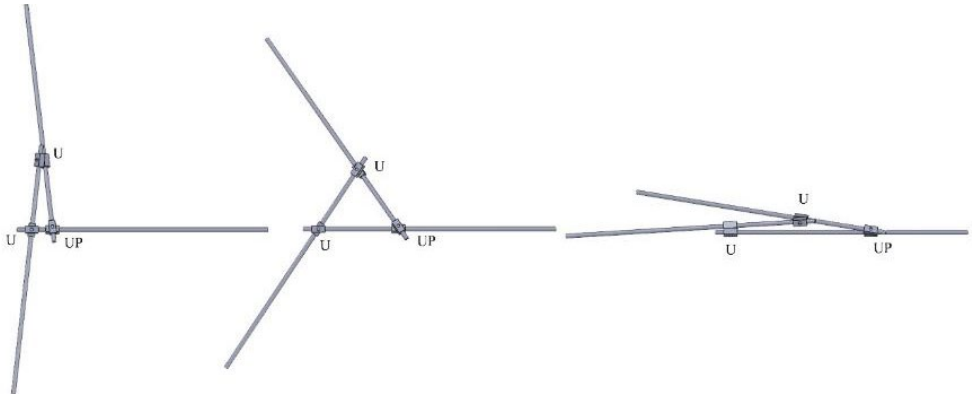

Figure 5.3. U-UP-U fan motion.

The calculation of the mobilities will not be given from this part since this chapter studies only single DoF fans. In Figure 5.4, the P joint is shifted to the supported nexor, different than Figure 5.2, to see the change in the motion, which can be seen in Figure 5.5.

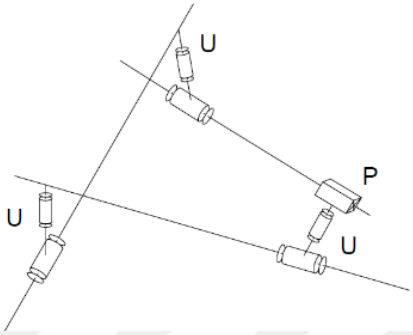

Figure 5.4. U-PU-U fan.

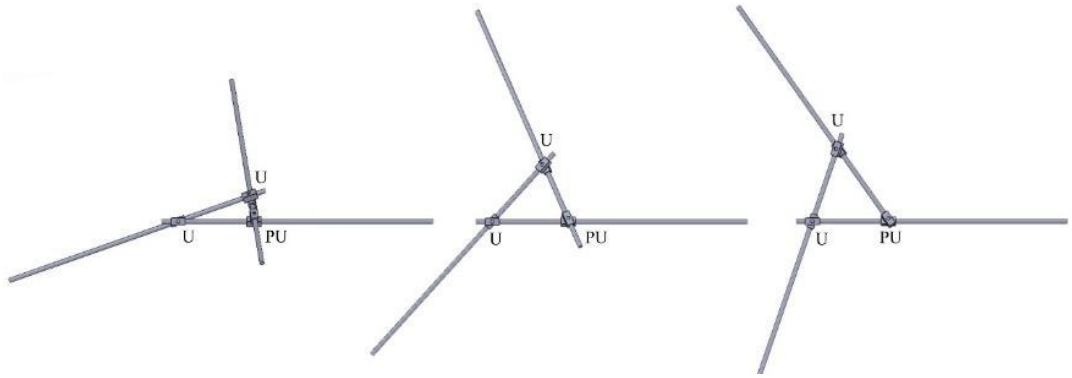

Figure 5.5. U-PU-U fan motion.

In Figure 5.6, one more P joint is added to one of the intersection points, and one R joint is canceled. Two nexors have P joints, meaning there are two variable engagement lengths (Figure 5.7).

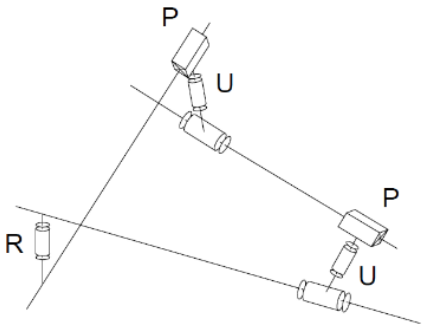

Figure 5.6. PU-PU-R⊥ fan.

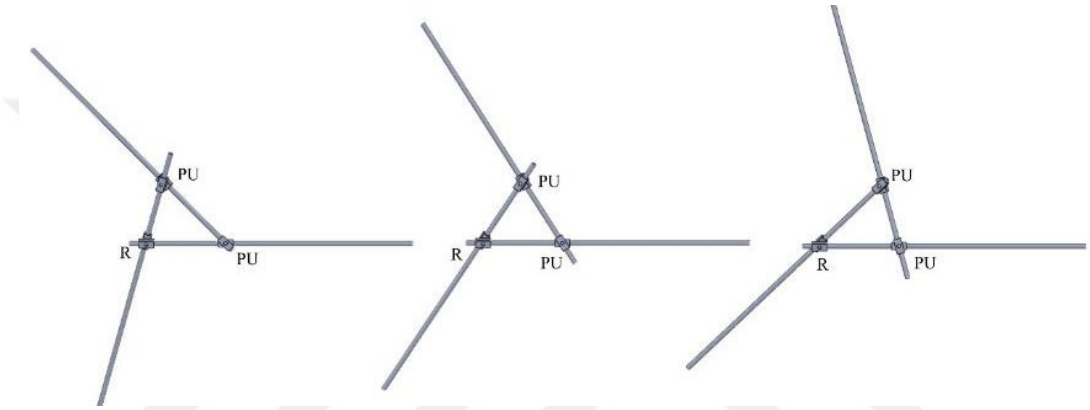

Figure 5.7. PU-PU-R⊥ fan motion

The organization of the joints PU (Figure 5.6) is changed as UP (Figure 5.8) to see the change in the motion. The change in engagement lengths is clearly seen in Figure 5.9.

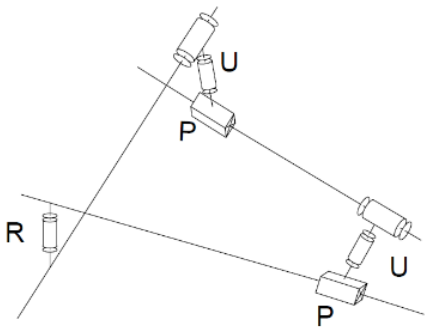

Figure 5.8. UP-UP-R⊥ fan.

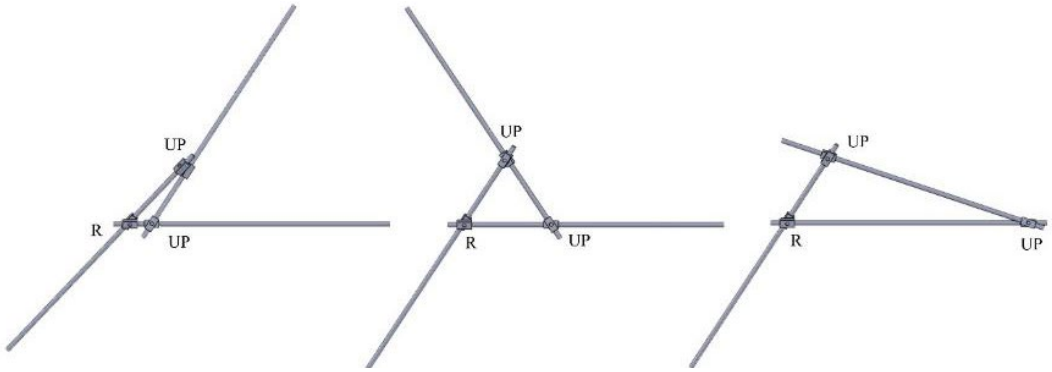

Figure 5.9. UP-UP-R$_\perp$ fan motion.

In Figure 5.10, there are two P and five R joints whose two engagement lengths are variable. The P joints are on one intersection point at which one is at the support, and the other is at the supported nexor. The motion of the fan can be seen in Figure 5.11.

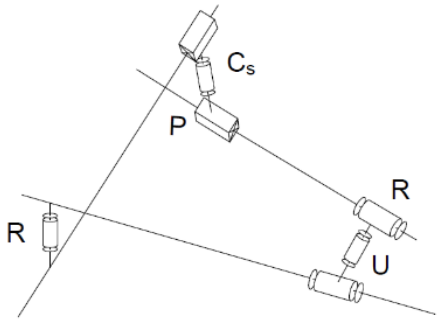

Figure 5.10. C$_s$P-R$_\parallel$U-R$_\perp$ fan.

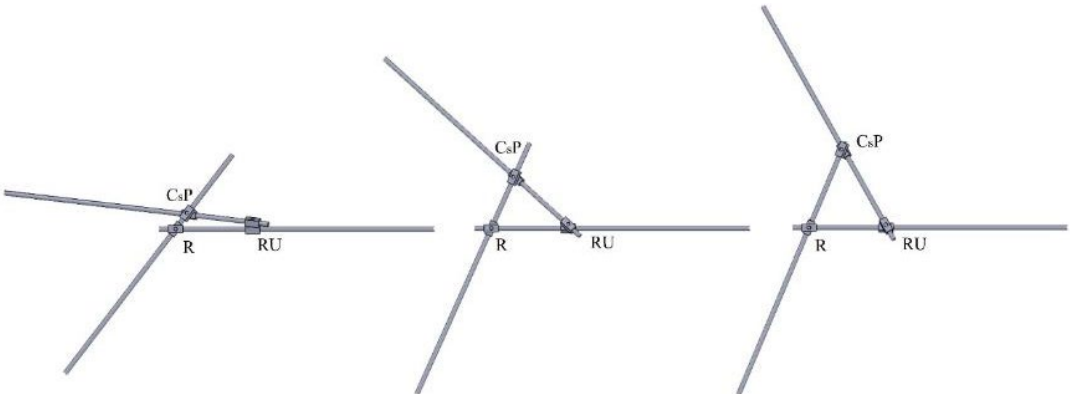

Figure 5.11. C$_s$P-R$_\parallel$U-R$_\perp$ fan motion.

In Figure 5.12, C_s-PU-U joints series fan is created. Both of the P joints are at the supported nexor. Two engagement lengths are variable. Its motion can be seen in Figure 5.13.

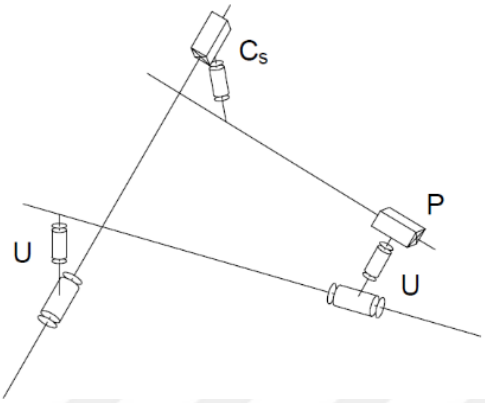

Figure 5.12. C_s-PU-U fan.

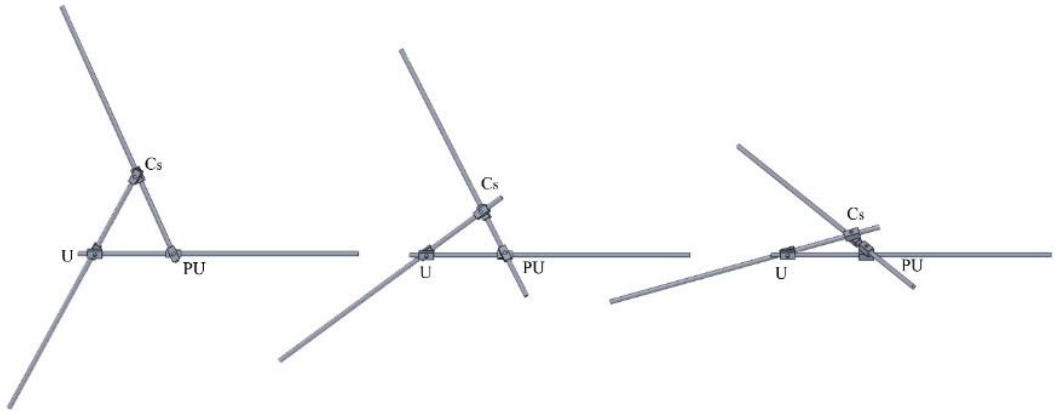

Figure 5.13. C_s-PU-U fan motion.

In Figure 5.14, three engagement lengths are variable because of the existence of three P joints. Even though it seems like there is no motion in Figure 5.15, there is a slight change in engagement lengths.

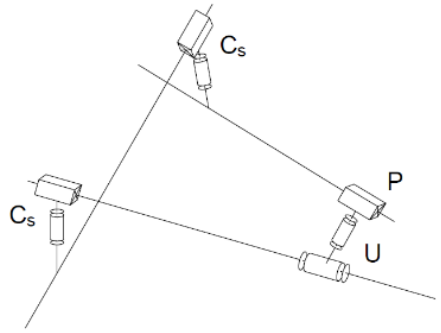

Figure 5.14. C_s-PU-C_s fan.

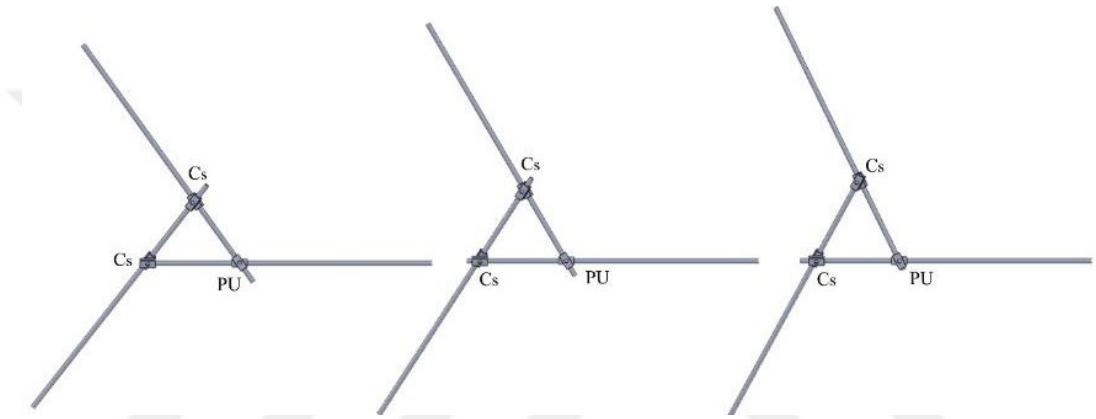

Figure 5.15. C_s-PU-C_s fan motion.

In Figure 5.16, U-PU-C_s fan is obtained. There are two P and five R joints. The engagement length is variable in the nexor where the P joint is. The motion of the fan can be seen in Figure 5.17.

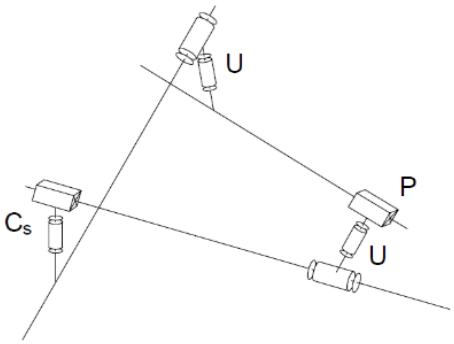

Figure 5.16. U-PU-C_s fan.

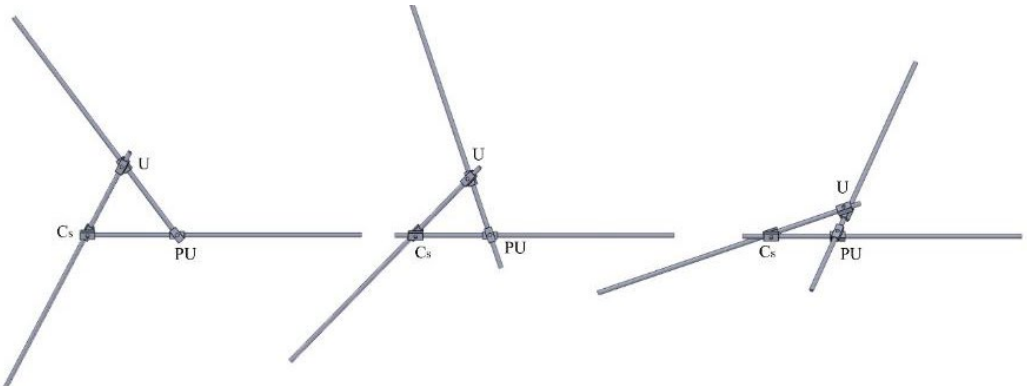

Figure 5.17. U-PU-C_s fan motion.

The organization of the intersection points is changed in Figure 5.18 to see the change in motion. While the engagement length variability is in the bottom and right nexor in Figure 5.17, it shifted to the bottom and left nexor in Figure 5.19.

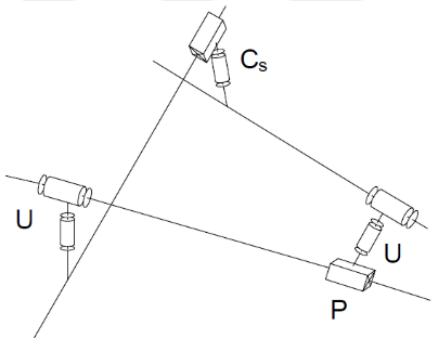

Figure 5.18. C_s-UP-U fan.

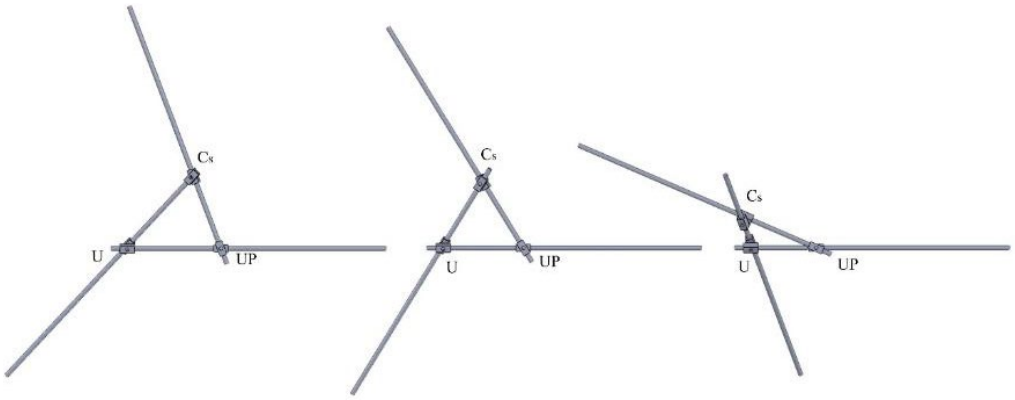

Figure 5.19. C_s-UP-U fan motion.

U joint is replaced with C_s joint in Figure 5.20. Its motion can be seen in Figure 5.21. Since there are three P joints, three engagement lengths are variable.

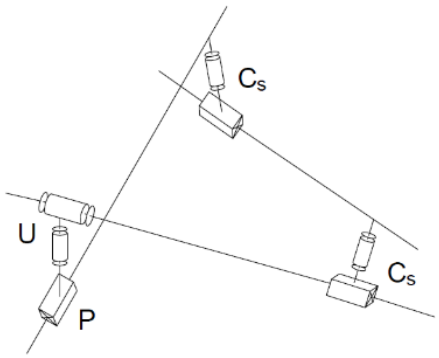

Figure 5.20. C_s-C_s-UP fan.

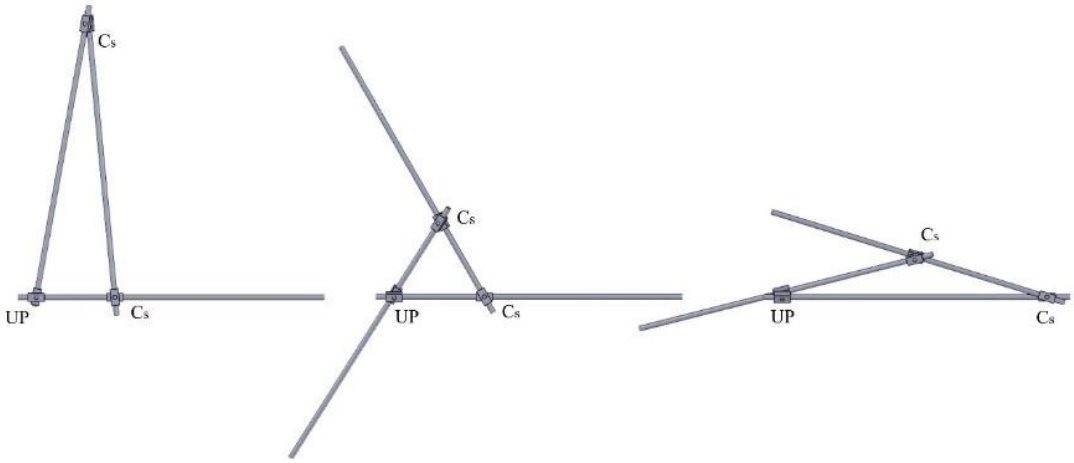

Figure 5.21 C_s-C_s-UP fan motion

In the following fan, the C joint is included at the two support nexors (Figure 5.22). Two engagement lengths are variable, as can be seen in Figure 5.23.

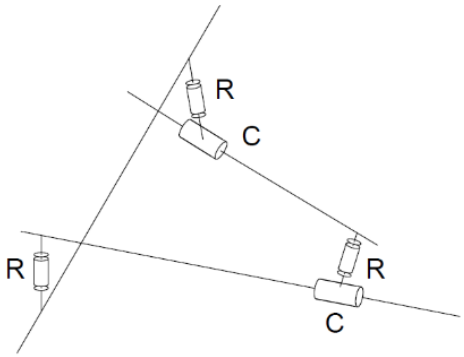

Figure 5.22. R⊥C -R⊥C -R⊥ fan.

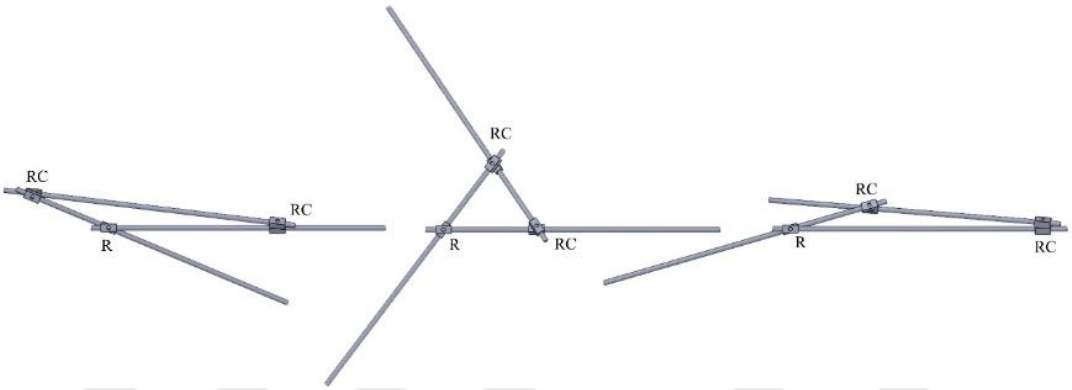

Figure 5.23. R⊥C -R⊥C -R⊥ fan motion.

C joint through the support nexor in one of the intersection points is switched and replaced through the supported nexor in Figure 5.24. The change in the motion can be seen in Figure 5.25.

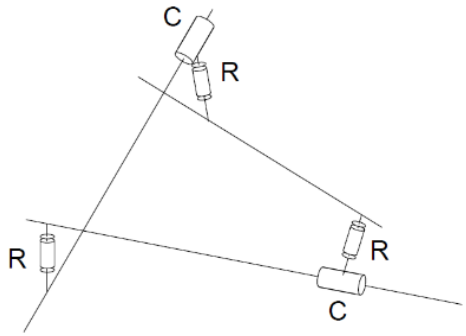

Figure 5.24. CR⊥-R⊥C-R⊥ fan.

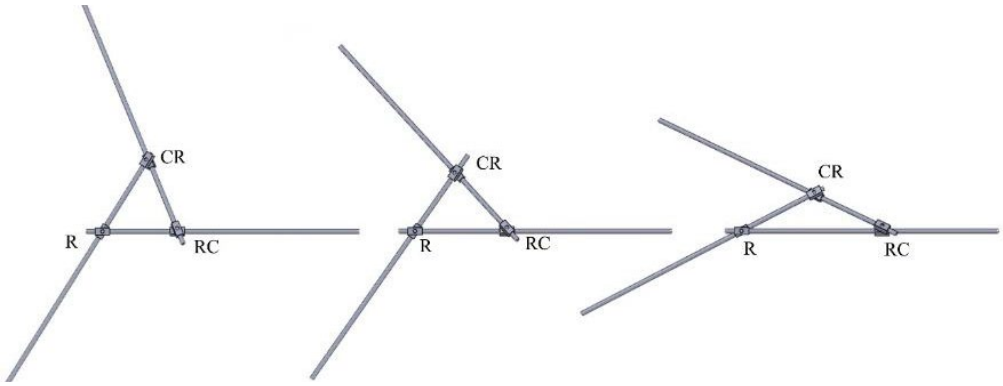

Figure 5.25. CR⊥-R⊥C-R⊥ fan motion.

In Figure 5.26, while one intersection point has CR⊥C joint series, the other two have only orthogonal R joints. There is only rotation at the two intersection points where the only R⊥ joints are. Two engagement lengths are variable, as can be seen in Figure 5.27.

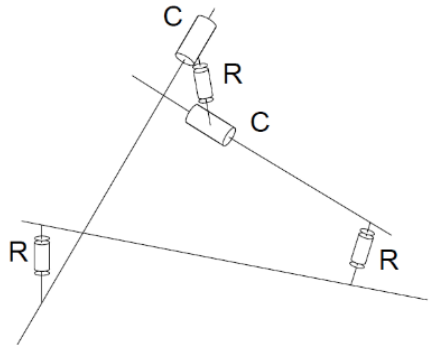

Figure 5.26. CR⊥C-R⊥-R⊥ fan.

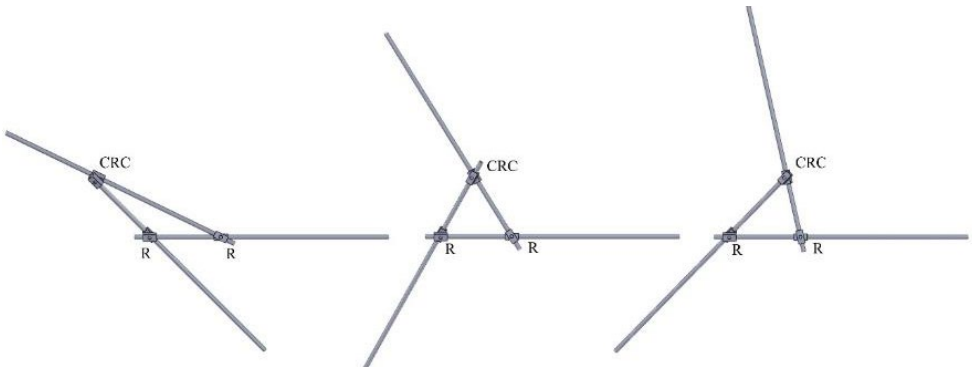

Figure 5.27. CR⊥C-R⊥-R⊥ fan motion.

In Figure 5.28, there are one C joint and five R joints. Only one nexor's engagement length is variable (Figure 5.29).

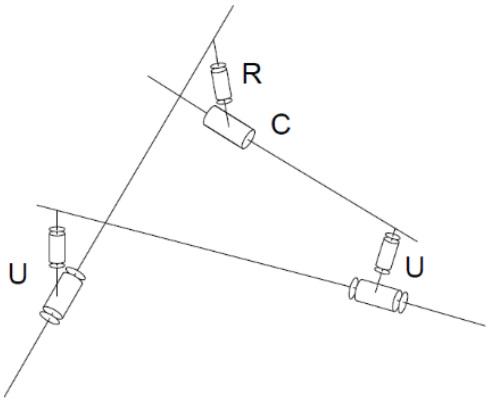

Figure 5.28. $R_{\perp}C$-U-U fan.

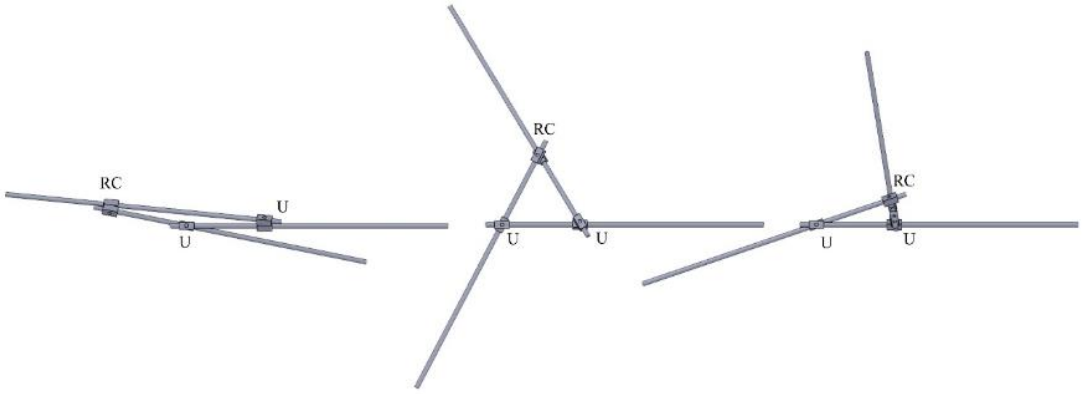

Figure 5.29. $R_{\perp}C$-U-U fan motion.

U joints in Figure 5.28 are replaced with C_s joints in Figure 5.30. Thus, the engagement lengths of three nexors become variable (Figure 5.31).

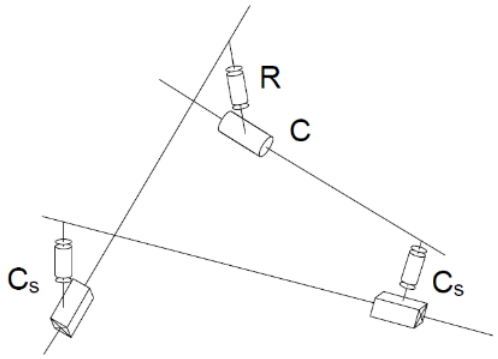

Figure 5.30. $R_{\perp}C\text{-}C_s\text{-}C_s$ fan.

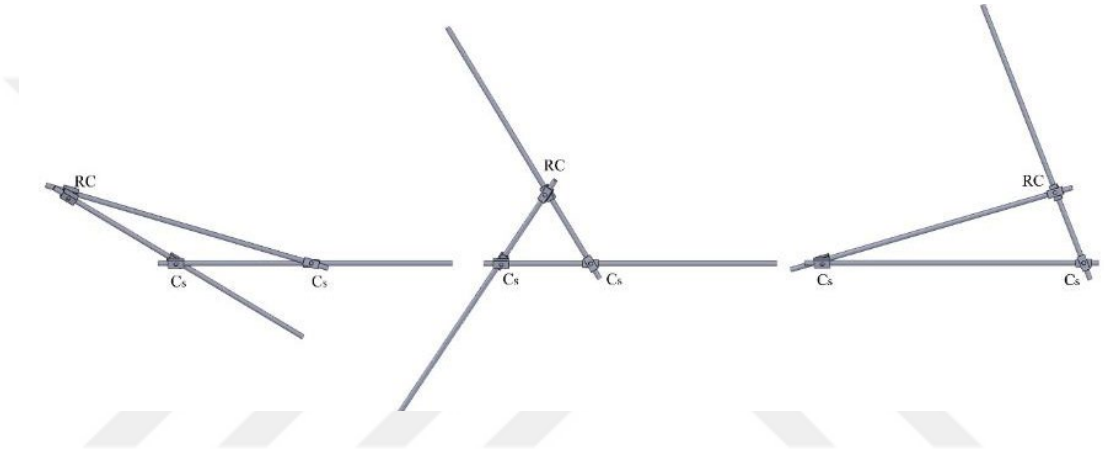

Figure 5.31. $R_{\perp}C\text{-}C_s\text{-}C_s$ fan motion.

In Figure 5.32, one of the P joints is removed, and an R joint is placed instead. By doing this, two engagement lengths become variable (Figure 5.33).

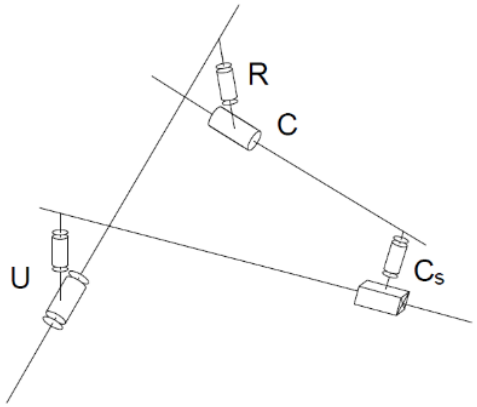

Figure 5.32. $R_{\perp}C\text{-}C_s\text{-}U$ fan.

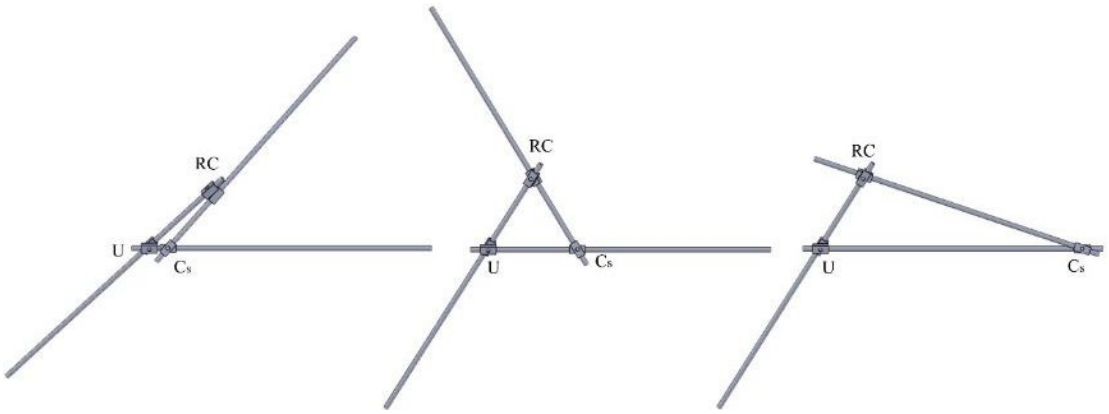

Figure 5.33. $R_{\perp}C$-C_s-U fan motion.

No single DoF fan is created without any sliding joints because of the involvement of excessive mobility in triangular fans. The motion changes according to the joint types for the other category in triangular fans. If there is a P joint, the engagement length is variable. If there is an R joint, the rotation motion can be seen. If there is a C joint, both rotation and translation motion can be observed in a fan. To conclude, there are general motions in triangular fans.

4.5. Quadrilateral Fans

In the first three single DoF RFs, the nexors are connected without using any sliding joints. In these fans, even though the engagement lengths are constant, the form of the engagement window is variable. Only three RF fans are having single DoF created with only R joints.

There need to be seven R joints to have a single DoF RF fan. In Figure 5.34, there are seven 1-DoF joints. The fan has a parallelogram motion; as two opposite intersection points come close, the other two opposing intersection points move away (Figure 5.35).

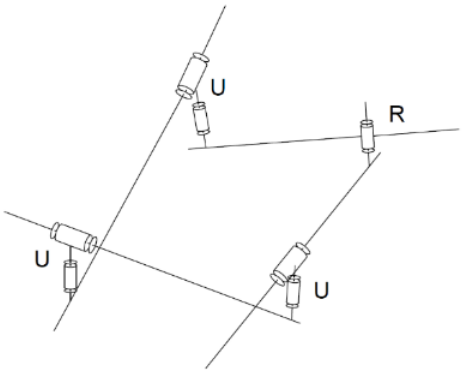

Figure 5.34. U- R⊥-U-U fan.

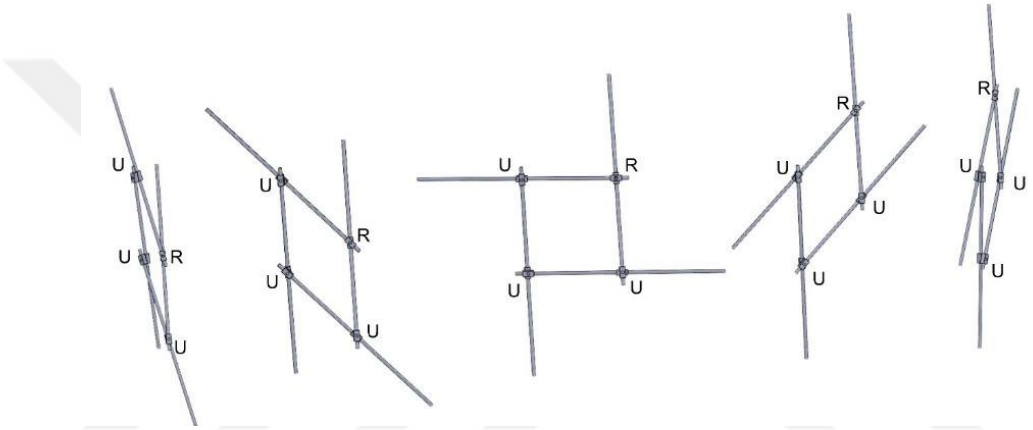

Figure 5.35. Motion of U- R⊥-U-U fan.

In Figure 5.36, R∥U-R⊥-U-R⊥ joint series fan is created. The fan is obtained with only R joints. The motion in Figure 5.37 is similar to the motion in Figure 5.35.

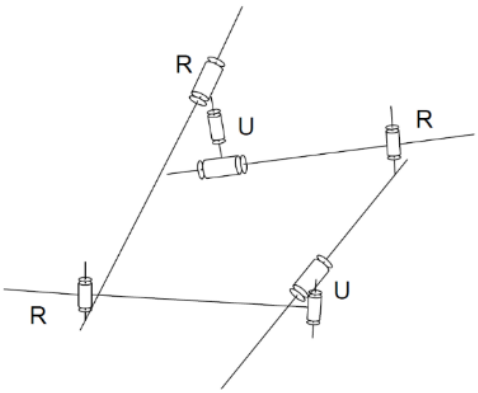

Figure 5.36. R∥U-R⊥-U-R⊥ fan.

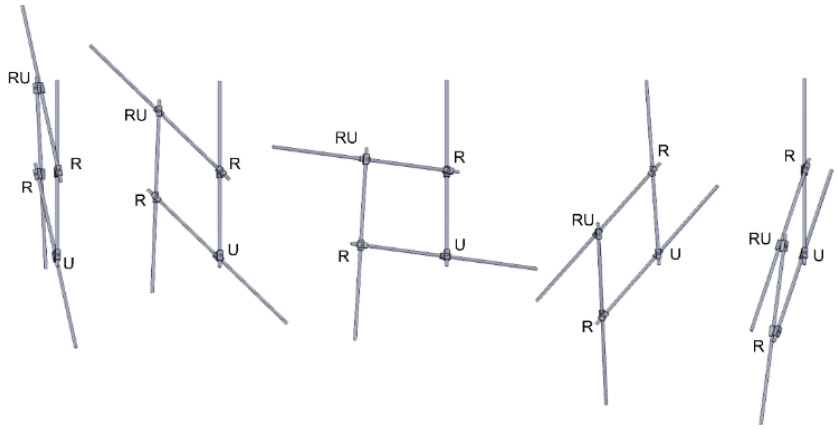

Figure 5.37. Motion of $R_{\parallel}U\text{-}R_{\perp}\text{-}U\text{-}R_{\perp}$ fan.

The joint series in Figure 5.36 is changed in Figure 5.38 to see the change in the motion. A parallelogram motion can be seen in Figure 5.39.

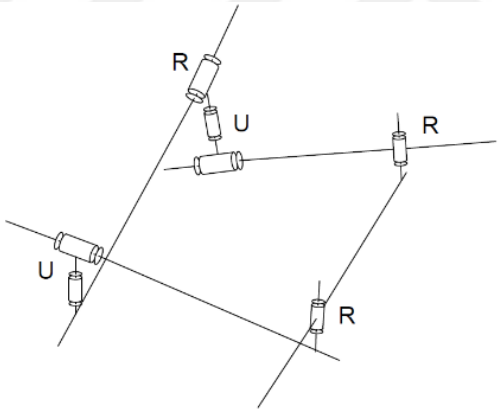

Figure 5.38. $R_{\parallel}U\text{-}R_{\perp}\text{-}R_{\perp}\text{-}U$ fan.

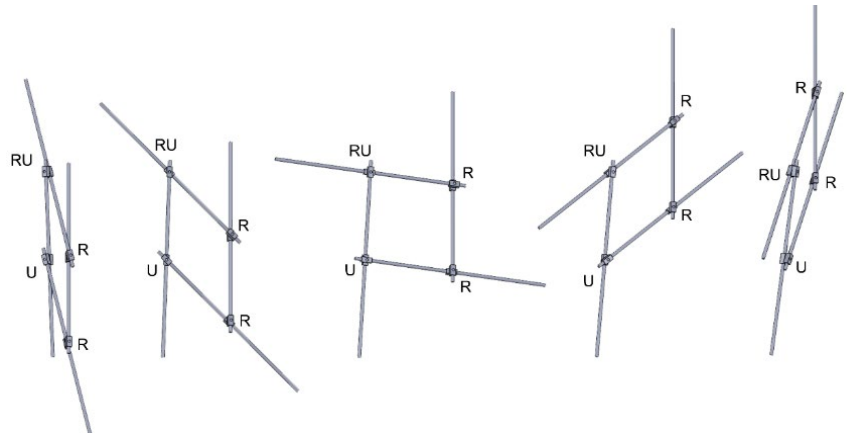

Figure 5.39. Motion of $R_{\parallel}U\text{-}R_{\perp}\text{-}R_{\perp}\text{-}U$ fan.

From this part, the nexors are connected with sliding joints. In these fans, the engagement lengths are not constant, and the form of the engagement window is variable. Several fans having a single DoF are analyzed, and the fans with excessive mobility are not shown.

In Figure 5.40, there are six R and one P joint. P joint is on the supported nexor. Since the P joint allows sliding, the engagement length of one nexor is variable (Figure 5.41).

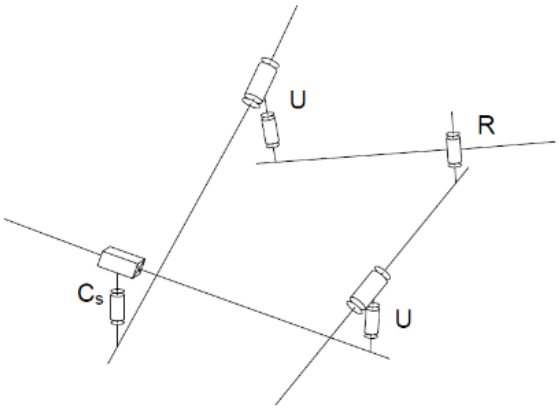

Figure 5.40. U-R$_\perp$-U-C$_s$ fan.

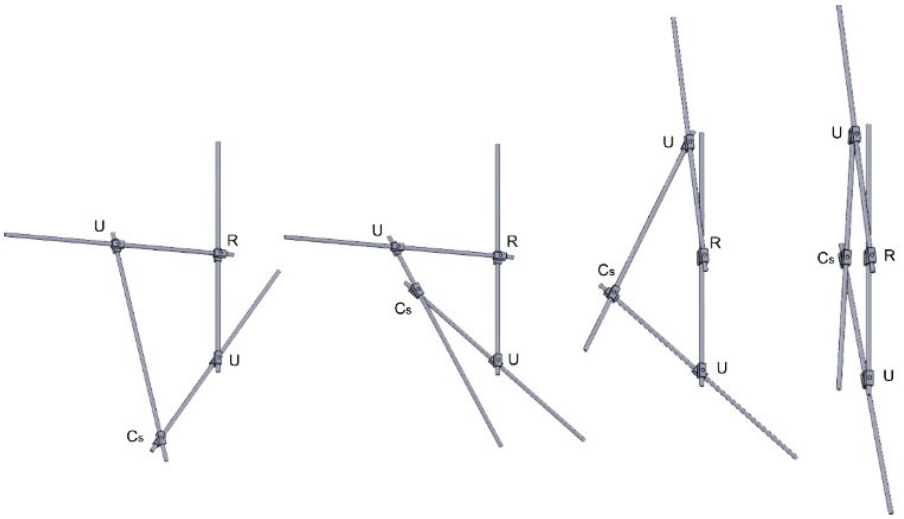

Figure 5.41. Motion of U-R$_\perp$-U-C$_s$ fan.

In Figure 5.42, one more P joint is used in one of the supported nexors instead of an R joint. Thereby, two engagement lengths are variable (Figure 5.43).

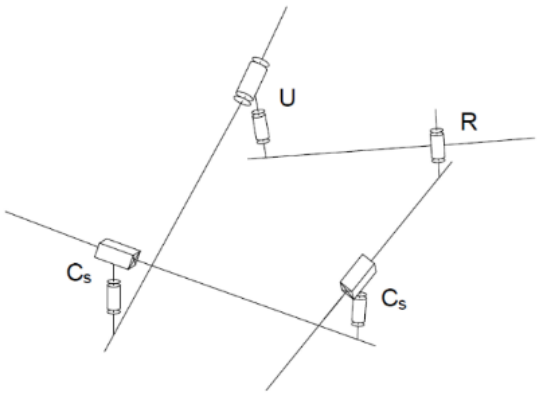

Figure 5.42. U-$R_{\perp}$-C_s-C_s fan.

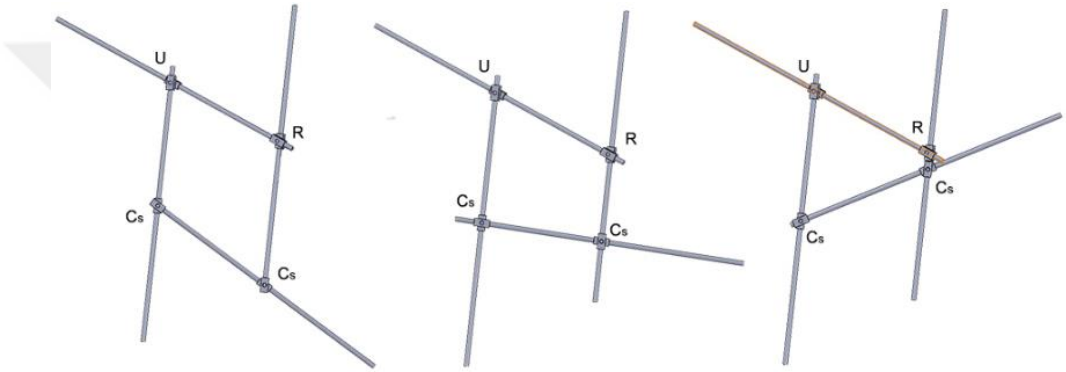

Figure 5.43. Motion of U- $R_{\perp}$-C_s-C_s fan.

In Figure 5.44, the series of joints are changed. While C_s joints were consecutive in the previous fan, C_s joints are placed opposite each other in this one. Two engagement lengths can vary (Figure 5.45).

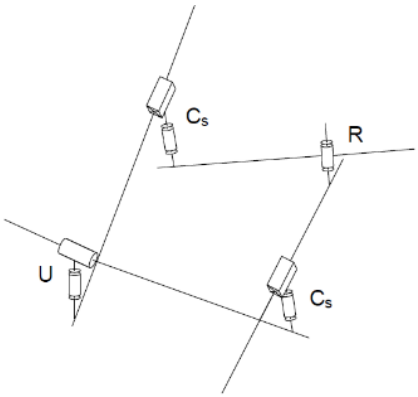

Figure 5.44. C_s-$R_{\perp}$-C_s-U fan.

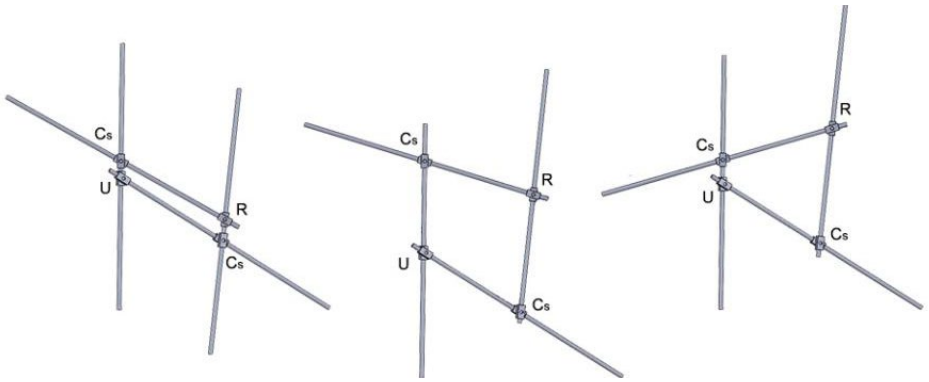

Figure 5.45. Motion of C_s-$R_\perp$-C_s-U fan.

In Figure 5.46, one more P joint is used instead of an R joint. Consequently, there are four R and three P joints. Thereby, the engagement lengths of the three nexors become variable (Figure 5.47).

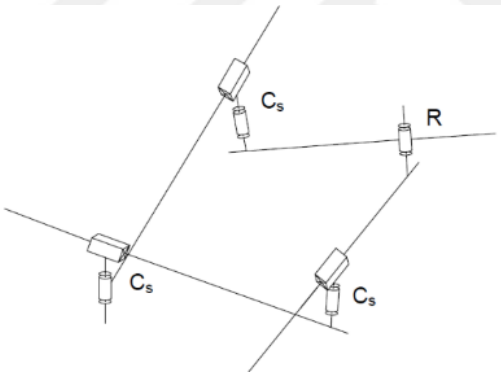

Figure 5.46. C_s-$R_\perp$-C_s-C_s fan.

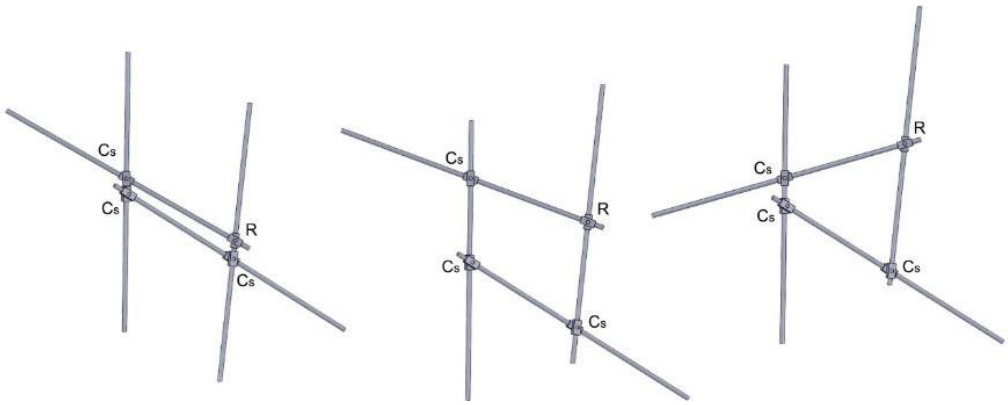

Figure 5.47. Motion of C_s-$R_\perp$-C_s-C_s fan.

There are six R and a P joints in Figure 5.48. One of the nexors' engagement lengths can change when the fan moves (Figure 5.49).

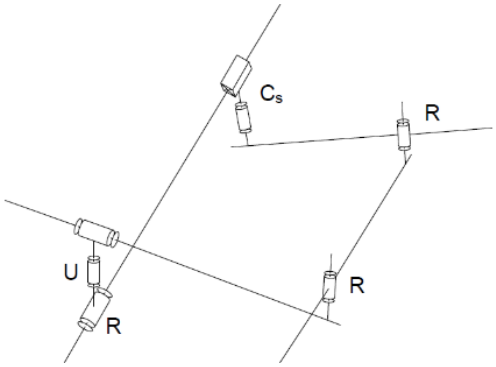

Figure 5.48. C_s-$R_\perp$-$R_\perp$-$UR_\parallel$ fan.

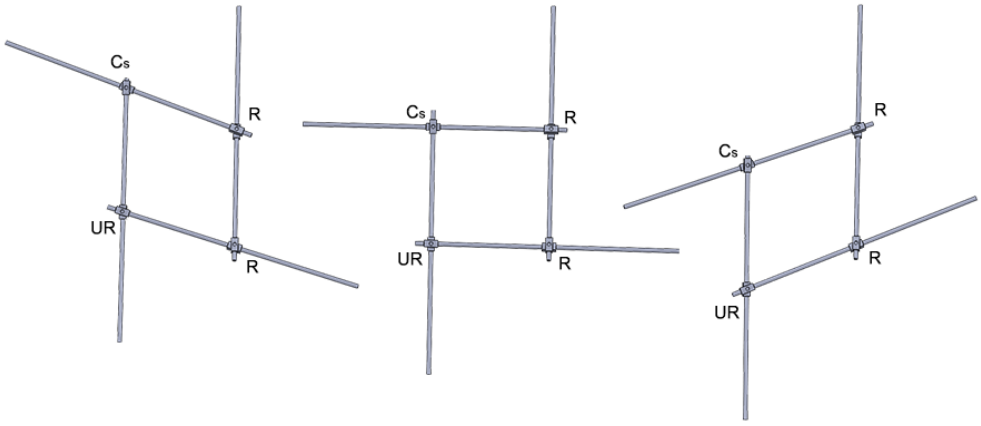

Figure 5.49. Motion of C_s-$R_\perp$-$R_\perp$-$UR_\parallel$ fan.

The series of joints are changed in Figure 5.50. While C_s and UR joint series were consecutive in the previous fan, they are opposite each other in this fan. The difference in motion can be seen in Figure 5.51.

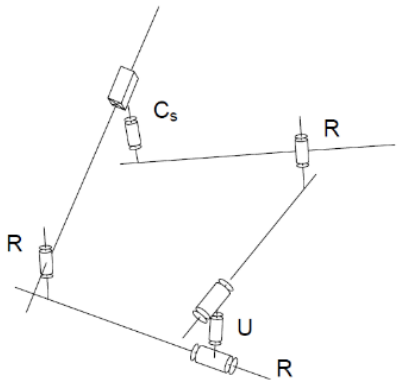

Figure 5.50. C_s-$R_\perp$-$UR_\parallel$-$R_\perp$ fan.

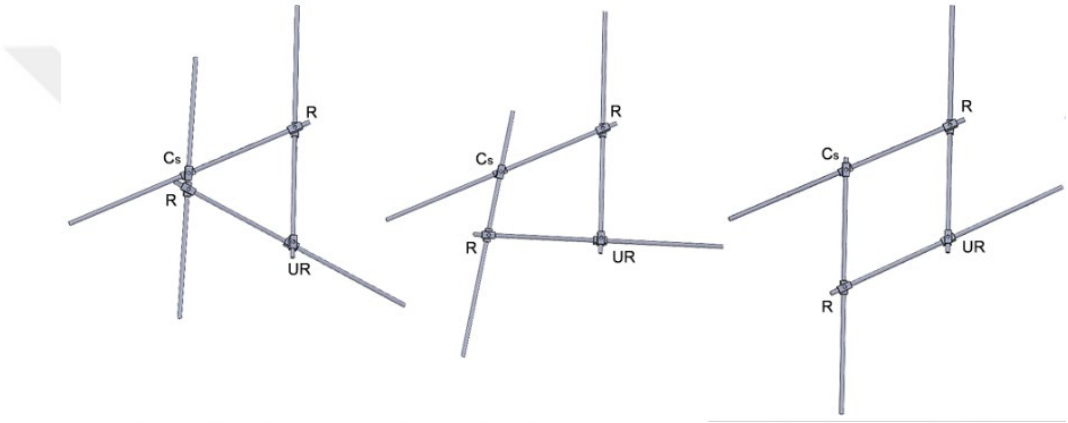

Figure 5.51. Motion of C_s-$R_\perp$-$UR_\parallel$-$R_\perp$ fan.

One nexor's engagement length is variable since there is one P joint in Figure 5.52. Other engagement lengths are constant (Figure 5.53).

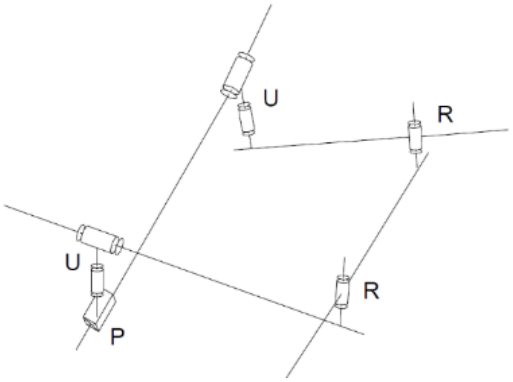

Figure 5.52. U-$R_\perp$-$R_\perp$-UP fan.

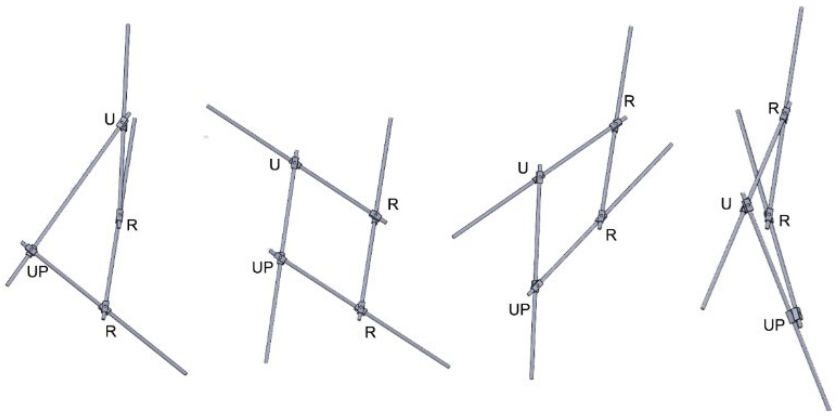

Figure 5.53. Motion of U-R⊥-R⊥-UP fan.

The series of joints are changed in Figure 5.54. While the U and UP joint series were consecutive in the previous fan, they are opposite each other in this fan. The change in the motion can be seen in Figure 5.55.

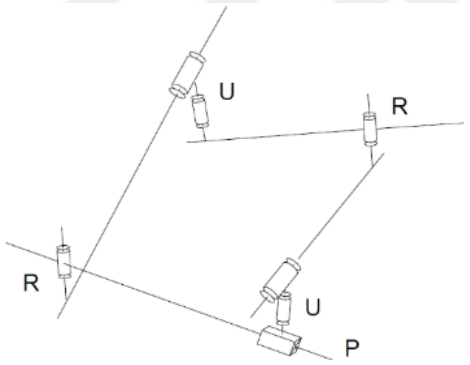

Figure 5.54. U-R⊥-UP-R⊥ fan.

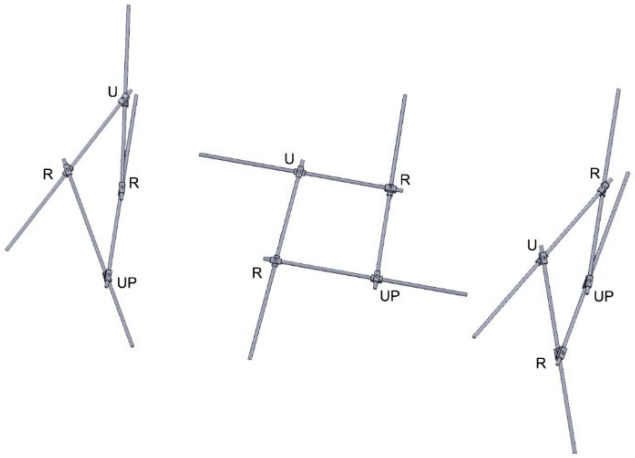

Figure 5.55. Motion of U-R⊥-UP-R⊥ fan.

One more P joint is added in the Figure 5.56 configuration, and the joint series is changed. Two P joints allow two engagement lengths to become variable in Figure 5.57.

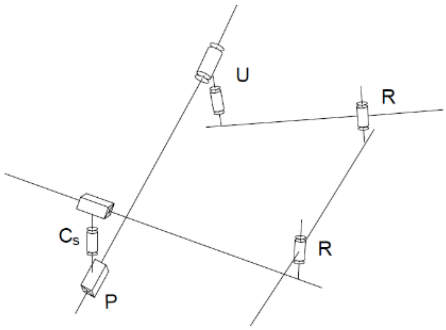

Figure 5.56. U-R⊥-R⊥-CsP fan.

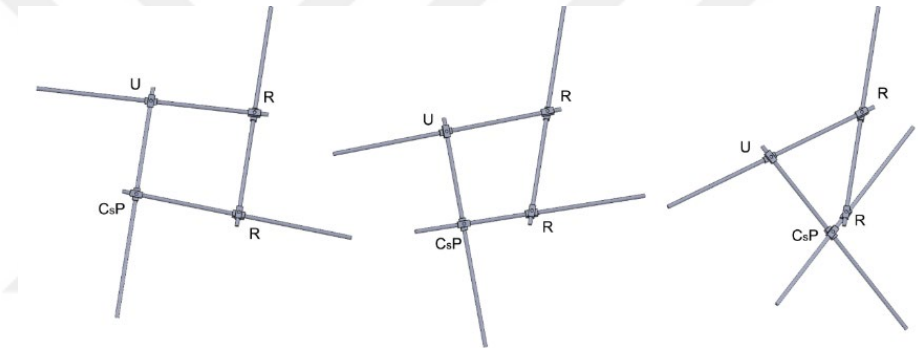

Figure 5.57. Motion of U-R⊥-R⊥-CsP fan.

The series of joints are changed in Figure 5.58. While U and CsP joint series were consecutive in the previous fan, they are opposite each other in this fan. The change in the fan motion can be seen in Figure 5.59.

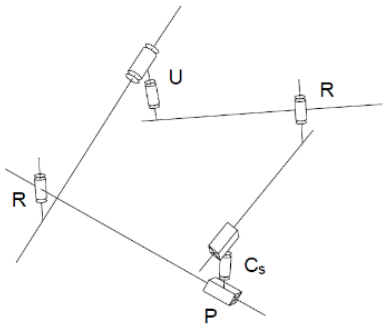

Figure 5.58 U-R⊥-CsP-R⊥ fan

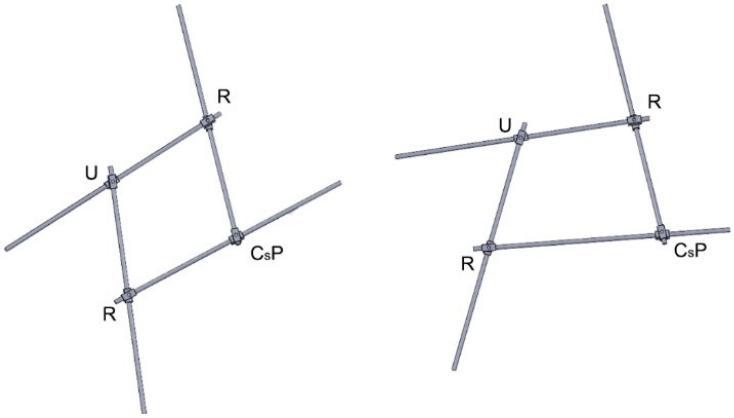

Figure 5.59. Motion of U-R⊥-CsP-R⊥ fan.

In Figure 5.60, there are two P and five R joints. Its motion can be seen in Figure 5.61.

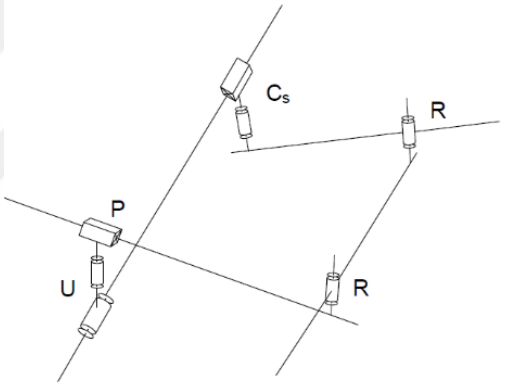

Figure 5.60. Cs-R⊥-R⊥-PU fan.

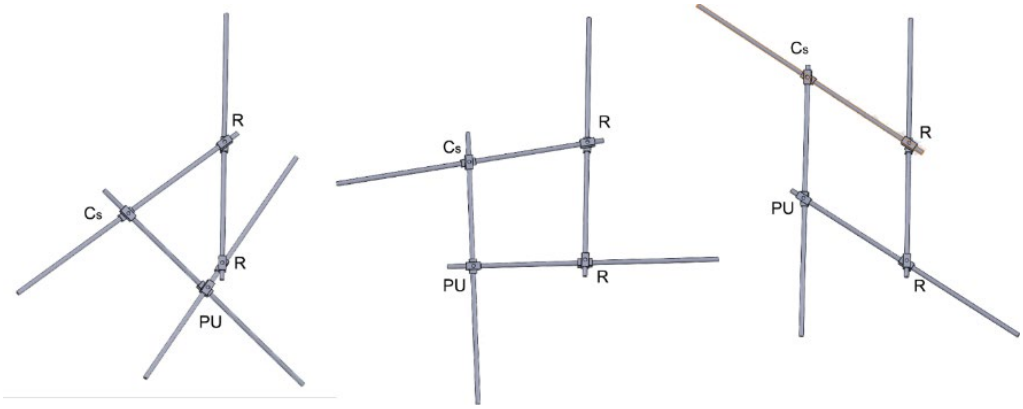

Figure 5.61. Motion of Cs-R⊥-R⊥-PU fan.

The series of joints are changed in Figure 5.62. While C_s and PU joint series were consecutive in the previous fan, they are opposite to each other in this fan. The difference in the motion can be seen in Figure 5.63.

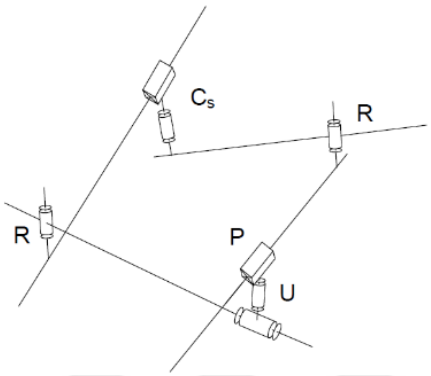

Figure 5.62. C_s-$R_\perp$-PU-$R_\perp$ fan.

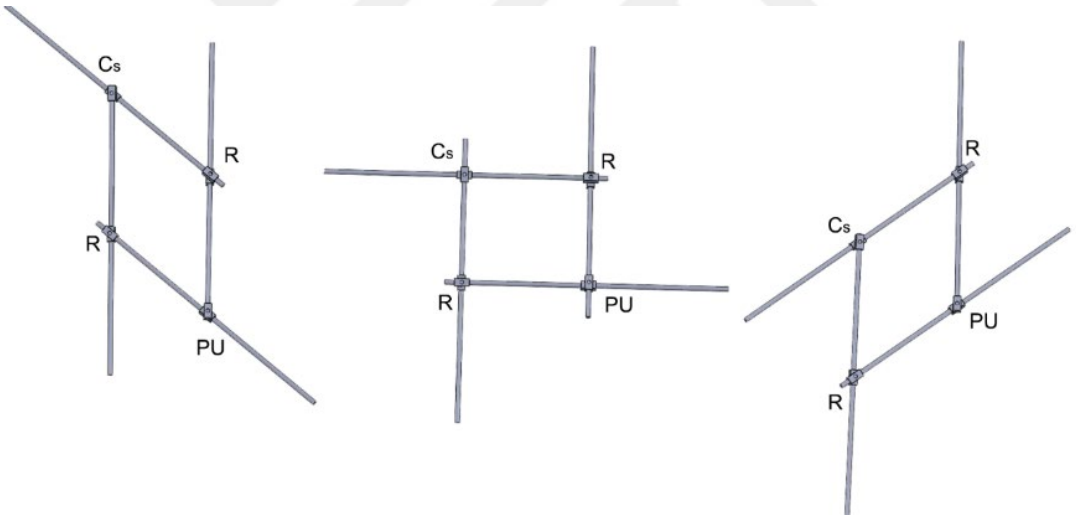

Figure 5.63. Motion of C_s-$R_\perp$-PU-$R_\perp$ fan.

A C joint is added to one of the intersection points (Figure 5.64). Its motion can be seen in Figure 5.65.

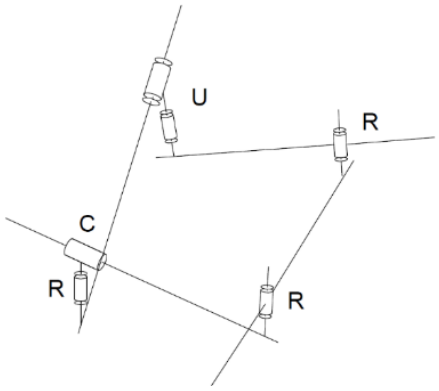

Figure 5.64. U-R⊥-R⊥-CR⊥ fan.

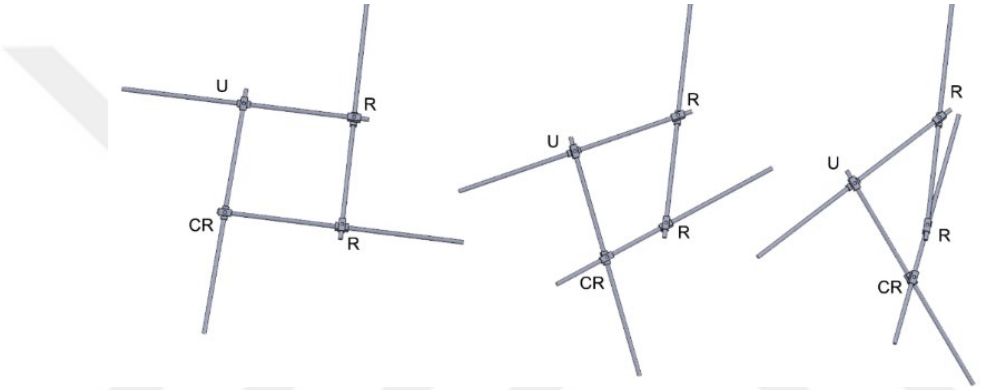

Figure 5.65. Motion of U-R⊥-R⊥-CR⊥ fan.

The series of joints are changed in Figure 5.66. While the U and CR⊥ joint series were consecutive in the previous fan, they are opposite each other in this fan (Figure 5.67).

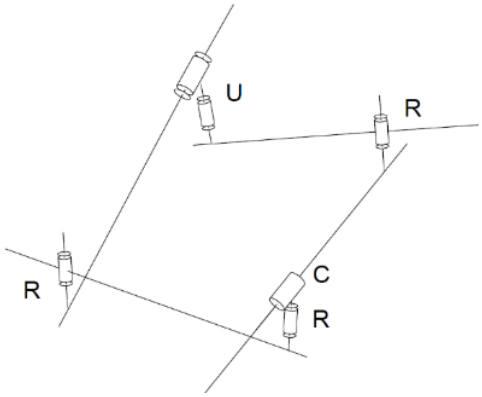

Figure 5.66. U-R⊥-CR⊥-R⊥ fan.

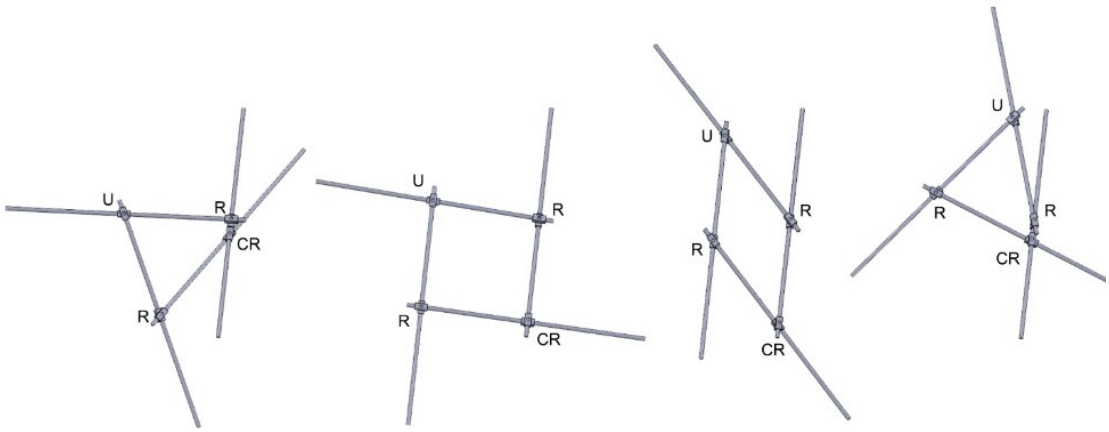

Figure 5.67. Motion of U-R⊥-CR⊥-R⊥ fan.

The series of CR⊥ is changed with R⊥C in Figure 5.68, and the change in motion is observed (Figure 5.69).

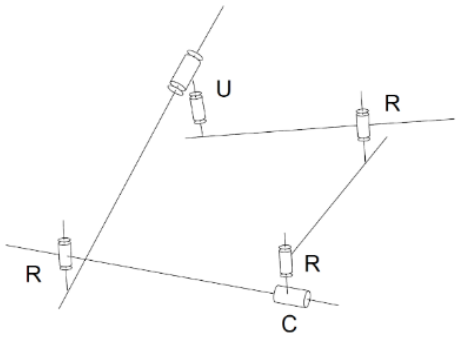

Figure 5.68. U-R⊥-R⊥C-R⊥ fan.

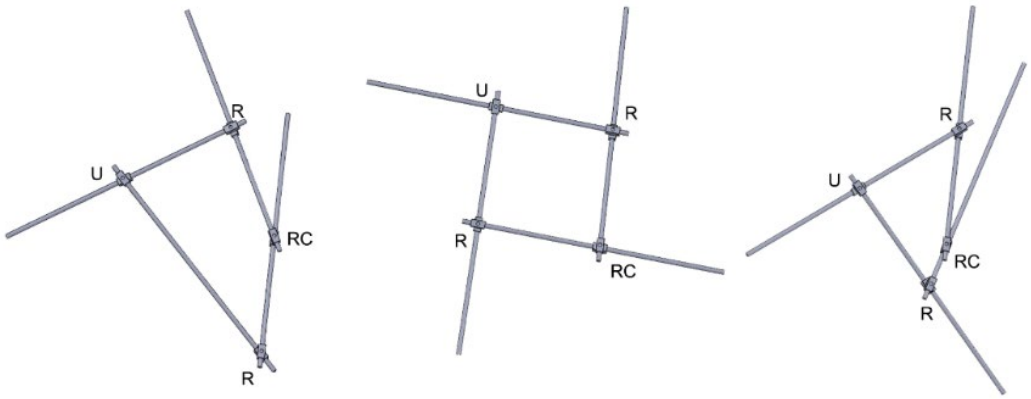

Figure 5.69 Motion of U-R⊥-R⊥C-R⊥ fan

There are one C, one P, and four R joints in Figure 5.70. Two engagement lengths are variable due to P and C joints (Figure 5.71).

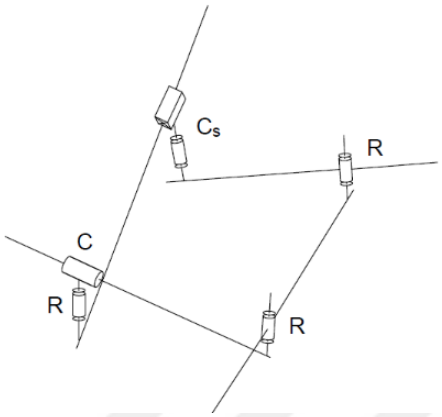

Figure 5.70. C_s-$R_\perp$-$R_\perp$-$CR_\perp$ fan.

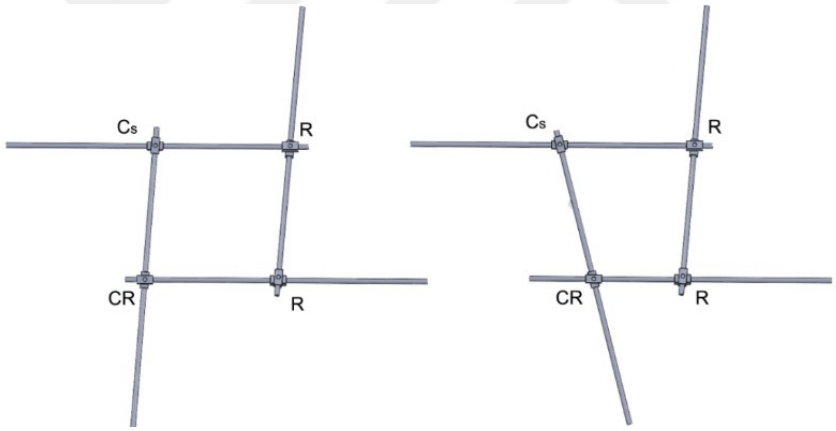

Figure 5.71. Motion of C_s-$R_\perp$-$R_\perp$-$CR_\perp$ fan.

The series of joints are changed in Figure 5.72. While C_s and $CR_\perp$ joint series were consecutive in the previous fan, they are opposite each other in this fan (Figure 5.73).

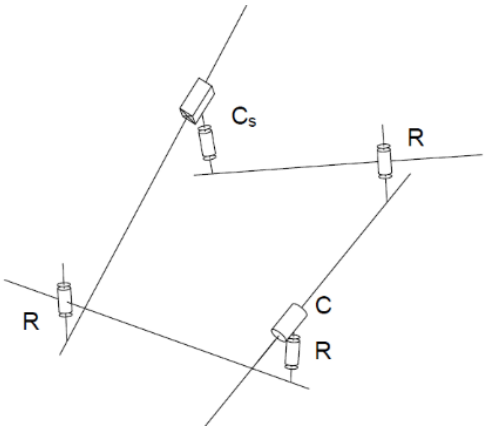

Figure 5.72. C_s-$R_\perp$-$CR_\perp$-$R_\perp$ fan.

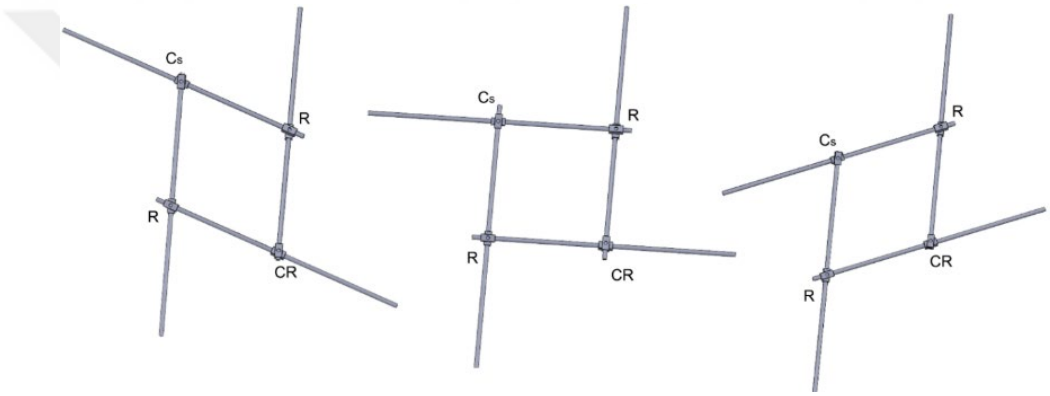

Figure 5.73. Motion of C_s-$R_\perp$-$CR_\perp$-$R_\perp$fan.

The series of $CR_\perp$ is changed with $R_\perp C$ in Figure 5.74, and the change in motion is observed (Figure 5.75).

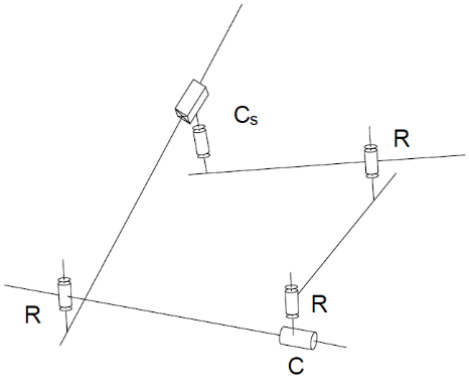

Figure 5.74. C_s-$R_\perp$-$R_\perp C$-$R_\perp$ fan.

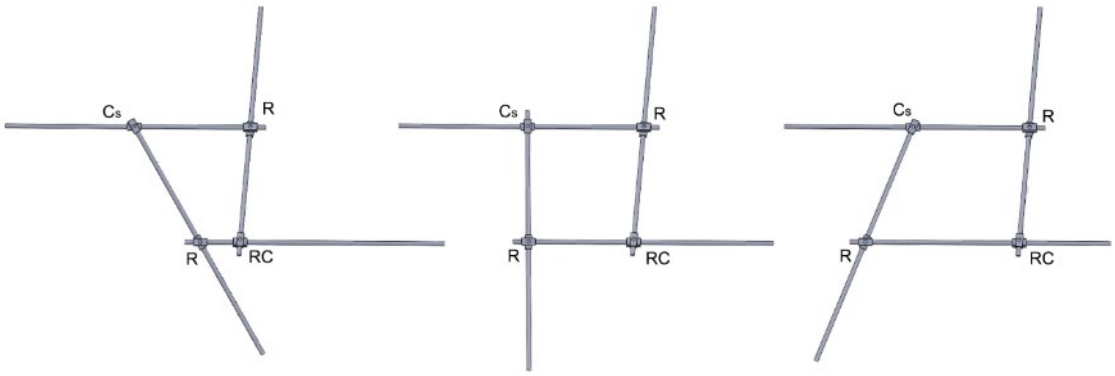

Figure 5.75. Motion of C_s-$R_\perp$-$R_\perp$C-$R_\perp$fan.

Three single DoF fans are found for the quadrilateral ones created without any sliding joints, and they have parallelogram motion. Some of the quadrilateral fans created with sliding joints also have parallelogram motion, but others haven't got specific motions which are general motions.

CHAPTER 6

NETWORKS FORMED BY USING ONLY R JOINTS

The 3d RF network is constructed piece by piece. It starts with a nexor, and another nexor is added to it to become a support, and another nexor is added to the previous nexor, and it continues so on. After several nexors are added, they create an RF network. But it is hard to know the final form of the network since many factors affect the form during the growth process. There are different types of studies to create networks from RFs. While some intend to create a planar RF network, some examine spatial RF networks.

According to Pugnale and Sassone (2014), there are three factors while designing an RF network:

- To define the fans that are going to be multiplied
- To study different types of assemblage options
- To select the joint types (Pugnale and Sassone, 2014)

Ruiz and Chilton (2002) described a classification system for RF fans to create networks. They examined combining convex and concave fans to create planar networks and polyhedra. Their classification system is composed of five items (Ariza Ruiz and Chilton, 2002):

- Number of nexors
- Single or double: Considering the prisms' diagonals, single fans are composed of nexors terminating at the reciprocal vertex, whereas double fans are composed of nexors extending to the full length of the prism diagonal.
- Positive or negative rotation: If the ends of nexors create a clockwise moment, it is called negative rotation. Otherwise, it is called positive rotation.
- Regular or irregular: regular fans have an equal length of nexors, height, and angles between nexors. Irregular fans are composed of variable lengths of nexors, the height of nexors from the ground, and the angle between the nexors
- Convex or concave: this is valid only for single fans since double fans are both convex and concave. If the outer ends of the nexors of the single fan are close to the

reference plane, it is convex; otherwise, it is concave (Figure 6.1) (Ariza Ruiz and Chilton, 2002).

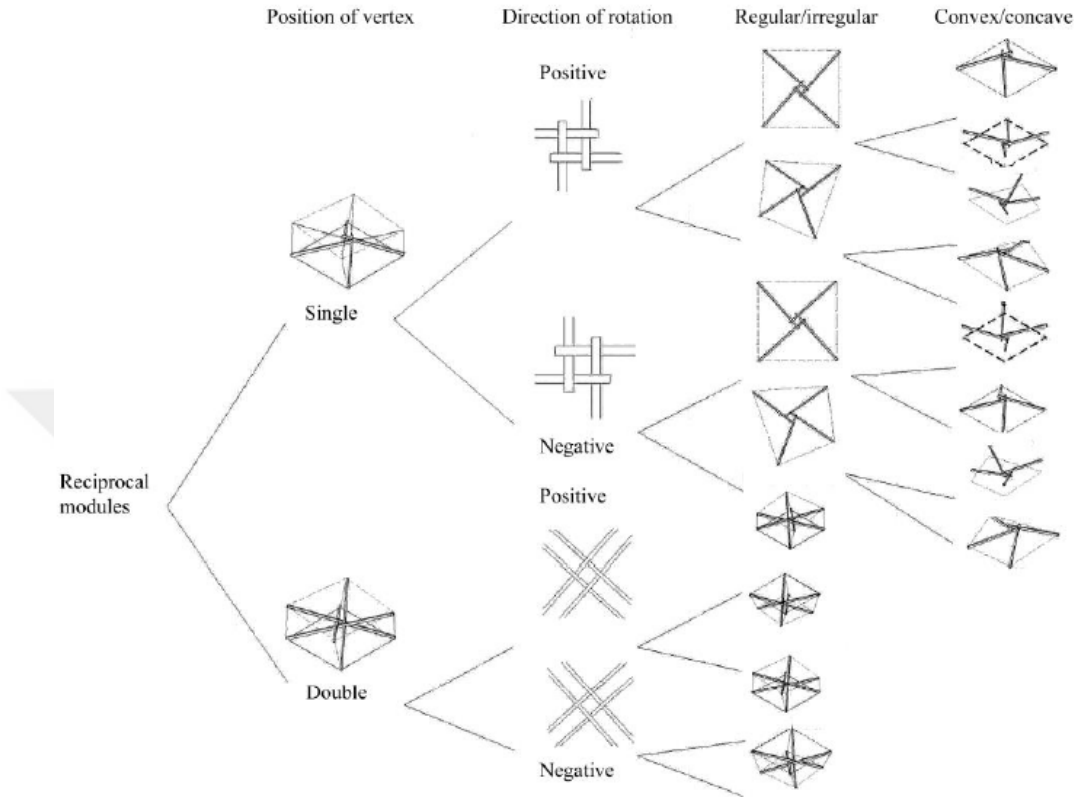

Figure 6.1. Classification Ariza Ruiz and Chilton proposed.
(Source: Ariza Ruiz and Chilton, 2002)

According to Palumba et al. (2019), there are two types of RF networks: inclined RFs and flat RFs. In the first type, nexors are placed on top of each other, and the fan is out of the plane. The nexors are on the same plane in the second type and create a flat form. There are three methods to create an RF network:

- starting with a fan and reaching to the surface, which is a bottom-up process
- starting with a surface and finding the fan that fits the surface, which is a top-down process
- dynamic relaxation or genetic algorithm methods start by finding the spatial definition of the chosen frame by reducing its geometrical errors from a non-compatible fan (Palumbo, Pone, and Lancia, 2019).

Moreover, Qi et al. (2019) studied two-dimensional hex-tri RF networks. The network with hex-tri units is arranged in rings about a center. In Figure 6.2, a) represents a unit, b) represents the first ring around a central unit, and c) represents the second ring around the first ring, and a central unit and whole system create the network (Figure 6.2) (Qi et al., 2019).

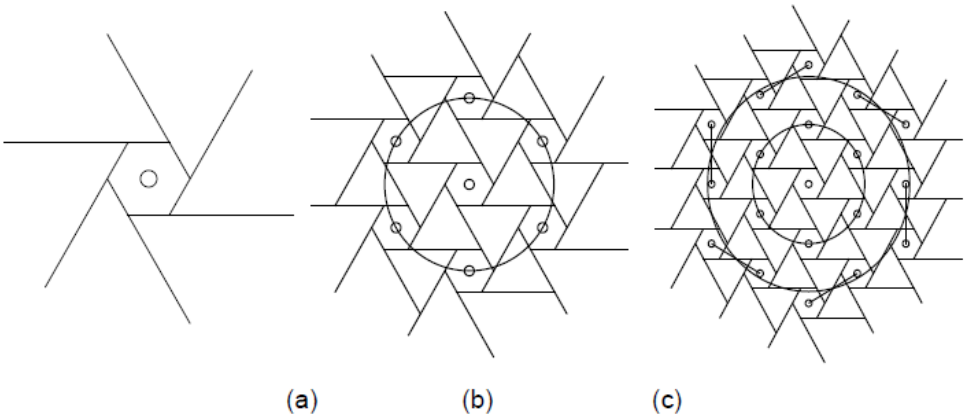

Figure 6.2. Hex-tri Multi Reciprocal Network.
(Source: Qi et al., 2019)

More RF network studies or projects are described in Chapter 2 apart from these studies.

This chapter of the thesis study aims to create a single DoF RF network by using identical 4-nexor fans. A 4-nexor fan is composed of only R joints, and an orthogonal R joint at every corner is specified as a must. The network starts with a single DoF 4-nexor RF fan and continues with adding nexors. Networks are divided into two categories according to the fan directions that are used: networks with only leftward fans and networks with both leftward and rightward fans.

5.1. Networks with only Leftward Fans

Only the leftward fan style is used to create networks in this section. Zero, single, and multi DoF networks are found.

The first network is created with $R_{\perp}$-U-U-U joint series fans. Every fan shares two nexors with its neighboring fans. In the model, it is not possible to connect nexors at

some point since the model reaches the zero DoF. So the network is shown with a drawing. A new fan occurs in the middle of the network when four fans are connected. The mobility formula is applied, and the result is -2, which means the network is a structure (Figure 6.3).

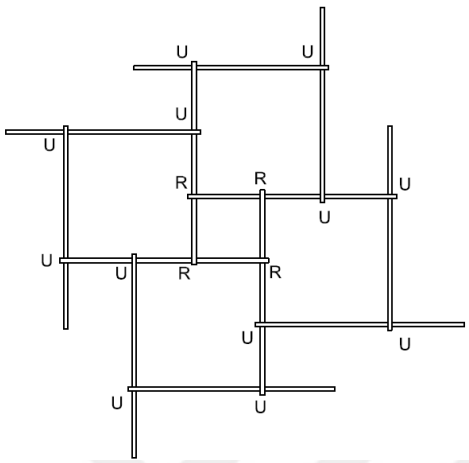

$\Sigma f_i = 28, \lambda_k = 6, L=5$

$$M = 28 - (6 * 5) = -2$$

Figure 6.3. Leftward style R⊥-U-U-U joint series network.

Since the previous network is a structure, the U-U-U-U joint series is used to increase the DoF. The connectivity sum equals 32, and the result becomes two, a multi-DoF network (Figure 6.4).

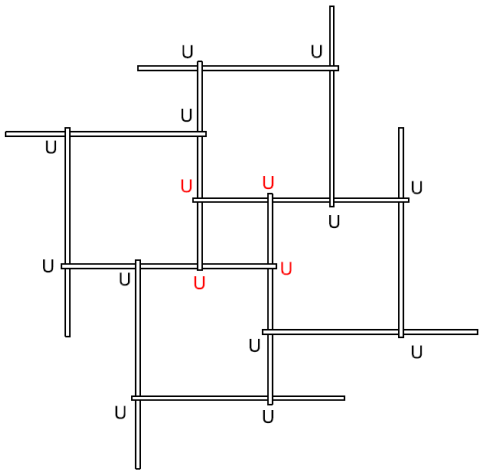

$\Sigma f_i = 32, \lambda_k = 6, L=5$

$$M = 32 - (6 * 5) = 2$$

Figure 6.4. Leftward style U-U-U-U joint series network.

Since the aim is to have a single DoF network, three DoF should be added to the first network, or one DoF should be extracted from the second network. One intersection point should have only one R joint in the final network (Figure 6.5).

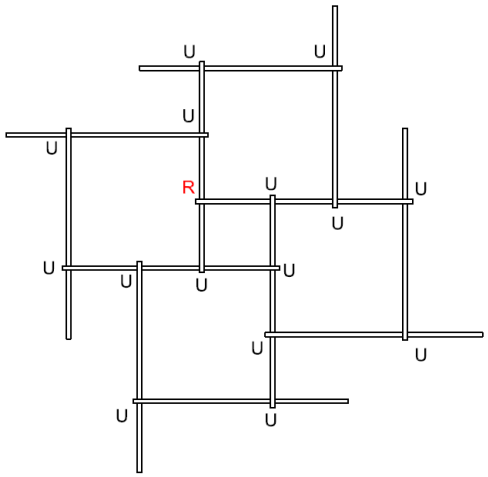

$\Sigma f_i = 31, \lambda_k = 6, L=5$

$$M = 31 - (6 * 5) = 1$$

Figure 6.5. Leftward style combination of $R_{\perp}$-U-U-U and U-U-U-U joint series network.

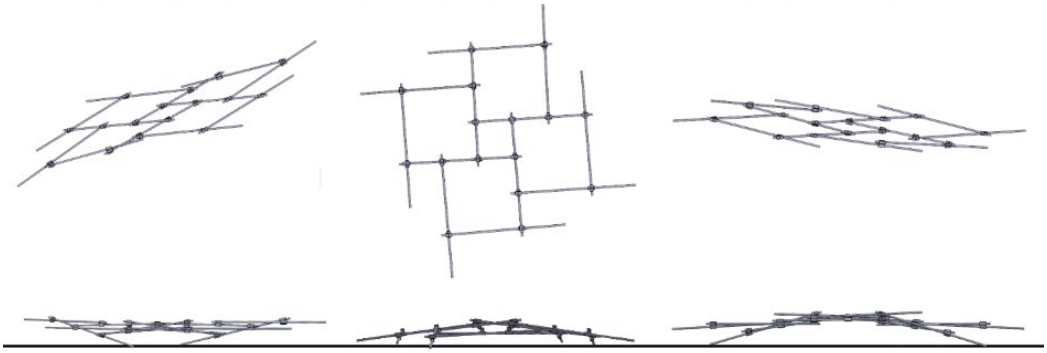

Figure 6.6. Leftward style combination of $R_{\perp}$-U-U-U and U-U-U-U joint series network motion in the top and side views.

The motion of the network can be seen in Figure 6.6. Since there are only R joints, only the rotation movement occurs. While two opposite corners get close to each other, the other two corners move away from each other during the motion in the top view. The form of the engagement windows changes from quadrilateral to rhombus. This kind of motion is called parallelogram motion and does not offer variation in the 3rd dimension (height).

5.2. Networks with both Leftward and Rightward Fans

In this part, both leftward and rightward fan styles are used to create networks. Two leftward and two rightward fans with $R_{\perp}$-U-U-U joints series are connected. A new quadrilateral fan occurs in the middle of the network when four fans are attached. Every fan shares two nexors with its neighboring fans. In the model, it is not possible to connect nexors at some point since the model reaches zero DoF. So the network is shown with a drawing. When the mobility formula is applied, the result takes a negative value, meaning the network is a structure (Figure 6.7).

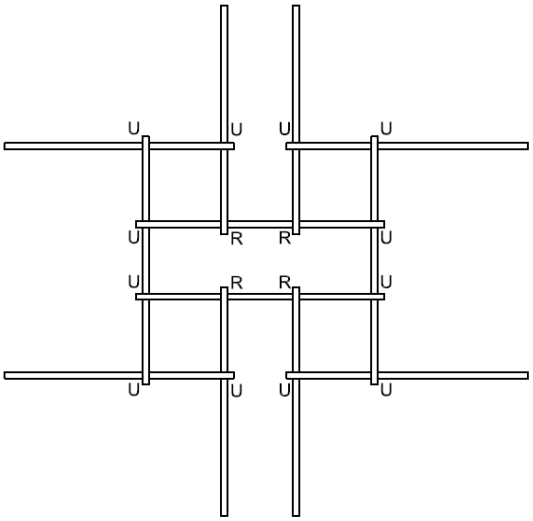

$\Sigma f_i = 28$, $\lambda_k = 6$, L=5

$$M = 28 - (6 * 5) = -2$$

Figure 6.7. Leftward and rightward style $R_{\perp}$-U-U-U joint series network.

The U-U-U-U joint series network is created by adding four R joints to the intersection points having only R. The network has two DoF (Figure 6.8).

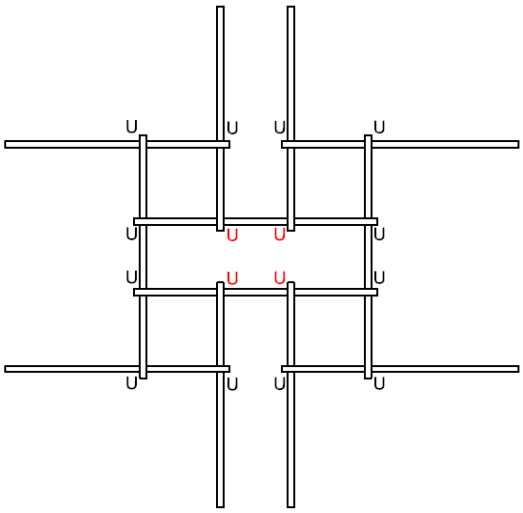

$\Sigma f_i = 32$, $\lambda_k = 6$, L=5

$$M = 32 - (6 * 5) = 2$$

Figure 6.8. Leftward and rightward style U-U-U-U joint series network.

Three DoF should be added to the first network, or one DoF should be extracted from the second network to reach a single DoF network. There should be only one intersection point in this network with only one R joint (Figure 6.9).

Since the network consists only of R joints, while two opposite corners get close to each other, the other two corners move away from each other during the motion in the top view (Figure 6.10). The network's motion in Figure 6.10 is parallelogram as in the single DoF leftward fans network.

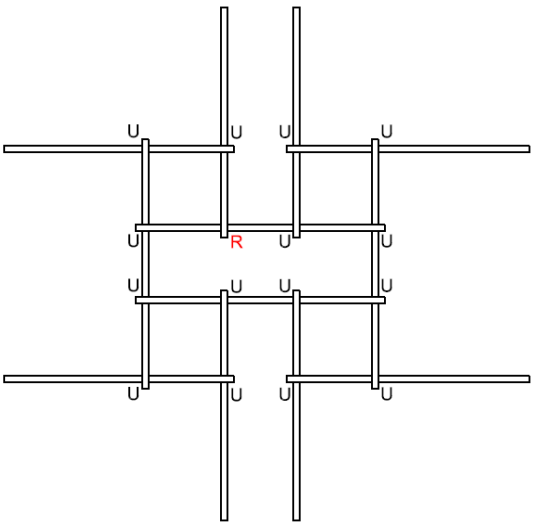

$\Sigma f_i = 31$, $\lambda_k = 6$, L=5

$$M = 31 - (6 * 5) = 1$$

Figure 6.9. Leftward and rightward style combination of $R_{\perp}$-U-U-U and U-U-U-U joint series network.

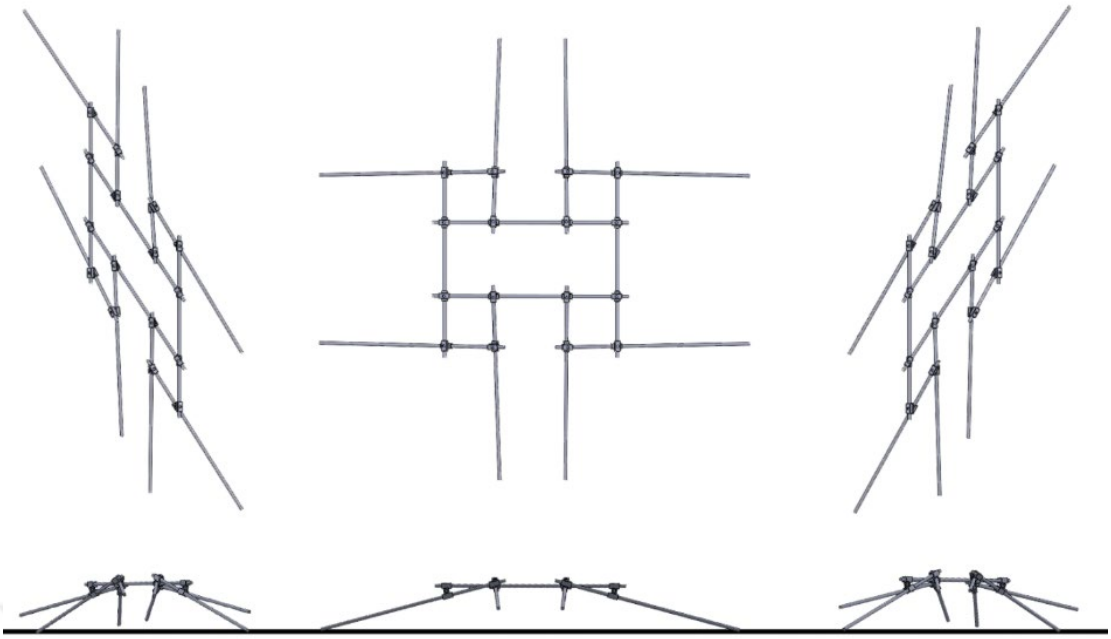

Figure 6.10. Leftward and rightward style combination of $R_{\perp}$-U-U-U and U-U-U-U joint series network motion in the top and side view.

CHAPTER 7

MOTION ANALYSIS OF SINGLE DOF RFS WITH MINIMUM NUMBER OF ORTHOGONAL R JOINTS VIA SIMULATIONS

The fan in Figure 5.34 is created with the U-R$_\perp$-U-U joint series in Chapter 5. Every nexor is connected with orthogonal R joints, and then three more R joints are added to obtain a single DoF. Its movement can be seen in Figure 5.35. Since the R joint allows rotation, the fan has a parallelogram motion in the top view, which means while the red dots are getting closer, the blue dots move away or vice versa (Figure 7.1). Because of the change in angles between nexors, only the engagement window's form is changing.

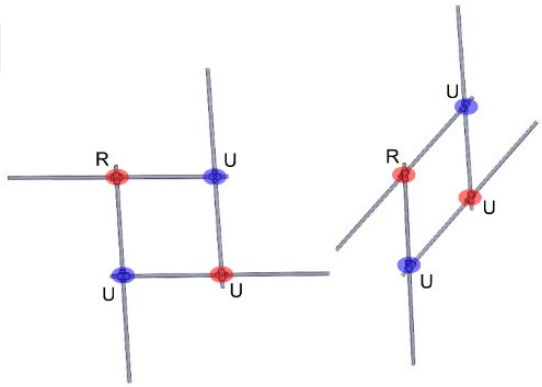

Figure 7.1. Parallelogram motion of the fan.

This chapter looks for motions where the fan changes its form from a large triangle to a small triangle or a square to a rectangle when viewed from the top view. An analogy is made as if the fans are two-dimensional. Thus, it can be said that the angle between nexors remains constant, but the engagement lengths change. This motion is called dilation motion for triangular fans and conformal motion for quadrilateral fans. Dilation motion is the resizing of the fan. Conformal motion preserves the angle between nexors but not necessarily the engagement lengths. The rotation between nexors should be

avoided to have a dilation and conformal motion due to the orthogonal R joints. Moreover, P joints are needed that give translation through nexor to make engagement windows of varying sizes.

6.1. Triangular Fans

The triangular fan in Figure 7.2 is connected with the PU-PU-P joint series. One connection point is thought to be welded instead of using an orthogonal R joint. Three nexors' engagement lengths are variable because of the three P joints. But there are also rotations that cause a general motion, as stated in Chapter 5. The motion of the fan can be seen in Figure 7.3.

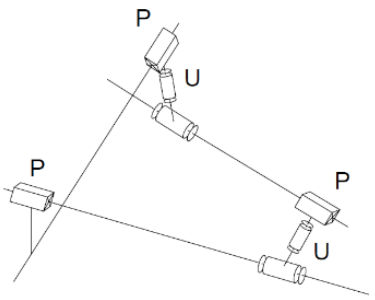

$\Sigma f_i = 7, \lambda_k = 6$

$M = 7 - 6 = 1$

Figure 7.2. PU-PU-P fan.

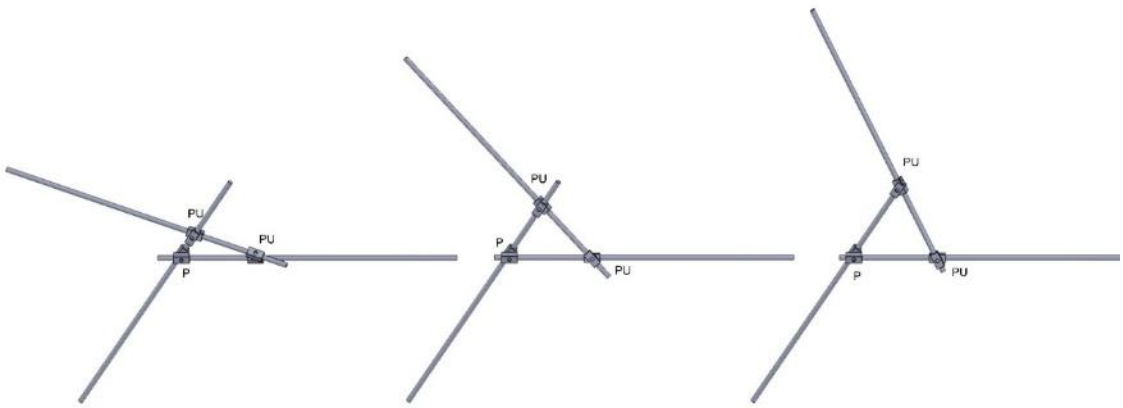

Figure 7.3. PU-PU-P fan motion.

One of the P joints in Figure 7.2 is replaced with an R joint in Figure 7.4a. Since two R joints exist in a nexor, there is excessive mobility. So, the PU-$R_{\parallel}$U-P joint series is a structure. Then the organization of the fan is changed in Figure 7.4b. There is no more excessive mobility. The motion of the PU-P-$R_{\parallel}$U fan can be seen in Figure 7.5.

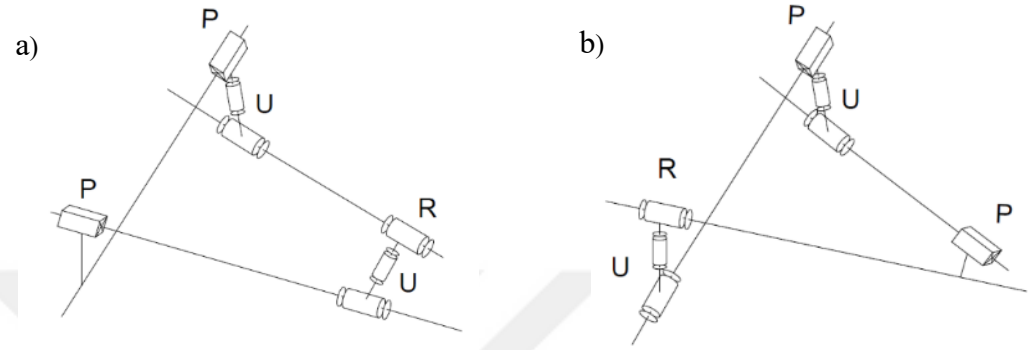

$\Sigma f_i = 7, \lambda_k = 6, E=1$
$M = 7 - 6 - 1 = 0$

$\Sigma f_i = 7, \lambda_k = 6$
$M = 7 - 6 = 1$

Figure 7.4. a) PU-$R_{\parallel}$U-P fan, b) PU-P-$R_{\parallel}$U fan.

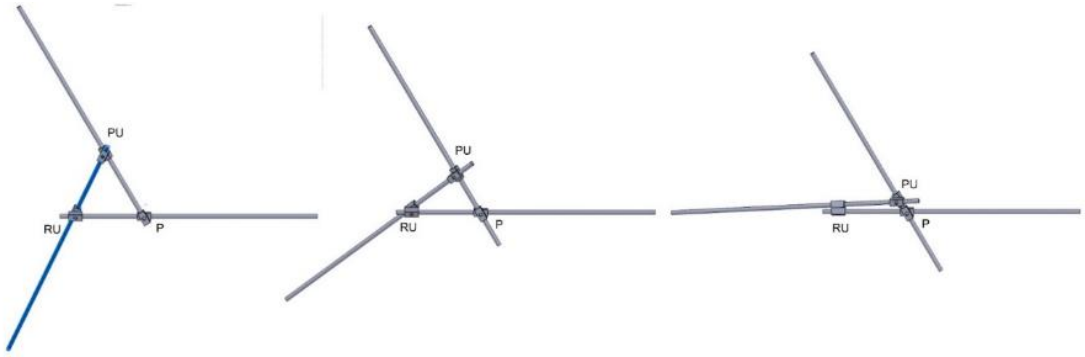

Figure 7.5. PU-P-$R_{\parallel}$U fan motion.

In Figure 7.6a PC_s-P-$R_{\parallel}$U fan is created. There is one nexor having excessive translation motion because of two P joints. This fan is unable to move. One of the P joints is replaced with an $R_{\parallel}$ joint to avoid excessive mobility. Thereby the fan has a single DoF. How the Figure 7.6b fan moves can be seen in Figure 7.7. After showing the fan in Figure 7.6a, the fans that have excessive mobility and the mobility calculations will not be shown in the continuation of this chapter. Only single DoF fans will be indicated.

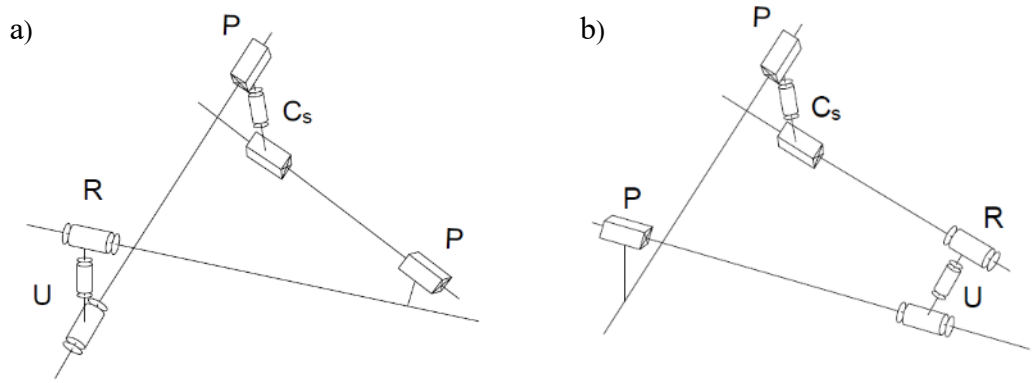

$\Sigma f_i = 7, \lambda_k = 6, E=1$
$M = 7 - 6 - 1 = 0$

$\Sigma f_i = 7, \lambda_k = 6$
$M = 7 - 6 = 1$

Figure 7.6. a) PC_s-P-$R_{\parallel}U$ fan, b) PC_s-$R_{\parallel}U$-P fan.

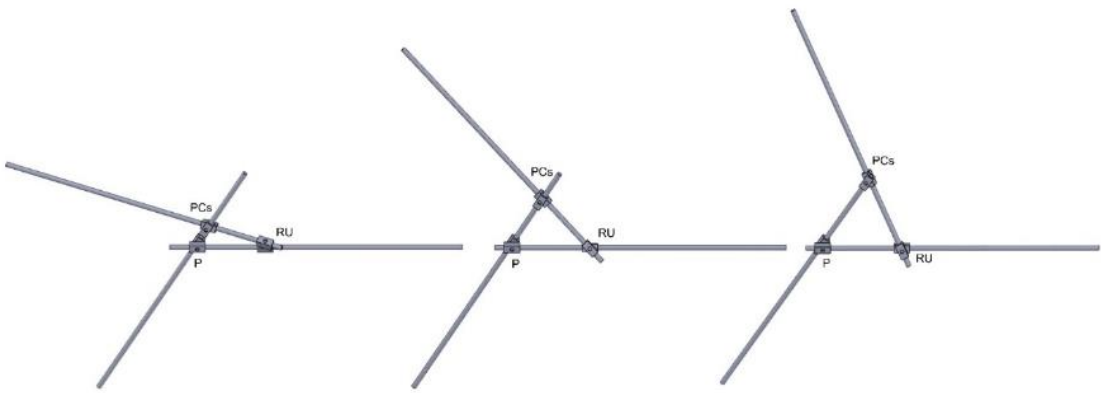

Figure 7.7. PC_s-$R_{\parallel}U$-P fan motion.

In Figure 7.8a, the UP-UP-$R_{\parallel}$ fan is created, and in Figure 7.9, its motion is observed. Since there are two P joints, only two engagement lengths are variable. In Figure 7.8b, the supported nexor with an $R_{\parallel}$ joint is made inactive, and the P joint is added to the support nexor. While the nexors having a P joint is expected to move, which causes the change in engagement length, the nexors having an $R_{\parallel}$ joint rotate and cause the change in form (Figure 7.10).

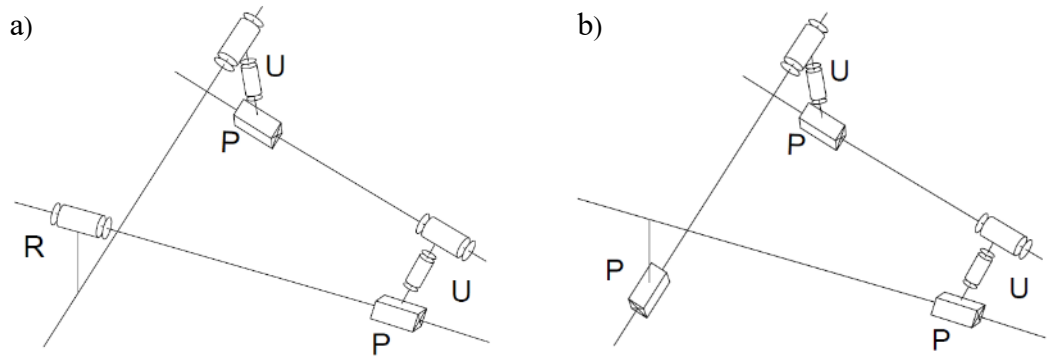

Figure 7.8. a) UP-UP-$R_{\parallel}$ fan, b) UP-UP-P fan.

Figure 7.9. UP-UP-$R_{\parallel}$ fan (Figure 7.8a) motion.

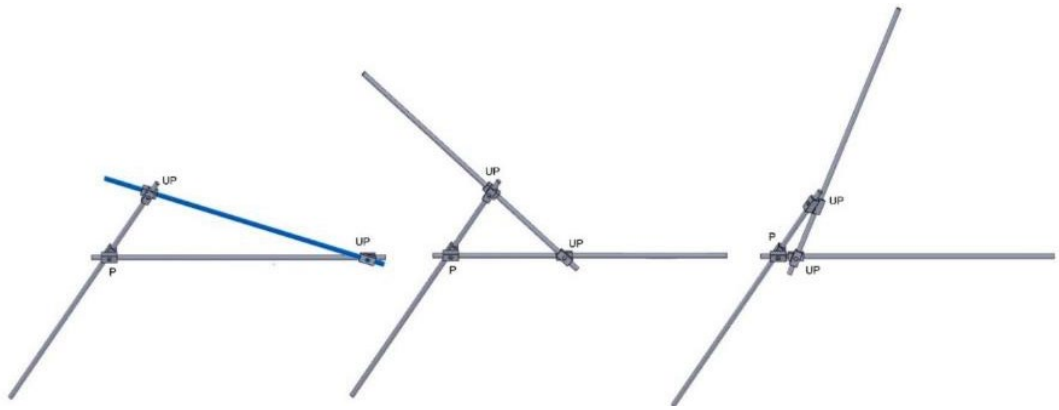

Figure 7.10. UP-UP-P fan (Figure 7.8b) motion.

In Figure 7.11a, C_sP-UP-$R_{\parallel}$ joint series fan is produced. While the $R_{\parallel}$ joint is along the supported nexor in Figure 7.11a, it is along the support nexor in Figure 7.11b. Their motions can be seen respectively in Figure 7.12 and Figure 7.13.

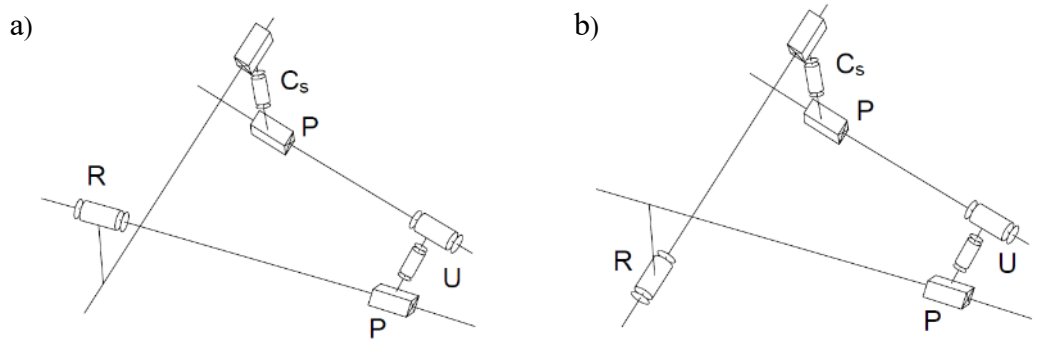

Figure 7.11. a) $C_sP\text{-}UP\text{-}R_{\parallel}$ fan, b) $C_sP\text{-}UP\text{-}R_{\parallel}$ fan.

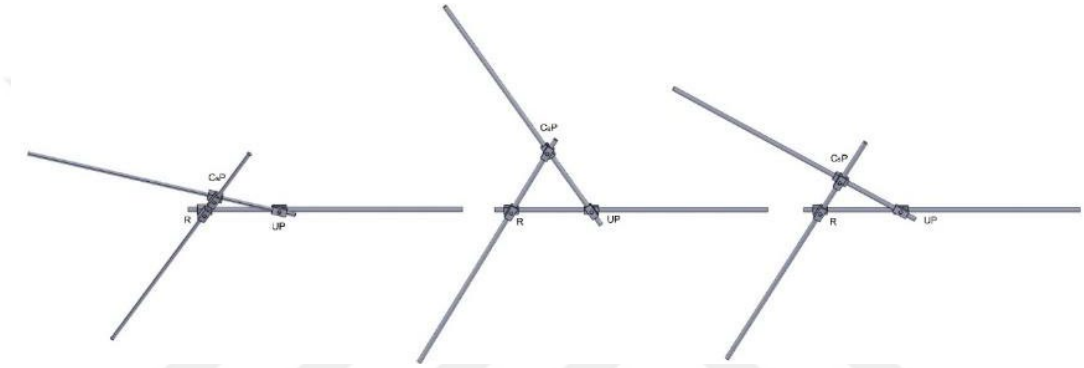

Figure 7.12. $C_sP\text{-}UP\text{-}R_{\parallel}$ fan (Figure 7.11a) motion.

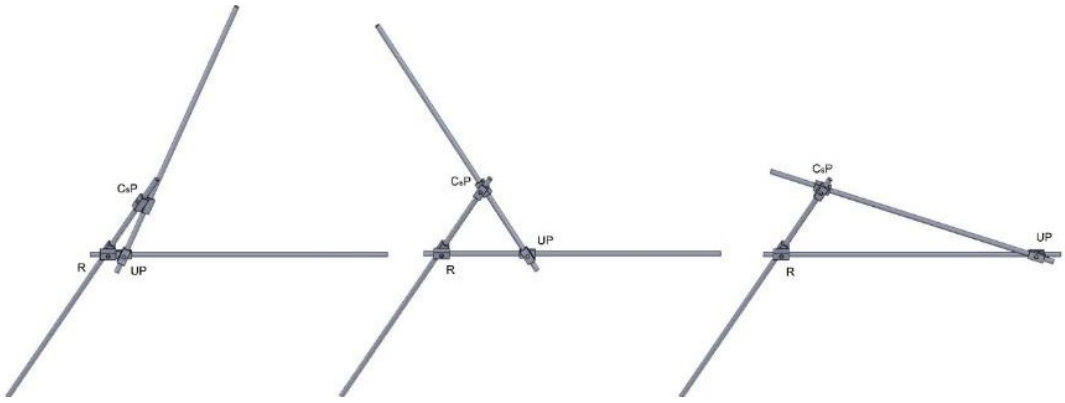

Figure 7.13. $C_sP\text{-}UP\text{-}R_{\parallel}$ fan (Figure 7.11b) motion.

$C_sP\text{-}R_{\parallel}R_{\parallel}\text{-}PR_{\parallel}$ joint series fan is constituted in Figure 7.14a. Then the position of the $R_{\parallel}$ and P joint along one nexor is switched to see the change in motion in Figure 7.14b. Their motions can be seen respectively in Figure 7.15 and Figure 7.16.

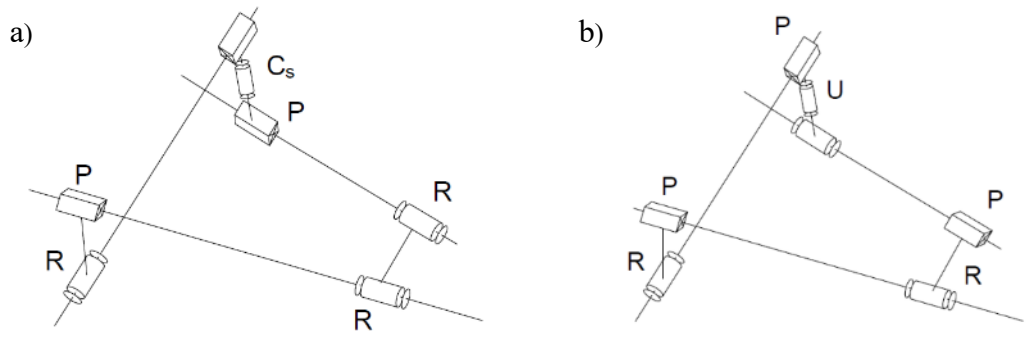

Figure 7.14. a) C_sP-$R_{\parallel}R_{\parallel}$-$PR_{\parallel}$ fan, b) PU-$PR_{\parallel}$-$PR_{\parallel}$ fan.

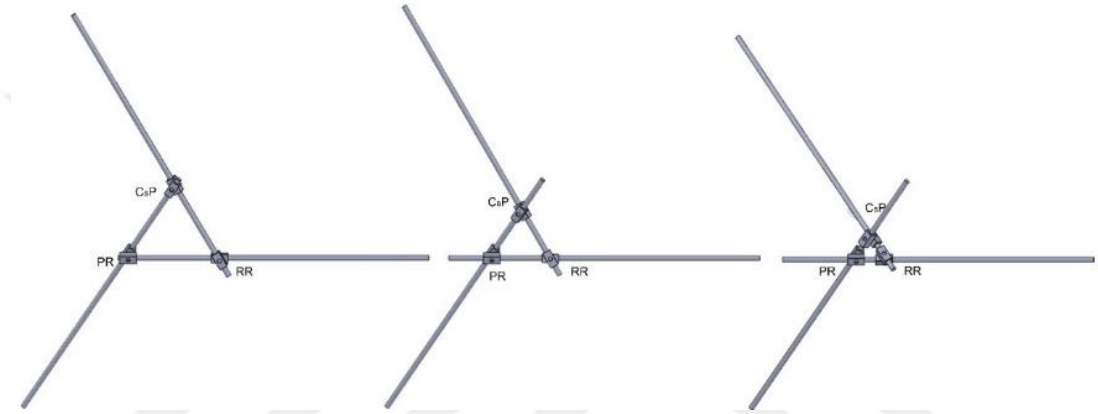

Figure 7.15. C_sP-$R_{\parallel}R_{\parallel}$-$PR_{\parallel}$ fan (Figure 7.14a) motion.

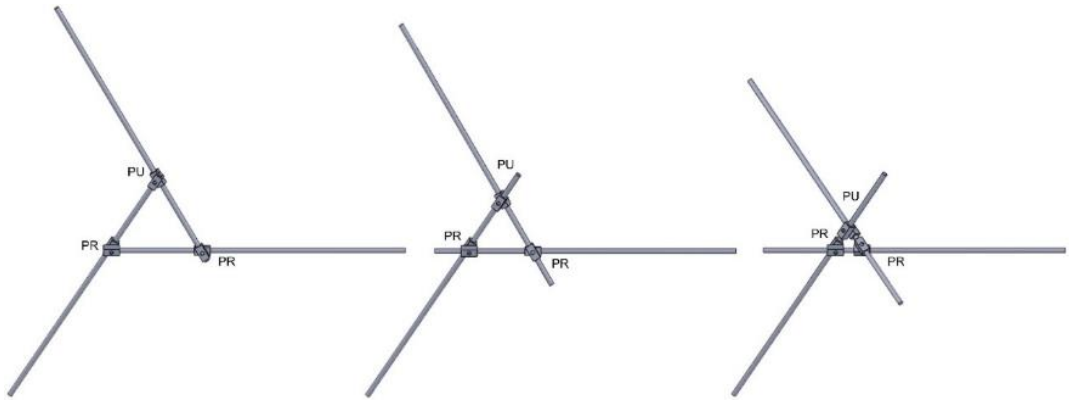

Figure 7.16. PU-$PR_{\parallel}$-$PR_{\parallel}$ fan (Figure 7.14b) motion.

UP-$R_{\parallel}$P-$R_{\parallel}$P joint series fan is produced in Figure 7.17a. Then the position of the $R_{\parallel}$ and P joint along one nexor is changed to see the change in motion in Figure 7.17b. Their motions can be seen respectively in Figure 7.18 and Figure 7.19.

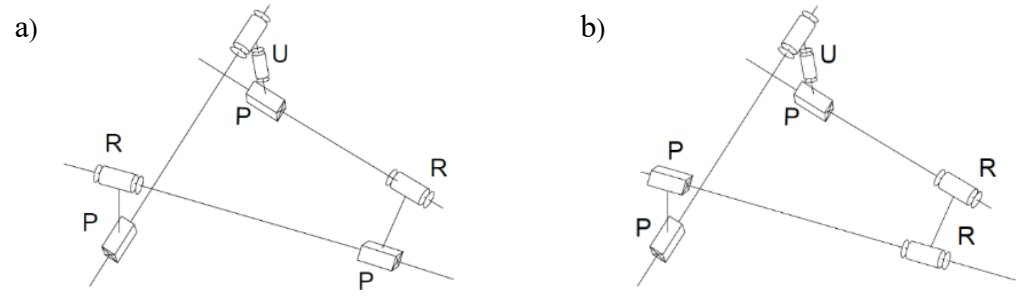

Figure 7.17. a) UP-R∥P-R∥P fan, b)UP-R∥R∥-PP fan.

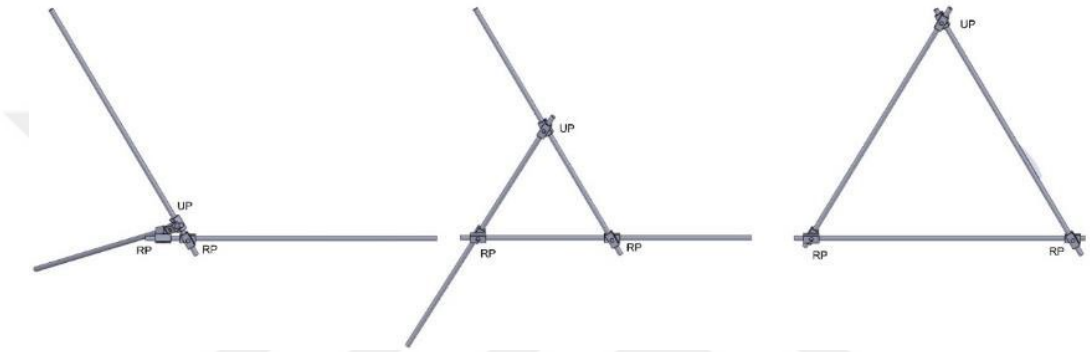

Figure 7.18. UP-R∥P-R∥P fan (Figure 7.17a) motion.

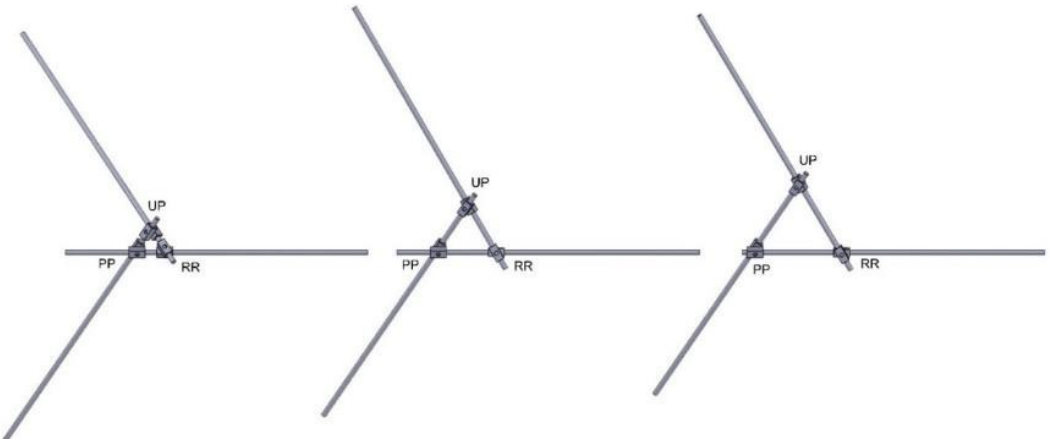

Figure 7.19. UP-R∥R∥-PP fan (Figure 7.17b) motion.

C, P, and R joints are used in Figure 7.20. The P joint in Figure 7.20a is replaced with the R∥ joint in Figure 7.20b to see the change in motion, which can be seen in Figure 7.21 and Figure 7.22.

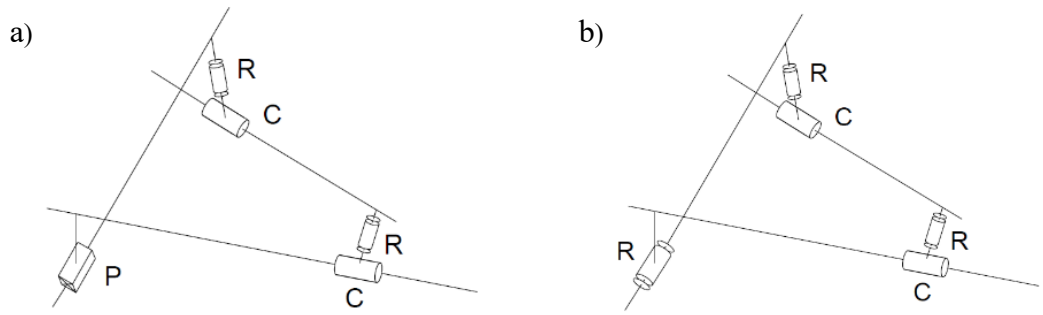

Figure 7.20. a) $R_{\perp}C\text{-}R_{\perp}C\text{-}P$ fan, b) $R_{\perp}C\text{-}R_{\perp}C\text{-}R_{\parallel}$ fan.

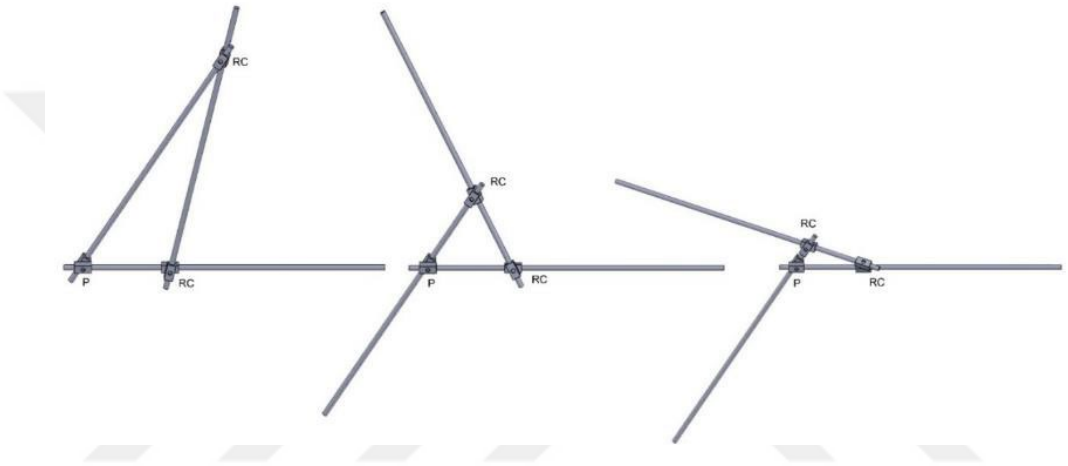

Figure 7.21. $R_{\perp}C\text{-}R_{\perp}C\text{-}P$ fan (Figure 7.20a) motion.

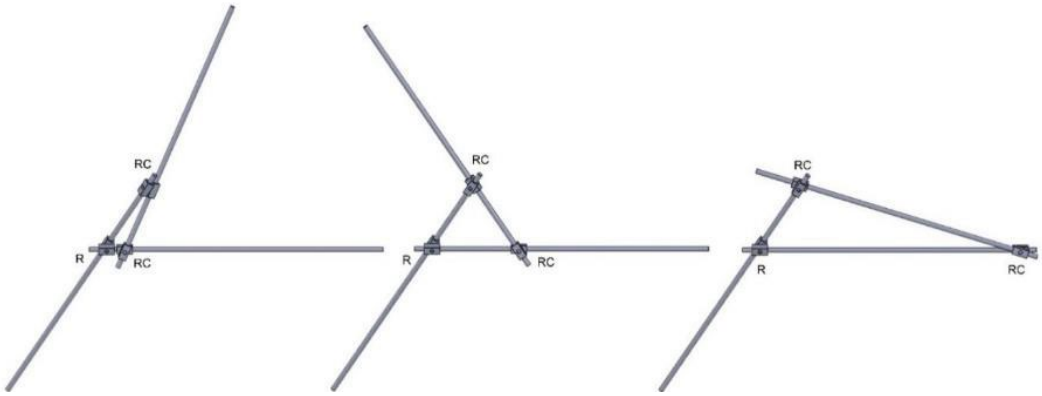

Figure 7.22. $R_{\perp}C\text{-}R_{\perp}C\text{-}R_{\parallel}$ fan (Figure 7.20b) motion.

In Figure 7.23, $CR_{\perp}\text{-}C\text{-}C$ joints series fan is created. Three engagement lengths are variable. Its motion can be seen in Figure 7.24.

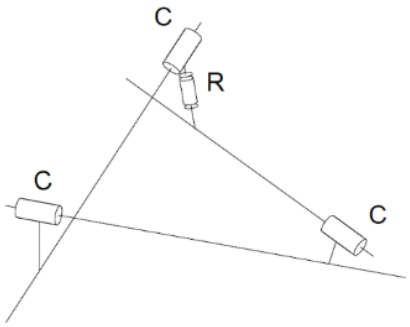

Figure 7.23. $CR_{\perp}$-C-C fan.

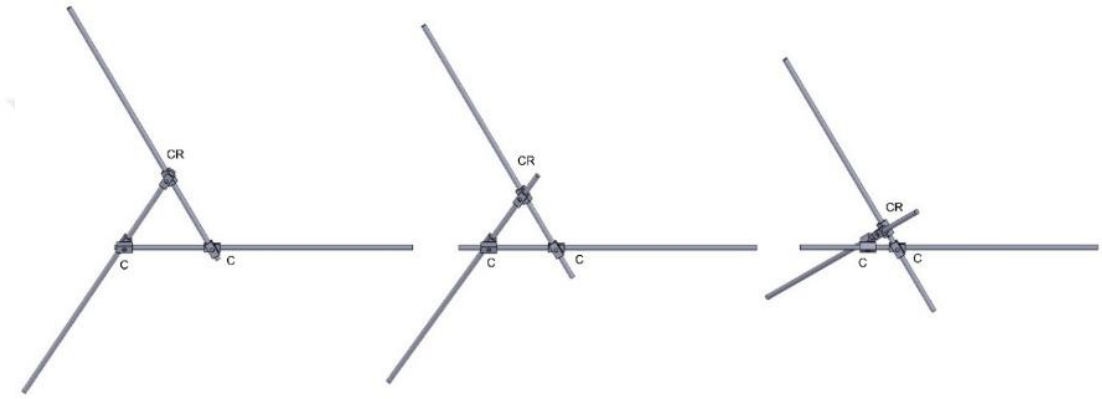

Figure 7.24. $CR_{\perp}$-C-C fan motion.

6.2. Quadrilateral Fans

In Figure 7.25a C_s-C_s-C_s-P joint series fan is created. When the motion is analyzed, it can be seen that the four nexors' engagement lengths are variable. In Figure 7.25b, the $R_{\parallel}$ joint is used along the supported nexor instead of the P joint, as in Figure 7.25a. In Figure 7.25c, the $R_{\parallel}$ joint is added along the support nexor. The differences between the fans' motions can be seen respectively in Figure 7.26, Figure 7.27, and Figure 7.28.

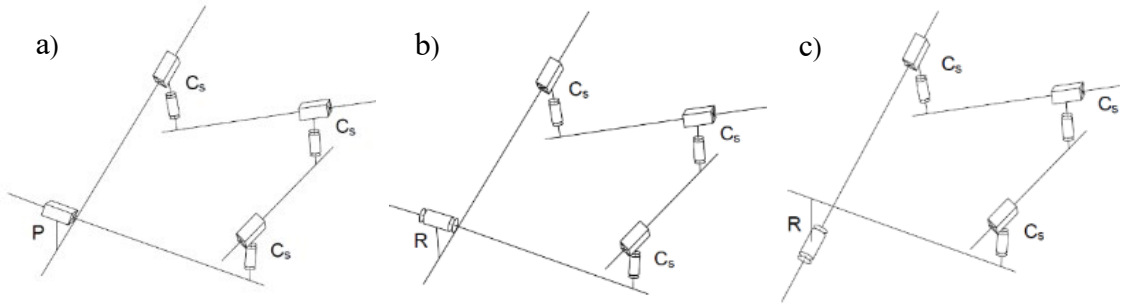

Figure 7.25. a) C_s-C_s-C_s-P fan, b) C_s-C_s-C_s-$R_{\parallel}$ fan, c) C_s-C_s-C_s-$R_{\parallel}$ fan.

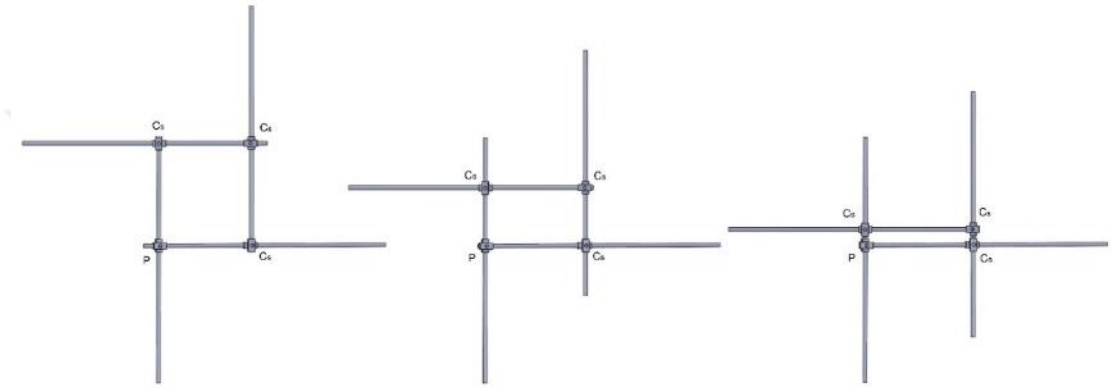

Figure 7.26. C_s-C_s-C_s-P fan motion (Figure 7.25a).

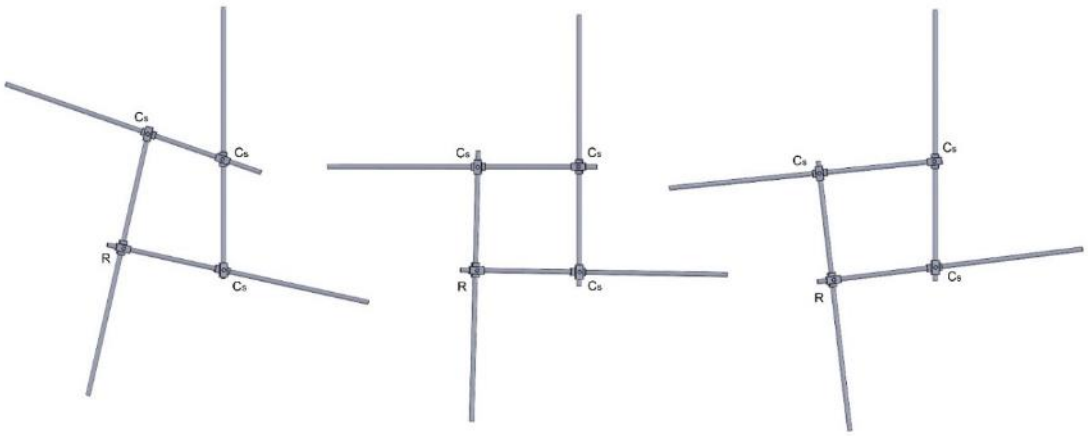

Figure 7.27. C_s-C_s-C_s-$R_{\parallel}$ fan motion (Figure 7.25b).

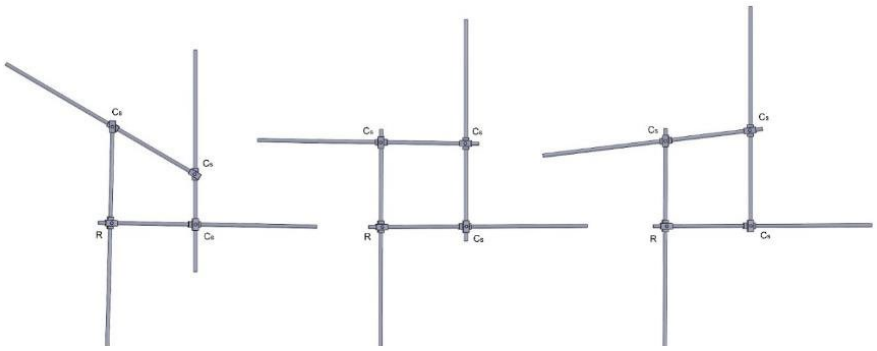

Figure 7.28. C_s-C_s-C_s-$R_{\parallel}$ fan motion (Figure 7.25c).

The organization of the joints in Figure 7.25 is changed in Figure 7.29, and it is aimed to see the change in the motions. The joints at the support nexors are placed to the supported nexors. The motions can be seen respectively in Figure 7.30, Figure 7.31, and Figure 7.32.

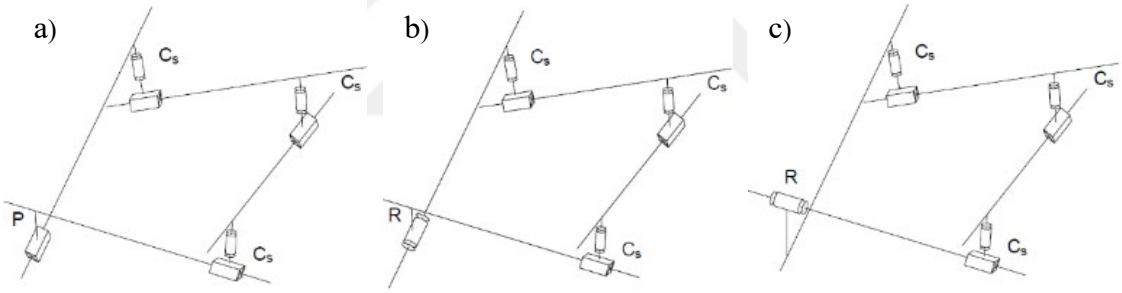

Figure 7.29. a) C_s-C_s-C_s-P fan, b) C_s-C_s-C_s-$R_{\parallel}$ fan, c) C_s-C_s-C_s-$R_{\parallel}$ fan.

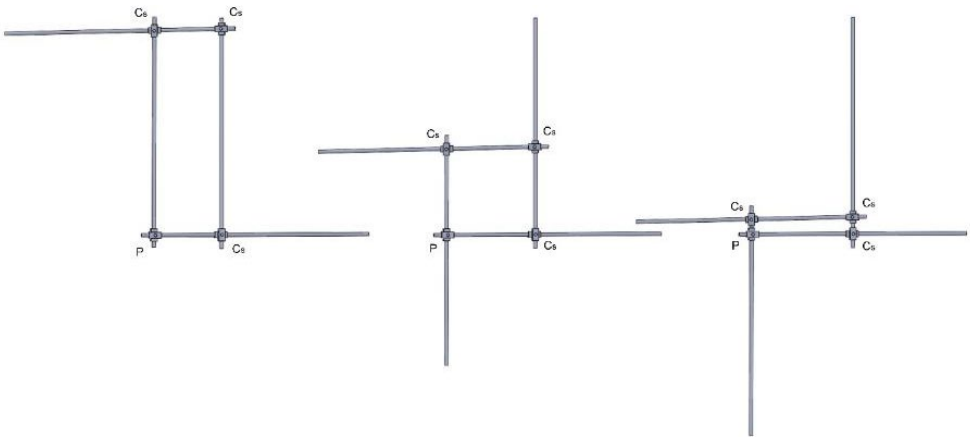

Figure 7.30. C_s-C_s-C_s-P fan motion (Figure 7.29a).

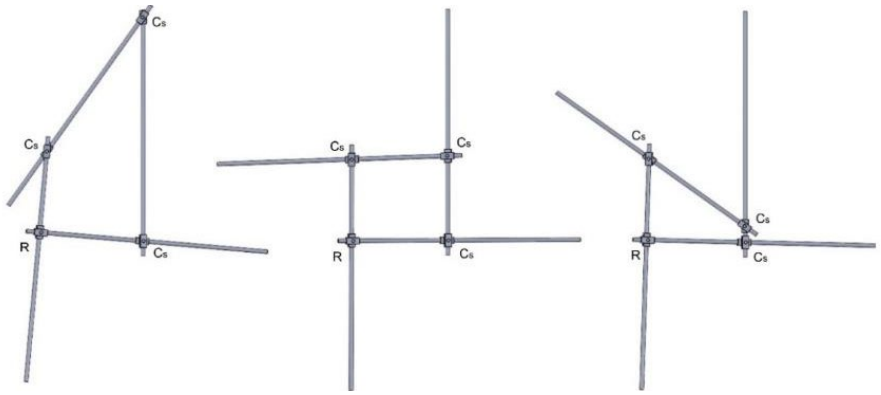

Figure 7.31. C_s-C_s-C_s-$R_\parallel$ fan motion (Figure 7.29b).

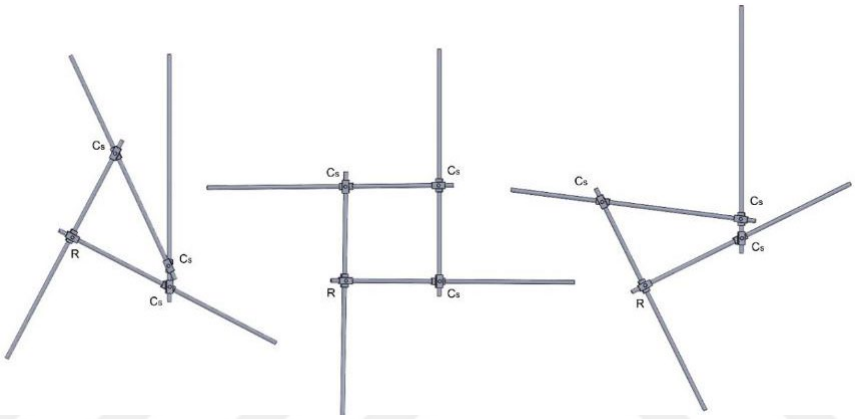

Figure 7.32. C_s-C_s-C_s-$R_\parallel$ fan motion (Figure 7.29c).

In Figure 7.33, all the nexors in the three fans are welded to each other except the last fan's one connection. Their motions can be seen in Figure 7.34, Figure 7.35, and Figure 7.36. While first fans' all engagement lengths are variable, second and third fans' three engagement lengths are varying.

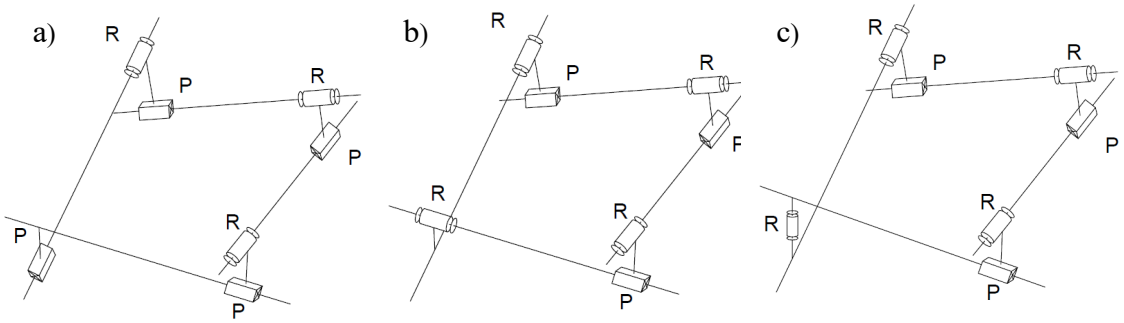

Figure 7.33. a) $R_\parallel$P-$R_\parallel$P-$R_\parallel$P-P fan, b) $R_\parallel$P-$R_\parallel$P-$R_\parallel$P-$R_\parallel$ fan, c) $R_\parallel$P-$R_\parallel$P-$R_\parallel$P-$R_\perp$ fan.

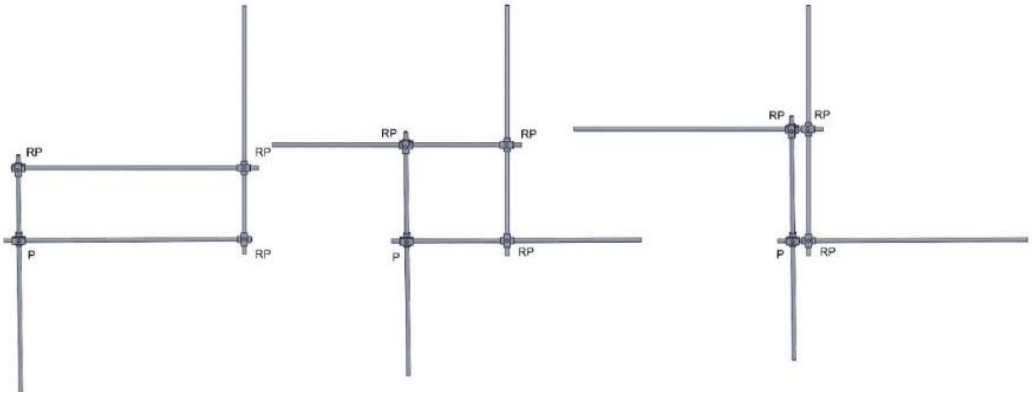

Figure 7.34 $R_{\parallel}P$-$R_{\parallel}P$-$R_{\parallel}P$-$R_{\perp}$ fan motion (Figure 7.33a)

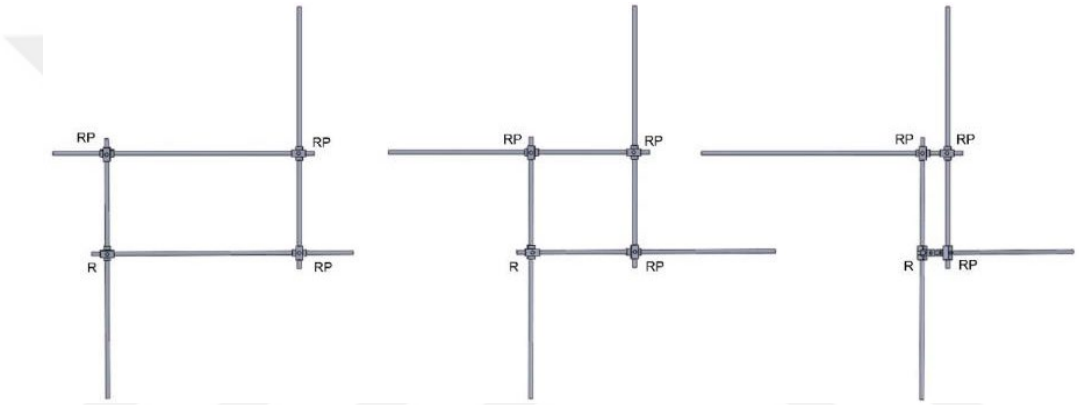

Figure 7.35. $R_{\parallel}P$-$R_{\parallel}P$-$R_{\parallel}P$-P fan motion (Figure 7.33b).

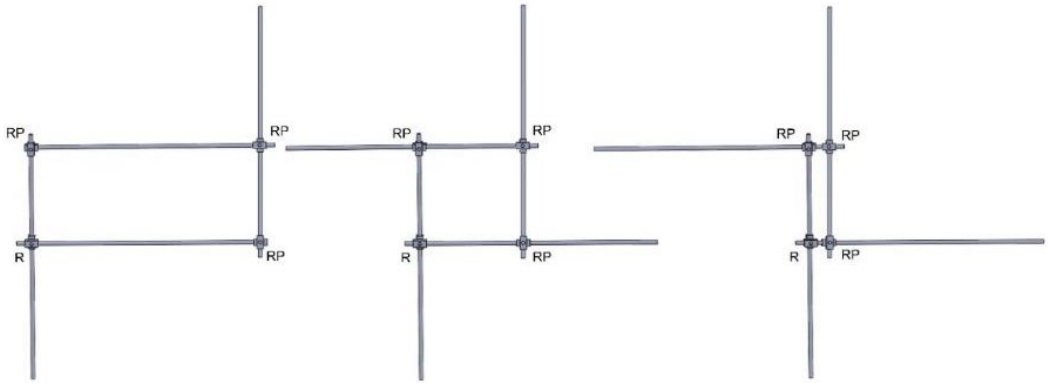

Figure 7.36. $R_{\parallel}P$-$R_{\parallel}P$-$R_{\parallel}P$-$R_{\parallel}$ fan motion (Figure 7.33c).

The organization of the $R_{\parallel}$ and P joints in Figure 7.33 is changed in Figure 7.37. While the joints at the support nexors are positioned to the supported nexors, the joints at

the supported nexors are placed to the support nexors. Their motions can be seen respectively in Figure 7.38, Figure 7.39, and Figure 7.40. They all have some kind of expanding and shrinking motion but are not conformal.

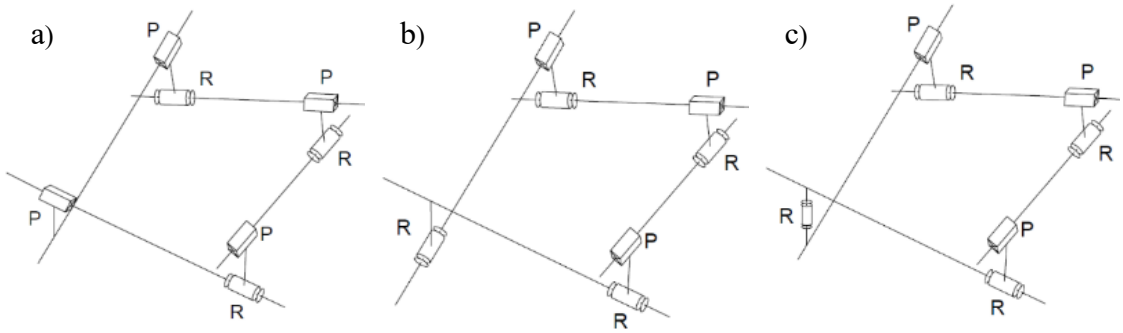

Figure 7.37. a) $PR_{\parallel}$-$PR_{\parallel}$-$PR_{\parallel}$-P fan, b) $PR_{\parallel}$-$PR_{\parallel}$-$PR_{\parallel}$-$R_{\parallel}$ fan, c) $PR_{\parallel}$-$PR_{\parallel}$-$PR_{\parallel}$-$R_{\perp}$ fan.

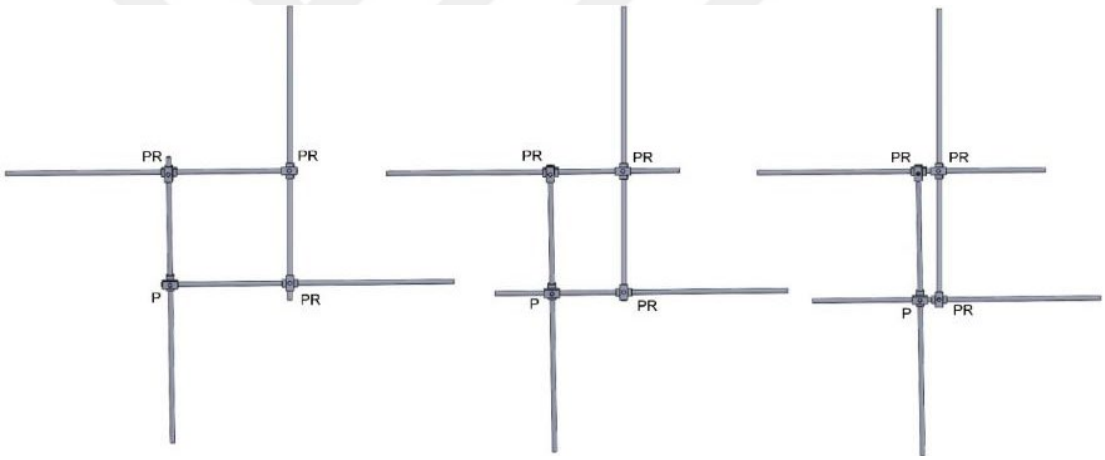

Figure 7.38. $PR_{\parallel}$-$PR_{\parallel}$-$PR_{\parallel}$-P fan motion (Figure 7.37a).

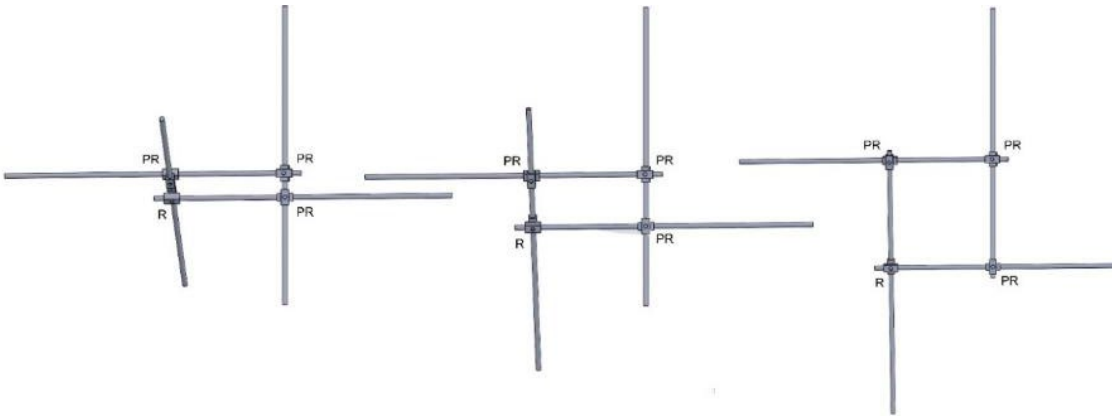

Figure 7.39. $PR_{\parallel}$-$PR_{\parallel}$-$PR_{\parallel}$-$R_{\parallel}$ fan motion (Figure 7.37b).

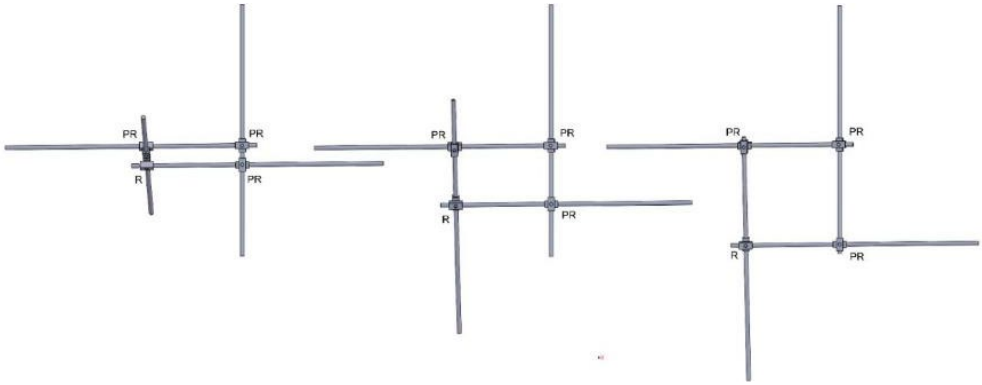

Figure 7.40. $PR_{\parallel}$-$PR_{\parallel}$-$PR_{\parallel}$-$R_{\perp}$ fan motion (Figure 7.37c).

In Figure 7.41, C joints are used at the support nexors. Every fan has the same joint connections except for one corner. In the first fan, P is used along the support nexor, whereas the $R_{\parallel}$ joint is used along the supported nexor in the second fan. In the third fan, the $R_{\perp}$ joint connects two nexors rather than welding. Their motions can be seen in Figure 7.42, Figure 7.43, and Figure 7.44.

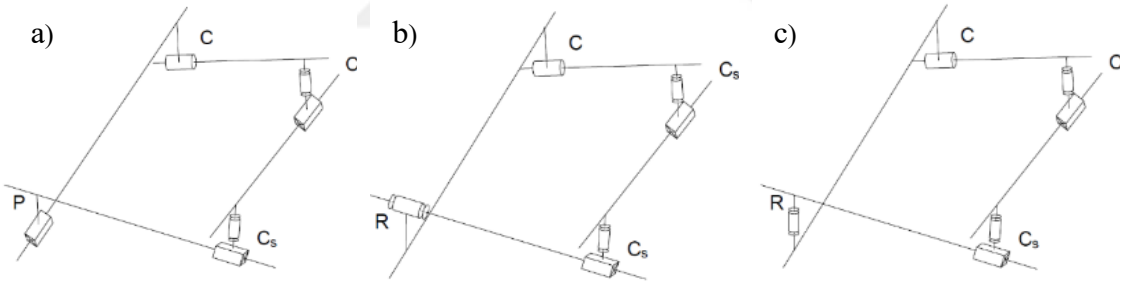

Figure 7.41. a) C-C_s-C_s-P fan, b) C-C_s-C_s-$R_{\parallel}$ fan, c) C-C_s-C_s-$R_{\perp}$ fan.

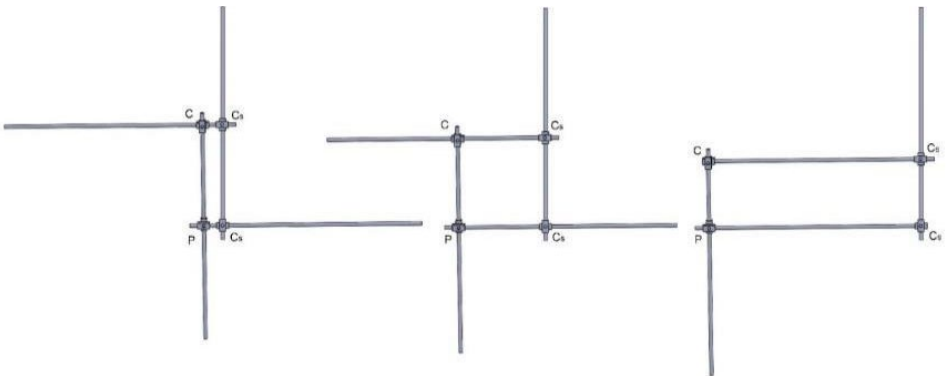

Figure 7.42. C-C_s-C_s-P fan motion (Figure 7.41a).

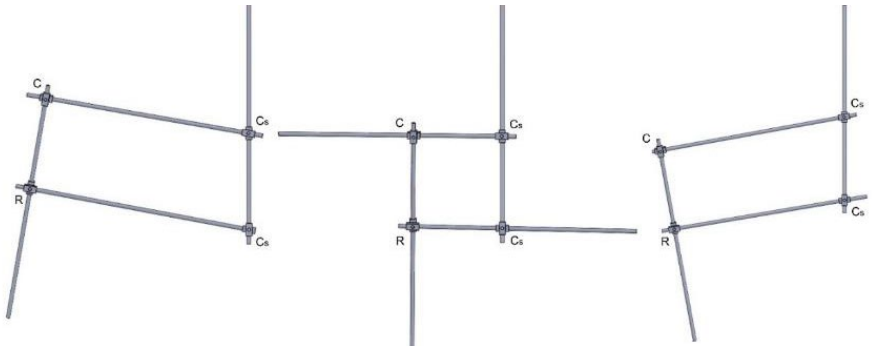

Figure 7.43. C-C_s-C_s-$R_{\parallel}$ fan motion (Figure 7.41b).

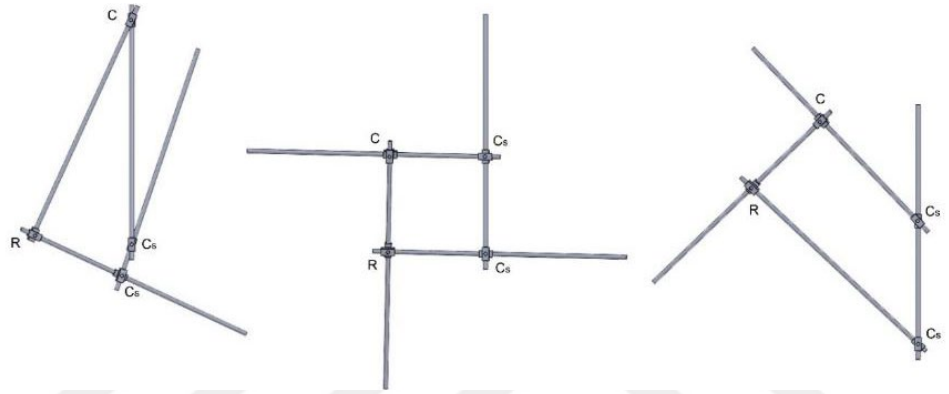

Figure 7.44. C-C_s-C_s-$R_{\perp}$ fan motion (Figure 7.41c).

In Figure 7.45, by reducing the number of C_s joints, one more C joint is added to every fan, different from Figure 7.41. Only one connection point connects two nexors with the orthogonal $R_{\perp}$ joint in Figure 7.45a and Figure 7.45b. The other three connections are done by welding and adding different types of joints along the nexors until the fans reach a single DoF. Their motions can be seen in Figure 7.46, Figure 7.47, and Figure 7.48.

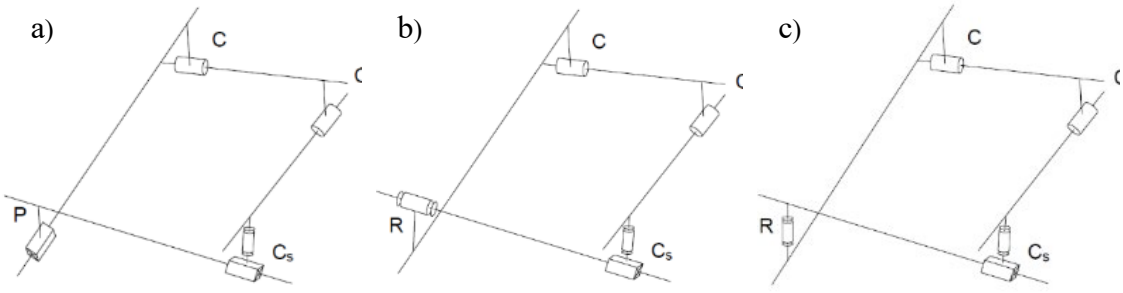

Figure 7.45. a) C-C-C_s-P fan, b) C-C-C_s-$R_{\parallel}$ fan, c) C-C-C_s-$R_{\perp}$ fan.

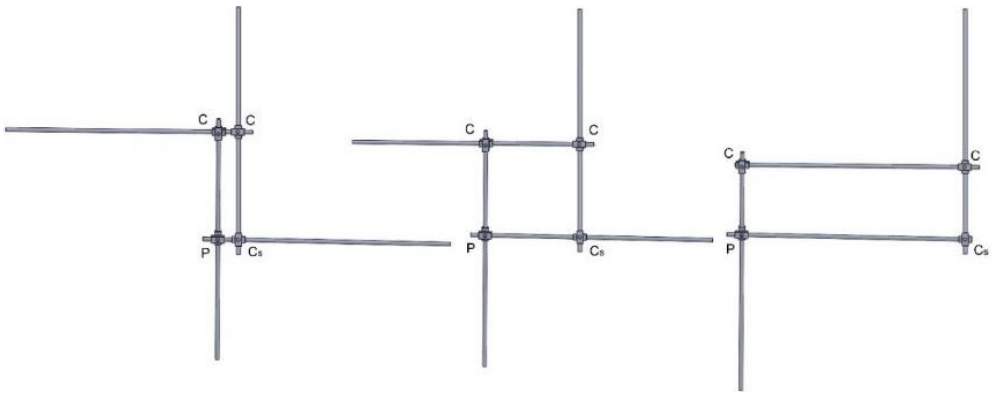

Figure 7.46. C-C-C_s-P fan motion (Figure 7.45a).

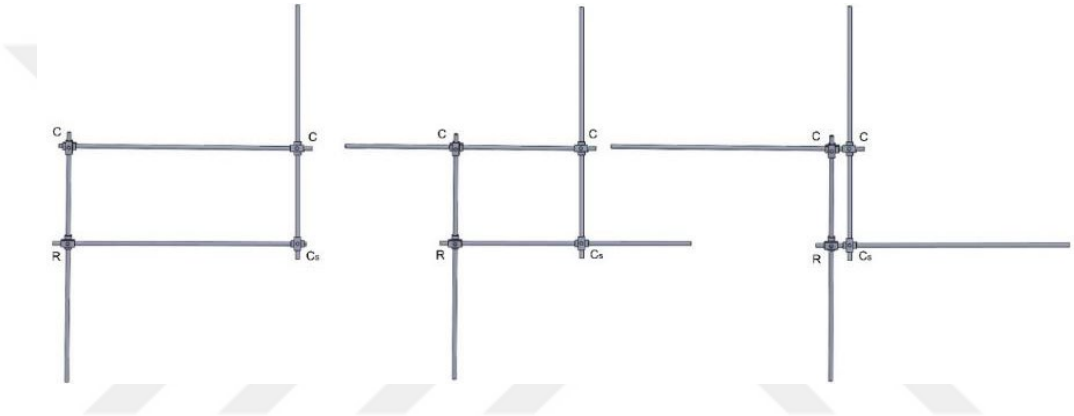

Figure 7.47. C-C-C_s-$R_{\parallel}$ fan motion (Figure 7.45b).

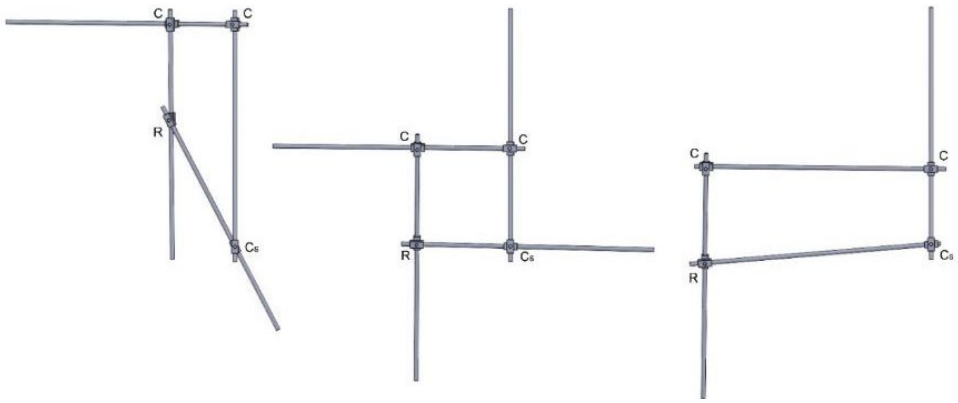

Figure 7.48. C-C-C_s-$R_{\perp}$ fan motion (Figure 7.45c).

In Figure 7.49, three connection points are welded, and there are C joints at the support nexors. The last connection point is connected either with an orthogonal R joint or welded. Their motions can be seen in Figure 7.50, Figure 7.51, and Figure 7.52.

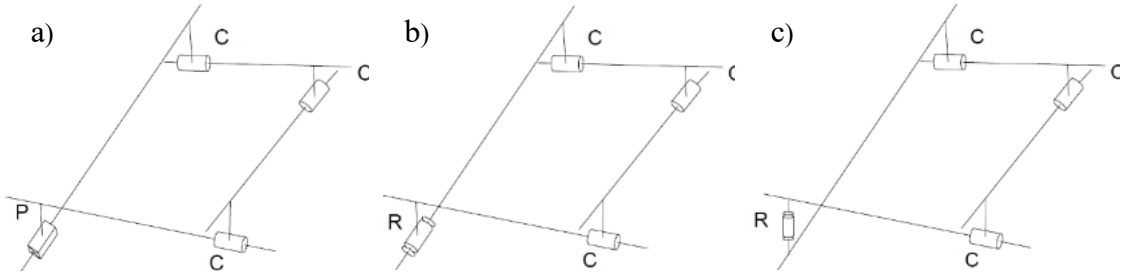

Figure 7.49. a) C-C-C-P fan, b) C-C-C-R$_{\parallel}$ fan, c) C-C-C-R$_{\perp}$ fan.

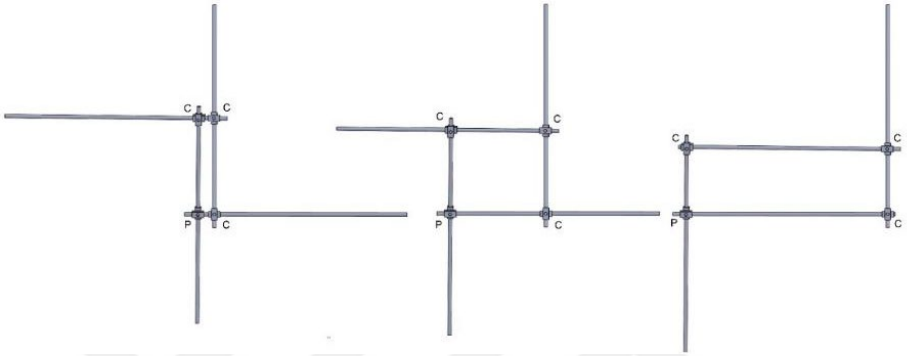

Figure 7.50. C-C-C-P fan motion (Figure 7.49a).

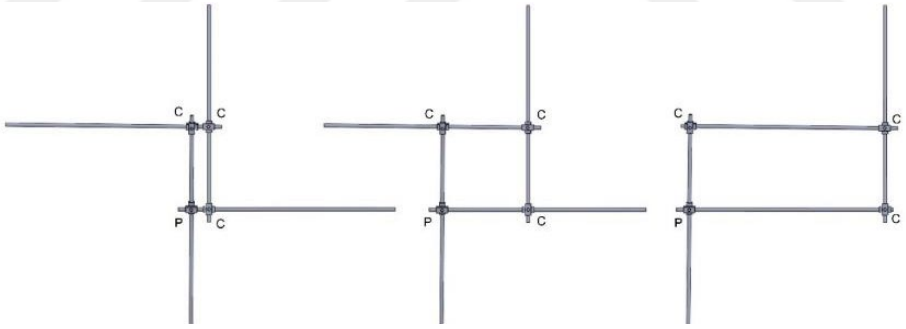

Figure 7.51. C-C-C-R$_{\perp}$ fan motion (Figure 7.49b).

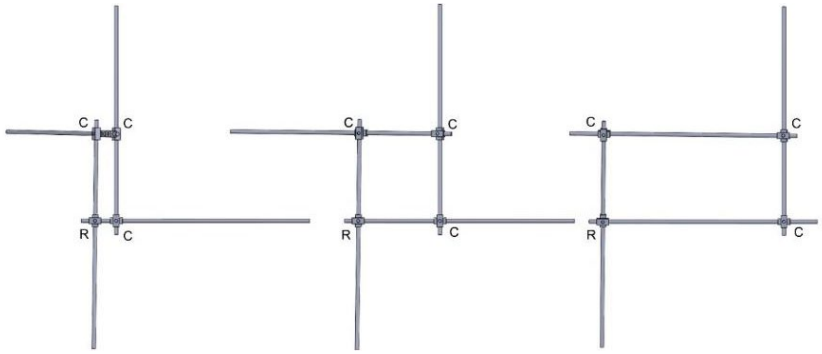

Figure 7.52. C-C-C-R$_{\parallel}$ fan motion (Figure 7.49c) .

The fans in Figure 7.53 are also tried. But none of the fans studied meet the conformal motion.

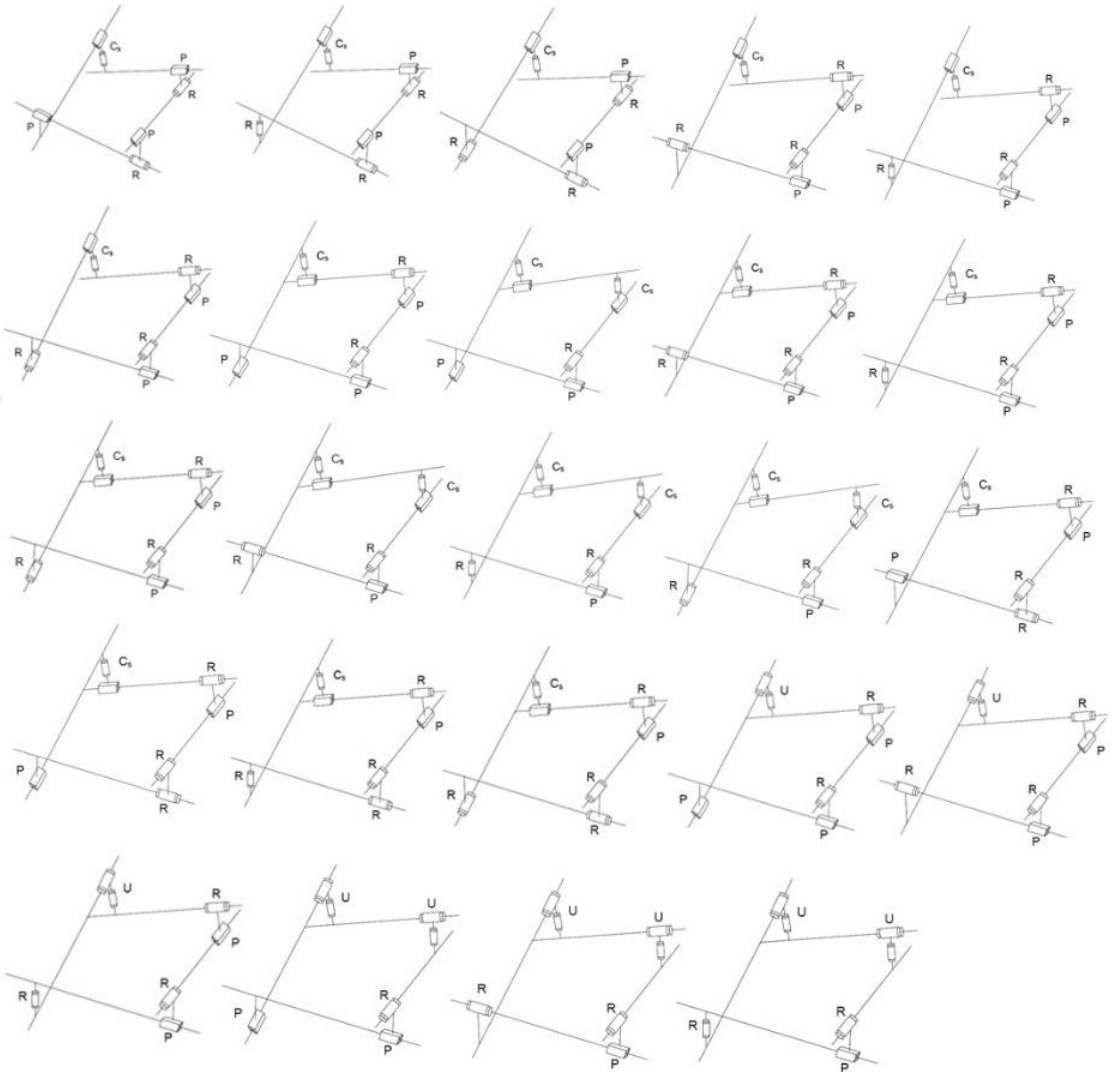

Figure 7.53. Quadrilateral fans.

6.3. Conclusion

Since the parallelogram motion and general motion that changes the angle between nexors and engagement lengths in Chapter 5 is undesirable, this chapter tries to eliminate the factors that cause these motions. So, this chapter investigates the shrinking and expanding motion in RF fans. In order to make this motion, an analogy has been made

by considering the fans as two-dimensional. In this motion, the fan is expected to transform from a large triangle to a small triangle or a square to a rectangle. This corresponds to the dilation motion for triangle fans and conformal motion for quadrilateral fans, in which the angle between the nexors remains constant, but the engagement lengths change. By reducing the orthogonal R joints, it is tried to get rid of the parallelogram and general motion. The effects of the variations of different joint series in fans are studied to achieve this. The possible fans with R, P, C, U, and C_s joints for triangular and quadrilateral fans are created to get the desired motions. The orthogonal R joints connecting the nexors are gradually reduced, and welding is used as a method of connection.

The triangular fans in Figure 7.54 have general motions. When the fans are analyzed, it is seen that they do not have the same characteristics that cause the non-symmetric motion. For example, while some of them have two P joints, some have three. It is thought that there should be three P joints for the synchronous motion. But looking at the result, the fans with three P joints did not give the desired motion either.

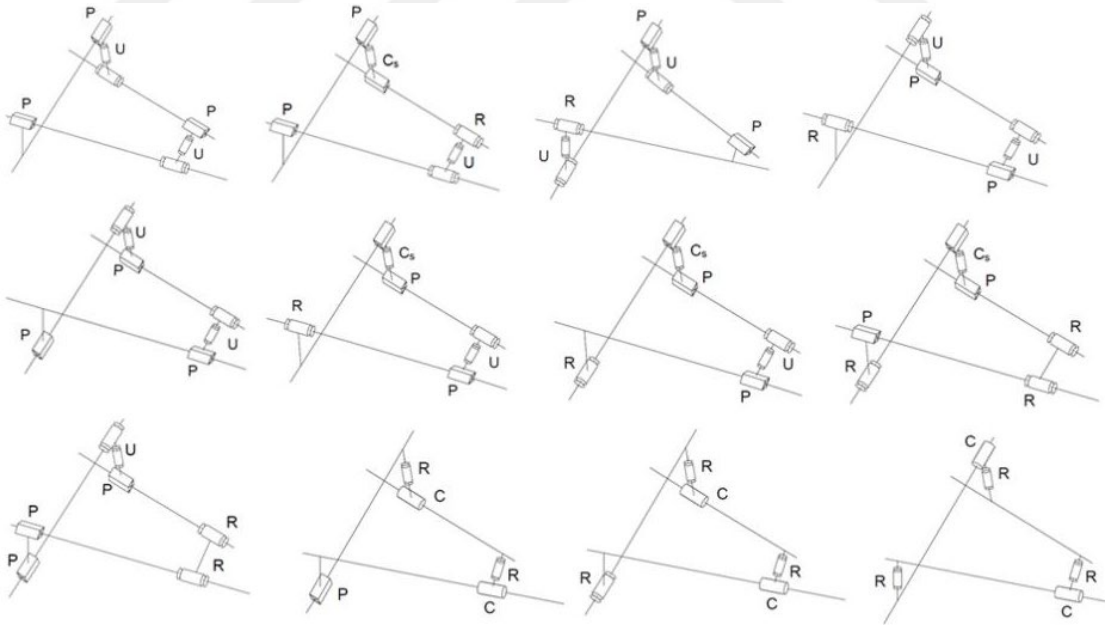

Figure 7.54. Triangular fans having general motions.

The fans in Figure 7.55 also have shrinking and expanding motions but not the desired one. This is due to the orthogonal $R_{\perp}$ joints. C_sP-$R_{\parallel}R_{\parallel}$-$PR_{\parallel}$ fan has three P and

four R joints. Because of the P joint, the fan has three changing engagement lengths, which give expanding and shrinking engagement windows. Even though the fan has a shrinking and expanding motion, the plane that the fan sits rotates during the motion, and nexors have variable engagement length dimensions. There are three P and four R joints in the PU-PR$_{\parallel}$-PR$_{\parallel}$ joint series fan, which means three variable engagement lengths exist. The fan's motion has a shrinking and expanding motion, but the engagement lengths become different as in the previous fans. The UP-R$_{\parallel}$P-R$_{\parallel}$P fan has three P and four R joints again. The fan has a shrinking and expanding motion, but the plane that the fan sits rotates during the motion. The CR$_{\perp}$-C-C joint series fan has three P and four R joints as in the previous fans, which have expanding and shrinking motions. This fan has variable engagement lengths, and the plane that the fan sits rotates. The result shows that the four fans in Figure 7.55 have the same characteristics as having three P and four R joints. But there are two types of motion: one has only variable nexor lengths, and the other has both varying nexor lengths and a rotating fan plane.

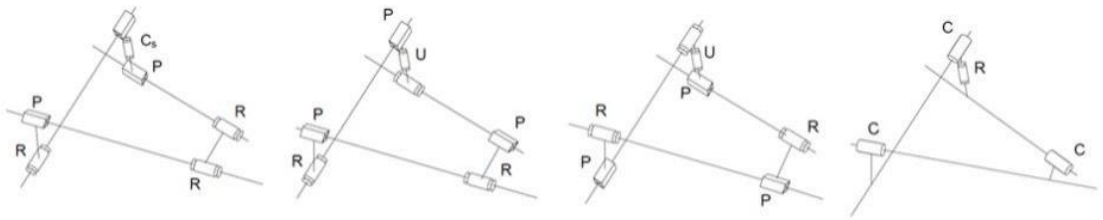

Figure 7.55. Triangular fans having general motions.

In quadrilateral fans, the fans in Figure 7.56 have general motions. The orthogonal R$_{\perp}$ joints connecting two nexors cause the change in the angle between two nexors. So, since the fans in Figure 7.56 have at least one R$_{\perp}$ joint, they have general motions.

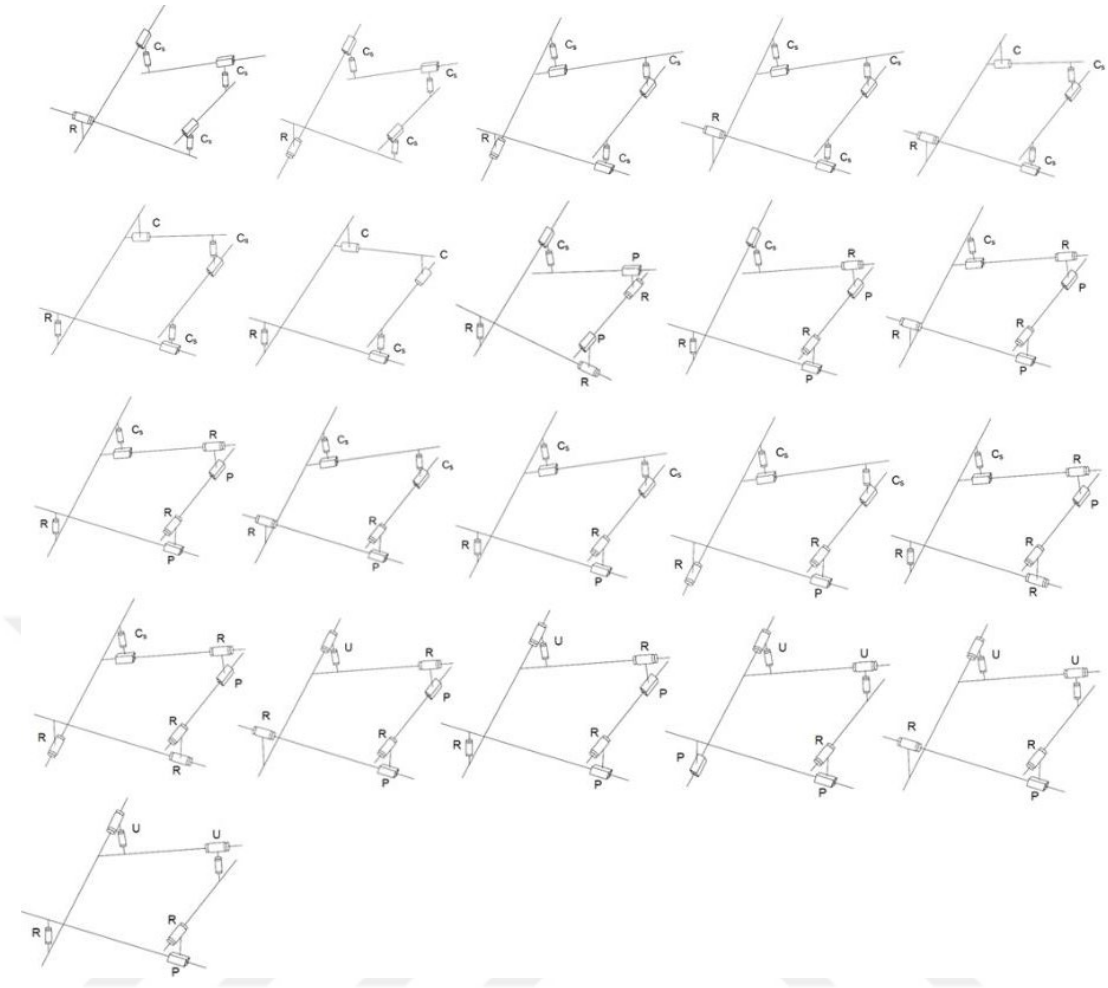

Figure 7.56. Quadrilateral fans having general motions.

Although the fans in Figure 7.57 appear to have a conformal kind of motion, the angle between two nexors slightly changes because of the nexors that are connected with the $R_{\perp}$ joints. Since these fans have at least one $R_{\perp}$ joint, they also have general motions.

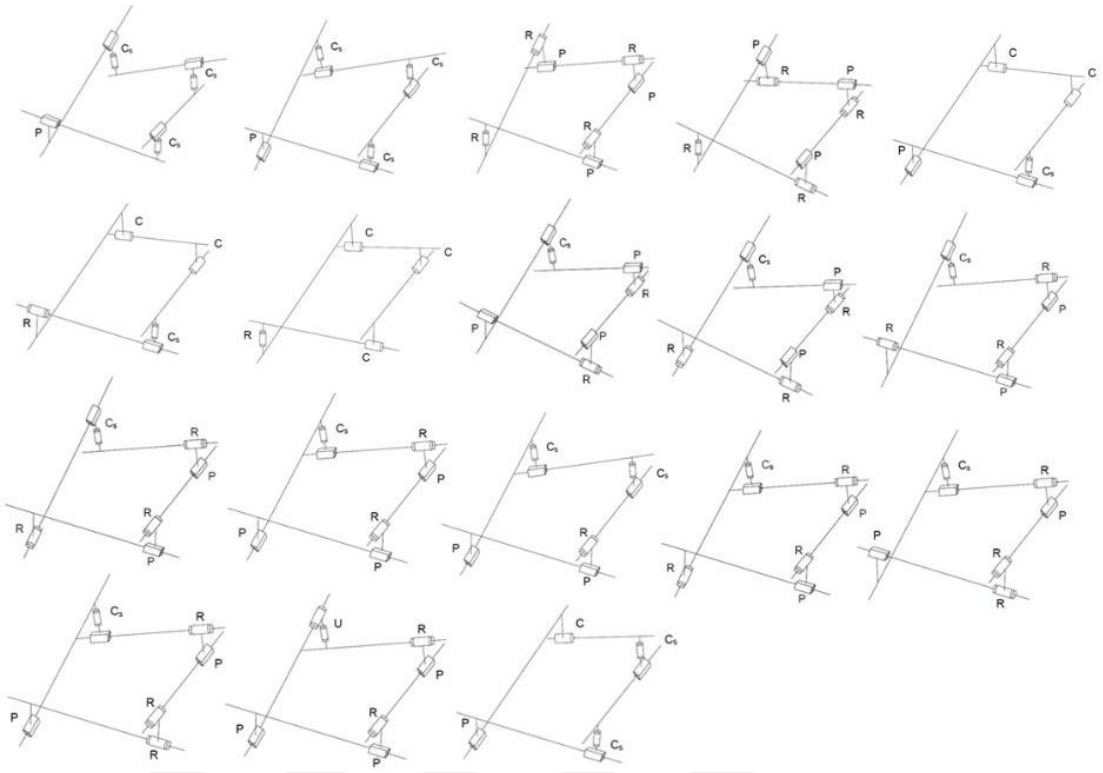

Figure 7.57. Quadrilateral fans having general motions.

The fans in Figure 7.58 have general motions too. There are four $R_{\parallel}$ and three P joints. Since this study aims to have a shrinking and expanding motion, all the engagement lengths should be variable. But the fans in this category have three variable engagement lengths. Eventually, the fans of this group do not meet the intended motion.

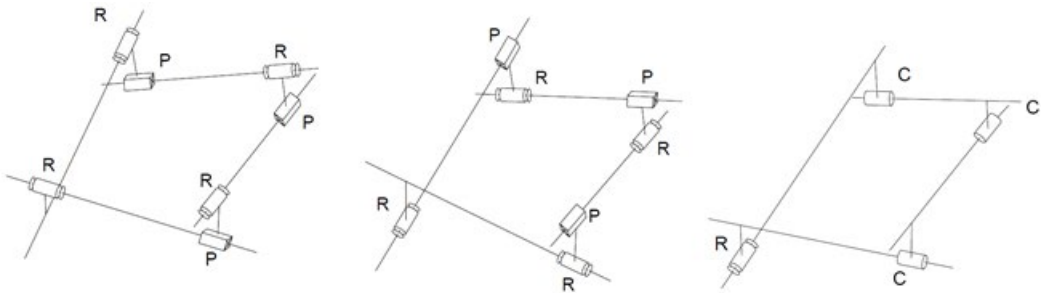

Figure 7.58. Quadrilateral fans having three P joints.

The fans in Figure 7.59 have three $R_{\parallel}$ and four P joints. The P joints meet the necessity of translation motion for four nexors. Any addition of the P joint will cause

excessive mobility, so the maximum number to have P joint is four. For this reason, the rest of the three joints should be $R_{\parallel}$. When their motions are observed, while two nexors become shorter, the other ones become longer. Moreover, there are rotating nexors. Since the DoF of every intersection point is not equal, conformal motion cannot be mentioned. Therefore, these fans also have general motion. For quadrilateral single DoF fans, conformal motion cannot be achieved.

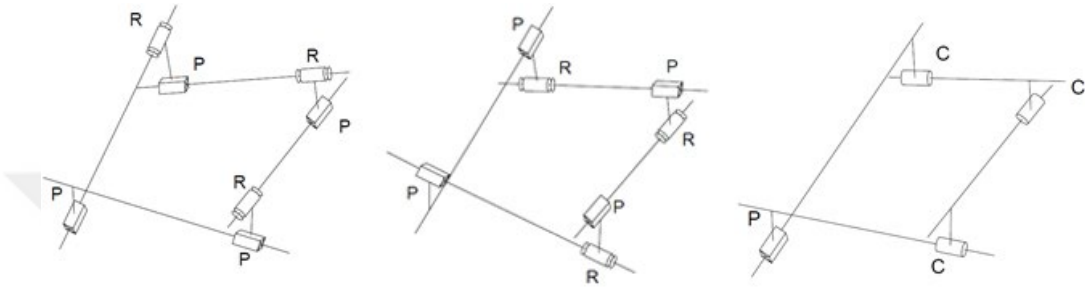

Figure 7.59. Quadrilateral fans having four P joints.

To conclude, there should be three P joints in triangular fans to change the engagement window area. The engagement lengths can be simultaneously shorter or longer during the motion. There should be four P joints for shrinking and expanding motion in quadrilateral fans. But it is not enough to have conformal motion. The angles between nexors change because of the R joints, which are not aimed. Results show that there is no dilation motion for single DoF triangular fans and conformal motion for single DoF quadrilateral fans. But it is possible to create some shrinking and expanding motions.

CHAPTER 8

MOTION ANALYSIS OF 2-DOF RFS AND NETWORKS

The intersection points should have the same number of joints of the same type to have dilation or conformal motion. To have M = 1, Σf_i should be 7. Corners can have 2-, 2-, and 3- DoF joints in triangular fans to have a single DoF motion. Since the DoF quantity at every corner is not equal, the motion is not conformal. When every corner has a 2-DoF joint- C is used in the example- RF has zero DoF, which is a structure (Figure 8.1). Moreover, when every corner has 3-DoF joints, the M = 3 which has multi DoF and is hard to control. So triangular fan is not studied.

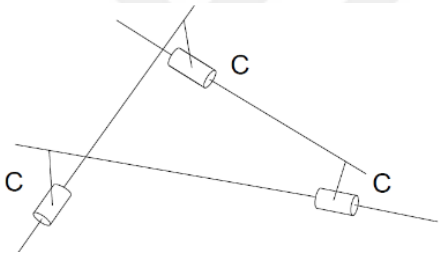

$\Sigma f_i = 6, \lambda_k = 6$

$M = 6 - 6 = 0$

Figure 8.1. C-C-C joint series triangular fan.

Then, a quadrilateral fan is analyzed. When every corner has a 2-DoF joint that is a C, M = 2, which is the fan that is going to be used in this chapter (Figure 8.2).

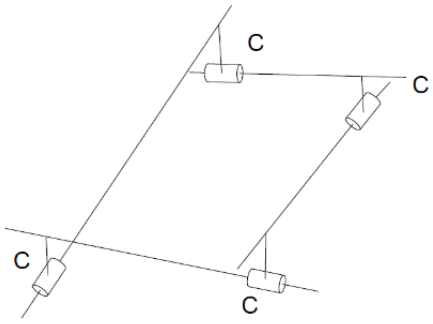

$\Sigma f_i = 8, \lambda_k = 6$

$M = 8 - 6 = 2$

Figure 8.2. C-C-C-C joint series quadrilateral fan.

M = 2 does not mean that the fan will have a conformal motion since it has several motions. But the desired motion can be obtained.

In two DoF mechanisms, there are two different motion modes depending on whether the angle between nexors is less than 90º or 90º. The one that is less than 90º is called motion mode 1, and the one that is 90º is called motion mode 2. The aim of this section is to show two different motion modes of a C-C-C-C joint series quadrilateral fan. A 70 cm long and 2.5 cm diameter nexors are used to create a fan. The conformal motion is intended which have changing engagement lengths, but not the angles in a two-dimensional analogy from the top view (Figure 8.3).

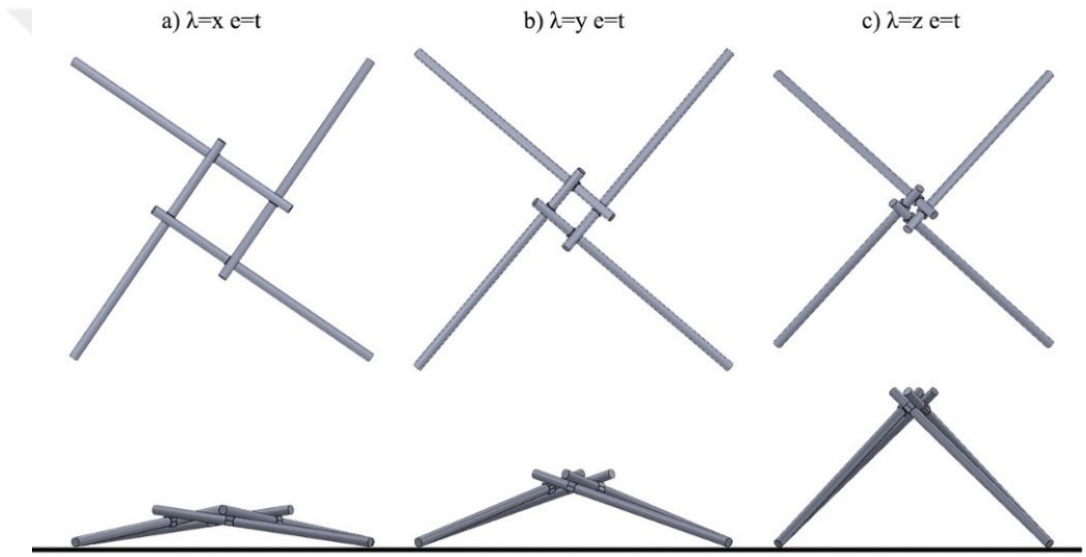

Figure 8.3. The change in the fan when the motion is applied.

Motion mode 1 is a two DoF fan with $\Sigma f_i=8$ and $\lambda_k=6$ where all nexors are radially symmetrical (Figure 8.4). It is conditioned as the ends of the nexors touch the ground, so the DoF of the fan becomes one. The angles between nexors (θ) must be equal in order for the ends of the nexors to touch the ground. Moreover, it is observed in section 3.3. that θ is never 90º in the ground contact condition (Table 3.4).

.

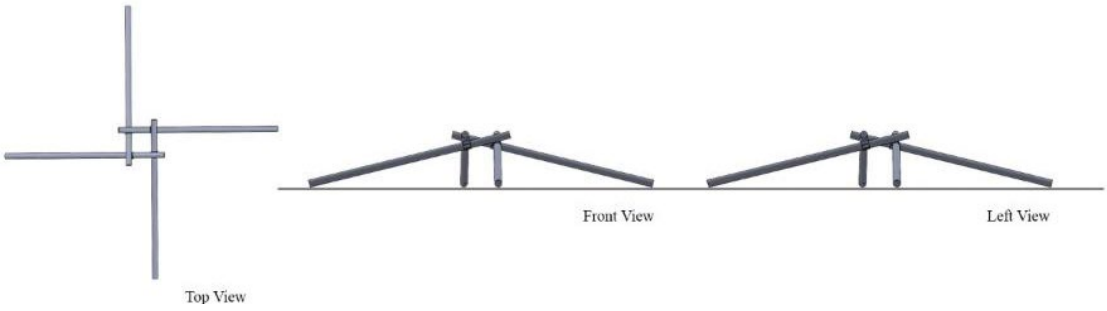

Figure 8.4. Motion mode 1.

The physical model is made from circular cross-sectioned wooden sticks and filament. They are cut in a wood workshop to have the intended length. All the lengths are equal to each other. The joints are printed in a 3d printer with the use of filaments. There is a hole through one face while a semi-hole in the next face (Figure 8.5b). This is because the nexors pass through the holes to provide diversity in the engagement length during the motion, and the endpoints of the nexors are fixed in the semi-holes.

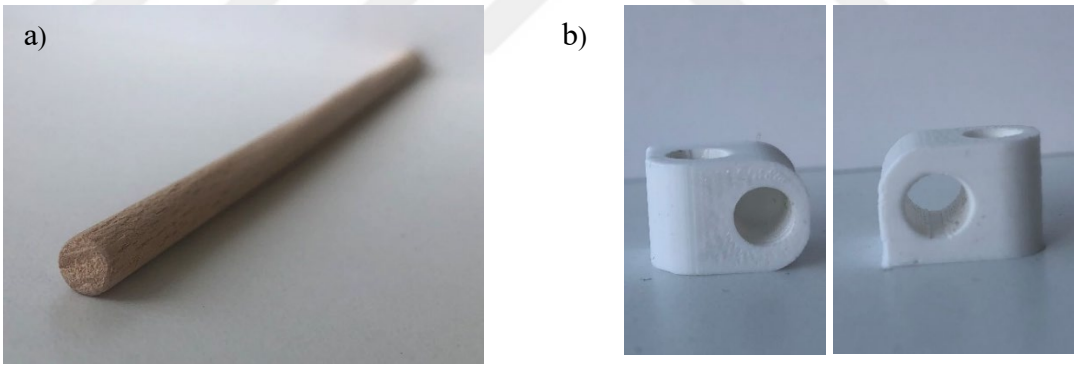

Figure 8.5. a) Wooden stick nexor, b) Joints from filaments.

After obtaining all the nexors and joints, the network is created by adhering to the layout. The fans used in the network are motion mode 1. The network has multi DoF, as seen in Figure 8.6.

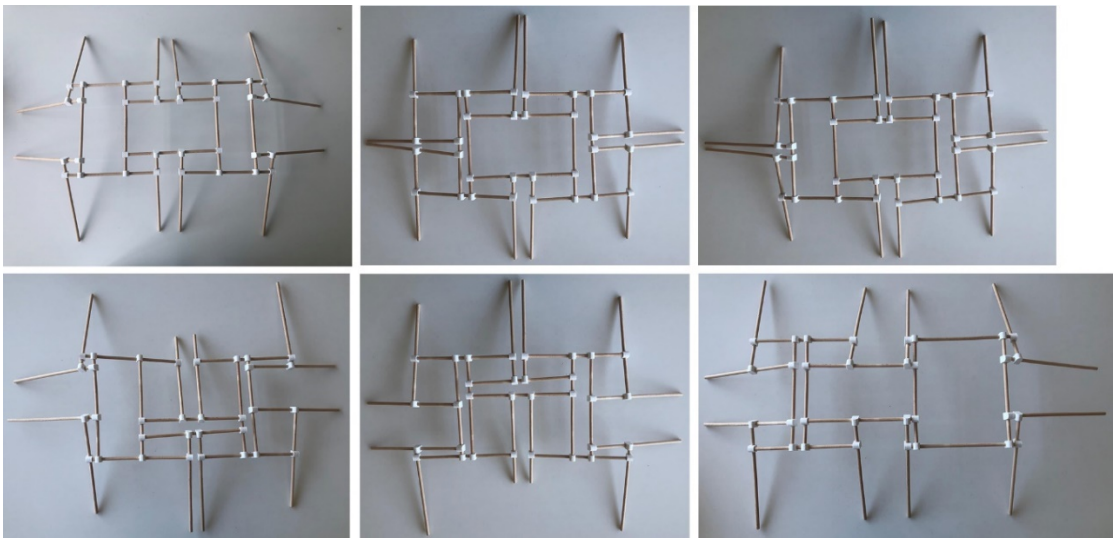

Figure 8.6. Physical model of a network from motion mode 1.

In the condition that the angle between nexors is 90º, a motion mode 2 is formed. Motion mode 2 is a two DoF fan with $\Sigma f_i=8$, and the angle between nexors (θ) is 90°. Thereby two nexors become parallel to each other (green) (Figure 8.7), and the condition of the ends of the nexors touching the ground is collapsed. Moreover, it is seen that two DoF, which are two R joints, remain passive during the motion, but the fan still has two DoF. Although Σf_i becomes six, it is found that the fan doesn't become a structure because the λ_k decreases to four.

$\Sigma f_i = 6, \lambda_k = 4, M = 6 - 4 = 2$

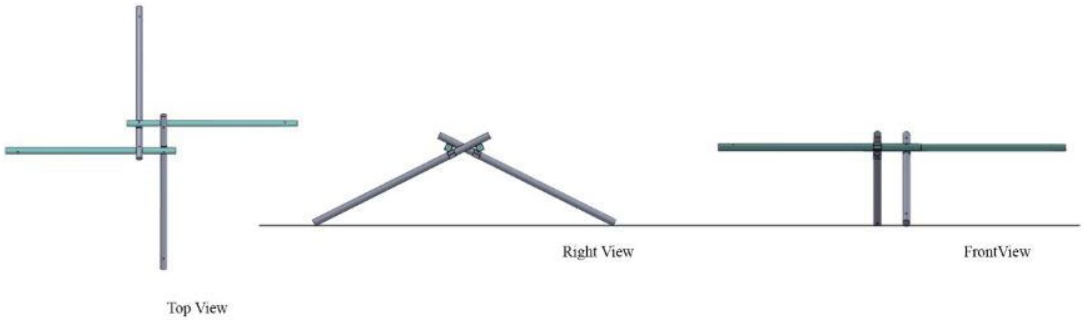

Figure 8.7. Motion mode 2.

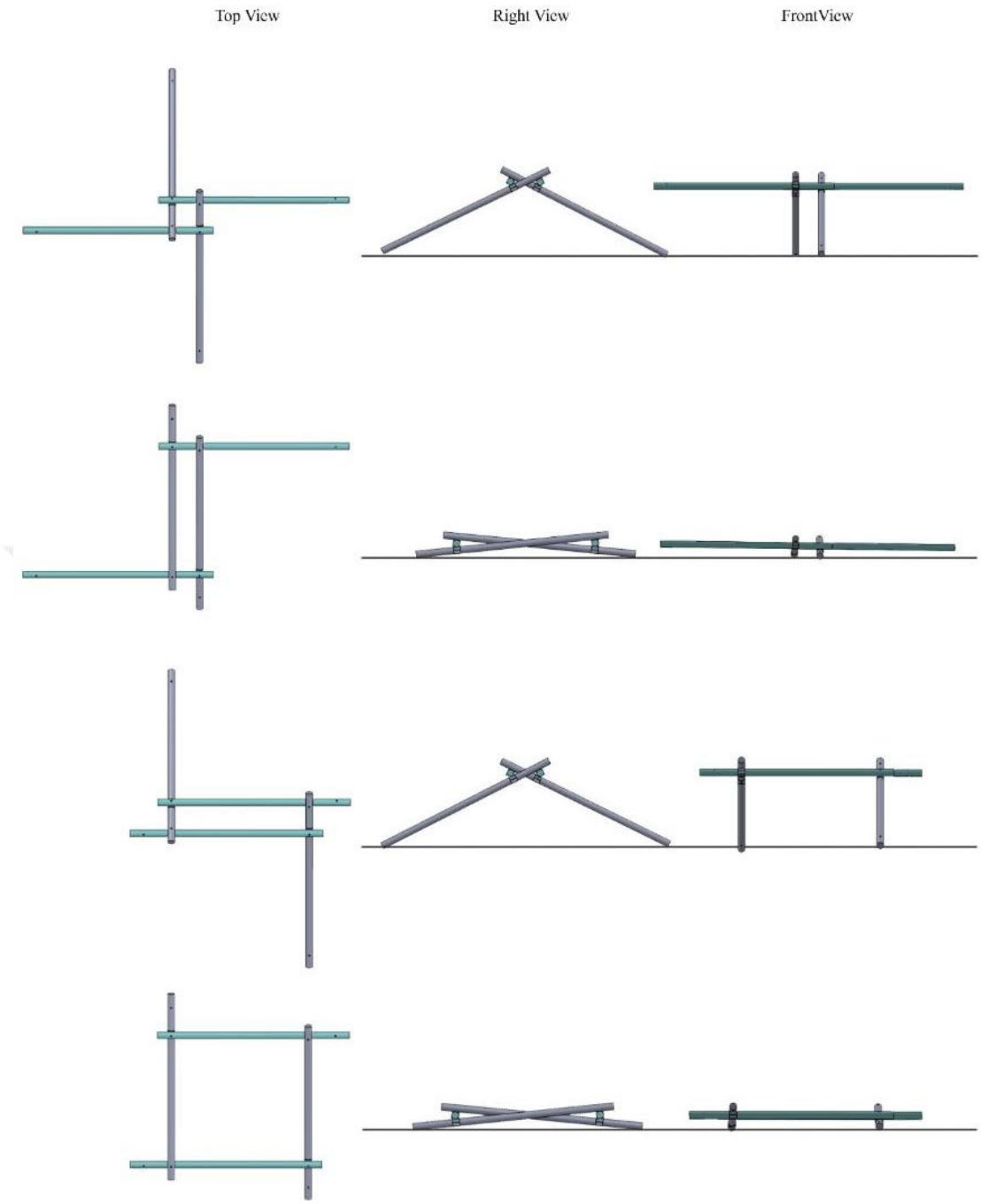

Figure 8.8. Motion of the motion mode 2 fan.

When viewed from the top view, it is seen that the nexors move left and right and up and down. Here, it can be said that there is translational motion in two axes. When viewed from the right view, as the width of the fan changes, there is an increase or decrease in the fan's height. This shows the translational motion on the 3rd axis. Moreover, there are rotations around an axis parallel to the green nexors' axis. Here, too, there is a rotational motion around an axis. As a result, there are three translational and one

rotational motion for motion mode 2, and therefore its λ_k is four. (Figure 8.8). Linear motion in 3d space, which is three translations and one rotation around an axis, is called Schoenflies displacement.

When the two R joints are neglected, two P and two C joints remain. Due to the inactivity of the two R joints, the non-parallel nexors are converted to square cross-section nexors that only allow translational motions (Figure 8.9).

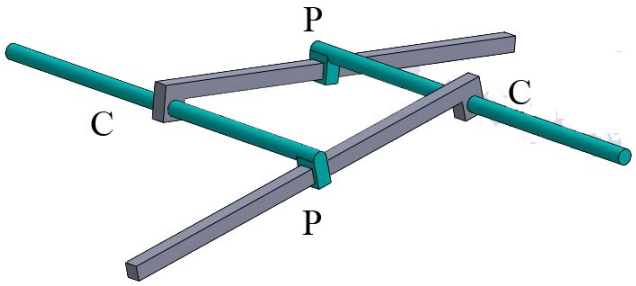

Figure 8.9. Motion mode 2 fan.

The motions of the fan can be seen in Figure 8.8. Four engagement lengths can be changed. The fan has a conformal motion from the top view. The height of the fan varies according to the changing engagement lengths.

7.1. Network 1 From Motion Mode 2

After that, a network is produced from the fans in which two nexors are parallel to each other (Figure 8.10). In the constructed network, the fans share their nexors with neighboring fans. Let the fan names be A, B, C, and D. The fans A and B share the nexor numbered 4, the fans B and D share nexor numbered 3, the fans A and D share nexor numbered 1, and the fans B and the share nexor numbered 3 (Figure 8.11).

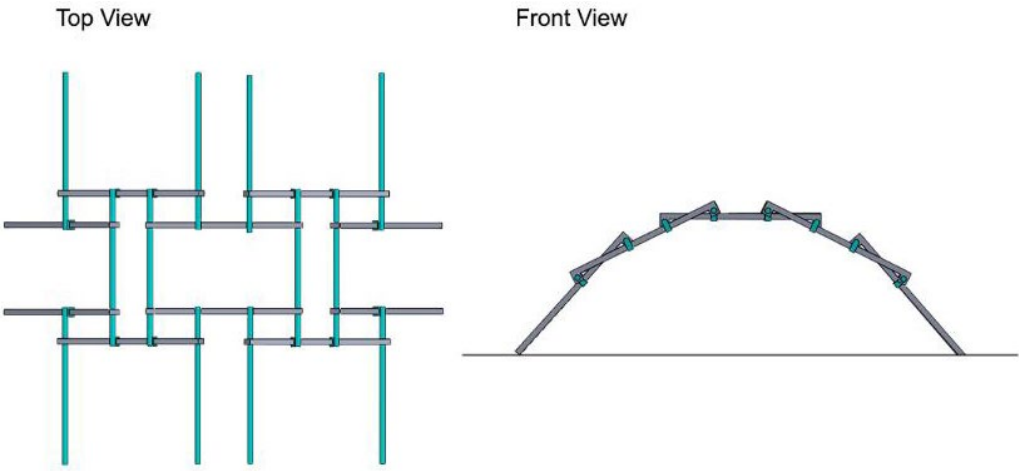

Figure 8.10. Network of motion mode 2.

In the multiplication process, the position and angle of each nexor are affected by its neighboring nexor. The green ones of the multiplicated nexors are positioned parallel to each other. The gray ones automatically take the necessary positions and angles depending on the neighboring nexors and fans.

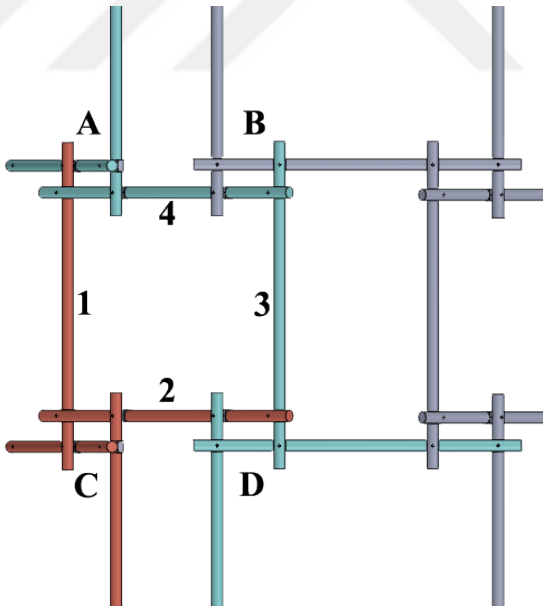

Figure 8.11. Common nexors of motion mode 2 fans.

There are two kinds of motions in the network. If the nexors that are not parallel are moved, the vault thickness changes (Figure 8.12b), and if the parallel nexors are moved, the curvature of the network is affected (Figure 8.12c).

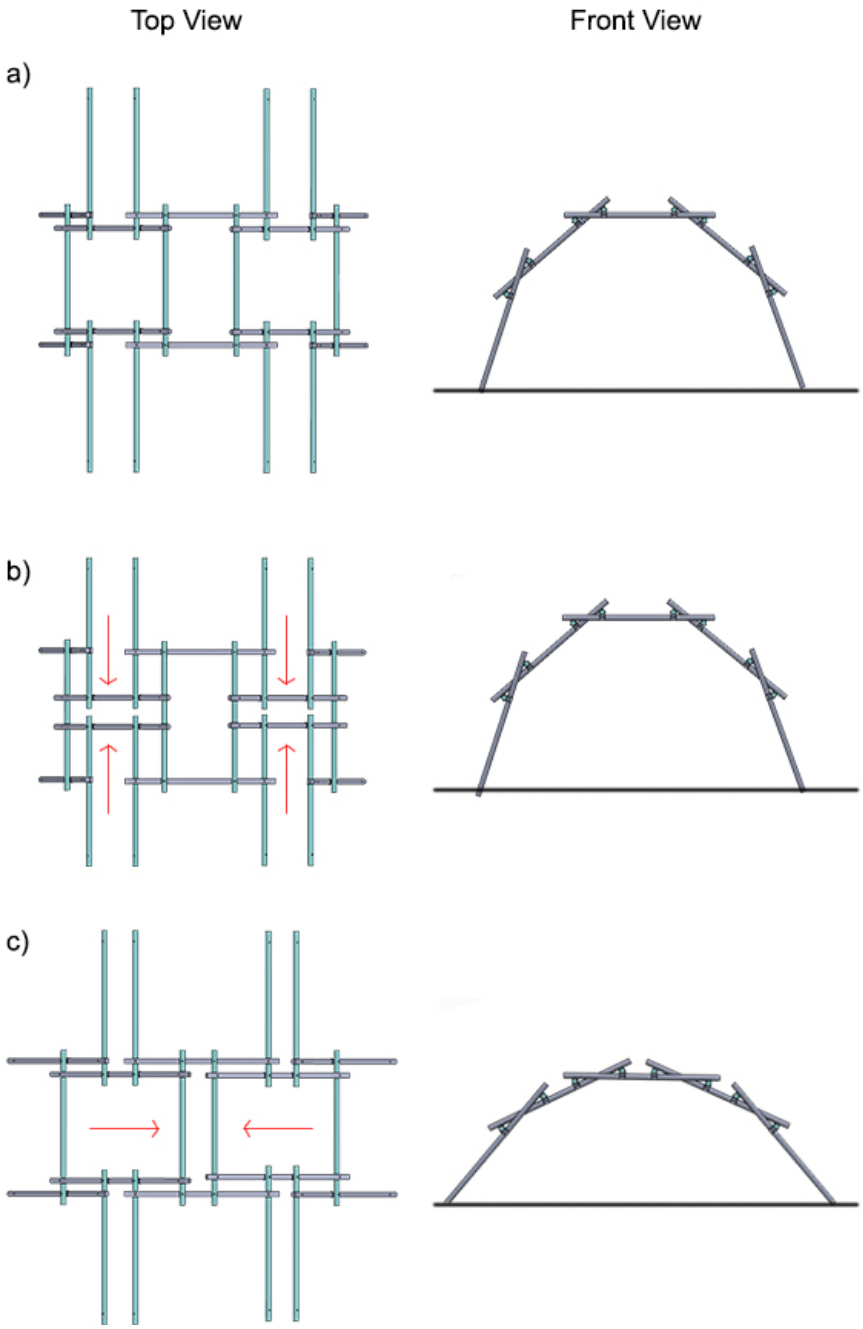

Figure 8.12. Network motion a) Initial state, b) Motion of the non-parallel nexors, and c) Motion of the parallel nexors.

Since the network has multi DoF, it has multiple motions, and some fan groups can move independently. When one of the nexors is pulled to the left, the vault's curvature changes, and the network leans towards the left (Figure 8.13).

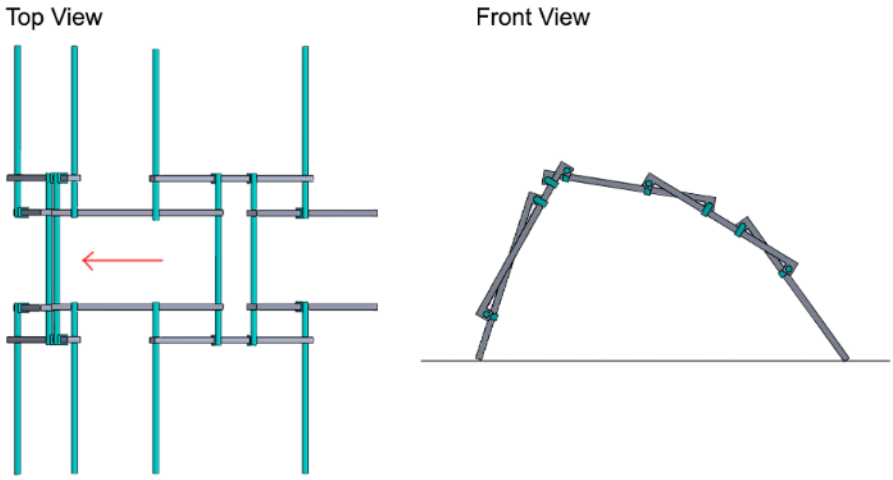

Figure 8.13. Network motion.

When the right part of the fan is pulled, the vault has a symmetric form, but the vault's curvature changes compared to its original state (Figure 8.14).

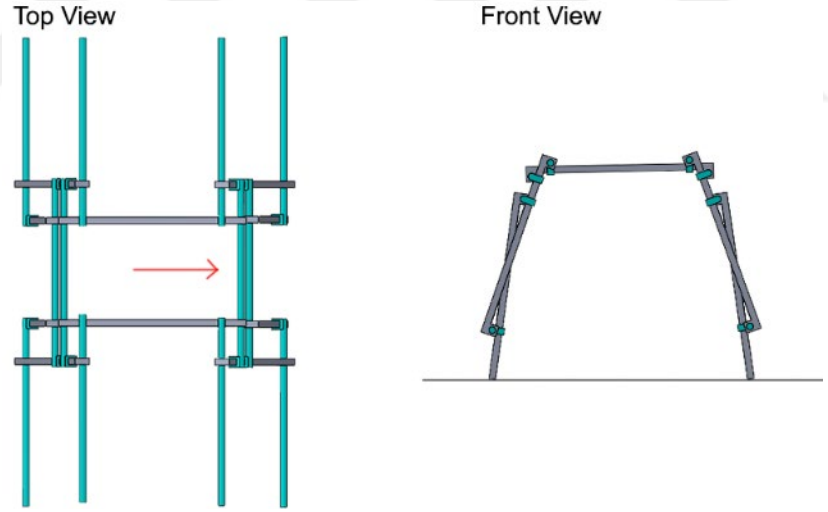

Figure 8.14. Network motion.

In Figure 8.15, the nexor indicated by the red arrow has been extended in the direction of the arrow. The gap in the middle of this part is closed. Moreover, the network curvature does not change.

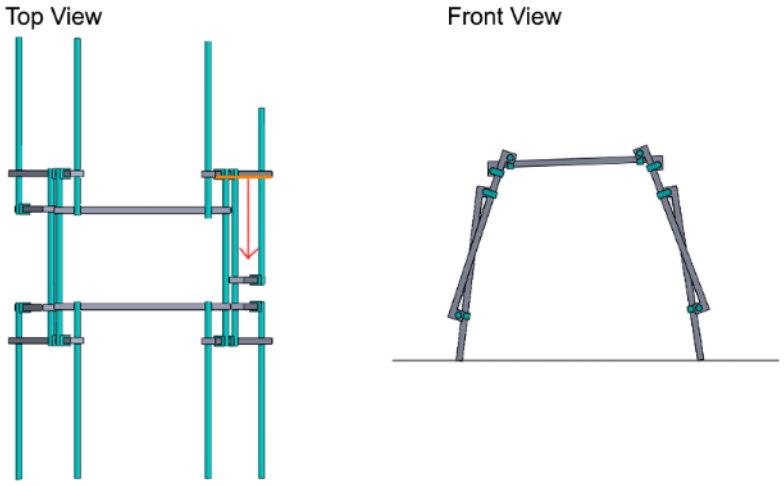

Figure 8.15. Network motion.

In Figure 8.16, the nexor shown with a red arrow is extended to the opposite side. As in the previous motion, the gap in the middle is closed, and this motion does not affect the network curvature.

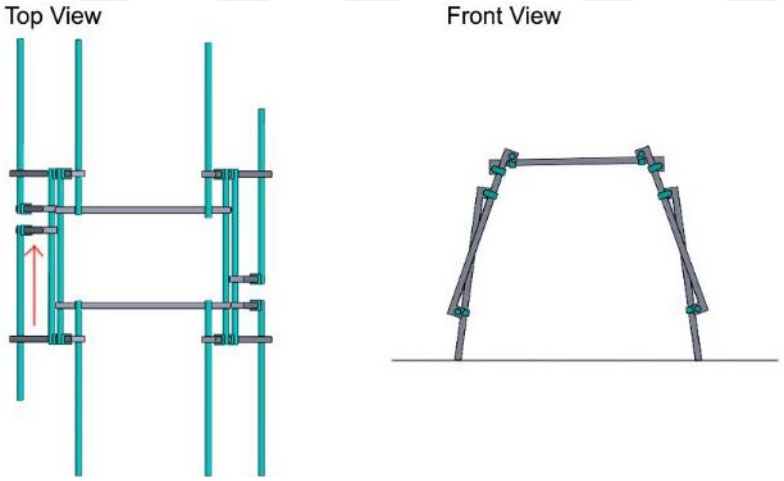

Figure 8.16. Network motion.

In Figure 8.17, the green nexors shown with red arrows are pushed to the right part of the network, and the fans they belong to have been enlarged. The gaps in the sections where the nexors are pushed were covered with the fans. The curvature of the network changes depending on the motion of the nexors.

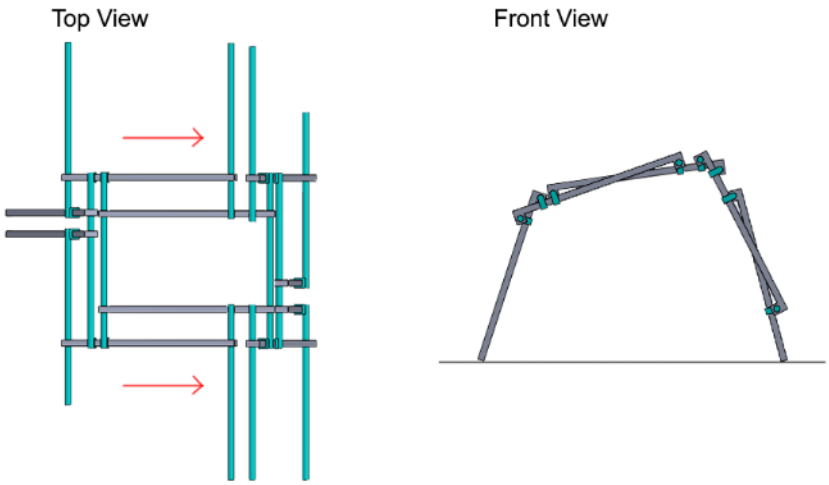

Figure 8.17. Network motion.

In Figure 8.18, the left end fans are made smaller in the direction of the arrow. The curvature of the network changes, and the left part gets higher.

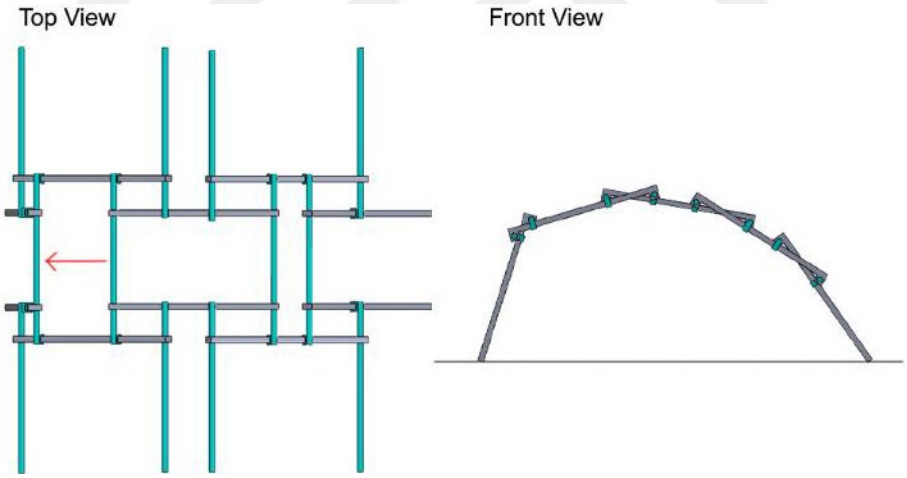

Figure 8.18. Network motion.

Moreover, the fans at the right end of the network are made smaller, and the curvature of the network changes (Figure 8.19).

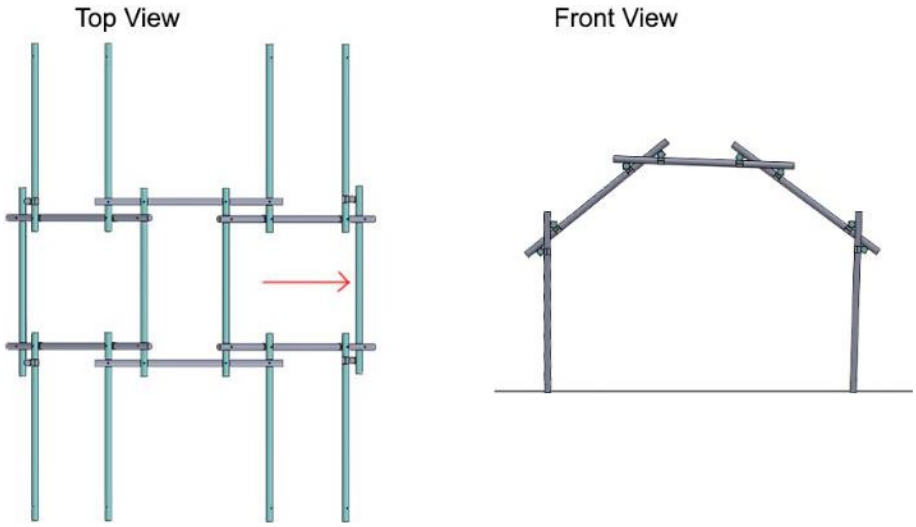

Figure 8.19. Network motion.

7.2. Network 2 From Motion Mode 2

It has been observed that, with the multiplication scheme shown in Figure 8.10, the network has multi DoF; thus, it is difficult to control the curvature. Then, a method is investigated to prevent the increase of the DoF affecting the network's curvature in the fan multiplication process. As a solution, the parallel nexors shown in green are made into a single nexor (There are two green nexors on each grey nexor. These green nexors are combined) (Figure 8.20). The kinematic diagrams of multi DoF and single DoF network curvatures are drawn in Figure 8.21. The nexors 4 and 5, 6 and 8, 9 and 11, 12 and 14 are combined. While Network 1 has 16 nexors, Network 2's nexor number decreases to 12. Network 1's connectivity sum is 20, so the mobility equals five. On the other hand, Network 2's Σf_i is 16; the mobility is one. Thus, the DoF affecting the curvature of the network is reduced to one.

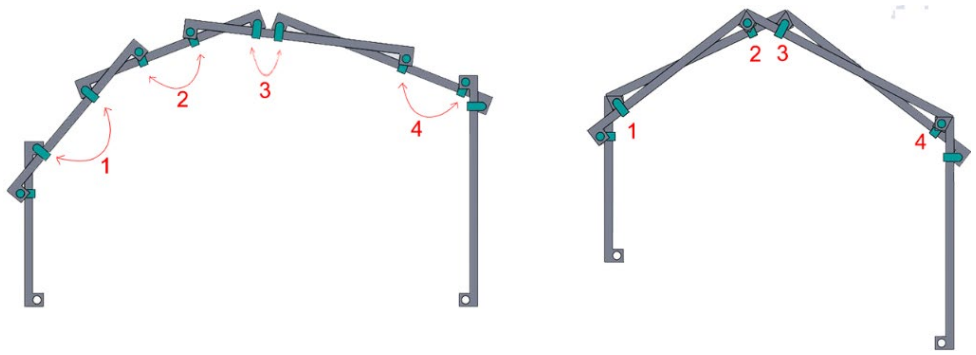

Figure 8.20. Nexors joined to reduce DoF.

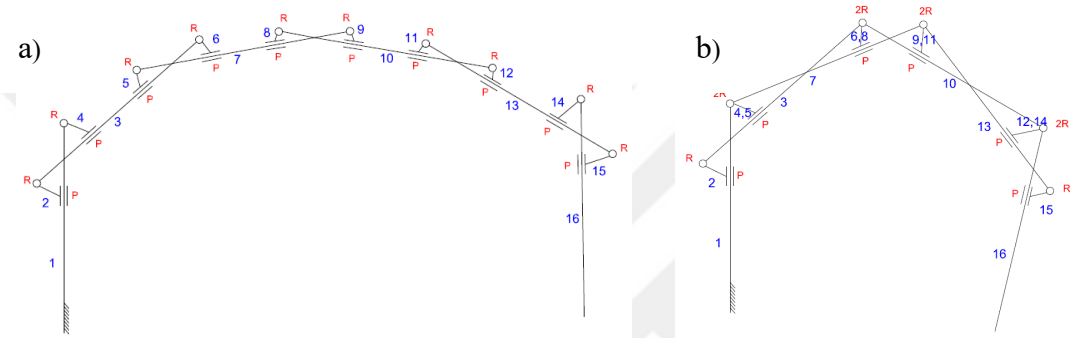

$\Sigma f_i = 20, \lambda_k = 3, L = 5$

$M = 20 - (3 * 5) = 5$

$\Sigma f_i = 16, \lambda_k = 3, L = 5$

$M = 16 - (3 * 5) = 1$

Figure 8.21. Kinematic diagrams and mobility calculations of network curvatures a) Network 1, b) Network 2.

After this part, a network that takes the form of a roll has been tried. In order to obtain a rollable network, it is necessary to use different nexor lengths so that the moving nexors do not collide with each other. While the lengths of the nexors in the parallel direction (green) remain constant, variations are made in the lengths of the gray nexors. Three different nexor lengths are used for this study. While the network takes the form of a roll in its most closed state, it takes the form of a vault in its most open state (Figure 8.22). Thus, the network can be moved and transferred to the desired location.

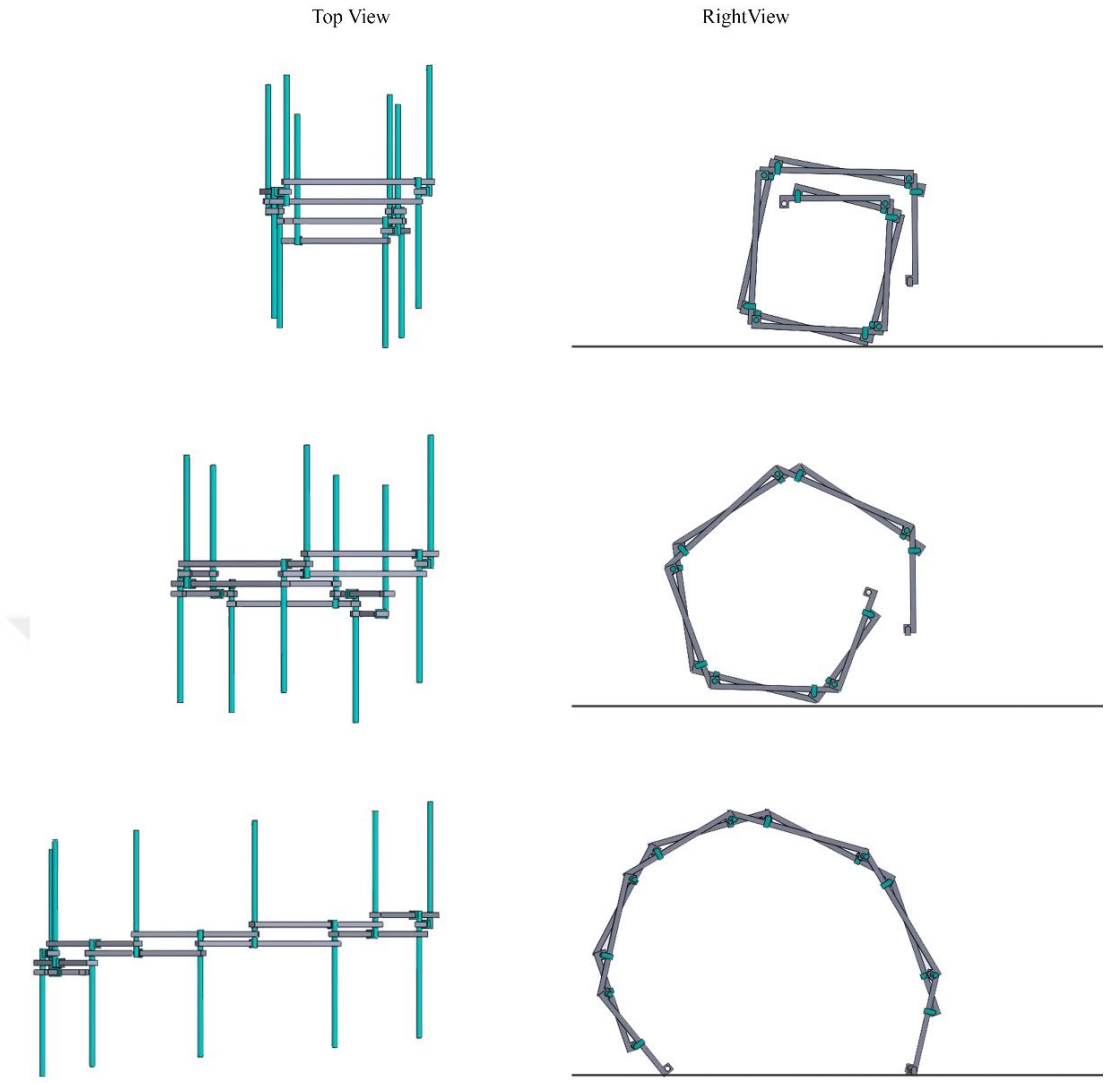

Figure 8.22. Motion of the network from the most closed situation to the most open.

The DoF in the direction that affects the thickness of the vault has not been interfered. Therefore, there is more than one DoF in this direction. The motion in the direction of thickness can be seen in Figure 8.23. In the figure, the thickness of all the fans has been increased, but the fans can also move independently. So, it is also possible to change the thickness of only one fan.

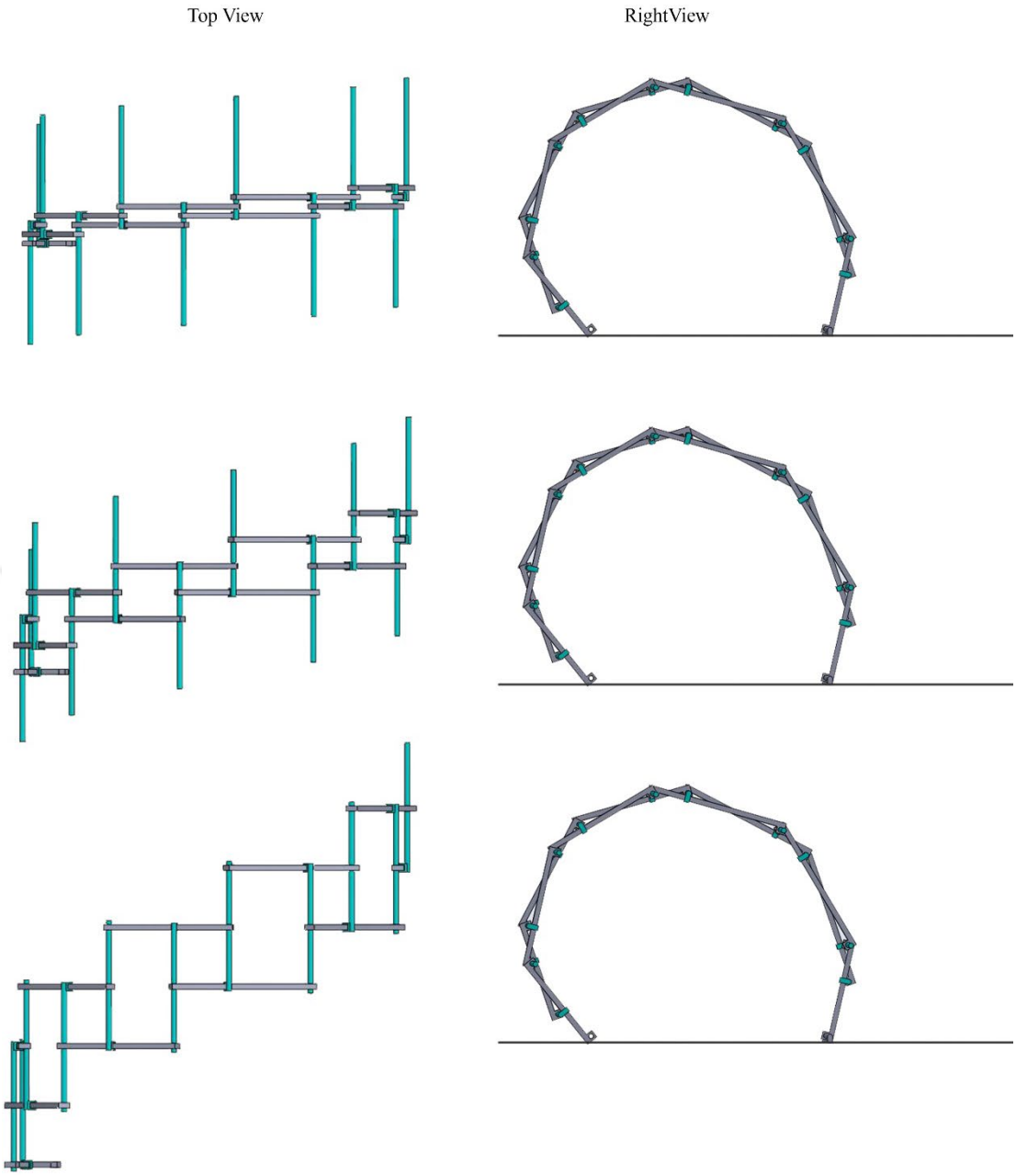

Figure 8.23. Motion in the direction of the thickness of the network.

To obtain the desired size of the vault, the fans can be multiplied as needed like in Figure 8.24.

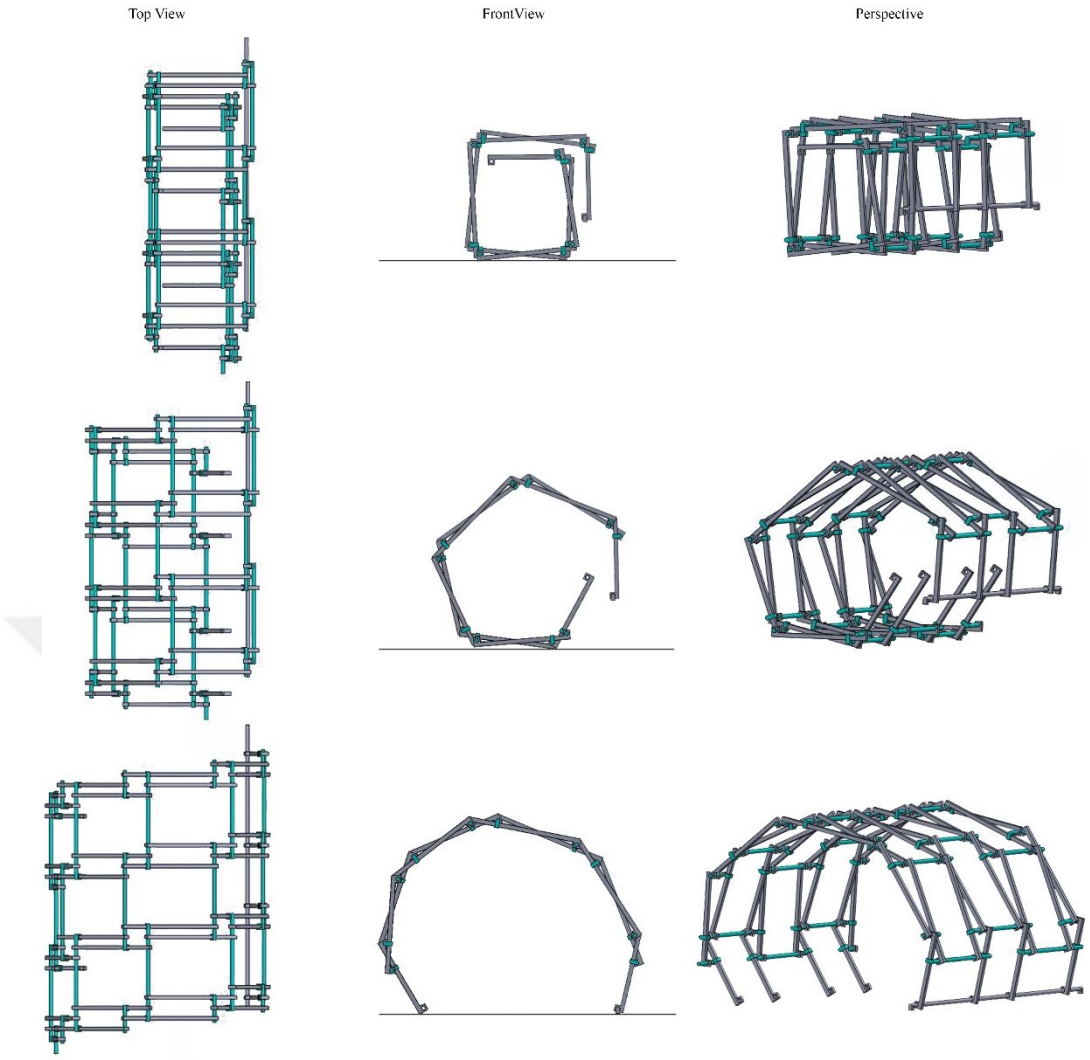

Figure 8.24. The motion sequence of the deployable network.

8.2.2. Physical Model of Network 2

Then, the physical model is produced. As mentioned before in Figure 8.9, there are two types of nexors: rectangular and circular cross-sectioned. The nexors are obtained from the box and tube aluminum (Figure 8.25). The nexors are cut in a metal workshop in the appropriate lengths.

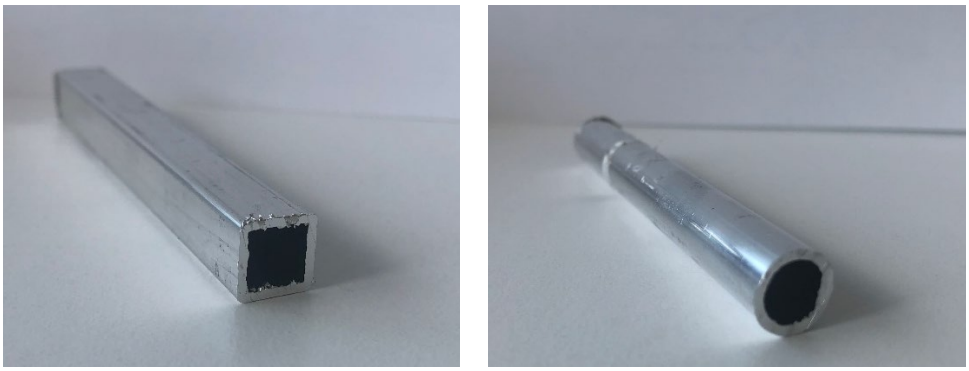

Figure 8.25. Box and tube aluminum.

As every nexor supports and is supported by each other, while a circular cross-sectioned nexor is on top of a rectangular one, in the next intersection point, a rectangular cross-sectioned nexor is on top of a circular one. To connect these two types of nexors, two connections are needed. The connections are printed in a 3d printer. There is a circular hole through a joint when there needs to be a C joint or a rectangular hole through a joint when there needs to be a P joint (Figure 8.26a). Half holes on the joints are for fixing the ends of the nexors (Figure 8.26b). No screwing is used in the model; all parts are telescopic.

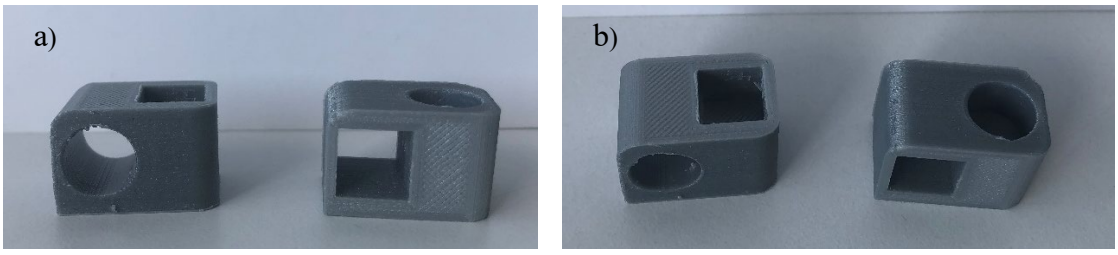

Figure 8.26. a) Hole through connection, b) Half holes on a connection .

After getting all the pieces, the nexors and joints are connected according to the network scheme (Figure 8.27). The model can roll in a most closed situation and be a vault in the most open condition.

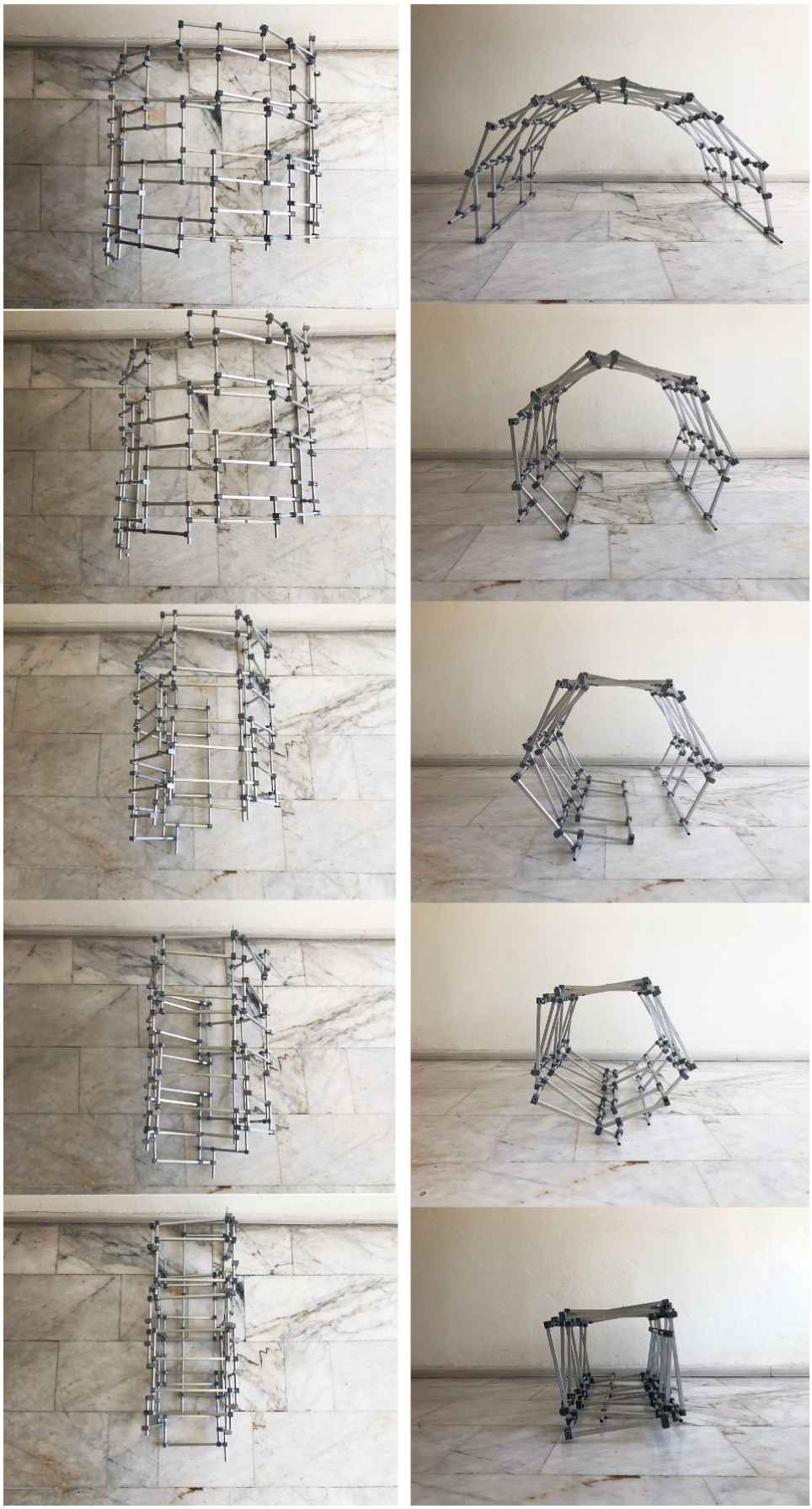

Figure 8.27. Physical model of network 2.

CHAPTER 9

MAIN ACHIEVEMENTS

This dissertation aims to develop movable RF fans and deployable RF networks. The first effort is to examine the elements of the RFs and study the previous studies. The definition of the RF is justified, and the components that make up the RFs are explained in detail. The literature review has been done regarding architectural and previous work. The previous studies show that there is a very limited number of studies for movable RF fans and no studies about 3-dimensional deployable RF networks.

The second attempt is to find the missing geometric information to design a movable RF fan. For this purpose, the joints' positions and orientations are found using the Denavit-Hartenberg parameters. Then, new trigonometric formulas are proposed to find the twist angle, the angle between the nexors and the horizontal plane, the fan's height, the distance between the nexor midpoint and the structure's center, and the base edge. Their relations with the increasing engagement length are shown in a table. A graph has been constituted to see the impact of the engagement length on the fan height and base edge. An unpredictable result is obtained in the analysis. The base edge value is expected to increase while the height decreases with the increasing engagement length. However, after the engagement length reaches a certain length, the height continues to decrease, while the base edge begins to decrease in that length. In other words, it is not possible to see a continuous increase or decrease of a base edge. So a designer should follow the process that is shown to reach an optimum result.

With the acquired geometric knowledge, it is possible to produce a fan that can be demountable. After deciding the engagement lengths for the desired height and base edge, the joints' locations and angles are determined to drill holes. As a result, a reconfigurable demountable fan is obtained that can be disassembled and reassembled at the desired engagement length, height, and base edge.

Since the aim is to have movable RF fans, mobility analysis is essential. After explaining the mobility and its calculation procedure, 3-, 4- and 5- nexor fans' mobility analyses have been made for zero, single and multi DoF.

Single or multi DoF fans are needed to create a deployable RF network. Since multi DoF fans are not easy to control, single DoF fans are selected to make motion analyses. Triangular and quadrilateral fans are created without sliding joints and with sliding joints. The kinematic diagrams of the fans are drawn, and their motions are simulated using Solidworks. While the quadrilateral fans without using P joints have parallelogram motion, the other fans, both triangular and quadrilateral, have no specific motion. If the motions are thought to be two-dimensional, as in the top view, the engagement lengths and the angles between nexors change, which is defined as a general motion.

The next effort is to create a network from a single DoF quadrilateral fan composed of R joints. Categorization has been made for the fan directions used to develop networks: networks with only leftward fans and networks with both leftward and rightward fans. Then the networks are divided into three according to their motion capabilities. The single DoF RF network has a parallelogram motion as it consists only of R joints.

Then, dilation motion for triangular fans and conformal motion for quadrilateral fans are looked for. While the fan's form changes from a large triangle to a small triangle or visa versa in dilation motion, the fan changes its form from a square to a rectangle or visa verse in conformal motion when viewed from the top view. An analogy has been made as if the fans are two-dimensional. Thus, while the engagement lengths change in both motions, the angle between the nexors remains constant. New fans are developed with R, P, C, U, and C_s joints to achieve the desired motions for triangular and quadrilateral fans. It has been seen from the simulations that the motions are either parallelogram or general.

A two DoF quadrilateral fan is investigated to reach conformal motion. The fan has the desired motion, which is conformal. Then, a multi-DoF network is created from this fan. Since it has several motions, it is hard to control. So, a new assembly method is searched. While the DoF in the thickness direction is not interfered with, the DoF in the curvature direction is reduced to single. By using three different nexor lengths, a deployable network is obtained. The network takes the form of a roll in its most closed state, and it takes the form of a vault in its most open state. Since the fans are multi DoF in the thickness direction, variations can be created in the thickness. The nexors can be used as much as needed to enlarge the network. If the deployment ratio of the network is

thought to be high, it is also possible to produce a demountable network. But it is beyond the scope of this thesis.

It has been seen that the new network is the same as the Da Vinci bridge in the direction of curvature. Da Vinci used simple joints in the bridge; on the other hand, revolute and prismatic joints are used in the proposed deployable RF network.

This research contributes to kinetic architecture by creating movable RF fans and deployable RF networks. In view of the changes occurring in the functional and spatial needs, this dissertation offers a deployable RF network that takes the form of a roll in the most closed situation and becomes a vault in the most open position. The RF network produced can meet the accommodation needs of architecture, military, and non-governmental organizations. It can be used as post-disaster emergency structures, exhibition stands, industrial tents, or roof shells.

REFERENCES

AKT II. 2012. “Coca Cola Beatbox.” 2012. https://www.akt-uk.com/projects/coca-cola-beatbox/.

Almaged, Mohammed. 2017. “Forward and Inverse Kinematic Analysis and Validation of the ABB IRB 140 Industrial Robot.” *International Journal Of Electronics, Mechanical And Mechatronics Engineering* 7 (2): 1383–1401.

Anastas, Youssef, Landolf Rhode-Barbarigos, and Sigrid Adriaenssens. 2016. “Design-to-Construction Workflow for Cell-Based Pattern Reciprocal Free-Form Structures.” *Journal of the International Association for Shell and Spatial Structures* 57 (2): 159–76. https://doi.org/10.20898/j.iass.2016.188.737.

Arias, C Martínez, and J Anaya Díaz. 2019. “Parametric Description of the Movement of Reciprocal Transformable Geometry Surfaces, for Adaptive Environment Materialization.” In *Structures and Architecture: Bridging the Gap and Crossing Borders*, edited by P. J. S. Cruz, 1st Edition, 793–800. London: CRC Press. https://doi.org/https://doi.org/10.1201/9781315229126.

Ariza Ruiz, J. O., and J C Chilton. 2002. “Networks Composed of Reciprocal Frame Modules.” In *Space Structures 5*, edited by G. A. R. Parke and P. Disney. London: Thomas Telford. https://www.researchgate.net/publication/299629592.

Bautista, Jorge. n.d. “Morfología de Las Cubiertas: Estructuras Recíprocas.” Bioconstruccion Online. Accessed April 11, 2022. https://bioconstrucciononline.com/estructuras-reciprocas/#:~:text=Los%20techos%20rec%C3%ADprocos%20incorporan%20geometr%C3%ADas,de%20estas%20con%20el%20todo.

Baverel, Oliver, and Messaoud Saidani. 1999. “The Multi-Reciprocal Grid System.” *Article in Journal of the International Association for Shell and Spatial Structures* 40 (1). https://www.researchgate.net/publication/283320301.

Baverel, Olivier. 2000. “Nexorades: A Family of Interwoven Space Structures.” Ph. D., University of Surrey.

Carlo, Biagio di. 2008. “The Wooden Roofs of Leonardo and New Structural Research.” *Nexus Network Journal*, 27–38. https://doi.org/10.1007/978-3-7643-8728-0_4.

Chilton, J C. 2009. “Development of Timber Reciprocal Frame Structures in the UK.” In *International Association for Shell and Spatial Structures*, edited by Alberto Domingo and Carlos Lazar, 1877–84. Valencia. https://www.researchgate.net/publication/50838924.

Chilton, J. C., B. C. Choo, and J. Yu. 1994. “Morphology of Reciprocal Three-Dimensional Grillage Structures.” In *Spatial Lattice and Tension Structures*, edited by J. F. Abel, J. W. Leonard, and C. U. Penalba, 1065–72. Atlanta.

Chilton, J C, B S Choo, and D Wilkinson. 1998. “A Parametric Analysis of the Geometry of Retractable Reciprocal Frame Structures.” In *Lightweight Structures in Architecture, Engineering and Construction*. https://www.researchgate.net/publication/321270413.

Chilton, John C, and Ban Seng Choo. 1992. “Reciprocal Frame Long Span Structures,” 100–109.

Choo, Ban Seng, Paula N Couliette, and John C Chilton. 1994. “Retractable Roof Using the ‘Reciprocal Frame.’” In *Places of Assembly and Long-Span Building Structures*, 49–54. https://doi.org/10.5169/seals-54118.

Clip Art ETC. n.d. “Caesar’s Bridge Over the Rhine.” Clip Art ETC. Accessed April 11, 2022. https://etc.usf.edu/clipart/79400/79426/79426_rhinebridge.htm.

Conway, John Horton, Heidi Burgiel, and Chaim Goodman-Strauss. 2008. *The Symmetries of Things*. A.K. Peters.

Douthe, C., and O. Baverel. 2009. “Design of Nexorades or Reciprocal Frame Systems with the Dynamic Relaxation Method.” *Computers and Structures* 87 (21–22): 1296–1307. https://doi.org/10.1016/j.compstruc.2009.06.011.

Freudenstein, F, and R Alizade. 1975. “On the Degree of Freedom of Mechanisms with Variable General Constraint.” In *Fourth World Congress on the Theory of Machines and Mechanisms*, 51–56.

Furuto, Alison. 2012. “Kreod / Chun Qing Li of Pavilion Architecture.” Archdaily. October 7, 2012. https://www.archdaily.com/275460/kroed-chun-qing-li-of-pavilion-architecture.

Gantes, Charalambos. 1991. “A Design Methodology for Deployable Structures.” Ph. D., Cambridge: Massachusetts Institute of Technology.

Garavaglia, Elsa, Attilio Pizzigoni, Luca Sgambi, and Noemi Basso. 2013. “Collapse Behaviour in Reciprocal Frame Structures.” *Structural Engineering and Mechanics* 46 (4): 533–47. https://doi.org/10.12989/sem.2013.46.4.533.

Gelez, Simon, Simon Aubry, and Bernard Vaudeville. 2011. “Behavior of a Simple Nexorade or Reciprocal Frame System.” *International Journal of Space Structures* 26 (4): 331–42. https://doi.org/10.1260/0266-3511.26.4.331.

Gheorghe, Andrei, and Robert Vierlinger. 2017. “DigDesFab15 Research Pavilion.” *Frontiers in Digital Humanities* 4 (September). https://doi.org/10.3389/fdigh.2017.00018.

Godthelp, Tom. 2019. “Timber Reciprocal Frame Structures.” Master, Eindhoven: Eindhoven University of Technology.

Griffiths, Alyn. 2017. “Stone Pavilion.” 2017. https://www.dezeen.com/2017/05/07/aau-anastas-gsa-research-laboratory-stone-pavilion-jericho-palestine/.

Gustafsson, Joel. 2016. “Connections in Timber Reciprocal Frames.” Master Thesis, Gothenburg: Chalmers University of Technology.

Hewett, C. A. 1974. *English Cathedral Carpentry*. https://doi.org/https://doi.org/10.1080/00665983.1974.11077553.

Houlsby, Guy T. 2014. “John Wallis and the Numerical Analysis of Structures.” *Nexus Network Journal* 16 (1): 207–17. https://doi.org/10.1007/s00004-014-0179-7.

“IFTooM Dictionaries Online.” n.d. Structure of Machines and Mechanisms. Accessed July 21, 2022. https://iftomm-terminology.antonkb.nl/2057/frames.html.

Karakoç, Zehra. 2017. “Yapı Örtüsü Olarak Mütekabil Elemanların İncelenmesi.” Master Thesis, İstanbul: Fatih Sultan Mehmet Vakıf University.

Kılıç, Övgü, and Ahmet Vefa Orhon. 2019. “Introduction of a Load Bearing System: RF Systems.” In *International Design and Engineering Symposium*, edited by Hakan Doygun, Aslı Güneş Gölbey, and Nurdan Erdoğan, 118–22. İzmir.

Lynch, Kevin (Kevin M.), and Frank C. Park. 2017. *Modern Robotics : Mechanics, Planning, and Control*.

McCarthy, J. M., and G. S. Soh. 2010. *Geometric Design of Linkages*. Edited by S. S. Antman, J. E. Marsden, and L. Sirovich. Springer Science & Business Media. www.springer.com/series/1390.

Mufazzal, Sameera. 2017. “Studies on Grübler’s Formula for Mobility and Connectivity.” In *Innovative Product Design & Development*, edited by Syed Wasiul Hasan Rizvi, 141–45.

Muñoz-Vidal, M., I. López-César, J. Pérez Valcárcel, and F. Suárez Riestra. 2019. “Deployable Structures of Reciprocal Crossed Arches.” In *Structures and Architecture: Bridging the Gap and Crossing Borders*, edited by P. J. S. Crus, 1st Edition. London: CRC Press. https://doi.org/https://doi.org/10.1201/9781315229126.

Palumbo, Arianna, Sergio Pone, and Daniele Lancia. 2019. “Digital Tool for Reciprocal Frame.” In *IASS Annual Symposium*, edited by C. Lázaro, K. U. Bletzinger, and E. Oñate. Barcelona. https://www.researchgate.net/publication/338864864.

Pantazis, Evangelos, and David Jason Gerber. 2014. “Material Swarm Articulations New View Reciprocal Frame Canopy Multi Agent Systems-Swarm Robotics View Project.” In *32nd ECAADe Conference*. Newcastle upon Tyne. https://doi.org/10.13140/2.1.1971.0405.

Parigi, Dario, and Poul Henning Kirkegaard. 2014. “The Reciprocalizer: An Agile Design Tool for Reciprocal Structures.” *Nexus Network Journal* 16 (1): 61–68. https://doi.org/10.1007/s00004-014-0176-x.

Parigi, Dario, and Alberto Pugnale. 2014. “Three-Dimensionality in Reciprocal Structures: Concepts and Generative Rules.” *Nexus Network Journal* 16 (1): 151–77. https://doi.org/10.1007/s00004-014-0183-y.

Parigi, Dario, and Mario Sassone. 2010. “The Design of a Planar Kinetic Reciprocal Frame.” In *Onternat’onal Association for Shell and Spatial Structures*, 1979–90. Shanghai: Chrina Architecture & Building Press.

Parigi, Dario, Mario Sassone, Poul Henning Kirkegaard, and Paolo Napoli. 2014. “Static and Kinematic Formulation of Planar Reciprocal Assemblies.” *Nexus Network Journal* 16 (1): 37–59. https://doi.org/10.1007/s00004-014-0175-y.

Pérez-Valcárcel, J., M. Muñoz-Vidal, F. Suárez-Riestra, Isaac R. López-César, and M. J. Freire-Tellado. 2021a. “A New System of Deployable Structures with Reciprocal Linkages for Emergency Buildings.” *Journal of Building Engineering* 33 (January). https://doi.org/10.1016/j.jobe.2020.101609.

Pérez-Valcárcel, J., M. Muñoz-Vidal, F. Suárez-Riestra, Isaac R. López-César, and M. J. Freire-Tellado. 2021b. “Deployable Cylindrical Vaults with Reciprocal Linkages for Emergency Buildings.” *Structures* 33 (October): 4461–74. https://doi.org/10.1016/j.istruc.2021.06.094.

Pizzigoni, Attilio. 2009. “A High Fiber Reinforced Concrete Prototype for Reciprocal Structures of Demountable Building.” In *International Association for Shell and Spatial Structures* , edited by Alberto Domingo and Carlos Lazaro, 1895–1906. Valencia. https://www.researchgate.net/publication/50838927_A_high_fiber_reinforced_concrete_prototype_for_reciprocal_structures_of_demountable_building.

Pizzigoni, Attilio. 2015. “Brunelleschi’s Bricks.” *Journal of the International Association for Shell and Spatial Structures* 56 (2): 137–48. https://www.researchgate.net/publication/287219959_Brunelleschi’s_bricks.

Popovic Larsen, Olga. 2007. *Reciprocal Frame Architecture*. Burlington: Architectural Press.

Popovic Larsen, Olga. 2009. “Reciprocal Frame Architecture in Japan.” In *International Association for Shell and Spetial Structures Symposium* , edited by Alberto Domingo and Carlos Lazaro, 1866–76. Valencia. https://moam.info/reciprocal-frame-architecture-in-japan_5c22675a097c474a018b456c.html.

Popovic Larsen, Olga. 2014. “Reciprocal Frame (RF) Structures: Real and Exploratory.” *Nexus Network Journal* 16 (1): 119–34. https://doi.org/10.1007/s00004-014-0181-0.

Popovic Larsen, Olga, and Daniel Sang-Hoon Lee. 2013. “Reciprocal Frames (RFs) Used for Quick-Built Deployable Emergency Shelters.” In *International Association for Shell and Spatial Structures (IASS) Symposium*, edited by J.B. Obrębski and R. Tarczewski. https://www.researchgate.net/publication/278409951.

Popovic, Olga. 1996. “Reciprocal Frame Structures.” Ph. D., University of Nottingham.

Pugnale, Alberto, Dario Parigi, Mario Sassone, and Poul H Kirkegaard. 2011. “The Principle of Structural Reciprocity: History, Properties and Design Issues.” In *IABSE-IASS Symposium 2011:Taller, Longer, Lighter*. London. https://www.researchgate.net/publication/271523220.

Pugnale, Alberto, and Mario Sassone. 2014. “Structural Reciprocity: Critical Overview and Promising Research/Design Issues.” *Nexus Network Journal* 16 (1): 9–35. https://doi.org/10.1007/s00004-014-0174-z.

Puyol, Ana Garcia. 2015. “Mass Customization of Reciprocal Frame Structures.” In *International Association for Shell and Spatial Structures*. Amsterdam.

Qi, Lin, Wenbo Zhang, Zifei Li, Ronglai Sun, and Xin Huang. 2019. “GEOMETRY CONSTRUCTION METHOD OF HEX-TRI RECIPROCAL FRAME.” *Civil Engineering Journal* 28 (4): 576–88. https://doi.org/10.14311/cej.2019.04.0048.

Rizzuto, J. P., and O. Popovic Larsen. 2010. “Connection Systems in Reciprocal Frames and Mutually Supported Elements Space Structure Networks.” *International Journal of Space Structures* 25 (4): 243–56. https://doi.org/https://doi.org/10.1260/0266-3511.25.4.243.

Rizzuto, J. P., M. Saidani, and J. C. Chilton. 2000. “The Self-Supporting Multi-Reciprocal Grid (MRG) System Using Notched Elements.” *International Association for Shell and Spatial Structures* 41 (133): 125–31. https://www.researchgate.net/publication/281684555_The_self-supporting_multi-reciprocal_grid_MRG_system_using_notched_elements.

Rizzuto, J. P., Messaoud Saidani, and J C Chilton. 2002. “Multi-Reciprocal Element (MRE) Space Structure Systems.” In *5th Conference on Space Structures*, 641–48. London. https://doi.org/10.13140/RG.2.1.2943.7921.

Roberti, Giulio Mirabella, Giuseppe Ruscica, and Vittorio Paris. 2021. “From the Herringbone Dome by Sangallo to the Serlio Floor of Emy (and Beyond).” *Curved and Layered Structures* 8 (1): 259–70. https://doi.org/10.1515/cls-2021-0023.

Saidani, M, and O Baverel. 1998. “Retractable Multi-Reciprocal Grid Structure.” *International Association for Shell and Spatial Structures* 39: 141–46.

Shigeru Ban Architects. 2002. “Bamboo Roof.” 2002. http://www.shigerubanarchitects.com/works/2002_bamboo-roof/index.html.

Song, Peng, Chi Wing Fu, Prashant Goswami, Jianmin Zheng, Niloy J. Mitra, and Daniel Cohen-Or. 2014. “An Interactive Computational Design Tool for Large Reciprocal Frame Structures.” *Nexus Network Journal* 16 (1): 109–18. https://doi.org/10.1007/s00004-014-0173-0.

Song, Peng, Chi-Wing Fu, Prashant Goswami, and Jianmin Zheng. 2013. “Reciprocal Frame Structures Made Easy.” *ACM Transactions on Graphics* 32 (4): 1–13. https://doi.org/https://doi.org/10.1145/2461912.2461915.

Thönnissen, Udo. 2014. “A Form-Finding Instrument for Reciprocal Structures.” *Nexus Network Journal* 16 (1): 89–107. https://doi.org/10.1007/s00004-014-0172-1.

Tsai, Lung-Wen. 1999. *Robot Analysis: The Mechanics of Serial and Parallel Manipulators*. John Wiley & Sons.

VITA

PERSONAL

Surname Name: Özen Gülçin

EDUCATION

Ph. D. İzmir Institute of Technology. The Graduate School of Engineering and Science. Department of Architecture (2016-2022)

Thesis: Design and Analysis of Deployable Reciprocal Frames

M. Sc. Yıldız Technical University. The Graduate of Science and Engineering, Computer Aided Architectural Design

Thesis: Design Inspired by Nature: Biomimicry

B. Arch. İzmir University of Economics. Faculty of Fine Arts and Design. Department of Architecture (2007-2012)
İzmir University of Economics. Faculty of Fine Arts and Design. Department of Interior Architecture and Environmental Design (2008-2013) (Minor Programme)

WORK EXPERIENCES

İzmir University of Economics. Directorate of Project and Construction. Architect (2013)
Yıldız Technical University. Department of Architecture. Research Assistant (2013-2016)
İzmir Institute of Technology. Department of Architecture. Research Assistant (2016-2022)
Pamukkale University. Department of Architecture. Research Assistant (2022-…)

PUBLICATIONS

Pekdoğan, T., Özen, G., Güçü, İ., and Gerçek, M. 2017. "An Empirical Investigation of the Housing Price Dynamics across the Districts of Izmir". In *International Congress on Politic, Economic and Social Studies (ICPESS)*. İzmir.
Özen, G. and Korkmaz, K. 2020. "Mobility Analysis of Reciprocal Frames". In *International Symposium of Architecture, Technology and Innovation 2020- Smart Buildings, Smart Cities (ATI)*, 160-169. İzmir.